THE DYNAMIC RESPONSE OF TIMBER SHEAR WALLS

By

James Daniel Dolan

B. Sc. (Civil Engineering) University of Montana

M. Sc. (Civil Engineering) University of Washington

A THESIS SUBMITTED IN PARTIAL FULFILLMENT OF

THE REQUIREMENTS FOR THE DEGREE OF

DOCTOR OF PHILOSOPHY

in

THE FACULTY OF GRADUATE STUDIES

CIVIL ENGINEERING

We accept this thesis as conforming

to the required standard

THE UNIVERSITY OF BRITISH COLUMBIA

October 1989

© James Daniel Dolan, 1989

In presenting this thesis in partial fulfilment of the requirements for an advanced degree at the University of British Columbia, I agree that the Library shall make it freely available for reference and study. I further agree that permission for extensive copying of this thesis for scholarly purposes may be granted by the head of my department or by his or her representatives. It is understood that copying or publication of this thesis for financial gain shall not be allowed without my written permission.

Civil Engineering
The University of British Columbia
2324 Main Mall
Vancouver, Canada
V6T 1W5

Date: October 9, 1989

Abstract

This thesis describes three numerical models, developed by the author, that predict the behavior of timber shear walls. Two of the models have been implemented in finite element programs. One program predicts the static behavior of shear walls and the other predicts the dynamic response to earthquakes. Both programs incorporate **1)** the ability to predict the ultimate load capacity of the walls, **2)** the effects of bearing between adjacent sheathing panels, **3)** the effects of bending in the sheathing, and **4)** the effect of bearing and gap formation between framing elements. The third model is a closed form mathematical model that was developed to predict the steady state response of shear walls to harmonic base excitations.

A series of experimental tests were performed to determine the load–deflection characteristics of single nail connections between the solid wood, used for framing, and sheathing materials. The load–deflection characteristics for these connections were used to predict the behavior of timber shear walls using the finite element models.

An extensive experimental program, consisting of five different tests and forty–two full size shear wall specimens, was conducted to verify the three numerical models. The experimental program included a new test that is representative of the earthquake loading for a ground floor wall of a three–storey North American apartment building.

The test results were also used to: **1)** compare the performance of waferboard with that of plywood sheathing, **2)** investigate the dynamic behavior of shear walls, **3)** investigate effects of out–of–plane deflections of the sheathing, and **4)** examine the anchoring connection that resists the overturning moment.

The merits and shortcomings of the five shear wall tests are discussed, along with their

future usefulness in determining the effects of changes in the construction techniques used for timber shear walls.

The dynamic model and shear wall test results are then used to investigate four design codes to see if shear walls, designed according to the various codes, adequately resist the loads experienced during earthquakes. A resistance factor for the design of shear walls is recommended for inclusion in the 1990 Canadian timber design code. The recommended resistance factor will result in the design loads specified by the code being more representative of the loads generated during an earthquake. Three important construction details are also discussed to inform the reader of possible problems that can be expected if these details are neglected during either design or construction. The details are: the hold–down anchor, framing corner connection, and sheathing connector.

Finally, recommendations are made as to the type of research that is required to develop a design procedure for timber shear walls, based on the actual dynamic characteristics of shear walls as well as reliability theory.

Table of Contents

Abstract ii

List of Tables xi

List of Figures xiv

Notation xix

Acknowledgements xxix

Dedication xxxi

1 Introduction 1

1.1 Background 1

1.2 Objectives 3

1.2.1 Methods for Achieving Objectives 4

1.3 Design Codes 5

1.4 Applications 6

1.5 Thesis Organization 7

1.6 Limitations of Study 9

2 Literature Survey 10

2.1 Introduction 10

2.2 Testing 11

2.2.1 Connections 11

2.2.2 Full Size Shear Walls 13
2.2.3 Full Size Buildings 16
2.3 Numerical Modeling 18
2.3.1 Connections 18
2.3.2 Shear Walls 19
2.3.3 Full Structures 20
2.4 Summary 21

3 Static Finite Element Model **23**
3.1 Introduction 23
3.2 Assumptions 24
3.3 The Framing Beam Element 26
3.4 Bi-Linear Corner Connector 31
3.5 The Sheathing Element 32
3.5.1 Kinematic Relationships 33
3.5.2 Stress-Strain Relationships 36
3.5.3 Finite Element Approximations and Shape Functions 38
3.5.4 Virtual Deformations 44
3.5.5 Virtual Work Equations 46
3.6 The Sheathing Connector Element 52
3.6.1 Geometry 53
3.6.2 Deflections 55
3.6.3 Connection Force 59
3.6.4 Energy Formulation of Stiffness Matrix 61
3.7 The Sheathing Bearing Connector Element 63
3.7.1 Geometry 64

3.7.2 Deflections 65
3.7.3 Connector Forces 66
3.7.4 Virtual Work 66
3.8 Global System of Equations and Solution 68
3.9 Summary 70

4 Closed Form Mathematical Model for Steady State Response 72
4.1 Introduction 72
4.2 Assumptions 74
4.3 Derivation 78
4.3.1 Numerical Solution of Equations 87
4.3.1.1 Numerical Example 88
4.4 Bounds on Frequency Response 88
4.5 Summary 91

5 Dynamic Finite Element Model 92
5.1 Introduction 92
5.2 Assumptions 92
5.3 Step-by-Step Integration Equations 96
5.4 Hysteretic Sheathing Connector Element Derivation 102
5.4.1 Connection Hysteresis Force 102
5.4.2 Energy Formulation of Stiffness Matrix 105
5.4.3 Error Checking 105
5.5 Energy Calculations 107
5.5.1 Energy Balance 110
5.6 Summary of Time-Step Solution Process 112
5.7 Summary 113

6 Connection Tests 115
6.1 Introduction . . . 115
6.2 Experimental Overview . . . 116
6.2.1 Objectives . . . 116
6.3 Testing Equipment . . . 117
6.4 Test Material . . . 119
6.4.1 Framing . . . 119
6.4.2 Sheathing . . . 123
6.4.3 Nails . . . 123
6.4.4 Screws . . . 123
6.4.5 Steel Angles . . . 124
6.5 Specimen Description . . . 124
6.5.1 Sheathing Connection Test Specimen . . . 124
6.5.2 Corner Connection Test Specimen . . . 126
6.6 Test Procedure . . . 128
6.6.1 Sheathing Connection Tests . . . 128
6.6.2 Static One–Directional Tests . . . 128
6.6.3 Static Cyclic Tests . . . 130
6.6.4 "Dynamic" Cyclic Tests . . . 131
6.6.5 Corner Connection Tests . . . 132
6.7 Results and Discussion . . . 133
6.7.1 Sheathing Connection Tests . . . 134
6.7.1.1 Static One–Directional . . . 134
6.7.1.2 Static Cyclic . . . 141
6.7.1.3 "Dynamic" Cyclic . . . 152
6.7.1.4 Overall Comparison . . . 161

6.7.2 Corner Connection Tests 164
6.8 Summary 165

7 Full-Size Shear Wall Test Descriptions and Procedures 167
7.1 Introduction 167
7.2 Test Equipment 168
7.2.1 Earthquake Table 168
7.2.2 Steel Four-Hinged Frame 168
7.2.3 Reaction Column 171
7.3 Data Acquisition 173
7.4 Test Specimen Materials 174
7.4.1 General 174
7.4.2 Steel Hold-Down Connections 174
7.5 Wall Specimen Configuration 175
7.6 Test Procedures 176
7.6.1 Static One-Directional Tests 176
7.6.2 Static Cyclic Tests 181
7.6.3 Free Vibration Tests 184
7.6.4 Sine Wave, Frequency Sweep Tests 185
7.6.5 Earthquake Tests 188
7.6.5.1 Background 188
7.6.6 Procedure 190
7.7 Data Analysis Procedures 192
7.7.1 Static Tests 192
7.7.2 Digital Filtering Method 196
7.7.3 Free Vibration Tests 198

7.7.4 Sine Wave Tests 198
7.7.5 Earthquake Tests 200
7.8 Summary 203

8 Full–Size Shear Wall Test Results **204**
8.1 Introduction 204
8.2 Static One–Directional Tests 206
8.3 Static Cyclic Tests 211
8.4 Free–Vibration Tests 217
8.5 Sinewave Frequency Sweep Tests 220
8.6 Earthquake Tests 220
8.7 General Discussion of Results 237
8.8 Summary 240

9 Verification of Mathematical Models **242**
9.1 Introduction 242
9.2 Static One-Directional Model 243
9.2.1 Plate Element Accuracy 243
9.2.2 Comparison to Test Results. 244
9.3 Closed Form Steady State Model 248
9.4 Dynamic Shear Wall Model 253
9.4.1 Comparison with Static Model 253
9.4.2 Time–Step Integration Accuracy Check 254
9.4.3 Hysteretic Sheathing Connector 255
9.4.4 Comparison with Test Results 256
9.5 Proposed Simplifications and Improvements to Models. 261
9.6 Summary 262

10 Design and Construction of Timber Shear Walls **264**

10.1 Introduction 264

10.2 Present Design Procedures 265

10.2.1 Overview of Codes 265

10.2.2 Comparison of Codes to Model Predictions and Test Results . . . 273

10.2.2.1 Seismic Loads 274

10.2.2.2 Deflections 279

10.3 Other Investigations 281

10.3.1 Effects of Using Adhesives 281

10.3.2 Effects of Aspect Ratio 283

10.4 Construction Details 287

10.4.1 Hold-Down Connection 287

10.4.2 Corner Connection 289

10.4.3 Sheathing Connectors 290

10.5 Summary 291

11 Conclusion **294**

11.1 Summary and Conclusions 294

11.2 Future Research 299

Bibliography **302**

List of Tables

4.1 Values of b_0 and b_1 for Each Iteration During the Solution of Numerical Example. 89

6.1 Types of Connection Tests Performed and Number of Specimens. 118

6.2 Sheathing Connection Test Displacements and Cycle Periods. 131

6.3 Load–Deflection Parameters Obtained From The Static One–Directional Sheathing Connection Tests Using Waferboard Sheathing. 138

6.4 Load–Deflection Parameters Obtained From The Static One–Directional Sheathing Connection Tests For Plywood Sheathing. 139

6.5 Load–Deflection Parameters Obtained From the Static Cyclic Sheathing Connection Tests. 144

6.6 Load–Deflection Parameters Obtained From The Static Cyclic Sheathing Connection Tests (Continued). 145

6.7 Load–Deflection Parameters Obtained From The Static Cyclic Sheathing Connection Tests (Continued). 146

6.8 Load–Deflection Parameters Obtained From The Static Cyclic Sheathing Connection Tests (Continued). 147

6.9 Load–Deflection Parameters Obtained From The Static Cyclic Sheathing Connection Tests (Continued). 148

6.10 Load–Deflection Parameters Obtained From The Static Cyclic Sheathing Connection Tests (Continued). 149

6.11 Load–Deflection Parameters Obtained From The Static Cyclic Sheathing Connection Tests (Continued). 150
6.12 Load–Deflection Parameters Obtained From The Static Cyclic Sheathing Connection Tests (Continued). 151
6.13 Load–Deflection Parameters Obtained From The Dynamic Cyclic Sheathing Connection Tests. 153
6.14 Load–Deflection Parameters Obtained From The Dynamic Cyclic Sheathing Connection Tests (Continued). 154
6.15 Load–Deflection Parameters Obtained From The Dynamic Cyclic Sheathing Connection Tests (Continued). 155
6.16 Load–Deflection Parameters Obtained From The Dynamic Cyclic Sheathing Connection Tests (Continued). 156
6.17 Load–Deflection Parameters Obtained From The Dynamic Cyclic Sheathing Connection Tests (Continued). 157
6.18 Load–Deflection Parameters Obtained From The Dynamic Cyclic Sheathing Connection Tests (Continued). 158
6.19 Load–Deflection Parameters Obtained From The Dynamic Cyclic Sheathing Connection Tests (Continued). 159
6.20 Load–Deflection Parameters Obtained From The Dynamic Cyclic Sheathing Connection Tests (Continued). 160
6.21 Overall Average Load–Deflection Parameters Obtained From The Sheathing Connection Tests for Waferboard Sheathing. 162
6.22 Overall Average Load–Deflection Parameters Obtained From The Sheathing Connection Tests for Plywood Sheathing. 163

7.1 Frequency and Corresponding Base Accelerations for Sine Wave Tests. . . 185

8.1 Overview of Full Size Shear Wall Tests. 205
8.2 Peak Load and Corresponding Deflection for Static One–Directional Shear Wall Tests. 208
8.3 Out–of–Plane Displacements of Sheathing, Mid–height and Midway Between Studs. 210
8.4 Exponential Curve Parameters Fit to Static One–Directional Test Data. . 211
8.5 Exponential Curve Parameters, Fit to Static Cyclic Test Data 213
8.6 Peak Loads for Each Cycle of Static Cyclic Tests (SI Units) 215
8.7 Peak Loads for Each Cycle of Static Cyclic Tests (Imperial Units). 216
8.8 Initial and Final Fundamental Frequencies for Shear Walls 218
8.9 Peak Values of Measured Displacements. 221
8.10 Peak Values of Measured Displacements. 222
8.11 Peak Acceleration at Top of Frame and Force at Top of Wall. 225
8.12 Peak Acceleration at Top of Frame and Force at Top of Wall. 226
8.13 Peak Displacement of Top of Wall Relative to the Base (SI). 227
8.14 Peak Displacement of Top of Wall Relative to the Base (Imperial). 228
8.15 Peak Displacement of Top of Wall Relative to the Base (SI). 229
8.16 Peak Displacement of Top of Wall Relative to the Base (Imperial). 230

9.1 Comparison of Predicted Versus Test Ultimate Load Capacity 247
9.2 Steady State Response of Shear Walls 249
9.3 Results of Accuracy Verification for **DYNWALL** 260

10.1 Comparison of Design Loads and Deflections with Test Results. 275

List of Figures

3.1 Framing Beam Element. 27

3.2 Corner Connector Load–Deflection Curve. 31

3.3 Sheathing Plate Element. 32

3.4 Loaded Shear Wall Configuration. 33

3.5 Representation of Deflections in Plate Element. 34

3.6 Sheathing Plate Element. 38

3.7 Exploded View of Shear Wall Model. 54

3.8 Sheathing Connector Element Geometry. 55

3.9 Load–Displacement Curves for Non–Linear Spring Connector Between Beams and Plate Elements 60

3.10 Sheathing Bearing Connector Element Configuration 64

3.11 Sheathing Bearing Connector Load–Deflection Curve. 66

4.1 Bi–Linear Hysteresis for a Theoretical Structure. 73

4.2 Equivalent Oscillator used to Represent Timber Shear Walls. 74

4.3 Typical Hysteresis Loop for Timber Shear Walls. 76

4.4 Idealization of Hysteresis Loop for Timber Shear Walls. 77

4.5 Frequency Response Function Curves for Timber Shear Walls. 85

4.6 The Left and Right Hand Sides of Equation 5.34. 86

4.7 The Idealized Hysteresis Loop When $R_0 \rightarrow \infty$. 90

5.1 Assumed Hysteresis Loop For Sheathing Connector Element. 96

5.2 Freebody Diagram of a General Object in Dynamic Equilibrium. 97
5.3 Typical Cyclic Load–Deflection Curve For a Timber Shear Wall. 103
5.4 Error Checking Parameters for Sheathing Connector. 107

6.1 Racking Versus Rigid Body Rotation Deflection. 119
6.2 Test Frame With Hydraulic Jack. 120
6.3 MTS Controller Used To Control The Hydraulic Jack. 121
6.4 Data Acquisition Equipment. 122
6.5 Corner Connection Test Specimen Configuration. 124
6.6 Sheathing Connector Load–Deflection Curve Parameters. 125
6.7 Sheathing Connection Test Specimen Configurations. 127
6.8 Typical Connection Test Displacement Patterns. 129
6.9 Locations of DC–DT's for Sheathing Connection Test Specimens. 130
6.10 Detail of Corner Connection. 132
6.11 Typical Load–Deflection Curve Obtained From The Static One–Directional Connection Test. 135
6.12 Typical Failure of Sheathing Connection Test Specimen. 136
6.13 Typical Failure of Sheathing Connection Test Specimen. 137
6.14 Average Load–Deflection Curves Using Exponential Curve Parameters. . 140
6.15 Nails After Connection Test Specimen Has Failed. 141
6.16 Typical Load–Deflection Curve Obtained From The Static Cyclic Sheathing Connection Test. 142
6.17 Typical Load–Deflection Curve Obtained From The Corner Connection Test. 165

7.1 Test Frame being Raised into Vertical Position. 169
7.2 Test Frame with Wall Specimen in Place for Testing. 170

7.3 Wall Specimen with Dead Load Applied. 171
7.4 Reaction Column with Arm Including Load Cell Attached to Testing Frame. 172
7.5 Hold-Down Connection Configuration. 175
7.6 Typical Configuration of Framing, Sheathing, and Connections Used in Full-Size Shear Wall Tests. 177
7.7 Displacement Patterns Used in Static Shear Wall Tests. 178
7.8 Location of Variables Measured During Static One-Directional Tests. . . 180
7.9 Steps Used to Correct the Load-Deflection Curves for the Static Tests. . 182
7.10 Location of Variables Measured During Static Cyclic Tests. 183
7.11 Location of Variables Measured During Sinewave, Frequency Sweep Tests. 187
7.12 Location of Variables Measured During Earthquake Tests. 193
7.13 Typical Load Versus Racking Deflection Curve for a Static One-Directional Test. 194
7.14 Typical Out-of-Plane Deflection Versus Racking Deflection Curve for a Static One-Directional Test. 195
7.15 Digital Filtering Procedure. 197
7.16 Comparison of a Filtered and Unfiltered Displacement Record. 199
7.17 Typical Acceleration Record for a Free Vibration Test of an Undamaged Shear Wall. 200
7.18 A Typical Racking Displacement Curve for a Sine Wave Test. 201
7.19 Free-Body Diagram of Testing Frame Column. 202

8.1 Load-Deflection Curves Obtained From The Static One-Directional Shear Wall Tests. 206
8.2 Typical Load-Deflection Curves Obtained From The Static Cyclic Shear Wall Tests. 212

8.3 Deformation Patterns for Racking Displacement of Typical Shear Wall. . 217
8.4 Typical Acceleration Records for the Base and Top of Wall. 234
8.5 Fourier Spectra for Acceleration Records Shown in Figure 8.4. 235
8.6 Plot of Amplification Factors versus Frequency. 236
8.7 Plot of Amplified Frequencies versus Time. 236

9.1 Finite Element Mesh used to Model a Fixed–Fixed Plate. 244
9.2 Comparison of Predicted Center Deflection of Plate with Distributed Load. 245
9.3 Comparison of Model's Predicted Load-Deflection Curves with Test Results. 246
9.4 Comparison of Steady State Model's Prediction and Test Results for Plywood Sheathed Walls. 250
9.5 Comparison of Steady State Model's Prediction and Test Results for Waferboard Sheathed Walls. 251
9.6 Comparison of the Predicted Steady State Responses for Plywood and Waferboard Sheathed Walls. 252
9.7 Three Member Frame Used to Check Time–Step Integration. 255
9.8 Hysteresis Loops for Connector in Shear Wall. 256
9.9 Test versus Predicted Frequencies in the Displacement Records. 258
9.10 Time–Histories for Test and Model. 259

10.1 Illustration of Ductility Concept. 266
10.2 Load and Strength Distributions. 269
10.3 Load–Deflection Curves for Design Code and Shear Wall. 272
10.4 Correct Load–Deflection Curves for Design Code. 273
10.5 Displacement Records for 4.8 m (16 ft) High Wall. 284
10.6 Bending versus Shear Deflection. 285
10.7 Displacement Records for Standard and Long Walls. 286

10.8 Hold–Down Connection Configuration. 288
10.9 Corner Connection Configuration. 289

Notation

Variables:

$\{a\}$ = Vector of nodal degrees–of–freedom or displacements.

a = The ratio of the load intercept to the peak load of the hysteresis, $\frac{P_1}{R_0}$.

a_g = The amplitude of the base or ground accelerations.

A = The cross–sectional area.

$\{\delta a\}$ = The vector of virtual displacements.

b = The constant amplitude ratio for Newton–Raphson solution.

$[B]$ = The strain–displacement matrix.

$C(R_0)$ = A function defined in Equation 4.25.

C_1 = A constant.

C_2 = A constant.

C_3 = A constant.

$[C]$ = The damping matrix.

$\{d\}$ = The vector containing the displacements of a general point within an element.

$\{d^*\}$ = A vector of displacements for a sheathing connector, oriented parallel and perpendicular to the axis of the beam element.

$[D]$ = Material properties matrix.

$[D_t]$ = The sheathing thickness times the material properties matrix, $t\,[D]$.

$[D_I]$ = The moment of inertia for a unit width of sheathing times the material properties matrix, $I\,[D]$.

$\mathcal{D}(t)$ = The energy dissipated by viscous damping at time t.

E = Modulus of elasticity.

E_i = Modulus of elasticity for an individual layer of plywood in the direction of interest.

$\mathbf{f_D(t)}$ = The non-linear force due to damping.

$\mathbf{f_I(t)}$ = The inertial resistance force.

$\mathbf{f_s(t)}$ = The non-linear structural resistance force.

$\mathbf{F}$ = A force.

F = A coefficient to account for soil variability in seismic design.

$\mathbf{F_1}$ = The force corresponding to the displacement, u_1.

$\mathbf{F_2}$ = The force corresponding to the displacement, u_2.

$\mathbf{F(x, \mu, t)}$ = The hysteresis force for a wall.

$\mathcal{F}$ = a factor to convert from the nominal yield load to the actual yield load.

$\mathbf{G_i}$ = Shear Modulus for an individual layer of plywood.

$\mathbf{G_{xy}}$ = Shear modulus in the X-Y plane.

$\mathbf{I}$ = The moment of Inertia.

I = The importance coefficient for seismic design.

$\mathbf{i}$ = Node variable.

$\{\mathbf{I}\}$ = The influence vector (identifies which degrees–of–freedom are effected by the dynamic loading).

$\mathcal{I}(t)$ = The energy input to the structure due to an earthquake at time (t).

$\mathbf{J_i(s)}$ = A shape function for a beam element.

$[\mathbf{J}]_\mathbf{b}$ = The matrix containing the Shape functions for a beam element.

$\mathbf{j}$ = Node variable.

$[\mathbf{k}]$ = The stiffness matrix for an individual finite element.

$\mathbf{K}$ = The individual connector stiffness.

K = A coefficient that accounts for structural ductility and damping.

$[\mathbf{K}]$ = The global stiffness matrix.

$\mathbf{K_0}$ = A parameter that defines the exponential equation of the initial loading curve for a nail connection or wall (the initial stiffness).

$\mathbf{K_2}$ = A parameter that defines the exponential equation of the initial loading curve for a nail connection or wall (the slope of the asymptotic line of the exponential curve.

$\mathbf{K_3}$ = A parameter that defines the slope of the linear decreasing section of the load–deflection curve of a nail connection or wall.

$\mathbf{K_4}$ = A parameter that defines slope of the hysteresis curves at 0 deflection (at the load intercept) for a nail connection or wall.

$\frac{\mathbf{K_0 R_0^*}}{\mathbf{P_0}}$ = The resonant amplitude ratio, which is a non-dimensional amplitude of the steady state oscillation at the resonant frequency.

$\left[\tilde{\mathbf{K}}(\mathbf{t})\right]$ = The apparent stiffness at time, t.

$\mathcal{K}(t)$ = the kinetic energy at time t.

l = The length of a beam element.

$[\mathbf{L}]_{\mathrm{sc}}$ = A matrix of the shape functions for the sheathing bearing connector.

$[\mathbf{L}(\xi, \eta)]$ = Shape function vector for the u–deflection fields.

$\mathcal{L}$ = A factor for converting the 5th percentile strength to the average strength.

m = The inertial mass.

[M] = The mass matrix.

$[\mathbf{M}(\xi, \eta)]$ = Shape function vector for the v–deflection fields.

$[\mathbf{N}(\xi, \eta)]$ = Shape function vector for the w–deflection fields.

$\{\mathbf{P}\}$ = The vector of applied loads.

$\mathbf{P_0}$ = A parameter that defines the exponential equation of the initial loading curve for a nail connection or wall (the load intercept for the asymptotic line of the exponential curve).

$\mathbf{P_1}$ = A parameter that defines the load intercept of the hysteresis curve for a nail connection or wall.

$\{\mathbf{P_{DL}}\}$ = A vector of general nodal dead load forces.

$\mathbf{P_{ELASTIC}}$ = The lateral load requirement for elastic structures.

$\mathbf{P_H}$ = The horizontal load at the top of the frame column.

$\mathbf{P_{TOP\ OF\ WALL}}$ = The load at the top of the wall.

$\mathbf{P_{YIELD}}$ = The lateral load at which a structure yields.

$\mathbf{P_{WALL}}$ = The actual lateral load experienced by a shear wall during an earthquake.

$\mathbf{P(t)}$ = The general dynamic loading.

$\left\{\tilde{\mathbf{P}}(\mathbf{t})\right\}$ = The apparent loading at time, t.

$\mathcal{P}$ = The amplitude of the sinusoidal forcing function on the equivalent oscillator.

$\{\mathbf{q}\}$ = A vector of distributed loads.

$\mathbf{R}$ = The amplitude of harmonic motion.

$\mathbf{R_0}$ = The steady-state amplitude of harmonic motion.

$\mathbf{R_0^*}$ = The resonant amplitude of harmonic motion.

$\overline{\mathbf{R}}$ = The average value of R for one cycle of harmonic motion.

$\mathcal{R}$ = The ratio of the desired damping to the critical damping for the fundemental frequency

s = The normalized local coordinate along the length of a beam element.

$\mathbf{S}$ = The surface area.

S = The seismic response factor.

$\mathbf{S(R_0)}$ = A function defined in Equation 4.26.

$[S]$ = The matrix of shape functions for a plate element.

t = Thickness of the sheathing in Chapter 3 and time everywhere else.

t_i = Thickness of an individual layer of plywood.

T = Surface traction forces.

$[T]$ = A transformation matrix for direction.

u = The displacement of a point in the X–direction.

u_1 = The largest positive displacement of a connector so far.

u_2 = The largest negative displacement of a connector so far.

u' = Displacement of a point in the X–direction.

$\{u(t)\}$ = A vector of general nodal displacements.

$\{\dot{u}(t)\}$ = A vector of general nodal velocities.

$\{\ddot{u}(t)\}$ = A vector of general nodal accelerations.

$\Delta\overline{u}$ = The relative displacement in the X–direction.

$\overline{u}_b$ = The displacement of a general point within a beam element in the X–direction.

$\mathcal{U}(t)$ = The strain energy plus energy dissipated by hysteretic damping at time t.

$\frac{\partial u}{\partial x}$ = The first partial derivative of u with respect to x or the change in the u displacement in the X–direction.

$\frac{\partial u}{\partial y}$ = The first partial derivative of u with respect to y or the change in the u displacement in the Y–direction.

$\frac{\partial^2 u}{\partial x \partial y}$ = Second partial derivative of the u displacement; first, with respect to x then with respect to y.

Δu_{max} = the deflection at peak load for a nail connection or wall.

v = the velocity ratio that represents the magnitude of the peak acceleration of the design earthquake.

$\mathbf{v}$ = Nodal displacement of a point in the Y–direction.

$\mathbf{v}'$ = Displacement of a point in the Y–direction.

$\mathbf{\Delta\overline{v}}$ = The relative displacement in the Y–direction.

$\mathbf{\overline{v}_b}$ = The displacement of a general point within a beam element in the Y–direction.

V = The lateral seismic force at the base of the structure.

$\mathbf{V}$ = Volume.

$\frac{\partial \mathrm{v}}{\partial \mathrm{x}}$ = The first partial derivative of v with respect to x or the change in the v displacement in the X–direction.

$\frac{\partial \mathrm{v}}{\partial \mathrm{y}}$ = The first partial derivative of v with respect to y or the change in the v displacement in the Y–direction.

$\frac{\partial^2 \mathrm{v}}{\partial \mathrm{x}\partial \mathrm{y}}$ = Second partial derivative of the v displacement; first, with respect to x then with respect to y.

$\mathbf{w}$ = Nodal displacement of a point in the Z–direction.

$\mathbf{w}'$ = Displacement of a point in the Z–direction.

$\mathbf{w}(\xi, \eta)$ = w deflection at the point (μ, η) inside an element.

$\frac{\partial \mathrm{w}}{\partial \mathrm{x}}$ = The first partial derivative of w with respect to x or the change in the w displacement in the X–direction.

$\frac{\partial \mathrm{w}}{\partial \mathrm{y}}$ = The first partial derivative of w with respect to y or the change in the w displacement in the Y–direction.

$\frac{\partial^2 \mathrm{w}}{\partial \mathrm{x}\partial \mathrm{y}}$ = Second partial derivative of the w displacement; first, with respect to x then with respect to y.

$\frac{\partial^2 w}{\partial x^2}$ = Second partial derivative of the w displacement with respect to x.

$\frac{\partial^2 w}{\partial y^2}$ = Second partial derivative of the w displacement with respect to y.

W = Body forces or weight of the structure.

x = The x–coordinate of a point.

$x(t)$ = The displacement of the top of the wall relative to the base.

$\dot{x}(t)$ = Velocity.

$\ddot{x}(t)$ = Acceleration.

Δx = Length of finite element in the X–direction.

X_s = The magnitude of the harmonic forcing function.

y = The y–coordinate of a point.

Y = The average yield resistance.

Δy = Length of finite element in the Y–directions.

z = The coordinate of a point or a distance measured along the Z–axis.

sig = The sign of a variable or function of variables.

α = The angle between the global coordinate system and the local coordinate system for a beam element.

β = Newmark–β constant.

γ = Newmark–β constant.

Δ = The change in a variable (used with a second variable such as u).

$\Delta_{E/Q}$ = The lateral deflection achieved during an earthquake.

Δ_{YIELD} = The lateral deflection at which a structure yields.

ϵ = A component of strain.

$\{\epsilon\}$ = Strain vector.

ϵ_{xy} = The shear strain in the X-Y plane.

ζ = Normalized local coordinated in the Z–direction for the plate element.

η = Normalized local coordinated in the Y–direction for the plate element.

θ = Variable defined in Equation 4.7.

θ_b = The counterclockwise rotation of a beam element node.

κ = The nondimensional ratio of the base excitation frequency to the resonant frequency of the structure, $\frac{\omega_g}{\omega_0}$. The variable is referred to as the frequency ratio.

ρ = density.

ϱ = A factor that is used to convert the characteristic strength to the average strength.

μ = The slope defined in Equation 4.2 and show in Figure 4.4.

ν = Poisson ratio.

ν_i = Same as ν, only for an individual layer of plywood.

ν_{xy} = Poisson ratio giving strain in the X-direction for a stress in the Y-direction.

ν_{yx} = Poisson ratio giving strain in the Y-direction for a stress in the X-direction.

ξ = Normalized Local coordinated in the X–direction for the plate element.

$\mathbf{\Pi}$ = The potential energy.

$\delta\mathbf{\Pi}$ = The first variation of the potential energy.

σ = Normal stress in the direction of interest.

σ_{xy} = Shear stress in the X–Y plane.

$\{\sigma\}$ = Stress vector.

τ = A time variable.

λ = The load factor for limit states design.

$\phi(\tau)$ = The phase of harmonic motion.

ϕ_0 = The steady-state phase of harmonic motion.

$\overline{\phi}$ = The average value of $\phi(\tau)$ for one cycle of harmonic motion.

ϕ = The capacity reduction factor for limit states design.

$\psi(\ )$ = Function for Equilibrium found by minimizing the potential energy.

ω = The frequency of the harmonic motion.

ω_1 = The fundamental frequency of the structure.

Superscripts:

$\mathbf{T}$ = Transpose of matrix or array.

$'$ = The first derivative of the variable if it has not been defined as part of the variable in the list above.

Subscripts:

$\mathbf{b}$ = Variable pertaining to beam elements.

$\mathbf{c}$ = Center of the plate element.

$\mathbf{C}$ = Compression.

$\mathbf{con}$ = Variable pertaining to a connector.

$\mathbf{g}$ = Variable pertaining to the base of wall
(or ground accelerations for earthquakes).

$\mathbf{P}$ = Variable pertaining to point P.

$\mathbf{P'}$ = Variable pertaining to point P'.

$\mathbf{Pl}$ = Variable pertaining to plate elements.

$\mathbf{s}$ = Variable pertaining to the secant stiffness.

$\mathbf{sc}$ = Variable pertaining to the sheathing bearing connector.

$\mathbf{t}$ = Variable pertaining to the tangent stiffness.

$\mathbf{T}$ = Tension.

$\mathbf{u}$ = Variable pertaining to the u–direction.

$\mathbf{v}$ = Variable pertaining to the v–direction.

$\mathbf{w}$ = Variable pertaining to the w–direction.

$\mathbf{x}$ = Variable pertaining to the X–direction.

$\mathbf{y}$ = Variable pertaining to the Y–direction.

$\mathbf{z}$ = Variable pertaining to the Z–direction.

$\mathbf{0}$ = Initial conditions.

∞ = Variable pertaining to infinity.

Acknowledgements

There have been so many people who have assisted me during the various tasks associated with the completion of this thesis, that I cannot hope to mention all of them here. I hope that no one will be offended if I neglect to acknowledge their help individually. It was very much appreciated, and I would not have been able to accomplish as much without their assistance.

I would like to first thank Professor Borg Madsen, the Chairman of my Advisory Committee, for the financial and technical advice he has given me over the years, as well as his personal advise and assistance during some difficult times.

Dr. R.O. Foschi is thanked for the many discussions and problem solving sessions that were so helpful while developing the finite element models.

The complement of my Advisory Committee, Dr. J.D. Barrett, Dr. S. Cherry, and Dr. S.F. Stiemer, are thanked for the advise and review of my manuscript.

For his help during not only the experimental work, but for the many discussions of the theoretical work, I thank Dr. André Filiatrault.

Dr. M.D. Olson is thanked for his help on numerous occasions in solving problems, in debugging the finite element programs.

The experimental section of this thesis would not have been possible without the assistance of the Laboratory technicians. Special thanks are extended to Dick Postgate, Bernie Merkli, Guy Kirsch, Rod Nussbaumer, Scott Jackson, and Max Nazar for their help with machining, welding, and electronics.

Jim Greig, Felix Yao, Gerard Canissius, Bryan Folz, and Damika Wickremesinghe are among the many research engineers and graduate students who helped with various

discussions, and in making computer equipment available to me.

The Waferboard Association, Council of Forest Industries of B.C., and Forintek Canada Corporation are thanked for their support with finances, equipment, and materials.

Finally, but certainly not least, I would like to thank my family and my wife, Desirée. My family is thanked for their financial and emotional support throughout my graduate career. Desirée is given special thanks, not only for the many hours of typing, editing and working on various experiments with me, but also for the patience and love she has shown me over the past four years.

Dedication

To my parents, Tom and Marie Dolan, who taught me that accomplishing anything worthwhile requires determination and perseverance.

Chapter 1

Introduction

1.1 Background

Houses, small office buildings, and light industrial buildings in North America have traditionally been constructed of timber. History has shown that common light frame construction used for these structures performs well when subjected to earthquakes. Two of the reasons timber structures have been successful in resisting earthquake loads are: **1)** the structures have been relatively light in mass, and **2)** the structural systems have had a large number of redundancies.

Shear walls are commonly used in low–rise timber buildings, to provide lateral support against wind and earthquake loads. Timber buildings usually have shear walls consisting of a light timber frame, clad with a panel product, such as plywood, waferboard, or oriented strand board. The sheathing is usually attached with nails that are spaced sufficiently close to provide the necessary stiffness and strength to resist the expected in–plane lateral loads. Most of these walls are not designed, but rather are constructed according to specifications that ensure a minimum strength and stiffness. Shear walls that are designed are checked by engineers or architects to ensure all the connections and components, as well as complete wall, will meet strength and serviceability requirements. These structural elements are used in many different types of timber buildings, such as single family houses, manufactured houses, and one to four storey buildings. While the

present and traditional methods of construction are similar, there are a few significant changes that have occurred recently that make a more accurate prediction of the behavior of timber buildings during earthquakes desirable. The multi–family structures being built today are larger than their predecessors from fifty years ago. In addition, concrete overlayments on floors, concrete tile on roofs, and other new, heavier materials are being used in the upper stories for fire protection, sound control, aesthetics, and reduced cost.

Other changes to the framing methods have also been made in order to utilize the construction materials more efficiently and reduce the cost of construction. Some of these changes include:

- increasing the spacing between wall studs,
- using staples or adhesives, rather than nails,
- and changing the type of sheathing panel used from plywood to new reconstituted panel products, such as waferboard and oriented strand board.

These are a few of the changes to how buildings are framed. The result of increasing the stud spacing is a reduced number of redundancies. The other two changes introduce new unknown variables to the building.

As the timber resources continue to be restricted by society, and as new innovative ideas are implemented to reduce construction costs or increase the energy efficiencies of buildings, more changes will be made to the construction techniques used in modern timber buildings. Due to these changes, the past experience can no longer prove the reliability of timber structures in the future. As demand for more efficient use of the timber in building construction increases, engineers will be called upon more and more to design buildings, using engineering knowledge and principles, rather than historical precedence. This will require that engineers have the design tools available to accurately

predict the behavior of the new buildings' structural elements when loaded by various environmental disasters, such as hurricanes and earthquakes. This thesis provides information and understanding of engineered timber shear walls used in apartment buildings and condominiums. The remainder of the discussion of shear walls will pertain to such walls.

1.2 Objectives

The primary objective of this study is to develop a numerical model that is capable of predicting the deflection of the top of timber shear walls, relative to the base, when subjected to dynamic earthquake loadings. This model is a general finite element model capable of describing the behavior of timber walls of various configurations and construction. Being general implies that shear walls constructed, using a variety of framing and sheathing materials, as well as walls with or without openings, can be modelled. While the program presented in this thesis is not meant for design work, future simplifications can be made to produce a model that will be easily used by engineers and architects as an aid in designing buildings. The model presented in this thesis is capable of representing the shear walls in sufficient detail to allow it to be used as a benchmark against which future simplified models can be compared to determine the amount of error introduced by simplifying assumptions. The data base information for the use of various fasteners in shear walls can be expanded more economically, using the finite element models presented in this thesis than by performing full size shear wall tests.

Other objectives of the study are:

- Develop a numerical model to accurately predict the static one-directional racking load–deflection curve and ultimate load capacity of timber shear walls (Chapter 3).

- Develop a mathematical model to predict the steady state response of timber shear walls (Chapter 4).
- Develop a dynamic test for timber shear walls that realistically represents the loading expected during an earthquake (Chapter 7).
- Investigate the effects of out–of–plane bending of sheathing, on the strength and stiffness of shear walls (Chapters 8 and 9).
- Compare the performance of plywood and waferboard sheathing to determine whether they should be given equal status as earthquake resisting materials (Chapters 8 and 9).
- Investigate the critical connections in shear walls (Chapters 6, 8, 9, and 10).
- Investigate the design procedure outlined by various design codes used in North America to see how walls designed by these codes actually perform (Chapter 10).
- Present an example of an analysis using the developed program (Chapter 10).

1.2.1 Methods for Achieving Objectives

The objectives dealing with modelling have been met by the three numerical models that the author has developed and are implemented in the following computer programs,

- **SHWALL** is the general finite element program that predicts static one–directional racking behavior of timber shear walls.
- **FREWALL** is the implementation of the closed–form mathematical model that predicts steady state response of timber shear walls.

- **DYNWALL** is the general finite element model that predicts the dynamic response of timber shear walls to random base accelerations, such as earthquakes.

All three models have been verified, using the results of an extensive testing program of full size shear walls, and are now available from the author upon request. However, as stated before, the intent of these models was not for use as design tools, but rather to be used to correctly investigate the detailed behavior of timber shear walls. The results of this thesis indicate several simplifications that can be made to reduce the computation time required for analysis and make the models more useful for design purposes. These simplifications will be made in the near future and the simplified versions of the models, along with user manuals, will be available to the public for general use.

The data required in order to use the numerical models are: **1)** the material properties of sheathing and framing, and **2)** the average load–deflection curve for the connectors used to attach the sheathing to the framing. The material properties for framing and sheathing can be found in the literature or obtained by either deriving the values using the principles of strength of materials, or testing suitable small specimens. The load–deflection curves for the connectors can be obtained by testing single connections, that are constructed in the same manner as the connections used in the full scale walls.

The remainder of the objectives were met by developing and conducting an extensive testing program of full size shear walls, and using the results to verify the dynamic model. The results of these tests and numerical simulations were analyzed in various ways to obtain answers for different objectives.

1.3 Design Codes

The current structural design codes for timber shear walls, used in Canada and the United States, are based on the results of static one–directional racking tests of full size

shear walls. For working stress design (WSD) codes, a factor of safety is used to ensure that the design stresses do not exceed the structural load capacity. The ultimate load capacity is divided by the factor of safety to obtain the reduced capacity used in design. For the current WSD codes, a factor of safety of 3.0 has been applied to either the ultimate load capacity (or corresponding deflection in the case of past numerical analysis work) to determine the allowable design capacity of timber shear walls. The allowable capacity is then presented to the designer as a table of design shear loads, dependent on the sheathing thickness, nail size, and nail spacing. The design capacity of the wall can be determined, knowing the unit load capacity from the design tables and the wall configuration.

Current design procedures have not been related to any dynamic test data, and as a result, it is unclear whether the resulting buildings are under– or over–designed. The fact that present design codes are not based on dynamic data could also cause the adjoining structural elements, such as floors, ceiling, foundations, and connections, to be under– or over–designed. The performance of timber buildings, designed to resist earthquakes, is therefore highly questionable. This study therefore investigates the accuracy of the current North American design codes by comparing the design shear for walls that were tested with shear values recorded during the dynamic tests. The effects of using adhesives are also investigated, since the design code has not addressed adhesives at all. A detailed investigation of the design codes is, however, beyond the scope of this study.

1.4 Applications

The results presented in this thesis provides knowledge of the dynamic behavior of timber shear walls. As such, the testing procedures used for the tests of full–size shear walls can be used as a performance tests for comparing different panel products and

methods of attaching the sheathing. Each of the tests give information about the wall's behavior in response to a particular type of loading.

The three computer models can also be used to predict the behavior of timber shear walls for static one–directional loading, harmonic loadings, such as equipment vibrations, and general random dynamic loadings, such as earthquakes. All the current North American design codes are based on tests that used essentially one type of nail, which was manufactured by one supplier. The finite element models can be used to expand the information base to nails manufactured by other suppliers or even to completely different types of connectors. After the load–deflection properties of the various sheathing connectors are determined, their use in walls can be investigated using the finite element models rather than by performing full size shear wall tests. This will allow the design codes to eventually provide the engineer with alternatives to the use of nails for attaching the sheathing in shear walls. The models provide a far less expensive method of investigating various topics pertaining to shear walls, than using full size tests. Finally, the models serve as benchmarks to which simplified models can be compared to verify their accuracy. This will eventually lead to design tools for engineers.

1.5 Thesis Organization

This thesis is organized such that the three numerical models are derived first. Subsequently, the physical tests performed are presented and finally, the accuracy of the models is determined.

Chapter 2 describes the various research that has previously been conducted. The topics include work on connections, testing of full size shear walls and buildings, modelling of shear walls, diaphragms and buildings.

Chapter 3 presents the derivation of the Static Finite Element Model, **SHWALL**.

This model is capable of describing the load–deflection behavior of timber shear walls of any configuration, and constructed of orthotropic or isotropic materials. Each element used in the model is derived separately. The method of combining the various elements, and solving a general problem is presented at the end of the chapter. This model is restricted to static one–directional loading in the plane of the wall.

In Chapter 4, a Closed Form Mathematical Model, **FREWALL**, used to predict the steady state behavior of timber shear walls, subjected to harmonic base excitations, is derived. A method for solving the equations is then presented, along with a numerical example.

Chapter 5 describes the Dynamic Finite Element Model, **DYNWALL**. The general step–by–step integration equations are first derived, followed by the required changes to the connector element used in the static model. The energy calculations used in the model are derived next and, finally, a summary of the time–step solution process is given.

Chapter 6 describes the test procedure and results from tests conducted to determine the load–deflection curves for the nail connections in shear walls. Load–deflection curves are used by the various models as data to determine load–deflection relationships for the connector elements.

Chapter 7 describes the full–size shear wall tests and procedures, along with the procedures followed in analyzing the data.

In Chapter 8, the results of the full–size shear wall tests are presented and discussed.

Chapter 9 details the verification of the accuracy for each of the numerical models. In addition to the usual patch tests and Eigenvalue tests, each of the models are compared to full size shear wall test results to see how accurately they predict the behavior of shear walls.

Chapter 10 discusses the design and construction of timber shear walls. Present design procedures are discussed and comparisons are made between design code requirements

and test results. It is shown that the current design codes underestimate the loads generated during earthquakes and a value for the resistance factor is recommended for inclusion in the proposed 1990 Canadian design code. Various construction details of timber shear walls are discussed at the end of the chapter. These details are considered critical for a shear wall to perform as a lateral supporting element in a timber building, and the discussion further draws attention to their importance.

1.6 Limitations of Study

The models described in this thesis are general and, therefore, capable of describing the load–deflection behavior of any timber shear wall. The models are limited only by the ability to describe the load–deflection curve of various connectors and materials used in the construction of timber shear walls. Nail connections using 8d or 63.5 mm (2.5 in) hot dipped galvanized common nails, Spruce–Pine–Fir (SPF) framing, and either plywood or waferboard sheathing are the main materials considered in this thesis. However, the use of adhesives and other connectors are discussed and modelled.

An extensive investigation of the various fasteners, sheathing materials, framing materials, and multiple earthquake and wind loadings was considered beyond the scope of this thesis. A detailed investigation of the various design codes was not considered part of this study. Also, no attempt at formulating a new design procedure, nor has a reliability investigation, been made.

Chapter 2

Literature Survey

2.1 Introduction

This chapter represents an overview of the research that have been performed on topics relevant to this thesis. The chapter is comprised of two sections. The first section includes testing of connections, full size shear walls, and full size buildings. The second section addresses modeling of shear walls and buildings. A general comment that can be made regarding research done in the past is that most of the research has been limited to the static behavior of connections and shear walls, with particular interest in determining the ultimate static, one–directional load capacities of connections and shear walls. Little research has addressed the cyclic or dynamic behavior of timber connections, shear walls or buildings.

An extensive bibliography on diaphragms was written by Carney (1975) and later updated by Peterson (1983). These bibliographies cover most of the pertinent published work on diaphragms and shear walls from 1927–82.

2.2 Testing

2.2.1 Connections

Many of the early investigations of timber shear walls concentrated on determining the effects of nailed connections on the performance of shear walls. This trend continued into the 1960's and 1970's with studies like those by Westman and McAdoo (1969), Wilkinson and Laatsch (1970), and Senft and Suddarth (1971). The initial stiffness or ultimate load capacity of various fasteners subjected to static one–direction withdrawal or shear was studied. Non–linear effects between the initial elastic loads and the ultimate loads were neglected in the early research. For instance, Westman and McAdoo (1969), determined the withdrawal resistance of nails in Douglas–Fir and Western Hemlock with the grain orientation considered as the one variable, while Senft and Suddarth (1971) considered the differences between plain and galvanized nails along with moisture content on the withdrawal resistance. Perkins (1971) continued to study single connectors by testing specimens to determine the ultimate load capacities for the withdrawal of nails in Red Pine, and Carsol (1970, 1972), and Eckelman (1975) reported on the withdrawal of screws.

Around 1975, the objective for connection tests shifted from determining the fastener performance in the framing material to investigating complete connections of framing and sheathing. Walford (1976) tested nail joints in order to determine the allowable loads for use in the design of diaphragms. Also, Hilton, et. al. (1976) found that nail spacing does not affect the stiffness of the connection, only the load capacity. Polensek (1976) studied the nail connection properties for future use in design of wood–stud walls subjected to static one–directional loading. Sturn (ATC-7-1, 1980) investigated multiple types of fasteners, but again reported static one–directional ultimate load capacities.

The effects of dynamic cyclic loading of nailed joints was studied by Soltis and

Mtenga (1985). They found no significant difference in the load capacity of the particular joint they tested, when loaded statically or dynamically.

Dowrick (1986) classified various types of timber connections based on the hysteresis loop shape.

Polensek and Bostendorff (1987), and Chou and Polensek (1987) researched the damping and stiffness of nailed joints, and found damping ratios between 10% and 40% for plywood sheathing connections. These damping ratios, along with joint stiffness, were significantly reduced when connections were constructed green and then allowed to dry before testing.

Polensek and Schimel (1986) investigated the effects of sheathing nails on the uplift of the end studs in shear walls. They found that adding extra nails in the sheathing corners of the walls increased the stiffness of the wall and reduced the uplift.

Turnbull and Lefkovitch (1986) found that steel gusset plates increased both the stiffness and strength of nailed joints compared to plywood gusset plates. They also found that 5–ply plywood gusset joints were stronger than 4–ply gusset joints.

An experimental study of joints using nails and screws in combination with adhesives by Van Wyk (1986) showed that the nails and screws contributed very little to the strength and stiffness of the joints. A study by Cunningham (1988) showed similar results. Hoyle (1988) proposed a design method for nailed–glued joints for use in diaphragms. Hoyle also pointed out the problem of guaranteeing the required glue line thickness during construction.

Foschi (1982) reported on the load–slip curve of nailed waferboard and Douglas–Fir connections. An exponential equation was fit to the load–deflection curve for use in modeling full size shear walls.

Tests of plywood and solid wood nailed joints, by Lhuede (1988), showed that load capacities of the joints were higher than joints between two solid pieces of wood. The

nails were cut to ensure equal penetration, and were obtained for both plywood and solid wood specimens. The effect of varying the sheathing thickness to nail diameter was also investigated.

Salinas and Massé (1988) investigated the reliability of nailed connections of plywood splices of truss cords. They found that structures, designed by either the limit states design or working stress design formats, had acceptable reliability indexes.

2.2.2 Full Size Shear Walls

Until the mid-1940's, timber buildings used so-called "let–in" corner bracing or diagonal lumber sheathing to provide the lateral resistance to wind and earthquake loads. Panel sheathing began to be used for shear walls in the late 1940's.

The standard procedure for testing shear wall panels that is followed in North America is the American Society of Testing Materials E72–77 (1981). The E72–77 standard is the test procedure which was used to determine the racking resistance of shear walls for use in the various building codes in North America.

The ASTM E72–77 test was used by Tissel (revised, 1977) to evaluate the relative effectiveness of plywood sheathed shear walls and let–in diagonal corner bracing. The test results for 2.4×2.4 m (8×8 ft) shear walls showed that walls partially sheathed with plywood have an ultimate load capacity as high as let–in corner braced walls. These tests along with those reported by Tissel and Eliott (revised, 1986) for diaphragms and Adams (revised, 1987) for shear walls were used as the basis for the allowable shear capacities in the United States building codes.

The International Council of Building Officials (ICBO) used experimental and analytical results as a basis for allowing waferboard to be considered as an equivalent to

plywood in shear walls and diaphragms. The experimental results used were for diaphragm tests conducted by Atherton (1982, 1983), and shear wall tests conducted by TECO (1980, 1981). The analytical results were provided by Foschi (1982).

Källsner (1984) tested shear wall panels with fiber board, plywood, particle board, and plasterboard sheathing. The study found that the load capacity of shear walls constructed with more than one sheathing material could be calculated by adding the load capacities for the shear walls sheathed with each material separately. The study also showed that the racking resistance of the shear walls was proportional to the length of the wall, minus any sections containing openings. Patton–Mallory, et. al. (1984) found the same results using plywood and gypsum wallboard sheathing.

The effects of glueing the sheathing to the framing was investigated by Thurston and Flack (1980). They found that glued sheathing provided a higher ultimate load capacity, but not a higher stiffness for shear walls. The hold–down anchors, at the bottom of the end studs, were shown to be important in determining the racking performance of shear walls.

The stud spacing was shown to be significant in the load capacity of shear walls by De Klerk (1985). It was observed that the load capacity increased with a decrease in the stud spacing. However, a corresponding increase in stiffness was not observed.

Sheathing panels of the same thickness were shown, by Kamiya (1986), to have higher stiffness and strength when the panel width is increased. He showed that using the 1.2×2.4 m (4×8 ft) sheathing panels, commonly used in North America, resulted in higher stiffness and load capacity of shear walls than using the 0.9×2.4 m (3×8 ft) sheathing panels, commonly used in Japan.

Thurston and Hutchison (1984) investigated the cyclic loading of timber shear walls, along with proposing a model to relate the results of tests using small scale specimens to the performance of full size shear panels.

Griffiths (1984) compared the procedures and results of the ASTM E72–77 and ASTM E564–76 tests, and concluded that the ASTM E564–76 test is superior to the ASTM E72–77 test, but it is still not perfect. The difference between the two ASTM Standard tests is that the ASTM E72–77 test uses two tie rods that run along each of the end studs. The tie rods eliminate the uplift effects of the overturning moment. Griffith's study found that the ASTM E72–77 test overestimated the test specimen stiffness and strength due to the use of tie down rods. Tissel (1989) discussed these tests with a similar conclusion being drawn. Tissel also discussed the earthquake shear wall tests, used by Stewart (1987) and the author.

Stewart (1987) and Dean, et. al. (1986) investigated the dynamic behavior of plywood shear walls. They used a dynamic test that subjected the test specimen to earthquake loads, similar to the one presented in this thesis. The loads generated during the tests were up to twice the design loads required by the New Zealand design code. The test used an inertial mass and excited the base of the wall specimen with an acceleration record representing the design earthquake. Stewart, et. al. (1988) also concluded that nails exhibited good ductility and damping characteristics.

Falk and Itani (1986, 1987) tested shear walls and diaphragms to determine the dynamic characteristics. They found that the natural frequency ranged from 8–29 Hz, and damping the ratio ranged from 9% to 34%. The results obtained were for the shear walls and diaphragms without an inertial mass, which would account for the high natural frequencies obtained. The study by Falk and Itani also showed the linear relation between the load capacity of shear walls and the length without openings.

The effect of overdriving nails and effectively forcing the head of the nail to penetrate the face of the sheathing panel was investigated with dynamic tests of shear walls by Gray and Zacher (1988). The study used a cyclic, reversing deformation to test the shear walls. They found that overdriving nails can result in sudden, non–ductile failures

of shear walls and that gypsum shear walls have poor performance in dynamic loading. The dynamic tests were considered by Gray and Zacher to disclose important information about the damping and hysteretic effects of shear walls that is not available from the static, monotonic tests.

2.2.3 Full Size Buildings

A few buildings have been tested to investigate the performance of the various components when combined to form a complete structure. Soltis (1984) investigated structural failures of buildings as a result of earthquakes, and found that engineered structures generally performed better than non–engineered or marginally engineered structures. Soltis found that the connections between different components of the structures commonly failed, and that the connector failure sometimes progressed through large sections of the structure. In another study of the performance of light–framed wood buildings, Soltis (1984) indicated that buildings performed adequately if they are symmetric in plan and elevation, and have shear walls capable of resisting the lateral loading.

Boughton and Reardon (1984) performed simulated cyclone wind tests on a house and found that the floor and roof functioned well as diaphragms, while the walls resisted the lateral loads. The walls were adversely affected by the flexibility of the floor in bending, and by the connections between the walls and floor.

Buchanan (1984) gave an overview of the effects of the behavior of materials, as well as connections, on the overall performance of structures. He also proposed shear walls constructed with solid glue laminated sections and ductile steel coupling beams, as a lateral load resisting system for multi–storey timber buildings.

A qualitative assessment of the response of houses was given by McDowall (1984). He concluded that for racking walls to develop their full strength and stiffness, they must

be restrained to deform in plane and that the interaction between the floor, ceiling, and walls increases the lateral stiffness of the walls.

Sugiyama, et. al. (1988) tested a conventional Japanese wood frame house to investigate the effects of wall coverings and floor openings have on the lateral stiffness. They found that small openings in the floors had no effect on the lateral stiffness and that sheathing on walls above and below openings add some lateral stiffness to the structure. Local failures of let–in corner braces were also observed.

Sadakata (1988) tested a two–storey house to investigate the usefulness of a ductility connection, that was constructed using steel plates. The author found that these connections reduced the damage of the ground sill, but also reduced the lateral stiffness of the building.

Broughton (1988) reviewed the cyclone tests of full size houses and commented on the effectiveness of the testing apparatus and instrumentation. He found that the stiffness of the test equipment can influence the stiffness of structural components, and that the houses behaved in a manner similar to the one assumed by design codes for wind loads. He also found differences between the few proposed models and the test results.

Stewart, et. al. (1988, 1989) reported the results of full scale tests of manufactured, or pre-fabricated housing. They found the ultimate capacity of the manufactured houses to be much higher than the design capacity and the roof and floors behave as very stiff diaphragms.

Ohash and Sakamoto (1988) tested a house in order to investigate the effects of horizontal diaphragms on the overall performance of the building. They found that assuming elastic behavior allows the use of superposition in calculating deflections in the structure, and the calculated deflections were in reasonable agreement with the test results.

Most of the experimental research performed to date has concentrated on the ultimate load capacity of connections, walls, or complete buildings subjected to static one–directional loadings. This is due to the lack of technology that would allow dynamic tests to be conducted, and the working stress design format that the design codes have used, where allowable load capacities were specified. With the introduction of computers, dynamic testing has become feasible, and recently the cyclic and dynamic characteristics were investigated. These tests have only begun to determine parameters required for a good understanding of the dynamic behavior of timber shear walls.

2.3 Numerical Modeling

There have been numerous models proposed for modeling timber structures with most of the models, pertinent to this thesis, being used to predict the static behavior of shear walls. A few models predict the behavior of joints only, but most of these models are included in the larger programs for shear walls. Attempts have also been made to model complete structures.

2.3.1 Connections

Soltis, et. al. (1987) modeled the effects of grain orientation on joints between lumber members. Good agreement between their model and the tests of connections loaded in shear was found.

Kivell, et. al. (1981) proposed a hysteretic model for nailed timber joints that was based on a modified model used for concrete, the model allowed for the pinching effects of the hysteresis to be modeled.

Loferski and Polensek (1982) proposed a model using a series of straight lines to represent the nonlinear load–deflection curve for static one–directional loading. The

model was shown to be useful for evaluating the inelastic moduli of the load–slip curve of nailed connections.

Malhotra and Thomas (1982) extended the exponential model, proposed by Foschi (1974), to include the effects of gaps in connections and bearing between connection components, with good results.

Smith et. al. (1988) proposed a model for dowel connections that was verified using full bolted connections, but only looked at nails in single sheets of plywood, not full connections.

2.3.2 Shear Walls

A large number of models have been proposed for predicting the static racking behavior of timber shear walls. Many of the models, such as those proposed by Gupta and Kuo (1984), Källsner (1984), McCutcheon (1985), and Tuomi and McCutcheon (1987) used energy derivations to model the load–deflection characteristics of shear walls.

Gupta and Kuo (1987) used their model to investigate the uplift of studs in shear walls, while Patton–Mallory and McCutcheon (1987) extended their model to investigate shear walls sheathed on two sides with dissimilar materials.

Källsner (1984) used his proposed model to predict the static one–directional load–deflection behavior of walls with openings and of various lengths.

Finite element analysis has been used by quite a few of the more recent models with success. Foschi (1977, 1982) proposed a general finite element model that modeled the nail connections using an exponential curve. His model was used to prepare the proposal for allowing waferboard to be used as an equivalent to plywood in timber diaphragms and shear walls, for the United States.

Itani and Cheung (1984) proposed a similar general finite element model to predict

the racking performance of shear walls and static behavior of diaphragms.

Falk (1986) and Falk and Itani (1988) proposed a finite element model that reduced the number of degrees–of–freedom (DOF) required by modeling all of the connectors attached to each sheathing panel as one element.

None of the models discussed above addressed the cyclic or dynamic behavior of shear walls. One of the first models proposed for predicting the dynamic response of shear walls was proposed by Medearis (1969). This model was a single degree–of–freedom (SDOF) model that was capable of predicting the behavior of simple wall configurations to dynamic excitations. Stewart (1987) proposed another SDOF model for predicting the dynamic behavior of shear walls, but neither of these models were general in nature. Stewart, et. al. (1984) used this model to investigate the base shear force and inter–storey displacements of timber buildings during earthquakes. They found that the New Zealand design code underestimates the loads experienced during earthquakes.

Cheung and Itani (1984) proposed a theoretical procedure, using viscous damping, for determining the damping ratios for shear walls, but found that the model predicted a decrease in damping for increased displacements, while experimental data indicated the opposite trend.

Falk (1986) proposed an extension to his static finite element model to include dynamic response, and used it to predict the elastic behavior of shear walls. There was no inertial mass modeled, therefore, the response remained elastic.

2.3.3 Full Structures

Few models have been proposed for predicting the behavior of entire timber buildings, and none have been addressed the dynamic behavior of buildings. Naik, et. al. (1984) developed a mechanical model of springs for shear walls and rigid horizontal diaphragms

to model timber buildings.

Gupta and Kuo (1987) extended their shear wall model to three–dimensions to model simple structures with fair success.

Finally, Moody and Schmidt (1988) and Schmidt and Moody (1989) presented the predictions of the static behavior of simple timber buildings. Their model combined the distortion model used by McCutcheon (1985) for shear walls with the load–deflection model for connectors proposed by Foschi (1977). The model also assumed rigid diaphragms for the roof and floors.

As can be seen from the above review, emphasis was placed on modeling the static one–directional racking performance of shear walls. Only recently, have attempts at modeling the dynamic behavior of shear walls been made and, with the exception of the model proposed in this thesis, none of the models can predict the dynamic behavior of general shear walls. There have been only a few models proposed for modeling complete structures, and none of them address the connections between the various structural elements, such as the wall and floors, or the dynamic response.

2.4 Summary

An overview of the pertinent literature for experimental and numerical modeling of timber shear walls, and the connections affecting their performance, has been presented. It is evident that the majority of the research has been oriented towards the prediction of the load capacity for shear walls and diaphragms, subjected to static one–directional loading. The emphasis on the static behavior is largely due to the lack of technology required to conduct dynamic tests, such as one representing earthquake loading. With the introduction of computers and improved measuring devices, the emphasis has recently begun to shift towards studying the dynamic characteristics of timber shear walls. The

recent experimental studies have concentrated on determining the natural frequencies or damping characteristics of shear walls. The study by Stewart (1987) is the only study, other than this thesis, that has tested the shear wall specimens, using a test that closely represented the type of loading generated during an earthquake. This thesis extends the investigation of the dynamic behavior, and will hopefully contribute to the understanding of timber shear walls subjected to earthquakes.

Chapter 3

Static Finite Element Model

3.1 Introduction

This chapter will present the derivation of the static computer model, called **SHWALL**, used to predict the behavior of timber shear walls subjected to a static one–directional loading. **SHWALL** is an improved model that can predict the ultimate load capacity of timber shear walls. It also allows the work of this thesis to be related to the tests and models previously presented by other researchers. The assumptions on which the model is based are outlined first. Different finite elements used in the model are derived, and the methods used to combine the elements and to solve the problem are described. In all cases the finite element formulations use the tangential stiffness matrix. This allows the static model to be easily converted to the dynamic time–step model described in Chapter 6. The verification of the model's accuracy is discussed in Chapter 9.

The five finite elements included in the model are:

1. A general two–dimensional beam element used to model the framing (Section 3.3).
2. A bi–linear corner connector element used to model the connections between framing members (Section 3.4).
3. A plate element used to model the sheathing (Section 3.5).

4. A sheathing connector element consisting of a non–linear, three–dimensional spring element used to model the fasteners connecting the sheathing and framing (Section 3.6).

5. A bi–linear sheathing bearing connector used to model the bearing effects between adjacent sheathing panels (Section 3.7).

3.2 Assumptions

The assumptions used in the derivation of the static finite element model, **SHWALL**, are as follows:

1. The beam element used to model the framing will not deflect out of the plane of the wall. The program is not intended for modeling the out–of–plane bending of the overall wall, and all the loads are applied in the plane of the wall.

2. To satisfy the compatibility requirements for the axial displacements, the deflected shape for the beam element, parallel to the beam axis, is assumed to be linear.

3. The in–plane deflected shape for the beam element, perpendicular to the beam axis, is defined by a cubic polynomial so that compatibility of slope is maintained between beam elements.

4. Initial plane sections of the beam element are assumed to remain plane after deformations since the change in shear stress across the cross–section is assumed to be small.

5. The beam material obeys linear elastic, homogeneous, stress–strain relationships and never reaches yield. This assumption is made since failure of the sheathing

connector is the primary failure mode. Future improvements to the model can include failure of the framing.

6. The plate element used to model the sheathing obeys linear elastic, orthotropic stress–strain relationships. The sheathing material should not yield, except if very stiff or strong sheathing connectors are used. The element is orthotropic because plywood sheathing is an orthotropic material.

7. Layered sheathing materials, such as plywood, will be modeled as a non-layered material having average material properties obtained from sheathing panel tests, or derived using transformed sections. This assumption is used to simplify the sheathing element.

8. The in–plane deflections of the plate element are affected by the bending deflections (large deflection theory). Making this assumption allows the buckling effect of thin sheathing panels to be modeled.

9. The change in the thickness of the sheathing material due to deformations is negligible, i.e. crushing of the material does not occur. Crushing of the sheathing has not been observed in any full size shear wall tests that this author is aware of.

10. The effect of bearing between two adjacent sheathing elements is modeled by a bi–linear spring connector that prevents overlapping of the plate elements, but does not hinder separation. The relative movement parallel to the edge of the plate element is also not hindered by the spring connector. The bearing between sheathing panels is an important factor, affecting the stiffness of large diaphragms and shear walls.

11. The connection between the sheathing and the framing is modeled as three independent, non–correlated, non–linear spring connectors, with exponential load–deflection curves. Foschi (1977) has shown that the exponential model represents nail connectors well. Also, the three independent springs allow for future simplifications by eliminating some deflection directions if it is shown to not effect the resulting predictions significantly.

12. The spring connectors between the sheathing and the framing are modeled as having a maximum load. Then, as the deflection increases past the deflection corresponding to the maximum load, the load capacity decreases linearly to a value of zero. This accounts for the eventual total failure of an individual connector, such as when a nail pulls completely out of the framing and will allow the load capacity of the wall to be determined.

3.3 The Framing Beam Element

The beam element used in this model to represent the frame members is a common two–dimensional beam element, with a linear displacement field in the axial direction, and a cubic displacement field for the deflections which are perpendicular to the beam axis. The beam is assumed to not deflect in the Z–direction (out–of–plane direction).

Consider the beam element of length l, shown in Figure 3.1. The three degrees of freedom u, v, and θ, representing the displacements in the X– and Y– directions, and the counterclockwise rotation, respectively, are assigned to each of the nodes i and j. If it is assumed that the deformation of any point on the beam can be described by the

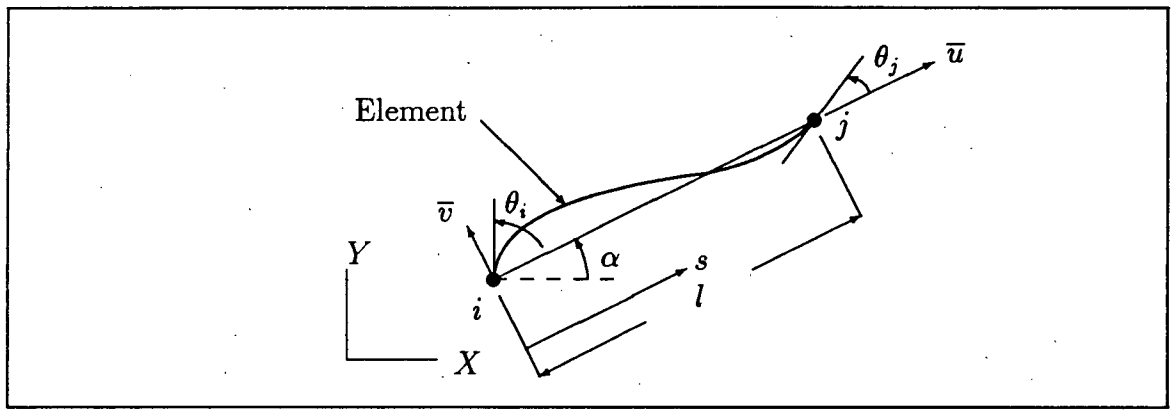

Figure 3.1: Framing Beam Element.

displacements $\overline{u}_b$ and $\overline{v}_b$, then these two displacements can be determined by the functions,

$$\overline{u}_b = J_1(s)\overline{u}_{b_i} + J_4(s)\overline{u}_{b_j} \tag{3.1}$$

$$\overline{v_b} = J_2(s)\overline{v}_{b_i} + J_3(s)\overline{\theta}_{b_i} + J_5(s)\overline{v}_{b_j} + J_6(s)\overline{\theta}_{b_j} \tag{3.2}$$

where, s is a local coordinate along the length of the beam starting at node i,

$$s = \frac{l}{2}(1+\tau) \tag{3.3}$$

τ is a local coordinate that has a range of values from -1 at node i to $+1$ at node j, and

$$\begin{aligned} J_1(s) &= 1.0 - s/l \\ J_2(s) &= 1.0 - 3(s/l)^2 + 2(s/l)^3 \\ J_3(s) &= s - 2s^2/l + s^3/l^2 \\ J_4(s) &= s/l \\ J_5(s) &= 3(s/l)^2 - 2(s/l)^3 \\ J_6(s) &= -s^2/l + s^3/l^2 \end{aligned} \tag{3.4}$$

Equations 3.1 and 3.2 can be written in matrix form as,

$$\{d\}_b = [J]_b \{a\}_b \tag{3.5}$$

where,

$$\{d\}_b = \begin{Bmatrix} \overline{u}_b \\ \overline{v}_b \end{Bmatrix} \quad , \quad \{a\}_b = \begin{Bmatrix} u_{b_i} \\ v_{b_i} \\ \theta_{b_i} \\ u_{b_j} \\ v_{b_j} \\ \theta_{b_j} \end{Bmatrix} \text{ and, } \quad [J]_b^T = \begin{bmatrix} J_1(s) & 0 \\ 0 & J_2(s) \\ 0 & J_3(s) \\ J_4(s) & 0 \\ 0 & J_5(s) \\ 0 & J_6(s) \end{bmatrix} \tag{3.6}$$

The strain matrix for the beam element is

$$\{\epsilon\}_b = \begin{Bmatrix} \partial u \ / \ \partial x \\ -z\partial^2 v \ / \ \partial x^2 \end{Bmatrix} \tag{3.7}$$

This equation can be reformulated, using Equation 3.5 as

$$\{\epsilon\}_b = [B]_b \{a\}_b \tag{3.8}$$

where

$$[B]_b = \begin{bmatrix} \dfrac{\partial J_1(s)}{\partial x} & 0 & 0 & \dfrac{\partial J_4(s)}{\partial x} & 0 & 0 \\ 0 & -z\dfrac{\partial^2 J_2(s)}{\partial x^2} & -z\dfrac{\partial^2 J_3(s)}{\partial x^2} & 0 & -z\dfrac{\partial^2 J_5(s)}{\partial x^2} & -z\dfrac{\partial^2 J_6(s)}{\partial x^2} \end{bmatrix} \tag{3.9}$$

The stresses associated with the strains can be written as,

$$\{\sigma\}_b = E_b \{\epsilon\}_b \tag{3.10}$$

where E_b is the modulus of elasticity of the material used for the beam.

Now, the potential energy expression for one element is

$$\begin{aligned} \Pi_b \ = \ & \int_V \frac{1}{2} \{\epsilon\}_b^T \{\sigma\}_b \, dV - \int_V \{\epsilon\}_b^T E \{\epsilon_0\}_b \, dV \\ & + \int_V \{\epsilon\}_b^T \{\sigma_0\}_b \, dV - \int_V \{a\}_b^T W dV - \int_S \{a\}_b^T T dS \end{aligned} \tag{3.11}$$

Substituting Equations 3.8 and 3.10 into Equation 3.11, yields

$$\Pi_b = \frac{1}{2}\{a\}_b^T \left(\int_V [B]_b^T E [B]_b \, dV\right) \{a\}_b - \{a\}_b^T \{P\}_b \tag{3.12}$$

where the loads applied by an element to its nodes are

$$\{P\}_b = \int_V [B]_b^T E \{\epsilon_0\}_b \, dV - \int_V [B]_b^T \{\sigma_0\}_b \, dV + \int_V [J]_b^T W dV + \int_S [J]_b^T T dS \tag{3.13}$$

The first term in Equation 3.13 represents the loads due to initial strains, the second represents the loads due to initial stresses, the third represents the loads due to body forces, and the last term represents loads due to tractions on the element boundary.

To find the governing equations of equilibrium, which occur when the potential energy is at a minimum, the first variation of the potential energy, Π_b, is taken with respect to the displacements, $\{a\}_b$.

$$\delta\Pi_b = \{\delta a\}_b^T \left(\int_V [B]_b^T E [B]_b \, dV\right) \{a\}_b - \{\delta a\}_b^T \{P\}_b = 0 \tag{3.14}$$

Since virtual displacements, $\{\delta a\}_b$, are arbitrary, the equations of equilibrium are,

$$\psi(\{a\}_b) = \int_V [B]_b^T E [B]_b \{a\}_b - \{P\}_b = 0 \tag{3.15}$$

which can be written as

$$\psi(\{a\}_b) = [k]_b \{a\}_b - \{P\}_b = 0 \tag{3.16}$$

$[k]_b$ is the beam element stiffness matrix and can be expanded as,

$$[k]_b = \begin{bmatrix} \frac{EA}{l} & & & & & \\ 0 & \frac{12EI}{l^3} & & SYMMETRIC & & \\ 0 & \frac{6EI}{l^2} & \frac{4EI}{l} & & & \\ \frac{-EA}{l} & 0 & 0 & \frac{EA}{l} & & \\ 0 & \frac{-12EI}{l^3} & \frac{-6EI}{l^2} & 0 & \frac{12EI}{l^3} & \\ 0 & \frac{6EI}{l^2} & \frac{2EI}{l} & 0 & \frac{-6EI}{l^2} & \frac{4EI}{l} \end{bmatrix} \tag{3.17}$$

Since the lateral deformation of the beam is represented by a cubic function of s, and the axial deformation of the beam is represented by a linear function of s, the deformation will only be approximate if the beam is loaded with a distributed load along its length. For the few cases where this could create problems, such as a long member with a distributed load, the member can be subdivided into smaller beam elements to improve the analysis.

It should be noted, that since the beam element is assumed to follow the small deflection theory, and to be linear elastic, the secant and tangent stiffness matrices,$[k_s]_b$ and $[k_t]_b$, for the beam element are the same as the stiffness matrix, $[k]_b$.

3.4 Bi–Linear Corner Connector

The derivation of the corner connector element is essentially the same as the beam element derivation. This is possible because the connector can be thought of as a short beam element with a modulus of elasticity that changes, depending on the loading. The corner connector uses the load-deflection curve shown in Figure 3.2.

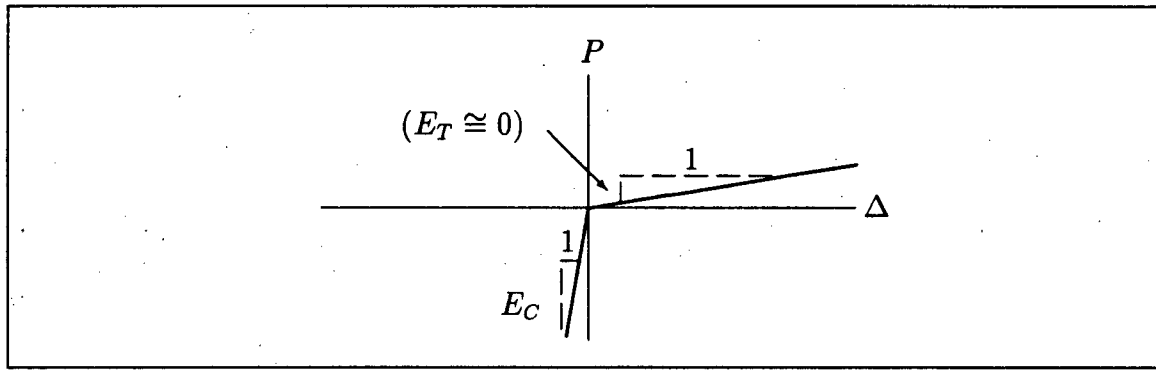

Figure 3.2: Corner Connector Load–Deflection Curve.

The modulus of elasticity for the connector in tension is E_T, and in compression it is E_C. Both of these values can be found from tests, or the modulus of elasticity of the framing material for compression perpendicular to grain could be used as the value of E_C. The cross–sectional area and moment of inertia of the connector can be adjusted, by changing the data, to give the appropriate stiffness in the rotational and axial directions.

The equation for the tangent stiffness matrix of the corner connector will be the same as the equation for the beam element tangent stiffness matrix, Equation 3.17, with the exception that the modulus of elasticity will be changed to either E_T or E_C for the connector.

3.5 The Sheathing Element

The sheathing is modeled using the two–dimensional, orthotropic plate finite element, shown in Figure 3.3. This element has a three–dimensional displacement field, but the thickness can be removed by integrating over the Z–direction, leaving a two–dimensional physical form. Hence, $z = 0$ and the nodes will be located on the center plane of the element.

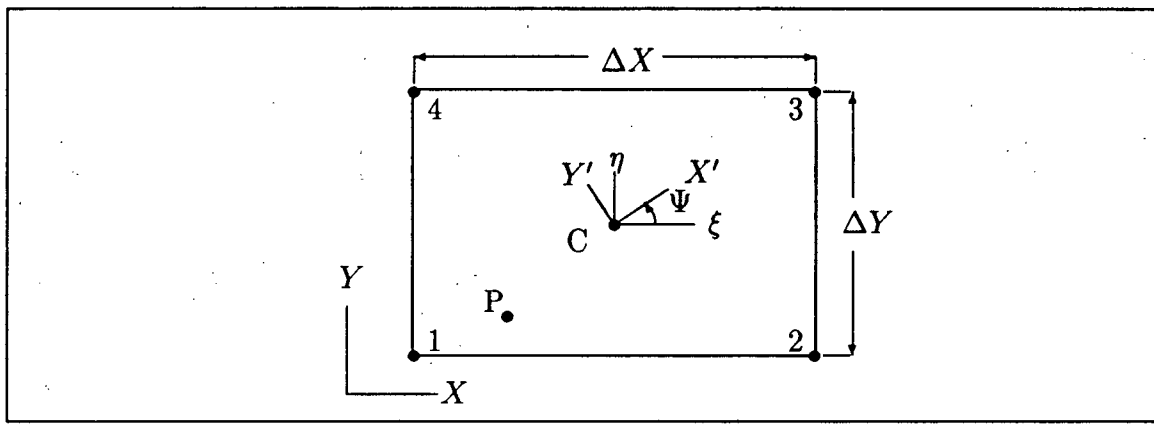

Figure 3.3: Sheathing Plate Element.

A cubic displacement field is required for compatibility of slopes between elements in the out–of–plane direction (Z–direction), and the same displacement field is desired in the in–plane (X– and Y–directions) to allow the bearing between elements to be modeled along part of the element edge. Therefore, a full cubic polynomial will be used to model the displacement fields in all three directions. These displacements will be defined as u, v, and w in the X–, Y–, and Z–directions, respectively.

3.5.1 Kinematic Relationships

The principal geometry and loading for shear walls are two–dimensional, as shown in Figure 3.4. This has lead to previous models, assuming that the entire problem is a two–dimensional problem. However, for thin sheathing materials, the out–of–plane deflections of the sheathing could have a marked effect on the stiffness and the strength. These bending deflections could lower the sheathing stiffness, and buckling of the sheathing has been observed in some walls. For this reason, the Z–direction deformations of the plate, along with the effects of large deflections, have been included.

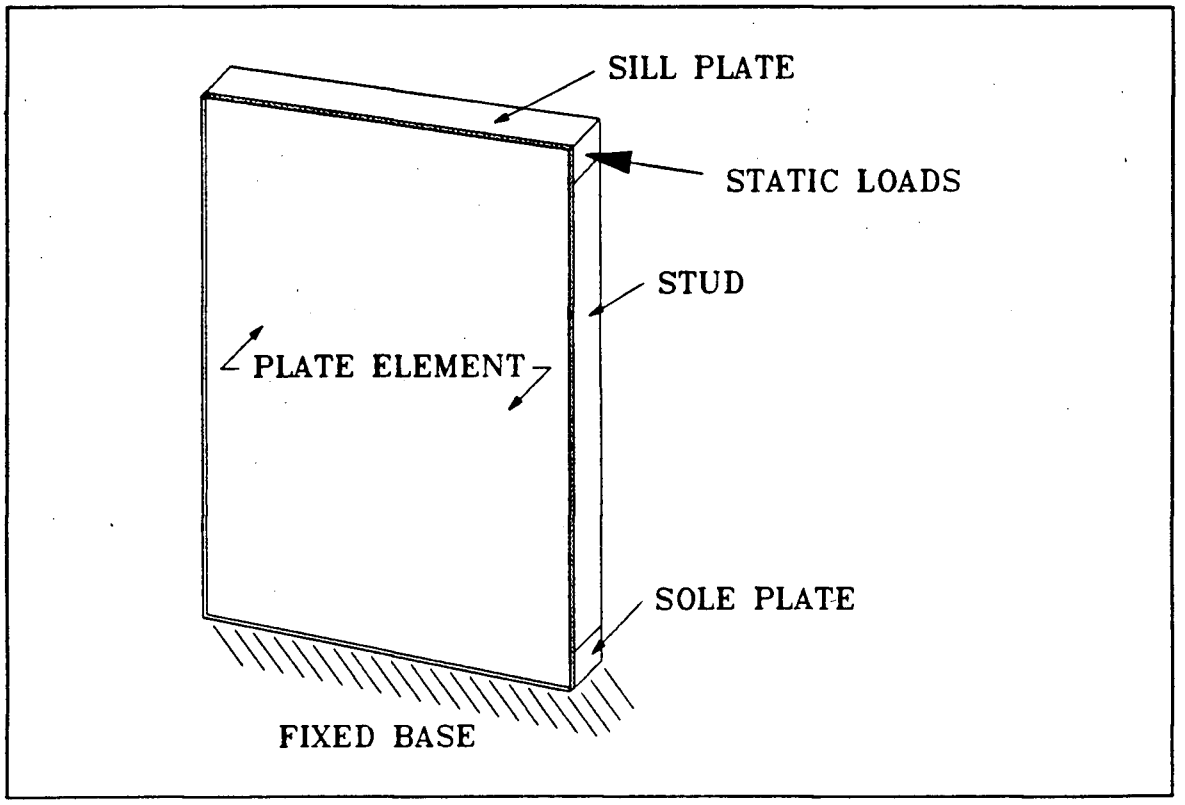

Figure 3.4: Loaded Shear Wall Configuration.

The sheathing material used for the walls modeled in this study, will be either plywood or waferboard panels. Each panel of sheathing can be represented by the plate element,

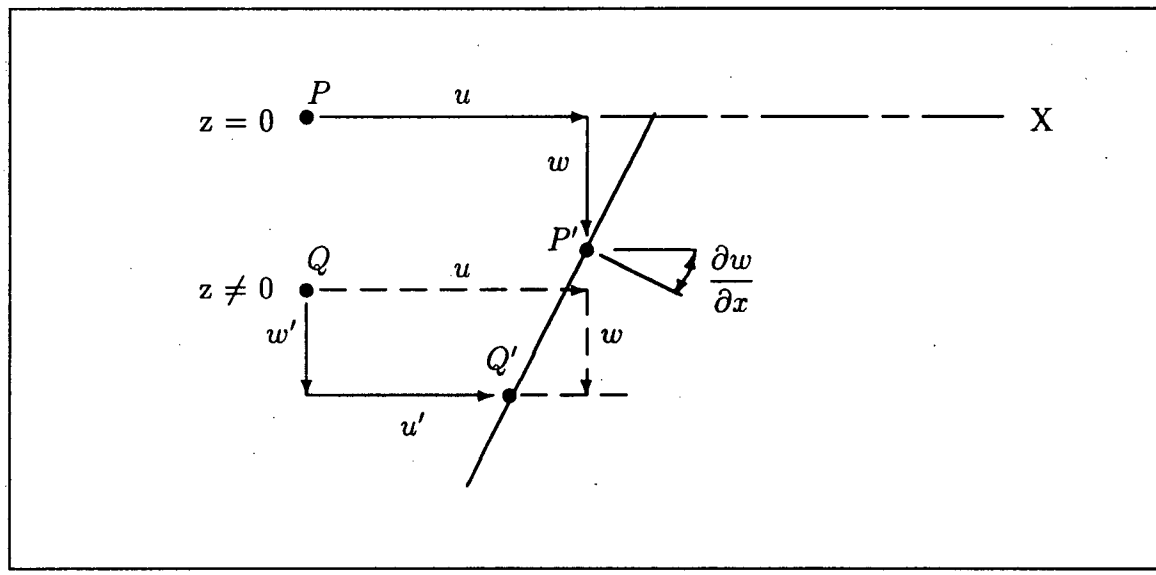

Figure 3.5: Representation of Deflections in Plate Element.

shown in Figure 3.3. Each element has 4 nodes, that are numbered locally 1–4 in a counter clockwise fashion, and will have dimensions ΔX, ΔY, and a thickness, t.

Consider an arbitrary point P inside an element. When the wall is loaded, point P will undergo displacements u, v, and w in the X–, Y–, and Z–directions, respectively. When a finite element approximation is used, these displacements will be defined by a polynomial expression within each element. To ensure convergence of the numerical solution, and continuity of the displacements u, v, and w, the polynomial must be continuous.

Consider Figure 3.5, which shows two positions in the X–Z plane, P and Q. Let point P lie on the mid–plane, $z = 0$, and point Q lie at a distance from the mid–plane, $z \neq 0$. Points P and Q have the same X– and Y–coordinates in the undeformed state. When loaded, point P undergoes displacements u and w, while point Q undergoes

displacements u' and w' which can be determined from Figure 3.5 as

$$\begin{aligned} u' &= u - z\frac{\partial w}{\partial x} \\ w' &= w \end{aligned} \tag{3.18}$$

These equations make the following assumptions:

1. Plane sections before bending remain plane after deformation.
2. Changes in the thickness due to deformation are negligible, i.e. crushing does not occur.

These assumptions can be made since shear deformations will be small, and the sheathing is not loaded in the out–of–plane direction. Similarly, the equation relating v' can be written as

$$v' = v - z\frac{\partial w}{\partial y} \tag{3.19}$$

The corresponding strains at point Q, including the second order effects due to large deflections, can now be calculated as follows:
in the X–direction,

$$\epsilon_{Pl_x} = \underbrace{\frac{\partial u}{\partial x} - z\left(\frac{\partial^2 w}{\partial x^2}\right)}_{\text{Elastic Theory}} + \underbrace{\frac{1}{2}\left(\frac{\partial w}{\partial x}\right)^2}_{\text{Large Displacement Term}} \tag{3.20}$$

in the Y–direction,

$$\epsilon_{Pl_y} = \frac{\partial v}{\partial y} - z\frac{\partial^2 w}{\partial y^2} + \frac{1}{2}\left(\frac{\partial w}{\partial y}\right)^2 \tag{3.21}$$

and the shear in the X–Y plane,

$$\epsilon_{Pl_{xy}} = \underbrace{\frac{\partial u}{\partial y} + \frac{\partial v}{\partial x} - 2z\frac{\partial^2 w}{\partial x \partial y}}_{\text{Elastic Theory}} + \underbrace{\frac{\partial w}{\partial x}\frac{\partial w}{\partial y}}_{\text{Large Deflection Term}} \tag{3.22}$$

Shear in the X–Z and Y–Z planes is neglected since the sheathing is thin, in relation to its in–plane dimensions.

3.5.2 Stress–Strain Relationships

Since plywood is an orthotropic material, it can be assumed that the sheathing material obeys linear elastic, orthotropic stress–strain relationships. These stress–strain relationships will be:

$$\begin{aligned} \sigma_{Pl_x} &= \frac{E_{Pl_x}}{C}\epsilon_{Pl_x} + \frac{\nu_{Pl_{xy}} E_{Pl_x}}{C}\epsilon_{Pl_y} \\ \sigma_{Pl_y} &= \frac{E_{Pl_y}}{C}\epsilon_{Pl_y} + \frac{\nu_{Pl_{yx}} E_{Pl_x}}{C}\epsilon_{Pl_x} \\ \sigma_{Pl_{xy}} &= G_{Pl_{xy}}\epsilon_{Pl_{xy}} \end{aligned} \tag{3.23}$$

where, σ_{Pl_x} and σ_{Pl_y} are the stresses in the X– and Y–directions, respectively, and $\sigma_{Pl_{xy}}$ is the shear stress in the X–Y plane. E_{Pl_x} and E_{Pl_y} are the average moduli of elasticity for the sheathing material in the X– and Y–directions, respectively. $G_{Pl_{xy}}$ is the average shear modulus in the X–Y plane. $\nu_{Pl_{xy}}$ and $\nu_{Pl_{yx}}$ are the Poisson ratios giving the strain in the X–direction for a stress in the Y–direction, and the strain in the Y–direction for a stress in the X–direction, respectively. ϵ_{Pl_x}, ϵ_{Pl_y}, and $\epsilon_{Pl_{xy}}$ are the axial and shear strains, given by Equations 3.20–3.22, and

$$C = 1 - \nu_{Pl_{xy}}\nu_{Pl_{yx}} \tag{3.24}$$

The material constants E_{Pl_x}, E_{Pl_y}, $G_{Pl_{xy}}$, $\nu_{Pl_{xy}}$, and $\nu_{Pl_{yx}}$ can be obtained by performing standard ASTM tests in the laboratory. The properties of plywood can also

be approximated using the following equations:

$$\begin{aligned} E_{Pl} &= \frac{\sum_{i=1}^{n} E_i t_i}{t} \\ \nu_{Pl} &= \frac{\sum_{i=1}^{n} \nu_i t_i}{t} \\ G_{Pl} &= \frac{\sum_{i=1}^{n} G_i t_i}{t} \end{aligned} \tag{3.25}$$

where E_{Pl}, ν_{Pl}, and G_{Pl} are the average modulus of elasticity, Poisson ratio, and shear modulus in the direction of interest, respectively. E_i, ν_i, and G_i are the modulus of elasticity, Poisson ratio, and shear modulus of the individual layer in the direction of interest, respectively. Here, t_i is the thickness of the individual layers, while t is the total thickness of the plywood panel. n is the total number of layers in the plywood panel.

If the definitions

$$\{\sigma_{Pl}\} = \begin{Bmatrix} \sigma_{Pl_x} \\ \sigma_{Pl_y} \\ \sigma_{Pl_{xy}} \end{Bmatrix} \quad \text{and} \quad \{\epsilon_{Pl}\} = \begin{Bmatrix} \epsilon_{Pl_x} \\ \epsilon_{Pl_y} \\ \epsilon_{Pl_{xy}} \end{Bmatrix} \tag{3.26}$$

are used, then Equations 3.23 can be written in matrix form as

$$\{\sigma\}_{Pl} = [D]_{Pl} \{\epsilon\}_{Pl} \tag{3.27}$$

where, $[D]_{Pl}$ is the material property matrix and contains the coefficients in Equations 3.23. The matrix $[D]_{Pl}$ will be,

$$[D]_{Pl} = \begin{bmatrix} \frac{E_{Pl_x}}{C} & \frac{\nu_{Pl_{xy}} E_{Pl_x}}{C} & 0 \\ \frac{\nu_{Pl_{yx}} E_{Pl_y}}{C} & \frac{E_{Pl_y}}{C} & 0 \\ 0 & 0 & G_{Pl_{xy}} \end{bmatrix} \tag{3.28}$$

3.5.3 Finite Element Approximations and Shape Functions

Figure 3.3 shows a single finite element used to model the sheathing. The element is a plate element with dimensions ΔX and ΔY, and a local coordinate system (ξ,η) centered at point C, the center of the element. The global coordinates of point C are (x_c,y_c).

The local coordinate system is shown in Figure 3.6 and the coordinates of any point inside the element can be calculated as

$$\begin{aligned} x &= x_c + \frac{\Delta X}{2}\xi \\ y &= y_c + \frac{\Delta Y}{2}\eta \end{aligned} \tag{3.29}$$

The sides of the element will have the coordinates $\xi = \pm 1$ and $\eta = \pm 1$ as shown in Figure 3.6.

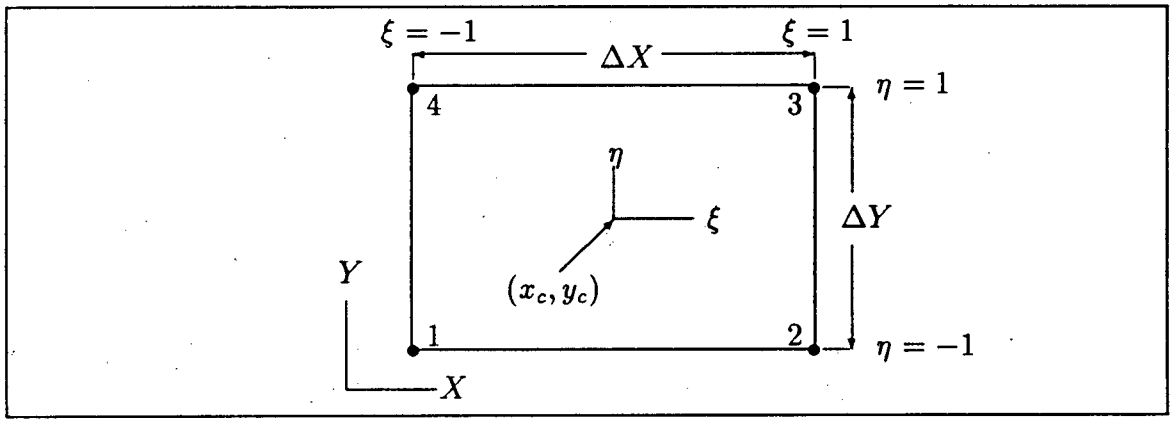

Figure 3.6: Sheathing Plate Element.

For the finite element approximation, the deflection fields u, v, and w will be assumed to be described by polynomial expressions in ξ and η. Each of the deflections will have four parameters at each of the four nodes. For the w deflection field, the parameters

will be w, $\frac{\partial w}{\partial x}$, $\frac{\partial w}{\partial y}$, and $\frac{\partial^2 w}{\partial x \partial y}$ at each node. The u and v directions will have similar parameters. Thus, there will be 12 degrees–of–freedom at each node, for a total of 48 degrees–of–freedom per plate element.

The polynomials used for all three displacement fields, along with the above degrees–of–freedom, will ensure continuity of slope between elements. This is required to provide continuity of the bending moment and allow the intra–element bearing surface to be described with reasonable accuracy.

The displacements of a point inside the plate element can be calculated as,

$$\begin{aligned} u(\xi,\eta) &= [L(\xi,\eta)]_{Pl} \{a\}_{Pl} \\ v(\xi,\eta) &= [M(\xi,\eta)]_{Pl} \{a\}_{Pl} \\ w(\xi,\eta) &= [N(\xi,\eta)]_{Pl} \{a\}_{Pl} \end{aligned} \tag{3.30}$$

Where, the element's degrees–of–freedom are assembled into a vector $\{a\}_{Pl}$ as follows:

$$\{a\}_{Pl} = \left\{ \begin{array}{c} u_1 \\ \partial u_1 \,/\, \partial x \\ \partial u_1 \,/\, \partial y \\ \partial^2 u_1 \,/\, \partial x \partial y \\ v_1 \\ \partial v_1 \,/\, \partial x \\ \partial v_1 \,/\, \partial y \\ \partial^2 v_1 \,/\, \partial x \partial y \\ w_1 \\ \partial w_1 \,/\, \partial x \\ \partial w_1 \,/\, \partial y \\ \partial^2 w_1 \,/\, \partial x \partial y \\ u_2 \\ \partial u_2 \,/\, \partial x \\ \vdots \\ w_4 \\ \partial w_4 \,/\, \partial x \\ \partial w_4 \,/\, \partial y \\ \partial^2 w_4 \,/\, \partial x \partial y \end{array} \right\} \tag{3.31}$$

The variables $u(\xi,\eta)$, $v(\xi,\eta)$, and $w(\xi,\eta)$ are the deflections at the point (ξ,η) on the plate element, and $[L(\xi,\eta)]_{Pl}$, $[M(\xi,\eta)]_{Pl}$, and $[N(\xi,\eta)]_{Pl}$ are vectors containing the

shape functions. The shape functions, $[L(\xi,\eta)]_{_{Pl}}$, can be identified from the following expression.

$$
\begin{aligned}
u(\xi,\eta) \quad = u_1 \quad & \Big(\frac{1}{4} - \frac{3}{8}\xi + \frac{9}{16}\xi\eta - \frac{3}{8}\eta + \frac{1}{8}\xi^3 - \frac{3}{16}\xi^3\eta \\
& + \frac{1}{16}\xi^3\eta^3 - \frac{3}{16}\xi\eta^3 + \frac{1}{8}\eta^3\Big) \\
+a\frac{\partial u_1}{\partial \xi} \quad & \Big(\frac{1}{8} - \frac{1}{8}\eta + \frac{3}{16}\xi\eta - \frac{3}{16}\eta - \frac{1}{8}\xi^2 + \frac{3}{16}\xi^2\eta \\
& + \frac{1}{8}\xi^3 - \frac{3}{16}\xi^3\eta + \frac{1}{16}\xi^3\eta^3 - \frac{1}{16}\xi^2\eta^3 - \frac{1}{16}\xi\eta^3 + \frac{1}{16}\eta^3\Big) \\
+b\frac{\partial u_1}{\partial \eta} \quad & \Big(\frac{1}{8} - \frac{3}{16}\xi + \frac{3}{16}\xi\eta - \frac{1}{8}\eta + \frac{3}{16}\xi\eta^2 - \frac{1}{8}\eta^2 \\
& + \frac{1}{16}\xi^3 - \frac{1}{16}\xi^3\eta - \frac{1}{16}\xi^3\eta^2 + \frac{1}{16}\xi^3\eta^3 - \frac{3}{16}\xi\eta^3 + \frac{1}{8}\eta^3\Big) \\
+ab\frac{\partial^2 u_1}{\partial \xi \partial \eta} \quad & \frac{1}{16}\Big(1 - \xi + \xi\eta - \eta - \xi^2 + \xi^2\eta + \xi^2\eta^2 + \xi\eta^2 - \eta^2 \\
& + \xi^3 - \xi^3\eta - \xi^3\eta^2 + \xi^3\eta^3 - \xi^2\eta^3 - \xi\eta^3 + \eta 3\Big) \\
+u_2 \quad & \Big(\frac{1}{4} + \frac{3}{8}\xi - \frac{9}{16}\xi\eta - \frac{3}{8}\eta - \frac{1}{8}\xi^3 + \frac{3}{16}\xi^3\eta \\
& - \frac{1}{16}\xi^3\eta^3 + \frac{3}{16}\xi\eta^3 + \frac{1}{8}\eta^3\Big) \\
+a\frac{\partial u_2}{\partial \xi} \quad & \Big(-\frac{1}{8} - \frac{1}{8}\xi + \frac{3}{16}\xi\eta + \frac{3}{16}\eta + \frac{1}{8}\xi^2 - \frac{3}{16}\xi^2\eta \\
& + \frac{1}{8}\xi^3 - \frac{3}{16}\xi^3\eta + \frac{1}{16}\xi^3\eta^3 + \frac{1}{16}\xi^2\eta^3 \\
& - \frac{1}{16}\xi\eta^3 - \frac{1}{16}\eta^3\Big) \\
+b\frac{\partial u_2}{\partial \eta} \quad & \Big(\frac{1}{8} + \frac{3}{16}\xi - \frac{3}{16}\xi\eta - \frac{1}{8}\eta - \frac{3}{16}\xi\eta^2 - \frac{1}{8}\eta^2 - \frac{1}{16}\xi^3 \\
& + \frac{1}{16}\xi^3\eta + \frac{1}{16}\xi^3\eta^2 - \frac{1}{16}\xi^3\eta^3 + \frac{3}{16}\xi\eta^3 + \frac{1}{8}\eta^3\Big) \\
+ab\frac{\partial^2 u_2}{\partial \xi \partial \eta} \quad & \frac{1}{16}\Big(-1 - \xi + \xi\eta + \eta + \xi^2 - \xi^2\eta - \xi^2\eta^2 + \xi\eta^2 \\
& + \eta^2 + \xi^3 - \xi^3\eta - \xi^3\eta^2 + \xi^3\eta^3 + \xi^2\eta^3 - \xi\eta^3 - \eta 3\Big) \\
+u_3 \quad & \Big(\frac{1}{4} + \frac{3}{8}\xi + \frac{9}{16}\xi\eta + \frac{3}{8}\eta - \frac{1}{8}\xi^3 - \frac{3}{16}\xi^3\eta \\
& + \frac{1}{16}\xi^3\eta^3 - \frac{3}{16}\xi\eta^3 - \frac{1}{8}\eta^3\Big)
\end{aligned}
$$

$$
\begin{aligned}
+a\frac{\partial u_3}{\partial \xi} \quad & \left(-\frac{1}{8}-\frac{1}{8}\xi-\frac{3}{16}\xi\eta-\frac{3}{16}\eta+\frac{1}{8}\xi^2+\frac{3}{16}\xi^2\eta\right. \\
& \left.+\frac{1}{8}\xi^3+\frac{3}{16}\xi^3\eta-\frac{1}{16}\xi^3\eta^3-\frac{1}{16}\xi^2\eta^3+\frac{1}{16}\xi\eta^3+\frac{1}{16}\eta^3\right) \\
+b\frac{\partial u_3}{\partial \eta} \quad & \left(-\frac{1}{8}-\frac{3}{16}\xi-\frac{3}{16}\xi\eta-\frac{1}{8}\eta+\frac{3}{16}\xi\eta^2+\frac{1}{8}\eta^2\right. \\
& \left.+\frac{1}{16}\xi^3+\frac{1}{16}\xi^3\eta-\frac{1}{16}\xi^3\eta^2-\frac{1}{16}\xi^3\eta^3+\frac{3}{16}\xi\eta^3+\frac{1}{8}\eta^3\right) \\
+ab\frac{\partial^2 u_3}{\partial \xi \partial \eta} \quad & \frac{1}{16}\left(1+\xi+\xi\eta+\eta-\xi^2-\xi^2\eta+\xi^2\eta^2-\xi\eta^2-\eta^2\right. \\
& \left.-\xi^3-\xi^3\eta+\xi^3\eta^2+\xi^3\eta^3+\xi^2\eta^3-\xi\eta^3-\eta 3\right) \\
+u_4 \quad & \left(\frac{1}{4}-\frac{3}{8}\xi-\frac{9}{16}\xi\eta+\frac{3}{8}\eta+\frac{1}{8}\xi^3+\frac{3}{16}\xi^3\eta\right. \\
& \left.-\frac{1}{16}\xi^3\eta^3+\frac{3}{16}\xi\eta^3-\frac{1}{8}\eta^3\right) \\
+a\frac{\partial u_4}{\partial \xi} \quad & \left(\frac{1}{8}-\frac{1}{8}\xi-\frac{3}{16}\xi\eta+\frac{3}{16}\eta-\frac{1}{8}\xi^2-\frac{3}{16}\xi^2\eta+\frac{1}{8}\xi^3\right. \\
& \left.+\frac{3}{16}\xi^3\eta-\frac{1}{16}\xi^3\eta^3+\frac{1}{16}\xi^2\eta^3+\frac{1}{16}\xi\eta^3-\frac{1}{16}\eta^3\right) \\
+b\frac{\partial u_4}{\partial \eta} \quad & \left(-\frac{1}{8}+\frac{3}{16}\xi+\frac{3}{16}\xi\eta-\frac{1}{8}\eta-\frac{3}{16}\xi\eta^2+\frac{1}{8}\eta^2\right. \\
& \left.-\frac{1}{16}\xi^3-\frac{1}{16}\xi^3\eta+\frac{1}{16}\xi^3\eta^2+\frac{1}{16}\xi^3\eta^3-\frac{3}{16}\xi\eta^3+\frac{1}{8}\eta^3\right) \\
+ab\frac{\partial^2 u_4}{\partial \xi \partial \eta} \quad & \frac{1}{16}\left(-1+\xi+\xi\eta-\eta+\xi^2+\xi^2\eta-\xi^2\eta^2-\xi\eta^2\right. \\
& \left.+\eta^2-\xi^3-\xi^3\eta+\xi^3\eta^2+\xi^3\eta^3-\xi^2\eta^3-\xi\eta^3+\eta 3\right) \qquad (3.32)
\end{aligned}
$$

Similar equations can be written for $v(\xi,\eta)$ and $w(\xi,\eta)$ from which $[M(\xi,\eta)]_{Pl}$ and $[N(\xi,\eta)]_{Pl}$ can be identified. Equations 3.30 can be reformulated as

$$\{d(\xi,\eta)\}_{Pl} = [S]_{Pl}\{a\}_{Pl} \qquad (3.33)$$

where

$$\{d(\xi,\eta)\}_{Pl} = \begin{Bmatrix} u(\xi,\eta) \\ v(\xi,\eta) \\ w(\xi,\eta) \end{Bmatrix} \qquad (3.34)$$

and

$$[S]_{Pl} = \begin{bmatrix} [L(\xi,\eta)]_{Pl} \\ [M(\xi,\eta)]_{Pl} \\ [N(\xi,\eta)]_{Pl} \end{bmatrix} \tag{3.35}$$

The shape functions shown in Equation 3.32, along with similar ones that could be written for $v(\xi,\eta)$ and $w(\xi,\eta)$, will ensure convergence of the solution as the number of finite elements used to model a given problem increases, by satisfying the criteria for completeness. The shape functions in all three directions are conforming, that is they ensure continuity of the displacement function and its slopes along all four element boundaries. This is required for w since the second derivatives of w are contained in the expression for the strains, as shown in Equations 3.20–3.22. Only the first derivatives of u and v are required for the strains in the X and Y–directions, but the higher order deflection fields will allow the intra-element bearing surface to be modeled more accurately. Zienkiewicz (1977) shows on how these shape functions can be found.

In order to identify the components of the shape function vector, the following identities must be taken into account:

$$\begin{aligned} \frac{\partial(\,)}{\partial\xi} &= \frac{\Delta x}{2}\frac{\partial(\,)}{\partial x} \\ \frac{\partial(\,)}{\partial\eta} &= \frac{\Delta y}{2}\frac{\partial(\,)}{\partial y} \\ \frac{\partial^2(\,)}{\partial\xi\partial\eta} &= \frac{\Delta x\Delta y}{4}\frac{\partial^2(\,)}{\partial x\partial y} \end{aligned} \tag{3.36}$$

3.5.4 Virtual Deformations

Substituting the finite element approximations from Equations 3.30 into Equations 3.20–3.22, the expressions for the strains, results in

$$\begin{aligned}
\epsilon_{Pl_x} &= \left[\frac{2}{\Delta x}\frac{\partial\left[L\left(\xi,\eta\right)\right]_{Pl}}{\partial\xi} - z\left(\frac{2}{\Delta x}\right)^2\frac{\partial^2\left[N\left(\xi,\eta\right)\right]_{Pl}}{\partial\xi^2}\right]\left\{a\right\}_{Pl} \\
&\quad + \frac{2}{\Delta x^2}\left\{a\right\}_{Pl}^T\frac{\partial\left[N\left(\xi,\eta\right)\right]_{Pl}^T}{\partial\xi}\frac{\partial\left[N\left(\xi,\eta\right)\right]_{Pl}}{\partial\xi}\left\{a\right\}_{Pl} \\
\epsilon_{Pl_y} &= \left[\frac{2}{\Delta y}\frac{\partial\left[M\left(\xi,\eta\right)\right]_{Pl}}{\partial\eta} - z\left(\frac{2}{\Delta y}\right)^2\frac{\partial^2\left[N\left(\xi,\eta\right)\right]_{Pl}}{\partial\eta^2}\right]\left\{a\right\}_{Pl} \\
&\quad + \frac{2}{\Delta y^2}\left\{a\right\}_{Pl}^T\frac{\partial\left[N\left(\xi,\eta\right)\right]_{Pl}^T}{\partial\eta}\frac{\partial\left[N\left(\xi,\eta\right)\right]_{Pl}}{\partial\eta}\left\{a\right\}_{Pl} \qquad (3.37) \\
\epsilon_{Pl_{xy}} &= \left[\frac{2}{\Delta y}\frac{\partial\left[L\left(\xi,\eta\right)\right]_{Pl}}{\partial\eta} + \frac{2}{\Delta x}\frac{\partial\left[M\left(\xi,\eta\right)\right]_{Pl}}{\partial\xi}\right. \\
&\quad \left. -2z\frac{4}{\Delta x\Delta y}\frac{\partial^2\left[N\left(\xi,\eta\right)\right]_{Pl}}{\partial\xi\partial\eta}\right]\left\{a\right\}_{Pl} \\
&\quad + \frac{4}{\Delta x\Delta y}\left\{a\right\}_{Pl}^T\frac{\partial\left[N\left(\xi,\eta\right)\right]_{Pl}^T}{\partial\xi}\frac{\partial\left[N\left(\xi,\eta\right)\right]_{Pl}}{\partial\eta}\left\{a\right\}_{Pl}
\end{aligned}$$

Equations 3.37 show that the strains in an element are a function of the nodal displacement vector, $\{a\}_{Pl}$, and is comprised of two components, a linear one, corresponding to the usual strain assumptions, and a quadratic one, corresponding to the large displacement assumptions.

Since the solution to the problem will be based on the principle of virtual work, an equation is required to describe the virtual change in the strain produced by a virtual

change in the nodal displacements is required. Let:

$$\begin{aligned}
\epsilon_{Pl_x} &= \left[[KX_1(\xi,\eta,\zeta)] + [KX_2(\xi,\eta,\zeta)] + \left[\frac{1}{2}MX(\xi,\eta)\right]\right]\{a\}_{Pl} \\
\epsilon_{Pl_y} &= \left[[KY_1(\xi,\eta,\zeta)] + [KY_2(\xi,\eta,\zeta)] + \left[\frac{1}{2}MY(\xi,\eta)\right]\right]\{a\}_{Pl} \\
\epsilon_{Pl_{xy}} &= \left[[KXY_1(\xi,\eta,\zeta)] + [KXY_2(\xi,\eta,\zeta)] + \left[\frac{1}{2}MXY(\xi,\eta)\right]\right]\{a\}_{Pl}
\end{aligned} \tag{3.38}$$

where the matrices $[KX_1]$, $[KX_2]$, $[KY_1]$, $[KY_2]$, $[KXY_1]$, $[KXY_2]$, $[MX]$, $[MY]$, and $[MXY]$ are given as:

$$\begin{aligned}
[KX_1(\xi,\eta,\zeta)] &= \frac{2}{\Delta x}\frac{\partial[L(\xi,\eta)]}{\partial\xi} \\
[KX_2(\xi,\eta,\zeta)] &= -\frac{4z}{\Delta x^2}\frac{\partial^2[N(\xi,\eta)]}{\partial\xi^2} \\
[KY_1(\xi,\eta,\zeta)] &= \frac{2}{\Delta y}\frac{\partial[M(\xi,\eta)]}{\partial\eta} \\
[KY_2(\xi,\eta,\zeta)] &= -\frac{4z}{\Delta y^2}\frac{\partial^2[N(\xi,\eta)]}{\partial\eta^2} \\
[KXY_1(\xi,\eta,\zeta)] &= \frac{2}{\Delta y}\frac{\partial[L(\xi,\eta)]}{\partial\eta} + \frac{2}{\Delta x}\frac{\partial[M(\xi,\eta)]}{\partial\eta} \\
[KXY_2(\xi,\eta,\zeta)] &= -\frac{8z}{\Delta x\Delta y}\frac{\partial^2[N(\xi,\eta)]}{\partial\xi\partial\eta} \\
[MX(\xi,\eta,\zeta)] &= \frac{4}{\Delta x^2}\{a\}_{Pl}^T\frac{\partial[N(\xi,\eta)]^T}{\partial\xi}\frac{\partial[N(\xi,\eta)]}{\partial\xi} \\
[MY(\xi,\eta,\zeta)] &= \frac{4}{\Delta y^2}\{a\}_{Pl}^T\frac{\partial[N(\xi,\eta)]^T}{\partial\eta}\frac{\partial[N(\xi,\eta)]}{\partial\eta} \\
[MXY(\xi,\eta,\zeta)] &= \frac{4}{\Delta x\Delta y}\{a\}_{Pl}^T\left[\frac{\partial[N(\xi,\eta)]^T}{\partial\xi}\frac{\partial[N(\xi,\eta)]}{\partial\eta}\right. \\
&\quad \left.+\frac{\partial[N(\xi,\eta)]^T}{\partial\eta}\frac{\partial[N(\xi,\eta)]}{\partial\xi}\right] \\
&= [RXY(\xi,\eta)]^T + [RXY(\xi,\eta)]
\end{aligned} \tag{3.39}$$

Now, the virtual change in the strains, given a virtual change in the displacements,

will be given by

$$\begin{aligned}
\delta\epsilon_{Pl_x} &= [[KX_1(\xi,\eta,\zeta)] + [KX_2(\xi,\eta,\zeta)] + [MX(\xi,\eta)]]\{\delta a\}_{Pl} \\
\delta\epsilon_{Pl_y} &= [[KY_1(\xi,\eta,\zeta)] + [KY_2(\xi,\eta,\zeta)] + [MY(\xi,\eta)]]\{\delta a\}_{Pl} \\
\delta\epsilon_{Pl_{xy}} &= [[KXY_1(\xi,\eta,\zeta)] + [KXY_2(\xi,\eta,\zeta)] + [MXY(\xi,\eta)]]\{\delta a\}_{Pl}
\end{aligned} \tag{3.40}$$

3.5.5 Virtual Work Equations

After substituting Equations 3.39 into Equations 3.37, the strain vector can be written as

$$\{\epsilon\}_{Pl} = \begin{bmatrix} [KX_1]+[KX_2] \\ [KY_1]+[KY_2] \\ [KXY_1]+[KXY_2] \end{bmatrix} \{a\}_{Pl} + \begin{bmatrix} \frac{1}{2}\{a\}_{Pl}^T[MX] \\ \frac{1}{2}\{a\}_{Pl}^T[MY] \\ \{a\}_{Pl}^T[RXY] \end{bmatrix} \{a\}_{Pl} \tag{3.41}$$

or

$$\{\epsilon\}_{Pl} = \left[[B_0]_{Pl} + [B_1]_{Pl}\right]\{a\}_{Pl} + [B_2]_{Pl}\{a\}_{Pl} \tag{3.42}$$

The virtual strain vector, $\{\delta\epsilon\}_{Pl}$, can be obtained from Equation 3.40 as

$$\{\delta\epsilon\}_{Pl} = \begin{bmatrix} [KX_1]+[KX_2] \\ [KY_1]+[KY_2] \\ [KXY_1]+[KXY_2] \end{bmatrix} \{\delta a\}_{Pl} + \begin{bmatrix} \{a\}_{Pl}^T[MX] \\ \{a\}_{Pl}^T[MY] \\ \{a\}_{Pl}^T[RXY] \end{bmatrix} \{\delta a\}_{Pl} \tag{3.43}$$

or

$$\{\delta\epsilon\}_{Pl} = \left[[B_0]_{Pl} + [B_1]_{Pl}\right]\{\delta a\}_{Pl} + [B_3]_{Pl}\{\delta a\}_{Pl} \tag{3.44}$$

$[B_0]_{Pl}$, $[B_1]_{Pl}$, $[B_2]_{Pl}$, and $[B_3]_{Pl}$, are the strain–displacement matrices which contain the derivatives of the shape functions. Matrices $[B_0]_{Pl}$ and $[B_1]_{Pl}$ are defined in Equations 3.45 and 3.46. The elements of matrices $[B_2]_{Pl}$ and $[B_3]_{Pl}$ can be found from Equations 3.41 and 3.43 in a similar manner.

$$
[B_0]_{Pl} = \begin{bmatrix}
\begin{matrix}1\end{matrix} & \begin{matrix}2\end{matrix} & \begin{matrix}3\end{matrix} & \begin{matrix}4\end{matrix} & \begin{matrix}5\end{matrix} & \begin{matrix}6\end{matrix} \\
\frac{2}{\Delta x}\frac{\partial L_1(\xi,\eta)_{Pl}}{\partial \xi} & \frac{2}{\Delta x}\frac{\partial L_2(\xi,\eta)_{Pl}}{\partial \xi} & \frac{2}{\Delta x}\frac{\partial L_3(\xi,\eta)_{Pl}}{\partial \xi} & \frac{2}{\Delta x}\frac{\partial L_4(\xi,\eta)_{Pl}}{\partial \xi} & 0 & 0 \\
0 & 0 & 0 & 0 & \frac{2}{\Delta y}\frac{\partial M_1(\xi,\eta)_{Pl}}{\partial \eta} & \frac{2}{\Delta y}\frac{\partial M_2(\xi,\eta)_{Pl}}{\partial \eta} \\
\frac{2}{\Delta y}\frac{\partial L_1(\xi,\eta)_{Pl}}{\partial \eta} & \frac{2}{\Delta y}\frac{\partial L_2(\xi,\eta)_{Pl}}{\partial \eta} & \frac{2}{\Delta y}\frac{\partial L_3(\xi,\eta)_{PL}}{\partial \eta} & \frac{2}{\Delta y}\frac{\partial L_4(\xi,\eta)_{Pl}}{\partial \eta} & \frac{2}{\Delta x}\frac{\partial M_1(\xi,\eta)_{Pl}}{\partial \xi} & \frac{2}{\Delta x}\frac{\partial M_2(\xi,\eta)_{Pl}}{\partial \xi}
\end{bmatrix}
$$

(3.45)

$$
\begin{bmatrix}
\begin{matrix}7\end{matrix} & \begin{matrix}8\end{matrix} & \begin{matrix}9\end{matrix} & \begin{matrix}10\end{matrix} & \begin{matrix}11\end{matrix} & \begin{matrix}12\end{matrix} & \begin{matrix}13\end{matrix} & \begin{matrix}14\end{matrix} & \dots & \begin{matrix}48\end{matrix} \\
0 & 0 & 0 & 0 & 0 & 0 & \frac{2}{\Delta x}\frac{\partial L_5(\xi,\eta)_{Pl}}{\partial \xi} & \frac{2}{\Delta x}\frac{\partial L_6(\xi,\eta)_{Pl}}{\partial \xi} & \dots & 0 \\
\frac{2}{\Delta y}\frac{\partial M_3(\xi,\eta)_{Pl}}{\partial \eta} & \frac{2}{\Delta y}\frac{\partial M_4(\xi,\eta)_{Pl}}{\partial \eta} & 0 & 0 & 0 & 0 & 0 & 0 & \dots & 0 \\
\frac{2}{\Delta x}\frac{\partial M_3(\xi,\eta)_{Pl}}{\partial \xi} & \frac{2}{\Delta x}\frac{\partial M_4(\xi,\eta)_{Pl}}{\partial \xi} & 0 & 0 & 0 & 0 & \frac{2}{\Delta y}\frac{\partial L_5(\xi,\eta)_{Pl}}{\partial \eta} & \frac{2}{\Delta y}\frac{\partial L_6(\xi,\eta)_{Pl}}{\partial \eta} & \dots & 0
\end{bmatrix}
$$

$$
[B_1] = \begin{bmatrix}
\begin{matrix} 1 & 2 & 3 & 4 & 5 & 6 & 7 & 8 \end{matrix} & 9 & 10 & 11 \\
0\ 0\ 0\ 0\ 0\ 0\ 0\ 0 & -\frac{4z}{\Delta x^2}\frac{\partial^2 N_1(\xi,\eta)_{Pl}}{\partial \xi^2} & -\frac{4z}{\Delta x^2}\frac{\partial^2 N_2(\xi,\eta)_{Pl}}{\partial \xi^2} & -\frac{4z}{\Delta x^2}\frac{\partial^2 N_3(\xi,\eta)_{Pl}}{\partial \xi^2} \\
0\ 0\ 0\ 0\ 0\ 0\ 0\ 0 & -\frac{4z}{\Delta y^2}\frac{\partial^2 N_1(\xi,\eta)_{Pl}}{\partial \eta^2} & -\frac{4z}{\Delta y^2}\frac{\partial^2 N_2(\xi,\eta)_{Pl}}{\partial \eta^2} & -\frac{4z}{\Delta y^2}\frac{\partial^2 N_3(\xi,\eta)_{Pl}}{\partial \eta^2} \\
0\ 0\ 0\ 0\ 0\ 0\ 0\ 0 & -\frac{8z}{\Delta x \Delta y}\frac{\partial^2 N_1(\xi,\eta)_{Pl}}{\partial \xi \partial \eta} & -\frac{8z}{\Delta x \Delta y}\frac{\partial^2 N_2(\xi,\eta)_{Pl}}{\partial \xi \partial \eta} & -\frac{8z}{\Delta x \Delta y}\frac{\partial^2 N_3(\xi,\eta)_{Pl}}{\partial \xi \partial \eta}
\end{bmatrix}
$$

(3.46)

$$
\begin{bmatrix}
12 & 13\ 14\ 15\ 16\ 17\ 18\ 19\ 20 & 21 & \cdots & 48 \\
-\frac{4z}{\Delta x^2}\frac{\partial^2 N_4(\xi,\eta)_{Pl}}{\partial \xi^2} & 0\ 0\ 0\ 0\ 0\ 0\ 0\ 0 & -\frac{4z}{\Delta x^2}\frac{\partial^2 N_5(\xi,\eta)_{Pl}}{\partial \xi^2} & \cdots & -\frac{4z}{\Delta x^2}\frac{\partial^2 N_{16}(\xi,\eta)_{Pl}}{\partial \xi^2} \\
-\frac{4z}{\Delta y^2}\frac{\partial^2 N_4(\xi,\eta)_{Pl}}{\partial \eta^2} & 0\ 0\ 0\ 0\ 0\ 0\ 0\ 0 & -\frac{4z}{\Delta y^2}\frac{\partial^2 N_5(\xi,\eta)_{Pl}}{\partial \eta^2} & \cdots & -\frac{4z}{\Delta y^2}\frac{\partial^2 N_{16}(\xi,\eta)_{Pl}}{\partial \eta^2} \\
-\frac{8z}{\Delta x \Delta y}\frac{\partial^2 N_4(\xi,\eta)_{Pl}}{\partial \xi \partial \eta} & 0\ 0\ 0\ 0\ 0\ 0\ 0\ 0 & -\frac{8z}{\Delta x \Delta y}\frac{\partial^2 N_5(\xi,\eta)_{Pl}}{\partial \xi \partial \eta} & \cdots & -\frac{8z}{\Delta x \Delta y}\frac{\partial^2 N_{16}(\xi,\eta)_{Pl}}{\partial \xi \partial \eta}
\end{bmatrix}
$$

If $\{P\}_{Pl}$ is the vector of applied loads, the principle of virtual work implies

$$\int_V \{\delta\epsilon\}_{Pl}^T \{\sigma\}_{Pl} \, dv - \{\delta a\}_{Pl} \{P\}_{PL} - \int_A [S]_{Pl} \{\delta a\}_{Pl} \{q\} \, da = 0 \tag{3.47}$$

where, $\{\sigma\}_{Pl}$ is given by Equation 3.27, $\{P\}$ is a vector of loads applied at the nodes of the plate element, and $\{q\}$ is a vector of distributed loads applied to the surface of the element. $\{q\}$ is defined as

$$\{q\} = \begin{Bmatrix} \text{distributed load in the X-direction} \\ \text{distributed load in the Y-direction} \\ \text{distributed load in the Z-direction} \end{Bmatrix}$$

The integration in Equation 3.47 is carried out over the volume and surface area of the element.

Substituting Equations 3.27, 3.42, and 3.44 into Equation 3.47,

$$\{\delta a\}_{Pl}^T \Big[\int_V \left[[B_0]_{Pl}^T + [B_1]_{Pl}^T + [B_3]_{Pl}^T \right] [D]_{Pl} \left[[B_0]_{Pl} + [B_1]_{Pl} + [B_2]_{Pl} \right] \{a\}_{Pl} \, dv - \{P\}_{PL} - \int_A [S]_{Pl}^T \{q\} \, dA \Big] = 0 \tag{3.48}$$

since $\{\delta a\}$ is arbitrary, the equations of equilibrium are,

$$\begin{aligned} \psi\left(\{a\}_{Pl}\right) = \int_V \Big(& [B_0]_{Pl}^T [D]_{Pl} [B_0]_{Pl} + [B_0]_{Pl}^T [D]_{Pl} [B_1]_{Pl} + [B_0]_{Pl}^T [D]_{Pl} [B_2]_{Pl} \\ & + [B_1]_{Pl}^T [D]_{Pl} [B_0]_{Pl} + [B_1]_{Pl}^T [D]_{Pl} [B_1]_{Pl} + [B_1]_{Pl}^T [D]_{Pl} [B_2]_{Pl} \\ & + [B_3]_{Pl}^T [D]_{Pl} [B_0]_{Pl} + [B_3]_{Pl}^T [D]_{Pl} [B_1]_{Pl} \\ & + [B_3]_{Pl}^T [D]_{Pl} [B_2]_{Pl} \Big) \{a\}_{Pl} \, dv - \{P\}_{Pl} = 0 \end{aligned} \tag{3.49}$$

where,

$$\{P\}_{Pl} = \{P\} - \int_A [S]_{Pl}^T \{q\} \, dA \tag{3.50}$$

If the $-z$ term is factored out of the matrix $[B_1]_{Pl}$,

$$[B_1]_{Pl} = -z \, [B_4]_{Pl} \tag{3.51}$$

The integration in Z-direction can be carried out term by term as follows,

$$\int_{-1}^{1}\int_{-1}^{1}\int_{-t/2}^{t/2}\frac{\Delta x}{2}\frac{\Delta y}{2}\left([B_0]_{Pl}^T[D]_{Pl}[B_0]_{Pl}\right)d\xi\ d\eta\ dz = \int_{-1}^{1}\int_{-1}^{1}\frac{\Delta x\ \Delta y}{4}\left([B_0]_{Pl}^T[D_t]_{Pl}[B_0]_{Pl}\right)d\xi\ d\eta$$

$$\int_{-1}^{1}\int_{-1}^{1}\int_{-t/2}^{t/2}\frac{\Delta x}{2}\frac{\Delta y}{2}\left([B_0]_{Pl}^T[D]_{Pl}[B_4]_{Pl}\right)(-z)d\xi\ d\eta\ dz = \int_{-1}^{1}\int_{-1}^{1}\frac{\Delta x\ \Delta y}{4}\left([B_0]_{Pl}^T[D_t]_{Pl}[B_4]_{Pl}\right)\frac{(-z)^2}{2}\Bigg|_{-t/2}^{t/2}d\xi\ d\eta = [0]$$

$$\int_{-1}^{1}\int_{-1}^{1}\int_{-t/2}^{t/2}\frac{\Delta x}{2}\frac{\Delta y}{2}\left([B_0]_{Pl}^T[D]_{Pl}[B_2]_{Pl}\right)d\xi\ d\eta\ dz = \int_{-1}^{1}\int_{-1}^{1}\frac{\Delta x\ \Delta y}{4}\left([B_0]_{Pl}^T[D_t]_{Pl}[B_2]_{Pl}\right)d\xi\ d\eta$$

$$\int_{-1}^{1}\int_{-1}^{1}\int_{-t/2}^{t/2}\frac{\Delta x}{2}\frac{\Delta y}{2}\left([B_4]_{Pl}^T[D]_{Pl}[B_0]_{Pl}\right)(-z)d\xi\ d\eta\ dz = \int_{-1}^{1}\int_{-1}^{1}\frac{\Delta x\ \Delta y}{4}\left([B_4]_{Pl}^T[D_t]_{Pl}[B_0]_{Pl}\right)\frac{(-z)^2}{2}\Bigg|_{-t/2}^{t/2}d\xi\ d\eta = [0] \tag{3.52}$$

$$\int_{-1}^{1}\int_{-1}^{1}\int_{-t/2}^{t/2}\frac{\Delta x}{2}\frac{\Delta y}{2}\left([B_4]_{Pl}^T[D]_{Pl}[B_4]_{Pl}\right)d\xi\ d\eta\ dz = \int_{-1}^{1}\int_{-1}^{1}\frac{\Delta x\ \Delta y}{4}\left([B_4]_{Pl}^T[D_I]_{Pl}[B_4]_{Pl}\right)d\xi\ d\eta$$

$$\int_{-1}^{1}\int_{-1}^{1}\int_{-t/2}^{t/2}\frac{\Delta x}{2}\frac{\Delta y}{2}\left([B_4]_{Pl}^T[D]_{Pl}[B_2]_{Pl}\right)(-z)d\xi\ d\eta\ dz = \int_{-1}^{1}\int_{-1}^{1}\frac{\Delta x\ \Delta y}{4}\left([B_4]_{Pl}^T[D_t]_{Pl}[B_2]_{Pl}\right)\frac{(-z)^2}{2}\Bigg|_{-t/2}^{t/2}d\xi\ d\eta = [0]$$

$$\int_{-1}^{1}\int_{-1}^{1}\int_{-t/2}^{t/2}\frac{\Delta x}{2}\frac{\Delta y}{2}\left([B_3]_{Pl}^T[D]_{Pl}[B_0]_{Pl}\right)d\xi\ d\eta\ dz = \int_{-1}^{1}\int_{-1}^{1}\frac{\Delta x\ \Delta y}{4}\left([B_3]_{Pl}^T[D_t]_{Pl}[B_0]_{Pl}\right)d\xi\ d\eta$$

$$\int_{-1}^{1}\int_{-1}^{1}\int_{-t/2}^{t/2}\frac{\Delta x}{2}\frac{\Delta y}{2}\left([B_3]_{Pl}^{T}[D]_{Pl}[B_4]_{Pl}\right)(-z)d\xi\ d\eta\ dz\ =$$
$$\int_{-1}^{1}\int_{-1}^{1}\frac{\Delta x\ \Delta y}{4}\left([B_3]_{Pl}^{T}[D_t]_{Pl}[B_4]_{Pl}\right)\frac{(-z)^2}{2}\Bigg|_{-t/2}^{t/2}d\xi\ d\eta\ =\ [0]$$

$$\int_{-1}^{1}\int_{-1}^{1}\int_{-t/2}^{t/2}\frac{\Delta x}{2}\frac{\Delta y}{2}\left([B_3]_{Pl}^{T}[D]_{Pl}[B_2]_{Pl}\right)d\xi\ d\eta\ dz\ =$$
$$\int_{-1}^{1}\int_{-1}^{1}\frac{\Delta x\ \Delta y}{4}\left([B_3]_{Pl}^{T}[D_t]_{Pl}[B_2]_{Pl}\right)d\xi\ d\eta$$

where,

$$[D_t]_{Pl} = t\,[D]_{Pl} \tag{3.53}$$

and

$$[D_I]_{Pl} = I_{Pl}\,[D]_{Pl} \tag{3.54}$$

t is the sheathing thickness and I_{Pl} is the moment of inertia for a unit width strip of the sheathing in the direction of interest.

Now, if Equations 3.52 are substituted into Equation 3.49, the resulting equation is

$$\begin{aligned}\psi\left(\{a\}_{Pl}\right) = \int_A \frac{\Delta x\ \Delta y}{2}\Big([B_0]_{Pl}^{T}[D_t]_{Pl}[B_0]_{Pl} + [B_0]_{Pl}^{T}[D_t]_{Pl}[B_2]_{Pl}\\ + [B_4]_{Pl}^{T}[D_I]_{Pl}[B_4]_{Pl} + [B_3]_{Pl}^{T}[D_t]_{Pl}[B_0]_{Pl}\\ + [B_3]_{Pl}^{T}[D_t]_{Pl}[B_2]_{Pl}\Big)\{a\}_{Pl}\,dA - \{P\}_{Pl} = 0\end{aligned} \tag{3.55}$$

This equation can be reformulated as

$$\psi\{a\} = [k_s]_{Pl}\{a\}_{Pl} - \{P\}_{Pl} = 0 \tag{3.56}$$

where the secant stiffness matrix, $[k_s]_{Pl}$, can be found as

$$\begin{aligned}[k_s]_{Pl} = \int_A \frac{\Delta x\ \Delta y}{2}\Big([B_0]_{Pl}^{T}[D_t]_{Pl}[B_0]_{Pl} + [B_0]_{Pl}^{T}[D_t]_{Pl}[B_2]_{Pl}\\ + [B_4]_{Pl}^{T}[D_I]_{Pl}[B_4]_{Pl} + [B_3]_{Pl}^{T}[D_t]_{Pl}[B_0]_{Pl}\\ + [B_3]_{Pl}^{T}[D_t]_{Pl}[B_2]_{Pl}\Big)\,dA\end{aligned} \tag{3.57}$$

Since, $[B_2]_{Pl}$ and $[B_3]_{Pl}$ are dependent on the displacements $\{a\}_{Pl}$, the stiffness matrix, $[k_s]_{Pl}$, is also dependent on $\{a\}_{Pl}$. Therefore, the solution will have to be an iterative one. A Newton–Raphson method employing the tangential stiffness is used to solve the problem.

If an initial trial solution, $\{a_1\}_{Pl}$, is found using Equation 3.55, and evaluating $[k_s]_{Pl}$ with $\{a\}_{Pl} = \{0\}$ as

$$\{a_1\}_{Pl} = [k_s]_{Pl}^{-1} \{P\}_{Pl} \tag{3.58}$$

then, an improved solution can be obtained using a truncated Taylor series as

$$\psi\left(\{a_{n+1}\}_{Pl}\right) = \psi\left(\{a_n\}_{Pl}\right) + \left(\frac{d\psi\left(\{a\}_{Pl}\right)}{d\{a_n\}_{Pl}}\right)\{\Delta a_n\}_{Pl} \tag{3.59}$$

where $\{a_{n+1}\}_{Pl} = \{a_n\}_{Pl} + \{\Delta a_n\}_{Pl}$ and

$$\begin{aligned}\left(\frac{d\psi\left(\{a\}_{pa}\right)}{d\{a_n\}_{Pl}}\right) &= \frac{d}{d\{a\}_{Pl}}\left(\int_A \frac{\Delta x\,\Delta y}{2}\left([B_0]_{Pl}^T [D_t]_{Pl} [B_0]_{Pl} + [B_0]_{Pl}^T [D_t]_{Pl} [B_2]_{Pl}\right.\right. \\ &\quad + [B_4]_{Pl}^T [D_I]_{Pl} [B_4]_{Pl} + [B_3]_{Pl}^T [D_t]_{Pl} [B_0]_{Pl} \\ &\quad \left.\left. + [B_3]_{Pl}^T [D_t]_{Pl} [B_2]_{Pl}\right)\{a_{n+1}\}_{Pl}\, dA\right) \\ &= [k_t]_{Pl}\end{aligned} \tag{3.60}$$

$[k_t]_{Pl}$ = the tangential stiffness matrix for the plate element.

3.6 The Sheathing Connector Element

The sheathing connector element models the material used to attach the sheathing to the framing of the shear wall. Traditionally, the connection has used common nails of sufficient length to provide the required strength for the connection. This connection has also been the weak link of the shear wall system. The predominant mode of failure has been the nails in this joint, either pulling out of the framing, or pulling through the

sheathing, or breaking. Yielding of the nails between the framing and sheathing, is also the main source of ductility for the wall system. The crushing of the wood fibers around the nail, the friction between the sheathing and framing, and yielding of the nails are the mechanisms for the wall to dissipate energy during loading.

Today, new methods of constructing timber shear walls utilize screws, staples, and adhesives to hold the sheathing to the framing. These new connections vary significantly in their behavior, from the traditional common nails. In some cases, the new fasteners may change the mode of failure in a shear wall from the ductile failure of the sheathing nail to one that is brittle, such as a tension failure in the end stud of the framing.

Since the sheathing connection has the most significant effect on the load–deflection and energy dissipating characteristics of the wall, it is important that it be modeled as realistically as possible. The following derivation of the connector element has been used to allow connections to be modeled as either a smeared line connector, such as an adhesive, or as a discrete connector, such as an individual nail.

Figure 3.7 shows an exploded view of a shear wall with the plate and beam elements, along with spring connectors that represent the sheathing connection connectors used in the model. This figure shows the essentials of how timber shear walls are modeled in the program, **SHWALL**.

3.6.1 Geometry

Figure 3.8a shows a sheathing element connected to a framing element. The sheathing element's nodes are numbered 1 to 4, and the beam element has nodes i and j. Assume points P and P' are a pair of points with the same X–Y coordinates in the unloaded state, except point P is located on the plate element, and point P' is located on the beam element.

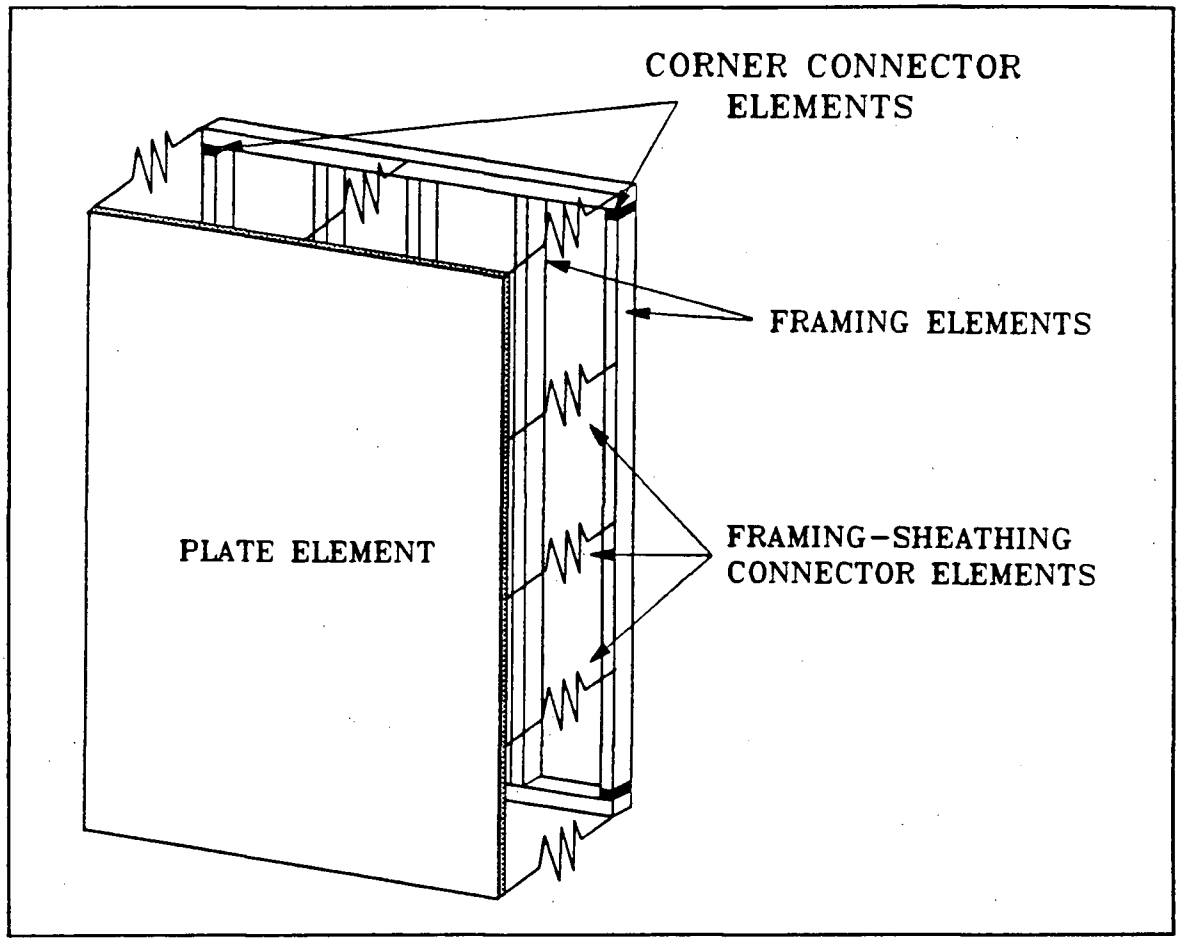

Figure 3.7: Exploded View of Shear Wall Model.

When the system is loaded, the relative displacement between points P and P' will represent the deformation of the connecting element at point P. Figure 3.8b shows two components of the connection deformation. Let $\Delta\bar{u}$ and $\Delta\bar{v}$ be the relative displacements of P with respect to P', parallel and perpendicular to the main axis of the beam element. The force required to produce this deformation will depend on the angle Θ and the load-deformation characteristics of the connector. In general, there will also be components of deflection and force in the Z–direction (out–of–plane direction).

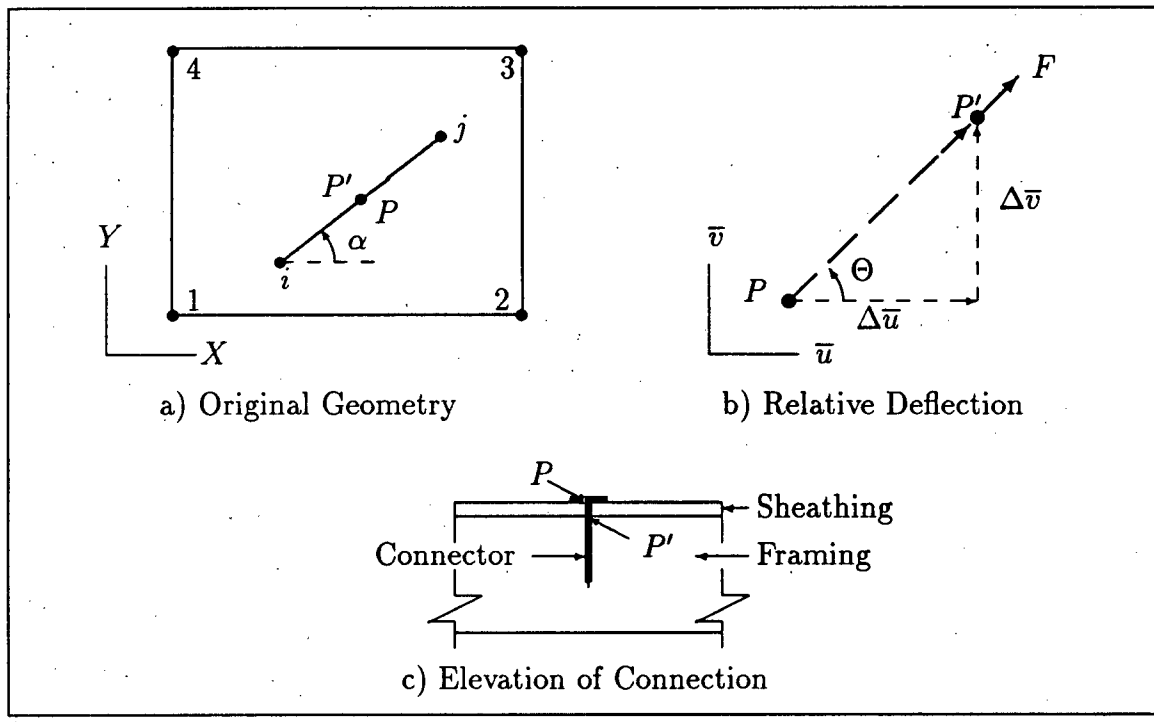

Figure 3.8: Sheathing Connector Element Geometry.

3.6.2 Deflections

The connector element will not have any nodes of its own, but will use the nodes and the associated DOF of the two elements it connects. Therefore, the sheathing connector will have a total of 56 DOF, 6 for the beam element, and 48 for the plate element. The relative deflection of P with respect to P' can be found by calculating the deflection of each point, then subtracting the deflections of P' from P.

The deflection of P' can be calculated using the local coordinate system shown in Figure 3.1 and Equation 3.5. The initial local coordinates of P' on the beam can be

calculated using the local variable s as,

$$\begin{aligned} x_{P'} &= x_i + s\cos\alpha \\ y_{P'} &= y_i + s\sin\alpha \end{aligned} \tag{3.61}$$

solving for s

$$s = \frac{x_{P'} - x_i}{\cos\alpha} = \frac{y_{P'} - y_i}{\sin\alpha} \tag{3.62}$$

The displacements $u_{P'}$ and $v_{P'}$ can be calculated using Equations 3.5 as

$$\{d\}^*_{P'} = \begin{Bmatrix} u^*_{P'} \\ v^*_{P'} \end{Bmatrix} = [J(s)]_b \{a\}_b \tag{3.63}$$

Since the displacements, $\{d\}^*_{P'}$ are oriented parallel and perpendicular to the beam's axis, they must be transformed to the plate element's coordinates as follows

$$\{d\}_{P'} = [T]\{d\}^*_{P'} = [T][J(s)]_b \{a\}_b = [J^*(s)]_b \{a\}_b \tag{3.64}$$

where

$$[T] = \begin{bmatrix} \cos\alpha & \sin\alpha & 0 & 0 & 0 & 0 \\ -\sin\alpha & \cos\alpha & 0 & 0 & 0 & 0 \\ 0 & 0 & 1 & 0 & 0 & 0 \\ 0 & 0 & 0 & \cos\alpha & \sin\alpha & 0 \\ 0 & 0 & 0 & -\sin\alpha & \cos\alpha & 0 \\ 0 & 0 & 0 & 0 & 0 & 1 \end{bmatrix} \tag{3.65}$$

The deflection $w_{P'} = 0$, since the beam is assumed to not deflect in the Z-direction.

The localized coordinates of point P can be found by reformulating equations 3.29

$$\begin{aligned} \xi_P &= \frac{2(x_P - x_c)}{\Delta x} \\ \eta_P &= \frac{2(y_P - y_c)}{\Delta y} \end{aligned} \tag{3.66}$$

The displacements u_P, v_P, and w_P can now be found from Equations 3.30 as

$$\begin{aligned} u_P &= [L(\xi_P, \eta_P)]_{Pl} \{a\}_{Pl} \\ v_P &= [M(\xi_P, \eta_P)]_{Pl} \{a\}_{Pl} \\ w_P &= [N(\xi_P, \eta_P)]_{Pl} \{a\}_{Pl} \end{aligned} \tag{3.67}$$

$[L(\xi_P, \eta_P)]_{Pl}$, $[M(\xi_P, \eta_P)]_{Pl}$, and $[N(\xi_P, \eta_P)]_{Pl}$ are the shape functions for the plate, evaluated at the local coordinates, (ξ_P, η_P).

Now, the connection deformation at point P–P' can be calculated as

$$\begin{aligned} \Delta u &= u_P - u_{P'} \\ \Delta v &= v_P - v_{P'} \\ \Delta w &= w_P - w_{P'} \end{aligned} \tag{3.68}$$

These equations can be written in a matrix formulation as

$$\begin{aligned} \Delta u &= [L(P - P')]_{con} \{a\}_{con} \\ \Delta v &= [M(P - P')]_{con} \{a\}_{con} \\ \Delta w &= [N(P - P')]_{con} \{a\}_{con} \end{aligned} \tag{3.69}$$

where,

$$[L\,(P-P')]^T_{con} = \begin{bmatrix} -J_1(s)\cos\alpha \\ -J_1(s)\sin\alpha \\ 0 \\ -J_4(s)\cos\alpha \\ -J_4(s)\sin\alpha \\ 0 \\ - \;- \;- \;- \;- \;- \;- \;- \;- \;- \\ [L\,(\xi_P,\eta_P)]_{Pl}\cos\alpha + [M\,(\xi_P,\eta_P)]_{Pl}\sin\alpha \end{bmatrix} \tag{3.70}$$

$$[M\,(P-P')]^T_{con} = \begin{bmatrix} L_2(s)\sin\alpha \\ -L_2(s)\cos\alpha \\ -L_3(s) \\ L_5(s)\sin\alpha \\ -L_5(s)\cos\alpha \\ -L_6(s) \\ - \;- \;- \;- \;- \;- \;- \;- \;- \;- \\ [-L\,(\xi_P,\eta_P)]_{Pl}\sin\alpha + [M\,(\xi_P,\eta_P)]_{Pl}\cos\alpha \end{bmatrix} \tag{3.71}$$

$$\{a\}_{con} = \begin{Bmatrix} \{a\}_b \\ - \;- \;- \;- \\ \{a\}_{Pl} \end{Bmatrix} \tag{3.72}$$

$$[N(P-P')]^T_{con} = \begin{bmatrix} 0 \\ 0 \\ 0 \\ 0 \\ 0 \\ 0 \\ - \; - \; - \; - \\ [N(\xi_P, \eta_P)]_{Pl} \end{bmatrix} \tag{3.73}$$

3.6.3 Connection Force

The load–deflection curves used for the connector is shown in Figures 3.9. The curve shown in Figure 3.9a is used for the forces in the X–Y plane, while the curve shown in Figure 3.9b is used for the out–of–plane forces. Figure 3.9a is shown for the absolute value of the deflection. The load would be negative for a negative deflection.

The force in the X–direction is initially modeled following the equation used by Foschi (1977),

$$|F_u| = (P_0 + K_2 |\Delta u|)\left(1 - \exp\left(\frac{-K_0 |\Delta u|}{P_0}\right)\right) \quad \text{for } |\Delta u| < |\Delta u|_{\max} \tag{3.74}$$

The curve used by Foschi is modified for deformations, $|\Delta u|$, larger than $|\Delta u|_{\max}$. The load capacity of the connector will decrease from the maximum load capacity according to the equation

$$|F_u| = \left[(P_0 + K_2 |\Delta u|_{\max})\left(1 - \exp\left(\frac{-K_0 |\Delta u|_{\max}}{P_0}\right)\right)\right] - K_3 (|\Delta u| - |\Delta u|_{\max}) \quad \text{for } |\Delta u| > |\Delta u|_{\max} \tag{3.75}$$

until a load capacity of 0 is reached.

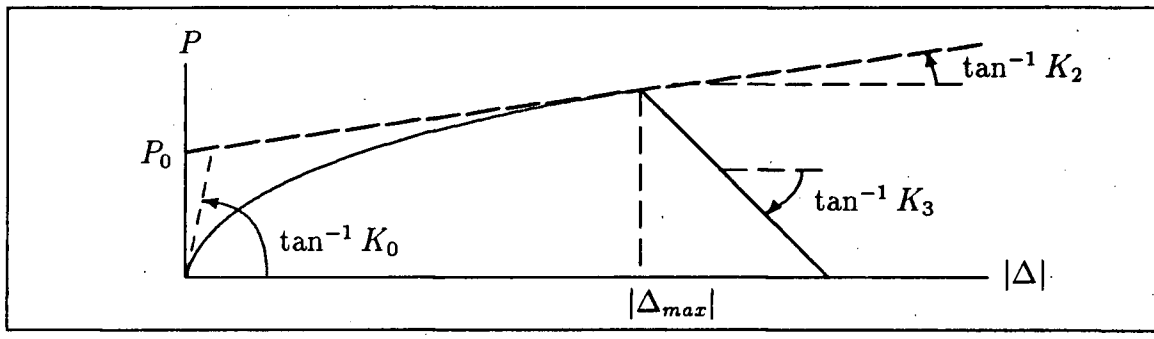

a) Curve for u and v Deflections

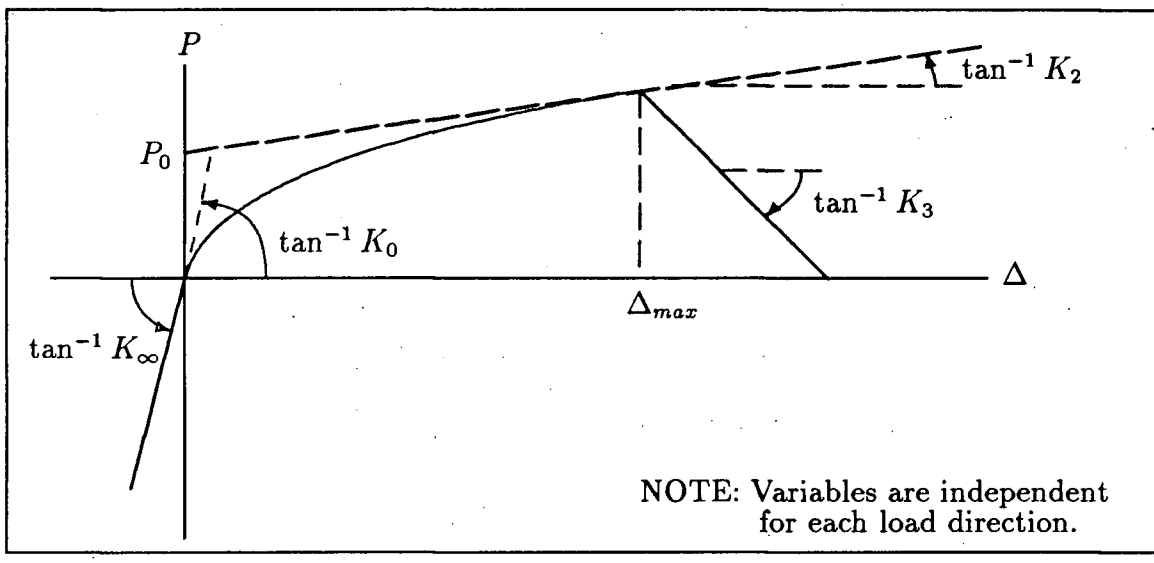

b) Curve for w Deflections (Out–of–Plane)

Figure 3.9: Load–Displacement Curves for Non–Linear Spring Connector Between Beams and Plate Elements

Similar equations can be written for the connector loads in the Y– and positive Z–directions. Deformations in the negative Z–direction would cause the plate element to bear on the framing. This possibility is accounted for in Figure 3.9b by the linear section of the curve in the negative load and displacement quadrant. The stiffness of the connector is changed in this case to a very high stiffness, to account for the additional stiffness of the sheathing bearing directly on the beams. The connector force in this case

can be calculated as

$$F_w = K_\infty \Delta w \qquad \text{for } \Delta w < 0 \tag{3.76}$$

The high stiffness, K_∞, results in high forces that prevent the sheathing from deflecting into the region defined by the beam elements. The plate element would be more flexible in bending if these bearing forces were not accounted for.

3.6.4 Energy Formulation of Stiffness Matrix

The total potential energy associated with the deformation of the connector over the length of the beam element is

$$\Pi_{con} = \int_0^{\Delta u} \left(\int_0^l \left((P_0 + K_2 \left|\Delta u\right|) \left(1 - \exp\left(\frac{-K_0 \left|\Delta u\right|}{P_0} \right) \right) ds \right) - \{P\}_{con} \right) du \tag{3.77}$$

To find the governing equations of equilibrium, which occur when the potential energy is at a minimum, the first variation of Equation 3.77 is performed with respect to $\{a\}_{con}$.

$$\begin{aligned} \delta\Pi_{con} \;=\; & \delta \{a\}_{con}^T \int_0^l \left[L \left(P - P' \right) \right]^T \left((P_0 + K_2 \left|\Delta u\right|) \left(1 - \exp\left(\frac{-K_0 \left|\Delta u\right|}{P_0} \right) \right) \right) \\ & dl \, \mathrm{sig}\left(\Delta u\right) - \delta \{a\}_{con}^T \{P\}_{con} = 0 \end{aligned} \tag{3.78}$$

where, sig(Δu) is the sign of the deflection.

Changing coordinates and substituting Equation 3.69

$$\begin{aligned} \delta\Pi_{con} \;=\; & \{\delta a\}_{con}^T \frac{nl}{2} \left(\int_{-1}^1 \left[L \left(P - P' \right) \right]_{con}^T \left(P_0 + K_2 \; \left| \left[L \left(P - P' \right) \right]_{con} \{a\}_{con} \right| \right) \right. \\ & \left. \left(1 - \exp\left(\frac{-K_1 \left| \left[L \left(P - P' \right) \right]_{con} \{a\}_{con} \right|}{P_0} \right) \right) \right. \\ & \left. \mathrm{sig} \left| \left[L \left(P - P' \right) \right]_{con} \{a\}_{con} \right| d\tau \right) - \{\delta a\}_{con}^T \{P\} = 0 \end{aligned} \tag{3.79}$$

where, n is the connector density. Since $\{\delta a\}_{con}$ is arbitrary, the equations of equilibrium are,

$$\begin{aligned}\psi(\{a\}_{con}) &= \frac{nl}{2}\int_{-1}^{1}([L(P-P')]_{con}(P_0 - K_2\ |[L(P-P')]_{con}\{a\}_{con}|) \\ &\left(1-\exp\left(\frac{-K_0\,|[L(P-P')]_{con}\{a\}_{con}|}{P_0}\right)\right) \\ &\text{sig}\,|[L(P-P')]_{con}\{a\}_{con}|\,ds) - \{P\} = 0\end{aligned} \tag{3.80}$$

The problem is to find $\{a\}_{con}$ so that $\psi(\{a\}_{con}) = 0$. The same iterative process is used as for the plate element in Equations 3.55–3.59, where the initial solution can be made using,

$$[k_{con}]_1 = \frac{nl}{2}\int_{-1}^{1}[L(P-P')]_{con}^{T}\,K_0\,[L(P-P')]_{con}\,d\tau \tag{3.81}$$

for the initial stiffness matrix, and

$$\begin{aligned}\frac{\partial\psi(\{a\}_{con})}{\partial\{a\}_{con}} = [k_t]_{con} &= \frac{nl}{2}\int_{-1}^{1}[L(P-P')]^{T}K_0 \\ &\left(1-\exp\left(\frac{-K_0\,|[L(P-P')]_{con}\{a\}_{con}|}{P_0}\right)\right)d\tau \\ &+\frac{nl}{2}\int_{-1}^{1}[L(P-P')]_{con}^{T}(P_0 + K_2\ |[L(P-P')]_{con}\{a\}_{con}|) \\ &\left(\frac{K_1}{P_0}\exp\left(\frac{-K_0\,|[L(P-P')]_{con}\{a\}_{con}|}{P_0}\right)\right)d\tau\end{aligned} \tag{3.82}$$

The tangent stiffness of the connector, $[k_t]_{con}$, will be a 54×54 symmetric matrix. The secant stiffness matrix for the connector, $[k_s]_{con}$, can be found from Equation 3.80 as,

$$\begin{aligned}[k_s]_{con} &= \frac{nl}{2}\int_{-1}^{1}([L(P-P')]_{con}(P_0 - K_2\ |[L(P-P')]_{con}\{a\}_{con}|) \\ &\left(1-\exp\left(\frac{-K_0\,|[L(P-P')]_{con}\{a\}_{con}|}{P_0}\right)\right)sig\,|[L(P-P')]_{con}\{a\}_{con}|\,ds\Bigg)\end{aligned} \tag{3.83}$$

The v and positive w directions will have similar equations.

For the linear regions of the load–deflection curve, such as the negative deflection region for Δw, the total energy to deform the connector is,

$$\Pi_{con} = \int_0^{\Delta w} \left(\int_{-1}^{1} \frac{nl}{2} F(w) d\tau - \{P\}_{con} \right) dw \tag{3.84}$$

Following the same process as that used for the exponential region of the load–deflection curve,

$$[k_s]_{con} = [k_t]_{con} = \frac{nl}{2} \int_{1-}^{1} \left([N(P - P')]_{con}^T K_\infty [N(P - P')]_{con} \right) d\tau \tag{3.85}$$

The equation for the stiffness matrices for the positive linear region is similar to Equation 3.85, except a stiffness equal to the stiffness at the maximum load replaces K_∞. The slope, K_3, can not be used to calculate the element stiffness matrix because a negative stiffness would mean energy could be generated by loading the member, which would violate the laws of physics.

Since the deflections of both the beam and the plate are cubic, a 4 point Gauss quadrature scheme is used to numerically integrate Equations 3.81, 3.83, and 3.85, when the connector is represented by a smeared line.

3.7 The Sheathing Bearing Connector Element

The sheathing bearing element, models the effects of two sheathing panels bearing on each other. This element is required to prevent adjacent elements from mathematically overlapping each other. Models that have been previously proposed, have either taken this effect into account, by giving adjacent plate elements common nodes, or have neglected the effect altogether.

Using common nodes between adjacent elements will overestimate the stiffness of the sheathing by not allowing the adjacent panels to move relative to each other, in the

direction perpendicular to the bearing. Models that neglect the effect of bearing will underestimate the sheathing stiffness, because the plate elements will be able to overlap each other with no resistance whatsoever.

Since the sheathing has the largest effect on the stiffness of a shear wall, provided the fasteners are sufficient to transfer the loads from the framing, it is imperative that this connector element model the effects of bearing, while allowing movement perpendicular to the bearing direction. The added stiffness of staggered joints, that has been shown to be significant in tests of diaphragms and large shear walls, will be accounted for by this finite element.

3.7.1 Geometry

Figure 3.10 shows the configuration of the sheathing bearing element. The element is modeled as a series of one–directional springs, connecting the edges of the two adjacent plate elements.

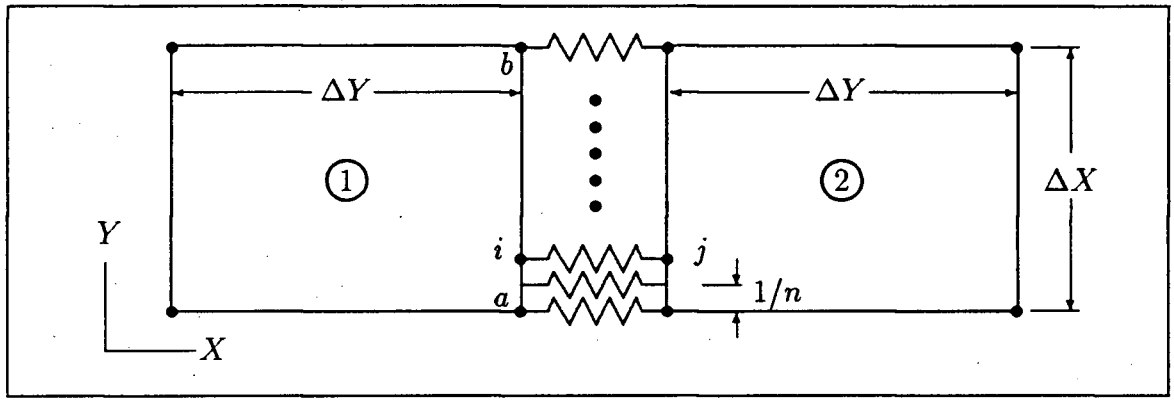

Figure 3.10: Sheathing Bearing Connector Element Configuration

3.7.2 Deflections

This bearing connector element will not have any nodes, but will use the nodes and associated degrees–of–freedom of the two plate elements that it joins. (This is the same method used for the sheathing connector, derived in Section 3.6 of this chapter.) If the connector were to have components of deflection in all directions, it would have a total of 96 degrees–of–freedom, 48 for each plate element connected. However, since the connector is only one–directional, 32 degrees–of–freedom are required, 16 for each plate element.

The deflections of points i and j, shown in Figure 3.10, can be calculated using Equations 3.30 as

$$\begin{aligned} u_i &= [L(\xi,\eta)_i]_{Pl}\{a\}_{Pl1} \\ u_j &= \left[L(\xi,\eta)_j\right]_{Pl}\{a\}_{Pl2} \end{aligned} \tag{3.86}$$

where, the subscripts $Pl1$ and $Pl2$ refer to plate elements 1 and 2 where, $[L(\xi,\eta)]_{Pl}$ is evaluated at points i and j.

The deflection for the connector between points i and j will then be

$$\Delta u_{con} = u_j - u_i \tag{3.87}$$

Substituting Equations 3.86 into Equation 3.87, and rearranging

$$\Delta u_{con} = [L]_{sc}\{a\}_{sc} \tag{3.88}$$

where

$$[L]_{sc} = \begin{bmatrix} -[L(\xi,\eta)]_{Pl1} \\ - - - - - \\ [L(\xi,\eta)]_{Pl2} \end{bmatrix} \quad \text{and} \quad \{a\}_{sc} = \begin{Bmatrix} \{a\}_{Pl1} \\ - - - - - \\ \{a\}_{Pl2} \end{Bmatrix} \tag{3.89}$$

3.7.3 Connector Forces

The force in the connector between points i and j can be found using the deflection calculated in Equation 3.88, and the load–deflection curve for the connector, shown in Figure 3.11. The force is

$$F = K_{sc}\Delta u_{con} \tag{3.90}$$

where,

$$\begin{aligned} K_{sc} &\approx 0 \quad \text{for} \quad \Delta u_{sc} > 0 \\ K_{sc} &\approx K_{\infty} \quad \text{for} \quad \Delta u_{sc} \leq 0 \end{aligned} \tag{3.91}$$

These equations will prevent the two plate elements from overlapping, while allowing the plate elements to separate.

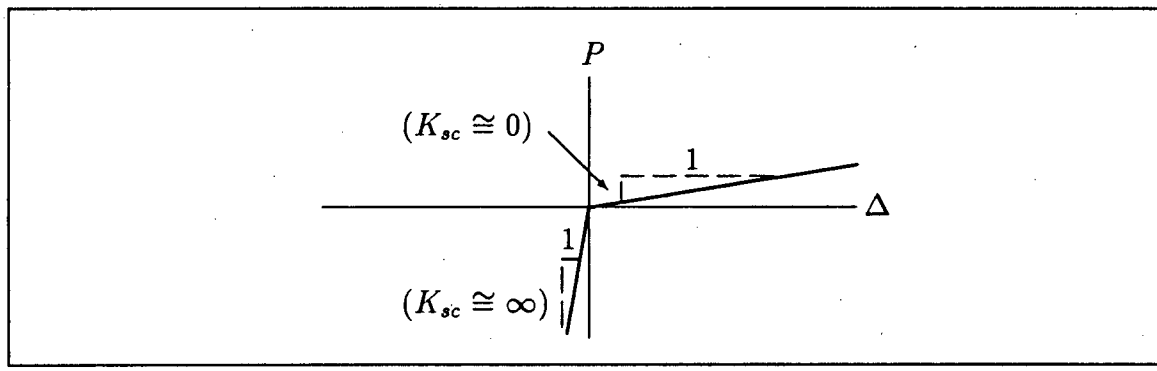

Figure 3.11: Sheathing Bearing Connector Load–Deflection Curve.

3.7.4 Virtual Work

The potential energy of the connector can be calculated as

$$\Pi_{sc} = \int_0^u \left(\int_a^b K_{sc}\Delta u_{sc} du \right) - \{P\}_{sc}\, du \tag{3.92}$$

Substituting Equation 3.88 into Equation 3.92, taking the first variation with respect to $\{a\}_{sc}$, and setting the result equal to zero to find the minimum potential energy,

$$\delta\Pi_{sc} = \{\delta a\}_{sc}^{T}\left(\int_{a}^{b}[L]_{sc}^{T}K_{sc}[L]_{sc}\,dy - \{P\}_{sc}\right) = 0 \tag{3.93}$$

changing coordinates

$$\delta\Pi_{sc} = \{\delta a\}_{sc}^{T}\left(\frac{n\Delta Y}{2}\int_{-1}^{1}[L]_{sc}^{T}K_{sc}[L]_{sc}\{a\}_{sc}\,d\eta - \{P\}_{sc}\right) = 0 \tag{3.94}$$

Since, $\{\delta a\}_{sc}$ is arbitrary,

$$\psi(\{a\}_{sc}) = \frac{n\Delta Y}{2}\int_{-1}^{1}[L]_{sc}^{T}K_{sc}[L]_{sc}\{a\}_{sc}\,d\eta - \{P\}_{sc} = 0 \tag{3.95}$$

This equation can be written as

$$\psi(\{a\}_{sc}) = [k_s]_{sc_x}\{a\}_{sc} - \{P\}_{sc} = 0 \tag{3.96}$$

where $[k_s]_{sc_x}$ is the secant stiffness matrix.

Finally, the tangent stiffness matrix is found by differentiating Equation 3.95 with respect to $\{a\}_{sc}$.

$$\frac{d\psi(\{a\}_{sc})}{d\{a\}_{sc}} = [k_t]_{sc_x} = \frac{n\Delta Y}{2}\int_{-1}^{1}[L]_{sc}^{T}K_{sc}[L]_{sc}\,d\eta \tag{3.97}$$

A similar equation for a connector oriented in the Y–direction can be derived in the same manner as

$$[k_t]_{sc_y} = \frac{n\Delta X}{2}\int_{-1}^{1}[M]_{sc}^{T}K_{sc}[M]_{sc}\,d\xi \tag{3.98}$$

The value chosen for the stiffness of the connector in compression must be large, relative to the stiffness of the connector in tension. However, if the stiffness is too high, the connection can cause local deformations in the plate element. These local deformations can result in the sheathing element buckling, and the global stiffness matrix for the wall becoming singular. The nodal deflections of the plate element can be monitored by the program user to see if the local deformations are significant or not.

3.8 Global System of Equations and Solution

The element equations for the problem are assembled into the global system of equations, using the direct stiffness method. A detailed description of the direct stiffness method can be found in most finite element books, such as Desai and Abel (1972) or Zienkiewicz (1977). Equations 3.16, 3.56, 3.80, and 3.95 are merged together to obtain the global system of equations for the problem as,

$$\psi\left(\{a\}_{n+1}\right) = \psi\left(\{a\}_n\right) + \frac{d\psi\left(\{a\}_n\right)}{d\{a\}}\{\Delta a\}_n \tag{3.99}$$

where,

$$\psi\left(\{a\}_n\right) = [K_s]_n \{a\}_n - \{P\} \tag{3.100}$$

and

$$\frac{d\psi\left(\{a\}_n\right)}{d\{a\}} = [K_t]_n \tag{3.101}$$

The arrays $\{a\}$ and $\{P\}$ will have the following form

$$\{a\} = \begin{Bmatrix} \{a\}_b \\ - - - \\ \{a\}_{Pl} \end{Bmatrix} \text{and} \quad \{P\} = \begin{Bmatrix} \{P\}_b \\ - - - \\ \{P\}_{Pl} \end{Bmatrix} \tag{3.102}$$

The two stiffness matrices $[K_s]_n$ and $[K_t]$, which are the secant and tangent stiffness matrices, respectively, will have the form

$$[K] = \left[\begin{array}{c|c} \begin{array}{c}\text{Framing Stiffness}\\ +\\ \text{Corner}\\ \text{Connector Stiffness}\\ +\\ \text{Sheathing}\\ \text{Connector Stiffness}\end{array} & \text{SYMMETRIC} \\ \hline \begin{array}{c}\\ \text{Sheathing}\\ \text{Connector Stiffness}\\ \\ \\ \\ \\ \end{array} & \begin{array}{c}\text{Sheathing Stiffness +}\\ \text{Sheathing Connector}\\ \text{Stiffness +}\\ \text{Sheathing Bearing}\\ \text{Connector Stiffness}\end{array} \end{array}\right] \tag{3.103}$$

The solution of the global system of equations will be an iterative process and will follow the steps listed below:

1. Solve the equation

$$\{a\}_1 = [K_s]^{-1}\{P\}$$

where $\{a\}_1$ is the initial solution for the displacements and $[K_s]_1$ is the initial secant stiffness matrix that is calculated using $\{a\} = \{0\}$.

2. Solve the equation

$$\{a\}_n = [K_t]_n^{-1}\{R\}$$

where $\{a\}_n$ is the improved solution for the displacements, $[K_t]_n$ is the tangent stiffness matrix which is calculated using $\{a\}_{n-1}$, and $\{R\}_n$ is the residual force

array which is calculated as,

$$\{R\}_n = \{P\} - [K_s]_{n-1} \{a\}_{n-1}$$

3. Check to see if the solution found is close enough to the true answer to satisfy the accuracy requirements. The program, **SHWALL**, uses the change in the displacements as the measure of accuracy. If the condition

$$\sqrt{\sum_{i=1}^{NDOF} \left[(a_i^2)_n - (a_i^2)_{n-1}\right]} \leq TOL \sqrt{\sum_{i=1}^{NDOF} (a_i^2)_{n-1}}$$

is satisfied, then the solution $\{a\}_n$ is considered to be accurate enough. If the accuracy condition is not satisfied, steps 2 and 3 are repeated. The variables $NDOF$ and TOL represent the number of DOF and the allowable tolerance for the problem, respectively. The iteration process is continued until the solution is found within the accuracy requirements.

3.9 Summary

The numerical model, **SHWALL**, has been described along with the assumptions on which the model is based. Each of the five finite elements used by the model have been derived in detail, and the method used to combine the element equations into the global system of equations has been described. Finally, the Newton–Raphson method used to solve the global equations has been outlined.

The improvements incorporated in **SHWALL** include:

- The ultimate load capacity of the sheathing connector has been accounted for. This allows the ultimate load capacity shear walls to be predicted.
- The effects of bearing between adjacent sheathing elements is modeled which improves the prediction of the wall stiffness.

- The connections between framing members is represented by a bi–linear element which allows the bearing between framing members to be modeled.

- The out–of–plane bending effects of the sheathing are accounted for. While the out–of–plane bending is not important for the thicker sheathing sizes, it may be an important effect for thin flexible sheathing materials.

The Newton–Raphson method used to solve the global equations is presented at the end of the Chapter. The model's accuracy is verified in Chapter 9, where the predicted load–deflection curve is compared to static shear wall test results, for both plywood and waferboard sheathed walls.

Chapter 4

Closed Form Mathematical Model for Steady State Response

4.1 Introduction

In an effort to facilitate the transition from static, one–directional analysis to dynamic earthquake analysis, an intermediate analytical model is presented in this chapter. The intermediate model is a closed form mathematical model that predicts the non–linear steady state response of timber shear walls, when subjected to harmonic excitations.

Many non–linear structures exhibit hysteretic behavior due to either the presence of Coulomb friction or the elastoplastic behavior of the material. Figure 4.1 shows an idealized bi–linear hysteresis for a structure. If a structure exhibits hysteretic behavior, its load–deflection curves for cyclic loading will have a looping shape, as shown in Figure 4.1. The area contained within the loop represents the energy dissipated by the structure. The possibility of predicting the response of systems that exhibit bi–linear hysteresis was investigated by Caughey (1960). A similar analysis, using bi–linear hysteresis, was successfully used by Filiatrault and Cherry (1988) to investigate the effects of friction dampers on the steady state response of steel–framed buildings. In this chapter, the derivations used by Caughey and Filiatrault are extended to predict the steady state response of timber shear walls, when subjected to harmonic excitations, by modifying

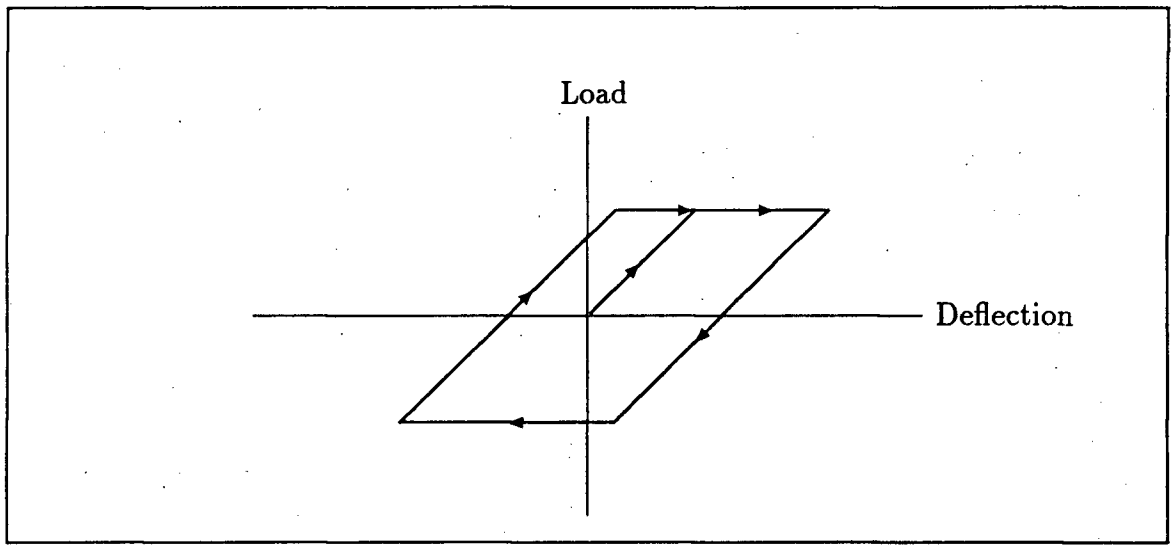

Figure 4.1: Bi–Linear Hysteresis for a Theoretical Structure.

the hysteresis to represent the pinching characteristics of nailed timber structures.

The ability to predict the responses of walls subjected to harmonic excitation would be helpful in estimating the structural integrity of buildings, for both new ones or those previously damaged during an earthquake. Not only does the steady state model give an indication of the natural frequency of walls, but it is also a quick method for estimating the maximum displacement expected during future earthquakes. The future prediction would require that an estimate be made of the previous deflections the wall has experienced, as well as the predominant frequency and acceleration magnitude of future earthquakes.

The governing assumptions are presented first, then the derivation of the model is given and the stability of the response of shear walls to harmonic excitation is discussed. A structure that exhibits stable response is defined by most authors, such as Thomson (1981), as one that has a single value for the response to each excitation. In other words, the structure will not exhibit a jump phenomenon analogous to the jump phenomenon in buckling analysis. Finally, an example of the model is presented and the

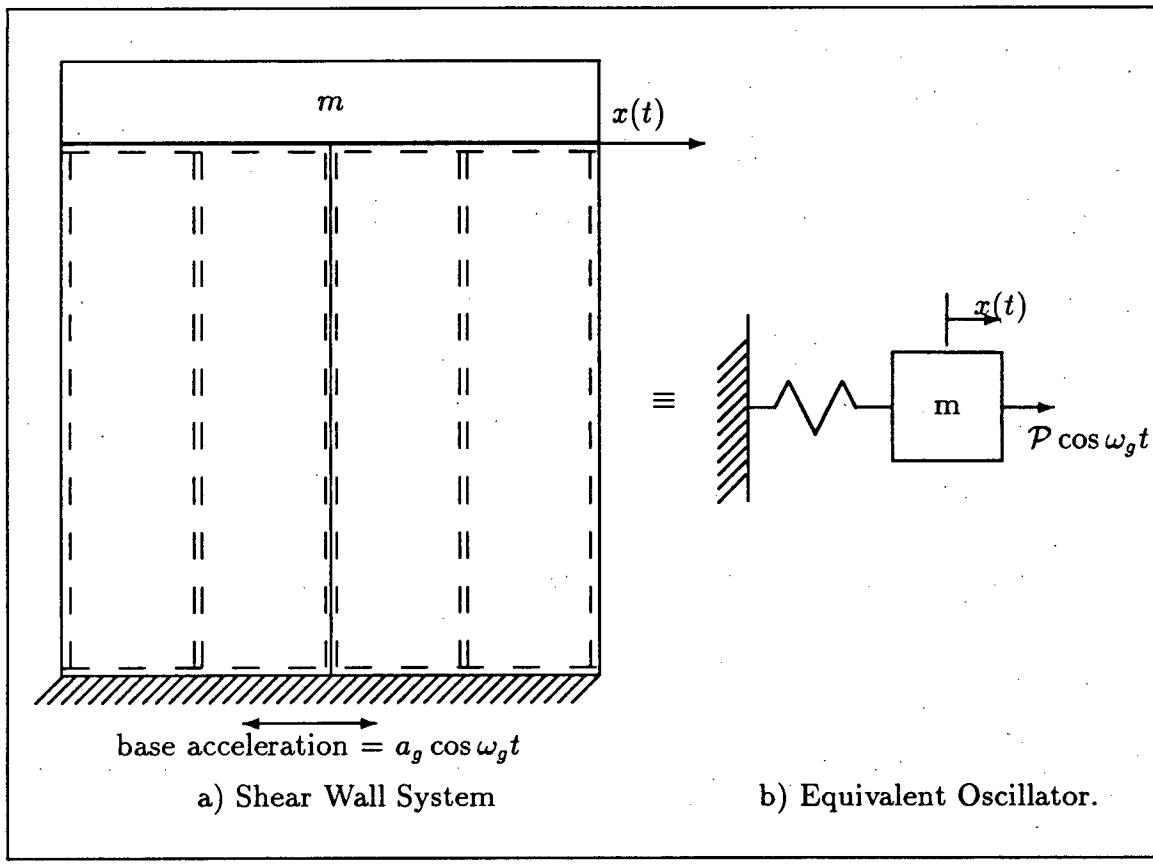

Figure 4.2: Equivalent Oscillator used to Represent Timber Shear Walls.

bounds of the resonant frequency of shear walls are investigated. To verify its accuracy, Chapter 9 shows the comparison of the model's predictions to the test results. The predicted response of the timber shear walls that are subjected to a variety of acceleration amplitudes is also discussed.

4.2 Assumptions

The closed form derivation requires that a few assumptions be made about the shear wall deflection and resulting hysteresis, in order to simplify the system. However, the resulting model will be used to predict the steady state response of full-scale shear walls,

by predicting the amplitude of the deflections for any given frequency and amplitude excitation.

The following assumptions were made for this analysis:

1. The shear wall is a single SDOF, non–linear oscillator. Many structures exhibit a similar steady state hysteresis to that of a nailed timber shear wall, therefore, a SDOF model can be easily adapted to other structures. Figure 4.2 shows this assumption pictorially. The displacement of the top of the wall relative to the base is represented by $x(t)$.

2. There is no viscous damping present. Therefore, the equivalent oscillator shown in Figure 4.2b does not include a dashpot. All of the energy dissipation is assumed to be due to the hysteretic characteristics of the spring. This assumption is made because most of the energy dissipation in nailed timber shear walls is due to yielding of the nails.

3. The hysteresis loop of timber shear walls can be idealized, using six linear line segments. Figure 4.3 shows a typical hysteresis curve for a plywood sheathed shear wall, and Figure 4.4 shows the idealized hysteresis loop that will be used in this model. The dashed lines in the figures represent an envelope curve of the peak load and the solid lines represent the hysteresis loops. The individual slopes of each line segment represent the corresponding segment of the true hysteresis curve. While the hysteresis can be represented by more line segments to represent the true hysteresis, six line segments was found to be sufficiently accurate.

4. While the load–deflection characteristic of shear walls is non–linear, the strength of the walls is assumed infinite. This assumption means the wall will not collapse due to loading or a displacement that is too high. The ultimate load capacity of

the walls was not included in the model at this time in order to keep the problem as simple as possible.

5. The steady state response of any structure is harmonic, therefore, a cosine or sine function can be used to represent the motion. For this model, a cosine function is assumed.

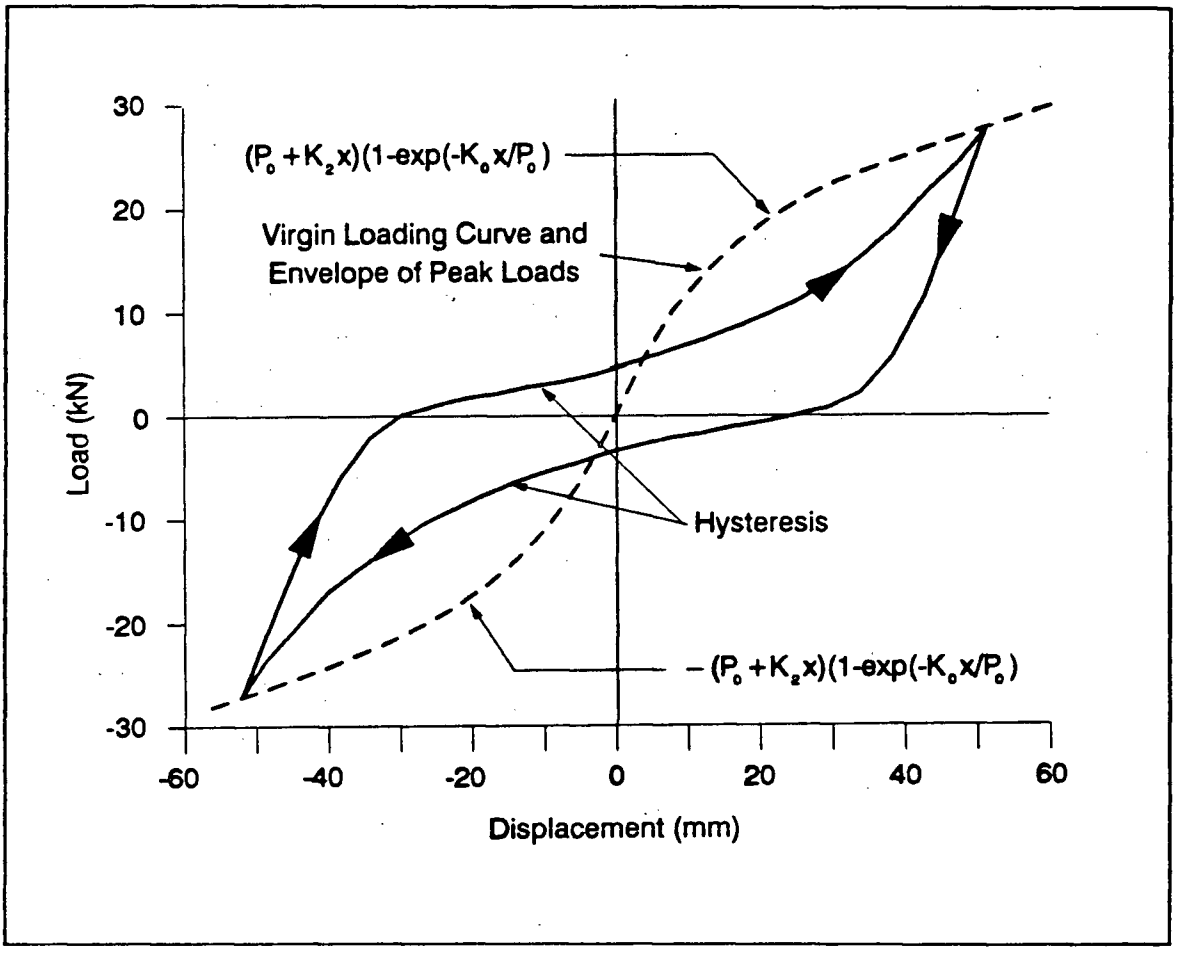

Figure 4.3: Typical Hysteresis Loop for Timber Shear Walls.

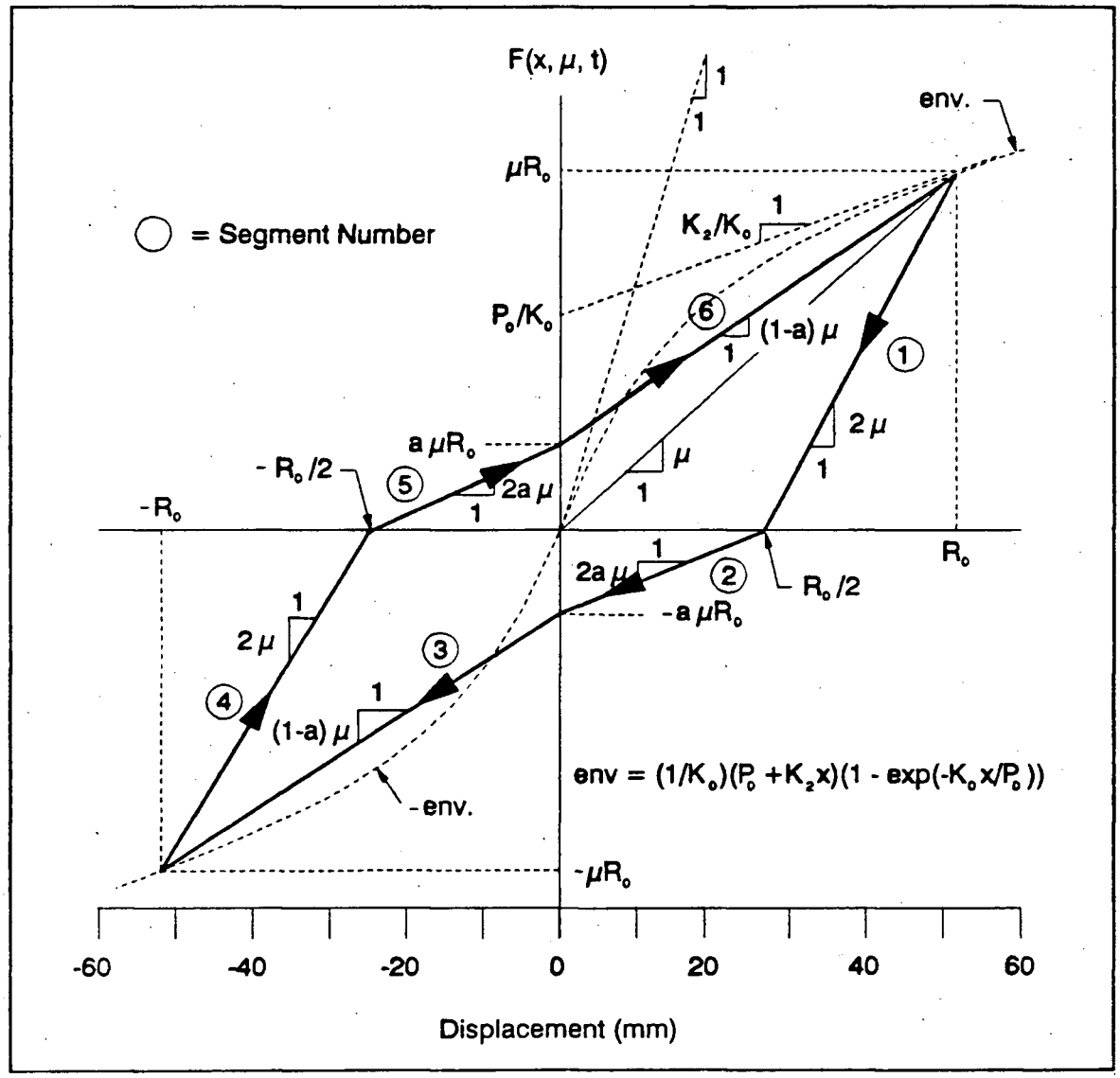

Figure 4.4: Idealization of Hysteresis Loop for Timber Shear Walls.

4.3 Derivation

The derivation of the closed form mathematical model begins with consideration of Figure 4.2b. The equation of motion for the spring oscillator can be written as,

$$m\ddot{x}(t) + K_0 F(x, \mu, t, a) = \mathcal{P} \cos \omega_g t \ . \tag{4.1}$$

where,

a = a constant representing the ratio of the load at zero deflection to the peak load for the hysteresis.

$x(t)$ = the displacement of the mass relative to the moving base.

$\ddot{x}(t)$ = the acceleration of the mass relative to the base.

K_0 = the initial stiffness of the wall.

$\mathcal{P}$ = $|-ma_g|$ = the absolute amplitude of the forcing function.

ω_g = the forcing function frequency.

t = the time.

m = the mass restrained by the shear wall, i.e. the mass of the system.

$F(x, \mu, t, a)$ = the hysteresis force per unit stiffness of the wall. This spring force is found using the idealized hysteresis curves, shown in Figure 4.4.

The parameter, μ, depends on the maximum displacement of the top of the wall, relative to the base of the wall. μ is defined as,

$$\mu = \frac{(P_0 + K_2 x)(1 - \exp(-K_0 x / P_0))}{K_0 x} \tag{4.2}$$

where, P_0, K_2, K_0, and a are found by testing full–scale shear walls in a static cyclic manner. The static cyclic test is conducted as described in Section 7.6.2, and the parameters, P_0, K_0, and K_2 are obtained using a least squares curve fitting routine to fit the equation for the numerator of Equation 4.2 to the test load–deflection curve. The parameter, a is found by calculating the ratio of the intercept load to the peak load for each test cycle.

By rearranging terms and using some variable substitutions, Equation 4.1 can be written as,

$$\frac{d^2x(\tau)}{d\tau^2} + F(x, \mu, t, a) = X_s \cos(\kappa, \tau) \tag{4.3}$$

where,

$$\kappa = \frac{\omega_g}{\omega_0} \tag{4.4}$$

$$\omega_0 = \sqrt{\frac{K_0}{m}}$$

$$\tau = \omega_0 t$$

$$X_s = \frac{\mathcal{P}}{K_0} = \frac{ma_g}{K_0}$$

Equation 4.3 is solved using the method of slowly varying parameters, i.e. the variables change little during one cycle of motion. The solution is assumed to be of the form,

$$x(\tau) = R(\tau)\cos(\kappa\tau + \phi(\tau)) \tag{4.5}$$

where $R(\tau)$ and $\phi(\tau)$ are the slowly varying amplitude and phase. Then,

$$\frac{dx(\tau)}{d\tau} = \dot{x}(\tau) = R'(\tau)\cos\theta - \kappa R(\tau)\sin\theta - \phi'(t)R(\tau)\sin\theta \tag{4.6}$$

where,

$$\theta = \kappa\tau + \phi(\tau) \tag{4.7}$$

If the system is assumed to be linear at any instant, then

$$R'(\tau)\cos\theta - \phi'(\tau)R(\tau)\sin\theta = 0 \tag{4.8}$$

Substituting Equation 4.8 into Equation 4.6 results in,

$$\frac{dx(\tau)}{d\tau} = \dot{x}(\tau) = -\kappa R(\tau)\sin\theta \tag{4.9}$$

Differentiating with respect to τ again,

$$\frac{d^2x(\tau)}{d\tau^2} = \ddot{x}(\tau) = -\kappa^2 R(\tau)\cos\theta - \kappa R'(\tau)\sin\theta - \kappa R(\tau)\phi'(\tau)\cos\theta \tag{4.10}$$

Substituting Equation 4.10 into Equation 4.3,

$$\begin{aligned} -\kappa R'(\tau)\sin\theta - \kappa R(\tau)\phi'(\tau)\cos\theta - \kappa^2 R(\tau)\cos\theta & \\ +F(R(\tau)\cos\theta, \mu, \tau, a) &= X_s\cos(\theta - \phi(\tau)) \end{aligned} \tag{4.11}$$

Multiplying Equation 4.8 by $(\kappa\cos\theta)$, and Equation 4.11 by $(\sin\theta)$, then subtracting, results in the equation,

$$-\kappa R'(\tau) - \kappa^2 R(\tau)\sin\theta\cos\theta + F(R(\tau)\cos\theta, \mu, \tau, a)\sin\theta = X_s\cos(\theta - \phi(\tau))\sin\theta \tag{4.12}$$

Multiplying Equation 4.8 by $(\kappa\sin\theta)$, and Equation 4.11 by $(\cos\theta)$, then adding, results in the equation,

$$\begin{aligned} -\kappa R(\tau)\phi'(\tau) - \kappa^2 R(\tau)\cos^2\theta + F(R(\tau)\cos\theta, \mu, \tau, a)\cos\theta = & \\ X_s\cos(\theta - \phi(\tau))\cos\theta & \end{aligned} \tag{4.13}$$

Since $R(\tau)$ and $\phi(\tau)$ are slowly varying, Equations 4.12 and 4.13 can be integrated over one cycle, with the variables $R(\tau)$ and $\phi(\tau)$ being replaced with their average values, $\bar{R}$ and $\bar{\phi}$. Therefore, integrating Equation 4.12,

$$\begin{aligned} -\kappa\bar{R}'\int_0^{2\pi} d\theta - \kappa^2\bar{R}\int_0^{2\pi}\sin\theta\cos\theta d\theta & \\ +\int_0^{2\pi} F\left(\bar{R}\cos\theta, \mu, \tau, a\right)\sin\theta d\theta &= X_s\int_0^{2\pi}\cos\left(\theta - \bar{\phi}\right)\sin\theta d\theta \end{aligned} \tag{4.14}$$

or,

$$-2\kappa\bar{R}' + S\left(\bar{R}\right) = X_s\sin\bar{\phi} \tag{4.15}$$

where,

$$S\left(\bar{R}\right) = \frac{1}{\pi}\int_0^{2\pi} F\left(\bar{R}\cos\theta, \mu, \tau, a\right)\sin\theta d\theta \tag{4.16}$$

Integrating Equation 4.13,

$$-\kappa\bar{R}\bar{\phi}'\int_0^{2\pi} d\theta - \kappa^2\bar{R}\int_0^{2\pi}\cos^2\theta d\theta + \int_0^{2\pi} F\left(\bar{R}\cos\theta,\mu,\tau,a\right)\cos\theta d\theta = X_s\int_0^{2\pi}\cos\left(\theta-\bar{\theta}\right)\cos\theta d\theta \tag{4.17}$$

or,

$$-2\kappa\bar{R}\bar{\phi}' - \kappa^2\bar{R} + C\left(\bar{R}\right) = X_s\cos\bar{\phi} \tag{4.18}$$

where,

$$C\left(\bar{R}\right) = \frac{1}{\pi}\int_0^{2\pi} F\left(\bar{R}\cos\theta,\mu,\tau,a\right)\cos\theta d\theta \tag{4.19}$$

The steady state response is obtained by setting $\bar{R}'$ and $\bar{\theta}'$ equal to zero in Equations 4.15 and 4.18. Therefore,

$$S\left(R_0\right) = X_s\sin\phi_0 \tag{4.20}$$

$$C\left(R_0\right) - \kappa^2 R_0 = X_s\cos\phi_0 \tag{4.21}$$

where, R_0 and ϕ_0 are the steady state amplitude and phase. Equation 4.20 can be rearranged as,

$$\phi_0 = \sin^{-1}\left[\frac{S\left(R_0\right)}{X_s}\right] \tag{4.22}$$

Substituting Equation 4.22 into Equation 4.21,

$$C\left(R_0\right) - \kappa^2 R_0 = X_s\cos\left[\sin^{-1}\left[\frac{S\left(R_0\right)}{X_s}\right]\right] = \pm\left[1-\left(\frac{S\left(R_0\right)}{X_s}\right)^2\right]^{1/2} X_s \tag{4.23}$$

Rearranging terms and dividing both sides of Equation 4.23 by R_0 results in

$$\kappa^2 = \frac{C\left(R_0\right)}{R_0} \pm \left[\left(\frac{X_s}{R_0}\right)^2 - \left(\frac{S\left(R_0\right)}{R_0}\right)^2\right]^{1/2} \tag{4.24}$$

This equation defines the frequency response function where,

$$C\left(R_0\right) = \frac{1}{\pi}\int_0^{2\pi} F\left(R_0\cos\theta,\mu,\tau,a\right)\cos\theta d\theta \tag{4.25}$$

and

$$S(R_0) = \frac{1}{\pi}\int_0^{2\pi} F(R_0\cos\theta, \mu, \tau, a)\sin\theta d\theta \tag{4.26}$$

Now, if Figure 4.4 is considered, and the variable substitution, $x = R_0\cos\theta$, is made, the integration required in Equations 4.25 and 4.26 can be carried out by integrating each segment of the hysteresis separately. The hysteresis force for each segment can be found from the following equations:

For segment (1):

x varies from R_0 to $R_0/2$ $\Rightarrow$ θ varies from 0 to $\pi/3$

$F(x,\mu,\tau,a) = 2\mu x - \mu R_0$ $\Rightarrow$ $F(R_0\cos\theta,\mu,\tau,a) = 2\mu R_0\cos\theta - \mu R_0$

For segment (2):

x varies from $R_0/2$ to 0 $\Rightarrow$ θ varies from $\pi/3$ to $\pi/2$

$F(x,\mu,\tau,a) = 2a\mu x - a\mu R_0$ $\Rightarrow$ $F(R_0\cos\theta,\mu,\tau,a) = 2a\mu R_0\cos\theta - a\mu R_0$

For segment (3):

x varies from 0 to $-R_0$ $\Rightarrow$ θ varies from $\pi/2$ to π

$F(x,\mu,\tau,a) = (1-a)\mu x - a\mu R_0$ $\Rightarrow$ $F(R_0\cos\theta,\mu,\tau,a) = (1-a)\mu R_0\cos\theta - a\mu R_0$

For segment (4):

x varies from $-R_0$ to $-R_0/2$ $\Rightarrow$ θ varies from π to $4\pi/3$

$F(x,\mu,\tau,a) = 2\mu x + \mu R_0$ $\Rightarrow$ $F(R_0\cos\theta,\mu,\tau,a) = 2\mu R_0\cos\theta + \mu R_0$

For segment (5):

x varies from $-R_0/2$ to 0 $\Rightarrow$ θ varies from $4\pi/3$ to $3\pi/2$

$F(x,\mu,\tau,a) = 2a\mu x + a\mu R_0$ $\Rightarrow$ $F(R_0\cos\theta,\mu,\tau,a) = 2a\mu R_0\cos\theta + a\mu R_0$

For segment (6):

x varies from 0 to R_0 $\Rightarrow$ θ varies from $3\pi/2$ to 2π

$F(x,\mu,\tau,a) = (1-a)\mu x + a\mu R_0 \Rightarrow F(R_0\cos\theta,\mu,\tau,a) = (1-a)\mu R_0\cos\theta + a\mu R_0$

Now $C(R_0)$ can be evaluated as,

$$C(R_0) = \frac{1}{\pi}\left[\int_0^{2\pi} F(R_0\cos\theta,\mu,\tau,a)\cos\theta d\theta\right]$$

$$\begin{aligned} C(R_0) = \frac{1}{\pi}\Bigg[&\int_0^{\pi/3}\left(2\mu R_0\cos^2\theta - \mu R_0\cos\theta\right)d\theta \\ &+\int_{\pi/3}^{\pi/2}\left(2a\mu R_0\cos^2\theta - a\mu R_0\cos\theta\right)d\theta \\ &+\int_{\pi/2}^{\pi}\left((1-a)\mu R_0\cos^2\theta - a\mu R_0\cos\theta\right)d\theta \\ &+\int_{\pi}^{4\pi/3}\left(2\mu R_0\cos^2\theta + \mu R_0\cos\theta\right)d\theta \\ &+\int_{4\pi/3}^{3\pi/2}\left(2a\mu R_0\cos^2\theta + a\mu R_0\cos\theta\right)d\theta \\ &+\int_{3\pi/2}^{2\pi}\left((1-a)\mu R_0\cos^2\theta + a\mu R_0\cos\theta\right)d\theta\Bigg] \end{aligned} \tag{4.27}$$

carrying out the iteration results in,

$$\begin{aligned} C(R_0) = \frac{1}{\pi}\Bigg[&\mu R_0\left(\theta + \frac{\sin 2\theta}{2} - \sin\theta\right)\Bigg|_0^{\pi/3} \\ &+ a\mu R_0\left(\theta + \frac{\sin 2\theta}{2} - \sin\theta\right)\Bigg|_{\pi/3}^{4\pi/3} \\ &+ \mu R_0\left(\left(\frac{\theta}{2} + \frac{\sin 2\theta}{4}\right) - a\left(\frac{\theta}{2} + \frac{\sin 2\theta}{4} + \sin\theta\right)\right)\Bigg|_{\pi/2}^{\pi} \\ &+ \mu R_0\left(\theta + \frac{\sin 2\theta}{2} + \sin\theta\right)\Bigg|_{\pi}^{4\pi/3} \\ &+ a\mu R_0\left(\theta + \frac{\sin 2\theta}{2} + \sin\theta\right)\Bigg|_{4\pi/3}^{3\pi/2} \\ &+ \mu R_0\left(\left(\frac{\theta}{2} + \frac{\sin 2\theta}{4}\right) - a\left(\frac{\theta}{2} + \frac{\sin 2\theta}{4} - \sin\theta\right)\right)\Bigg|_{3\pi/2}^{2\pi}\Bigg] \end{aligned} \tag{4.28}$$

Evaluating this equation at the limits results in the equation,

$$C(R_0) = \frac{(7-a)\pi - (1-a)3\sqrt{3}}{6\pi}\mu R_0 \tag{4.29}$$

In a similar way $S(R_0)$ can be evaluated as,

$$S(R_0) = -\frac{1+3a}{2\pi}\mu R_0 \tag{4.30}$$

Substituting Equation 4.2 into Equations 4.29 and 4.30,

$$C(R_0) = \left(\frac{(7-a)\pi - (1-a)3\sqrt{3}}{6\pi}\right)\left(\frac{(P_0 + K_2 R_0)(1 - \exp(-K_0 R_0/P_0))}{K_0}\right) \tag{4.31}$$

$$S(R_0) = -\left(\frac{1+3a}{2\pi}\right)\left(\frac{(P_0 + K_2 R_0)(1 - \exp(-K_0 R_0/P_0))}{K_0}\right) \tag{4.32}$$

Substituting Equations 4.31 and 4.32 into Equation 4.24, results in

$$\begin{aligned}\kappa^2 &= \left[\frac{(7-a)\pi - (1-a)3\sqrt{3}}{6\pi}\right]\left(\frac{P_0}{K_0 R_0} + \frac{K_2}{K_0}\right)\left(1 - \exp\left(\frac{-K_0 R_0}{P_0}\right)\right) \\ &\pm\left[\left(\frac{X_s}{R_0}\right)^2 - \left(\left(\frac{1+3a}{2\pi}\right)\left(\frac{P_0}{K_0 R_0} + \frac{K_2}{K_0}\right)\left(1 - \exp\left(-\frac{K_0 P_0}{P_0}\right)\right)\right)^2\right]^{1/2}\end{aligned} \tag{4.33}$$

This equation is the frequency response function (κ vs R_0) for timber shear walls. For particular values of P_0, K_0, K_2, a, and X_s, κ^2 can be found for specified values of R_0. Figure 4.5 shows the type of response curves produced if Equation 4.33 is graphed for various values of $X_s = \left(\frac{ma_g}{P_0}\right)$. The response, R_0 has been non-dimensionalized by multiplying by $\frac{K_0}{P_0}$. As shown in Figure 4.5, the response amplitude increases with the magnitude of the forcing function, X_s.

The effect of the forcing function frequency is also shown, with the peak response for each value of X_s representing the resonance condition. This shift in the resonant frequency is caused by the higher amplitude accelerations, inducing higher deflections of the shear wall. The higher deflections result in a lower overall stiffness which corresponds

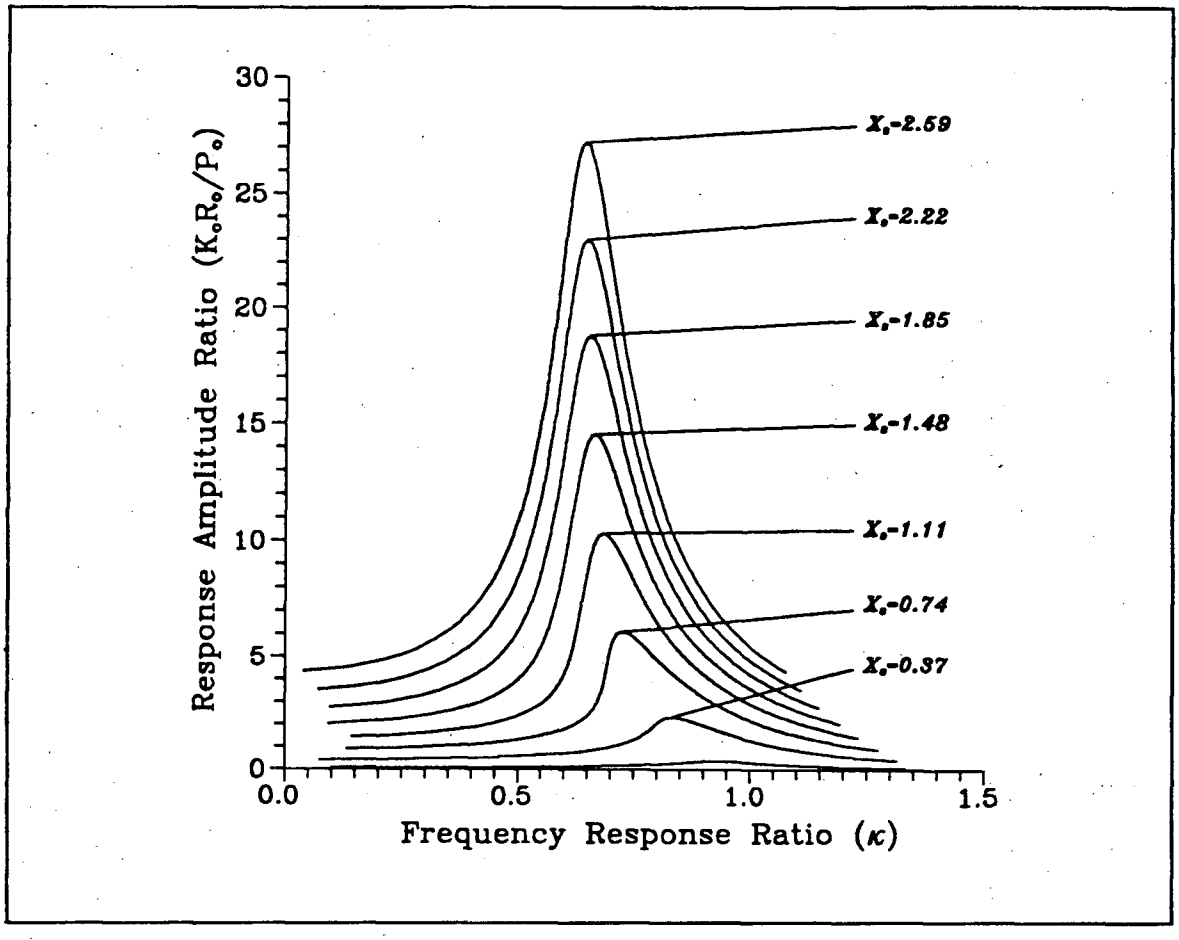

Figure 4.5: Frequency Response Function Curves for Timber Shear Walls.

to a lower frequency, provided the mass remains constant. Reasonance will occur where κ^2 has a double root. This condition occurs when,

$$\frac{X_s}{R_0^*} = \left(\frac{1+3a}{2\pi}\right)\left(\frac{P_0}{K_0 R_0^*} + \frac{K_2}{K_0}\right)\left(1 - \exp\left(-\frac{K_0 R_0^*}{P_0}\right)\right) \tag{4.34}$$

or,

$$2\pi X_s = (1+3a)\left(\frac{P_0}{K_0} + \frac{K_2 R_0^*}{K_0}\right)\left(1 - \exp\left(-\frac{K_0 R_0^*}{P_0}\right)\right)$$

Multiplying both sides by $\frac{K_0^2}{K_2 P_0}$ and reversing sides,

$$(1+3a)\left(\frac{K_0}{K_2} + \frac{K_0 R_0^*}{P_0}\right)\left(1 - \exp\left(-\frac{K_0 R_0^*}{P_0}\right)\right) = 2\pi\left(\frac{K_0}{K_2}\right)\left(\frac{ma_g}{P_0}\right) \tag{4.35}$$

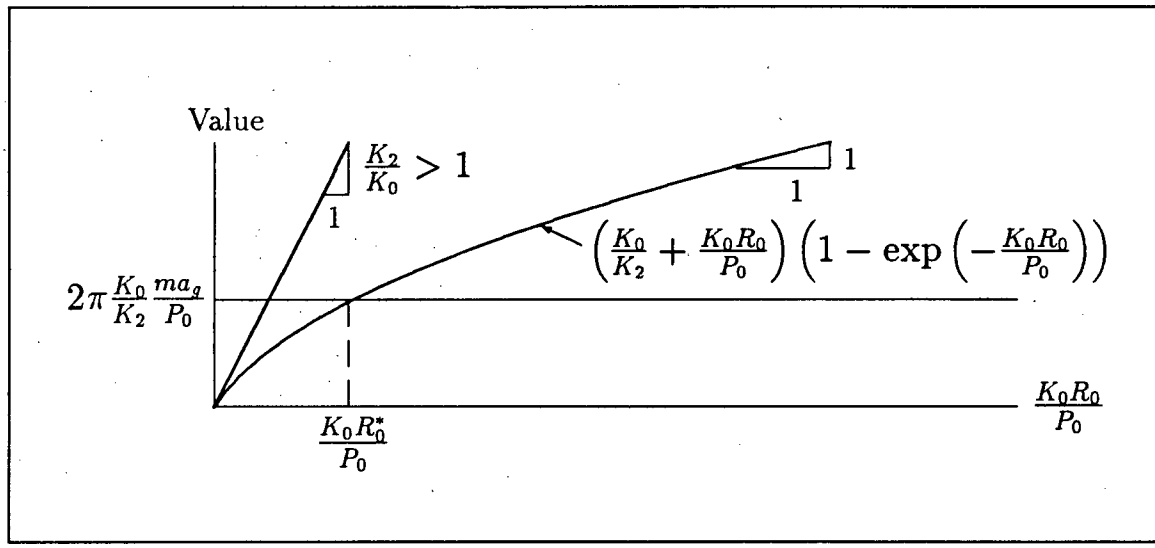

Figure 4.6: The Left and Right Hand Sides of Equation 5.34.

The above equation represents the resonant situation where, R_0^* is the resonant amplitude for the deflection. By looking at Equation 4.35, one can see that the left side is a single–valued, increasing function of $\frac{K_0 R_0^*}{P_0}$, while the right side is a positive constant. If the two sides of the equation are plotted on the same graph, as shown in Figure 4.6, the system can be seen as always being stable, i.e., for each magnitude acceleration, there is only one resonant response. This implies that the deflection should not have an unbounded amplitude at resonance, for finite values of a_g.

The resonant frequency ratio is obtained by substituting Equation 4.34 into Equation 4.33.

$$\kappa^* = \sqrt{\left[\frac{(7-a)\,\pi - (1-a)\,3\sqrt{3}}{6\pi}\right]\left(\frac{P_0}{K_0 R_0^*} + \frac{K_2}{K_0}\right)\left(1 - \exp\left(-\frac{K_0 R_0^*}{P_0}\right)\right)} \tag{4.36}$$

Equation 4.36 can be reformulated as,

$$\kappa^* = \sqrt{\left[\frac{(7-a)\,\pi - (1-a)\,3\sqrt{3}}{3+9a}\right]\frac{X_s}{R_0^*}} \tag{4.37}$$

or,

$$\kappa^* = \sqrt{\left[\frac{(7-a)\,\pi - (1-a)\,3\sqrt{3}}{3+9a}\right]\left(\frac{ma_g}{P_0}\right)\left(\frac{P_0}{K_0 R_0^*}\right)} \tag{4.38}$$

where, κ^* is the resonant frequency ratio.

4.3.1 Numerical Solution of Equations

Equation 4.35 can be rewritten as,

$$F(b) = C_1\,(C_2 + b)\,(1 - \exp(-b)) - C_3 = 0 \tag{4.39}$$

where,

$$\begin{aligned} C_1 &= (1+3a) \\ C_2 &= \left(\frac{K_0}{K_2}\right) \\ C_3 &= 2\pi\left(\frac{K_0}{K_2}\right)\left(\frac{ma_g}{P_0}\right) \\ b &= \frac{K_0 R_0^*}{P_0} \end{aligned} \tag{4.40}$$

Equation 4.39 can be solved using a Newton–Raphson iteration approach, as

$$b_1 = b_0 - \frac{F(b_0)}{F'(b_0)} = b_0 - \frac{[C_1\,(C_2 + b_0)\,(1 - \exp(-b_0)) - C_3]}{[C_1\,(1 - \exp(-b_0)) + C_1\,(C_2 + b_0)\exp(-b_0)]} \tag{4.41}$$

In order to solve Equation 4.42, an initial value of b_0 is assumed and the equation is solved for b_1. The value of b_1 is then used as the next trial value for b_0 and a new value for b_1 is calculated. The process is repeated until the values of b_0 and b_1 are acceptably close for the accuracy desired. The final value of b_1 can then be substituted into Equation 4.38 to determine the resonance frequency ratio, κ^*.

4.3.1.1 Numerical Example

To make the solution process more clear, an example can be used. Assume the values for the variables of Equation 4.39 are as follows:

$$\begin{aligned} C_1 &= 1.3 \\ C_2 &= 2.4 \\ C_3 &= 11.00 \end{aligned} \tag{4.42}$$

These values used for C_1, C_2, and C_3 are based on values of P_0, K_0, K_2, and a for the timber shear walls used in the cyclic tests described in Chapter 8.

An initial value of 1.0 was assumed for b_0, and an error in the answer of 0.01 was deemed acceptable. Following the procedure presented above, Equation 4.39 can be solved. The values of b_0 used in each iteration are shown in Table 4.1 along with the calculated values of b_1. As shown in Table 4.1, the values of b_0 and b_1 are sufficiently close after the 14th iteration, and the value of 6.07 is accepted as the correct resonance amplitude ratio, b or $\frac{K_0 R_0^*}{P_0}$. This value can now be substituted into Equation 4.38, and the resonant frequency ratio, κ^*, is found to be 0.729.

4.4 Bounds on Frequency Response

By considering Figure 4.6, one can see that the resonance amplitude ratio, $\frac{K_0 R_0^*}{P_0}$, increases with the amplitude of seismic force, ma_g. For a very small ma_g, $\frac{K_0 R_0^*}{P_0}$ is also small. If Figure 4.4 is considered, it can be seen that as the displacement, R_0, approaches 0, μ approaches 1. At the same time, a, approaches 0 and the stiffness of the

Table 4.1: Values of b_0 and b_1 for Each Iteration During the Solution of Numerical Example.

Iteration #	b_0	$b1$
1	1.00	4.67
2	4.67	5.09
3	5.09	5.36
4	5.36	5.54
5	5.54	5.68
6	5.68	5.78
7	5.78	5.86
8	5.86	5.92
9	5.92	5.96
10	5.96	6.00
11	6.00	6.02
12	6.02	6.04
13	6.04	6.06
14	6.06	6.07

wall, $(1-a)\,\mu$ will approach $\mu = 1$. Therefore,

$$\omega^*_{max} = \sqrt{\frac{K_0}{m}} \tag{4.43}$$

Equation 4.43 implies,

$$\kappa^*_{max} = \frac{\omega^*_{max}}{\omega_0} = \frac{\sqrt{K_0/m}}{\sqrt{K_0/m}} = 1 \tag{4.44}$$

For large $\frac{ma_g}{P_0}$, $\frac{K_0 R^*_0}{P_0}$ is also large, and the hysteresis of Figure 4.4 will approach the shape shown in Figure 4.7. It can be seen, for $R_0 \to \infty$, $\mu \to \frac{K_2}{K_0}$.

If $\mu = \frac{K_2}{K_0}$ is substituted into Equations 4.29 and 4.30,

$$C\,(R_0) = \left(\frac{(7-a)\,\pi - (1-a)\,3\sqrt{3}}{6\pi}\right)\left(\frac{K_2 R^*_0}{K_0}\right) \tag{4.45}$$

and,

$$S\,(R_0) = -\left(\frac{1+3a}{2\pi}\right)\left(\frac{K_2 R^*_0}{K_0}\right) \tag{4.46}$$

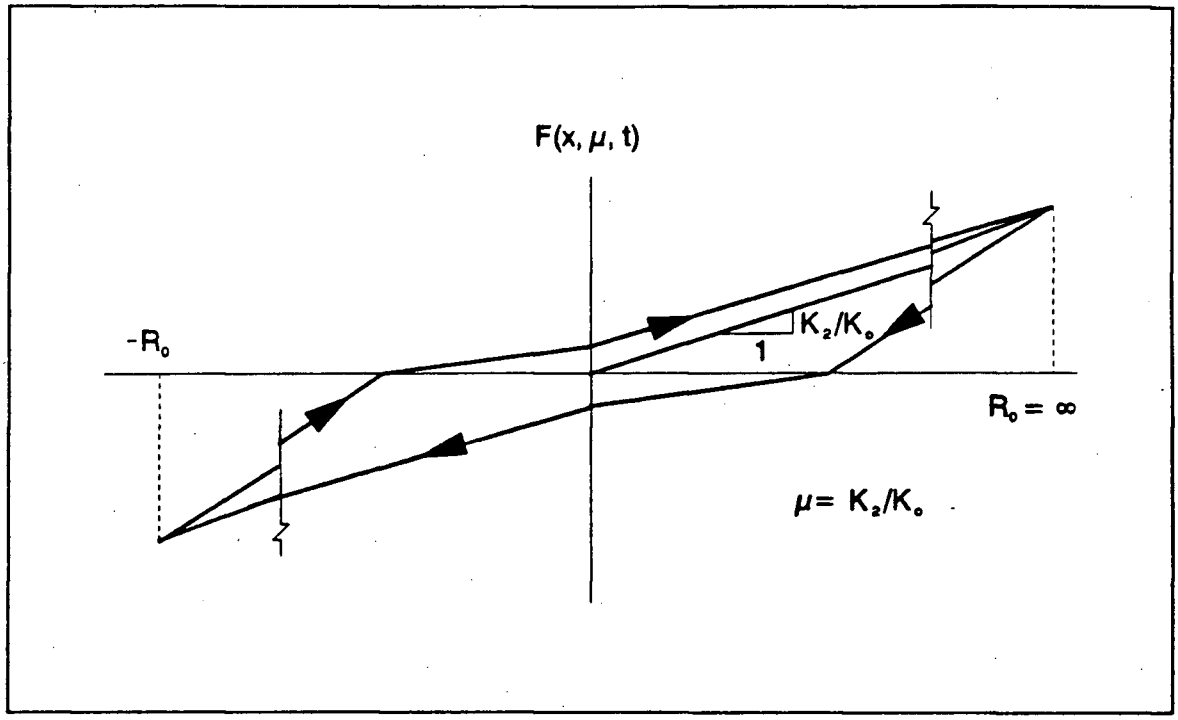

Figure 4.7: The Idealized Hysteresis Loop When $R_0 \rightarrow \infty$.

Substituting into Equation 4.24,

$$\kappa^2 = \left(\frac{(7-a)\pi - (1-a)3\sqrt{3}}{6\pi}\right)\left(\frac{K_2}{K_0}\right) \pm \left[\left(\frac{ma_g}{P_0}\frac{P_0}{K_0 R_0}\right)^2 - \left(\frac{1+3a}{2\pi}\frac{K_2}{K_0}\right)^2\right]^{1/2} \tag{4.47}$$

Resonance occurs when the second term equals 0. Therefore,

$$\kappa^*_{\min} = \sqrt{\frac{(7-a)\pi - (1-a)3\sqrt{3}}{6\pi}\left(\frac{K_2}{K_0}\right)} \tag{4.48}$$

From the above derivation, the resonant frequency ratio, κ^*, will have values in the following range for any amplitude of excitation force.

$$\sqrt{\frac{(7-a) - (1-a)3\sqrt{3}}{6\pi}\frac{K_2}{K_0}} \leq \kappa^* \leq 1 \tag{4.49}$$

4.5 Summary

A closed form mathematical model, used to predict the steady state response of timber shear walls, subjected to sinusoidal base excitation, has been derived. Given a base acceleration magnitude and frequency, the model predicts the steady state response of shear walls. The stability of the solution was investigated along with the bounds on the response frequency and a numerical example was used to clarify the solution process.

This mathematical model can be used to estimate the natural frequency (resonant frequency) of timber shear walls when subjected to various amplitude base excitations. Also, the peak displacements of shear walls subjected to earthquake excitations could be estimated, provided the predominant frequencies and amplitudes of the earthquake accelerations are known.

Chapter 5

Dynamic Finite Element Model

5.1 Introduction

This chapter outlines the derivation of the dynamic time–step numerical model, **DYNWALL**, used to predict the behavior of timber shear walls subjected to random dynamic base accelerations, such as earthquakes. The model incorporates the static one–directional loading model, **SHWALL**, that was derived in Chapter 3, with a modification of the sheathing connector element.

The assumptions for the model are outlined first. Equations for the time–step solution, the changes in the sheathing connector derivation, and energy balance are then derived. Finally, the entire solution process is summarized. The accuracy of the model is investigated in Chapter 9 where the predicted behavior of the model is compared to test results.

5.2 Assumptions

Since the static program, **SHWALL**, is incorporated in this model, all the assumptions pertaining to the derivation of **SHWALL** are included in the derivation of the dynamic model. In addition, assumptions regarding the hysteretic behavior of the sheathing connectors and dynamic behavior of the wall are made. The full list of assumptions is as

follows:

1. The beam element used to model the framing will not deflect out of the plane of the wall. The program is not intended for modeling the out–of–plane bending of the overall wall, and all the loads are applied in the plane of the walls.

2. To satisfy the compatibility requirements for the axial displacements, the deflected shape for the beam element, parallel to the beam axis, is assumed to be linear.

3. The in–plane deflected shape for the beam element, perpendicular to the beam axis, is defined by a cubic polynomial so that compatibility of slope is maintained between beam elements.

4. Initial plane sections of the beam element are assumed to remain plane after deformations since the change in shear stress across the cross–section is assumed to be small.

5. The beam material obeys linear elastic, homogeneous, stress–strain relationships and never reaches yield. This assumption is made since failure of the sheathing connector is the primary failure mode. Future improvements to the model can include failure of the framing.

6. The plate element used to model the sheathing obeys linear elastic, orthotropic stress–strain relationships. The sheathing material should not yield, except if very stiff and strong sheathing connectors are used. Also, the element is orthotropic because plywood sheathing is an orthotropic material.

7. Layered sheathing materials, such as plywood, will be modeled as a non-layered material having average material properties obtained from sheathing panel tests,

or derived using transformed sections. This assumption is used to simplify the sheathing element.

8. The in–plane deflections of the plate element are affected by the bending deflections (large deflection theory). Making this assumption allows the buckling effect of thin sheathing panels to be modeled.

9. The change in the thickness of the sheathing material due to deformations is negligible, i.e. crushing of the material does not occur. Crushing of the sheathing has not been observed in any full size shear wall tests that this author is aware of.

10. The effect of bearing between two adjacent sheathing elements is modeled by a bi–linear spring connector that prevents overlapping of the plate elements, but does not hinder separation. The relative movement parallel to the edge of the plate element is also not hindered by the spring connector. The bearing between sheathing panels is an important factor, affecting the stiffness of large diaphragms and shear walls.

11. The connection between the sheathing and the framing is modeled as three independent, non–correlated, non–linear spring connectors, with exponential load–deflection curves. Foschi (1977) has shown that the exponential model represents nail connectors well. Also, the three independent springs allow for future simplifications by eliminating some deflection directions if it is shown not to effect the resulting predictions significantly.

12. The spring connectors between the sheathing and the framing are modeled as having a maximum load. Then, as the deflection increases past the deflection corresponding to the maximum load, the load capacity decreases linearly to a value of zero. This accounts for the eventual total failure of an individual connector, such as when a

nail pulls completely out of the framing and will allow the load capacity of the wall to be determined.

13. The sheathing connector element will follow the hysteresis, shown in Figure 5.1, which closely resembles the hysteresis obtained from connection tests .

14. Accelerations are assumed to be constant during any time increment which will make the solution unconditionally stable.

15. All the material properties of the structure remain constant during any time increment. This implies that the tangent stiffness is used in this derivation; the stiffness will remain linear during the time increment, and can only change at the end of each time increment. As the time increment is reduced, the solution will approach the exact solution. The analysis using this solution must be performed twice to ensure that the error in the analysis is acceptable to the user.

16. If the error in the sheathing connector element becomes too large, in any given time increment, the solution process will be repeated for that time increment, using a smaller time increment. Due to the tangent stiffness being used for this analysis, the residual forces in the connectors could become large and cause localized problems in the analysis. The accuracy criteria used is described in Section 5.4.3.

17. The mass of the structure is assumed to remain constant for the entire solution, since the structural mass is not being consumed or changed in the process of resisting the loading.

18. The viscous damping for the shear wall will be assumed to be proportional to the

mass of the structure, which will eliminate the need to update the damping matrix as the analysis progresses.

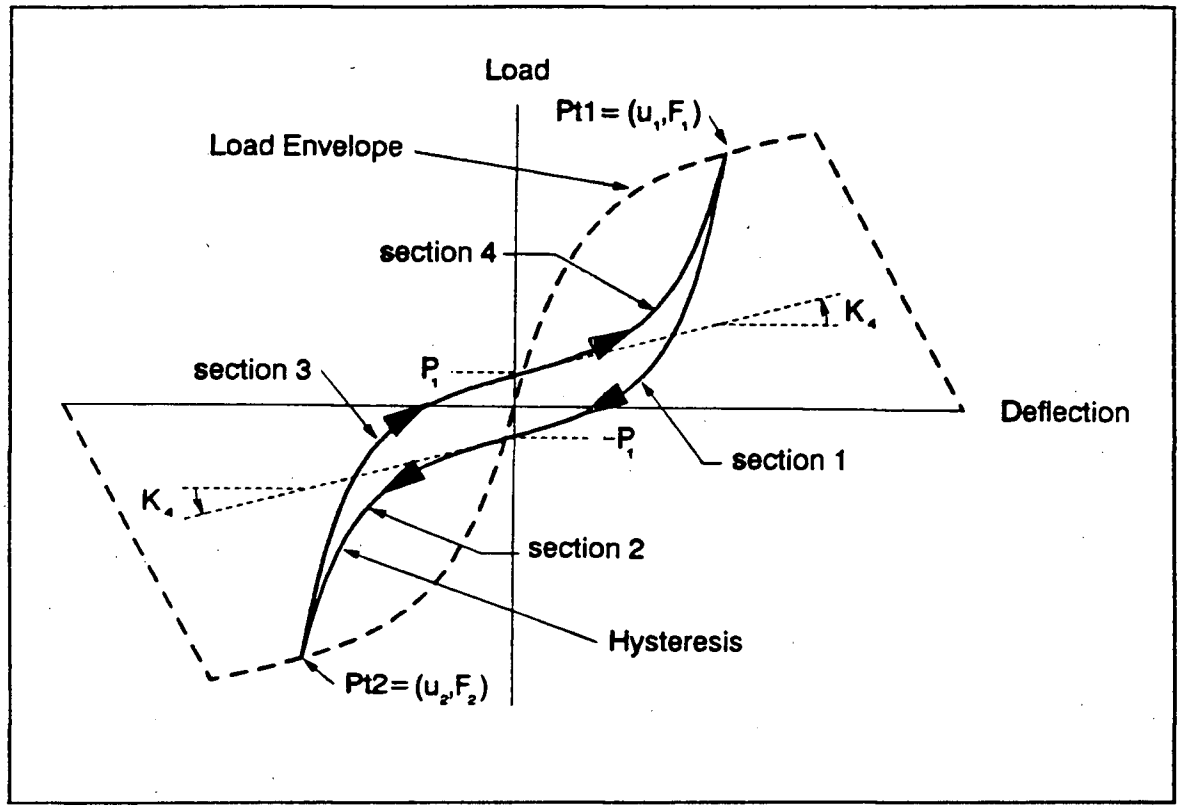

Figure 5.1: Assumed Hysteresis Loop For Sheathing Connector Element.

5.3 Step–by–Step Integration Equations

One procedure for performing non–linear dynamic analysis is the step–by–step integration procedure. This procedure was outlined by Clough (1975), and has been used by many researchers and design engineers to analyze structures that are required to resist dynamic loads.

Consider the free–body diagram, shown in Figure 5.2. The forces are defined as:

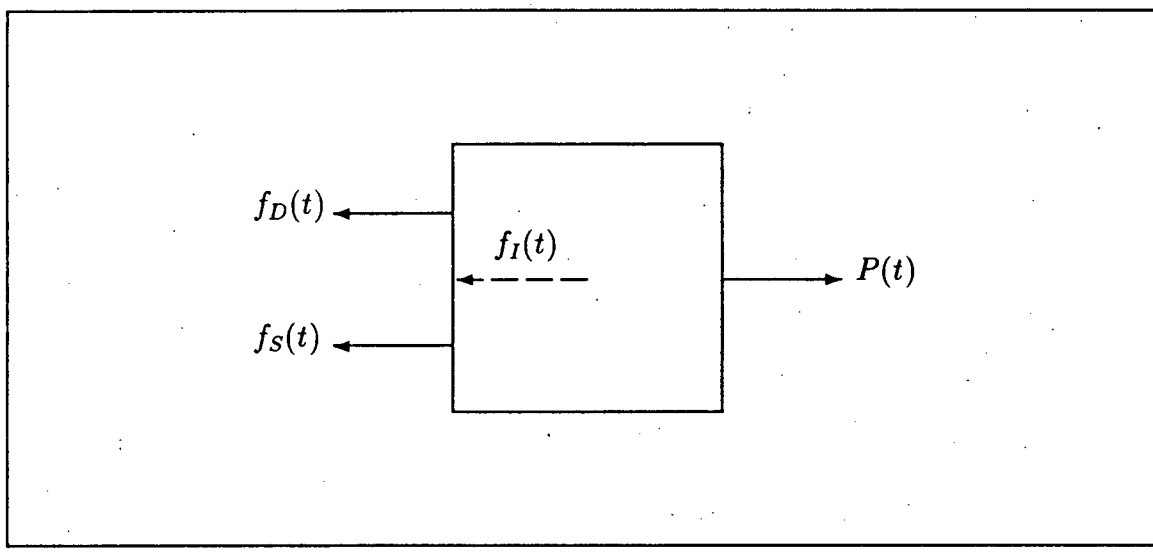

Figure 5.2: Freebody Diagram of a General Object in Dynamic Equilibrium.

$f_S(t)$ is the non–linear structural spring force, or the structural resistance force.

$f_D(t)$ is the non–linear force due to damping.

$f_I(t)$ is the inertial resistance force of the structure.

$P(t)$ is the general dynamic loading on the structure. The loading force used in this analysis represents earthquake loading, plus the dead load of the structure.

These forces are given by the following equations:

$$f_I(t) = [M]\{\ddot{u}(t)\} \tag{5.1}$$

$$f_D(t) = [C]\{\dot{u}(t)\} \tag{5.2}$$

$$f_S(t) = [K_t]\{u(t)\} \tag{5.3}$$

$$P(t) = -[M]\{I\}\,\ddot{u}_g(t) + \{P_{DL}\} \tag{5.4}$$

where,

$[M]$ = the mass matrix. The derivation of the mass matrix can be found in books on finite elements, such as those by Desai and Abel (1972), Zienkiewicz (1977), and Cook (1974).

$[C]$ = the damping matrix, which is mass–proportional, and is given by,

$$[C] = 2\Re\, \omega_1\, [M] \tag{5.5}$$

$\Re$ = the damping ratio (the ratio of the desired damping to the critical damping for the fundamental frequency of the structure).

ω_1 = the fundamental frequency of the structure.

$[K_t]$ = the tangent stiffness matrix which is given by Equation 3.103.

$\{I\}$ = the influence matrix, which consists of 1's and 0's, depending on whether the particular degree–of–freedom is directly effected by the ground accelerations.

$\{P_{DL}\}$ = the vector of structural dead loads.

If dynamic equilibrium is imposed at times, t and $t + \Delta t$, the resulting equations are

$$\begin{aligned} &[M]\{\ddot{u}(t)\} + [C]\{\dot{u}(t)\} \\ &\quad + [K_t(t)]\{u(t)\} \;=\; -[M]\{I\}\,\ddot{u}_g(t) + \{P_{DL}\} \end{aligned} \tag{5.6}$$

and

$$\begin{aligned} &[M]\{\ddot{u}(t+\Delta t)\} \\ &+ [C]\{\dot{u}(t+\Delta t)\} + [K_T(t)]\{u(t+\Delta t)\} \;=\; -[M]\{I\}\,\ddot{u}_g(t+\Delta t) + \{P_{DL}\} \end{aligned} \tag{5.7}$$

Subtracting Equation 5.6 from Equation 5.7 results in the incremental equation of motion,

$$[M]\{\Delta\ddot{u}(t)\} + [C]\{\Delta\dot{u}(t)\} + [K_t(t)]\{\Delta u(t)\} = -[M]\{I\}\Delta\ddot{u}_g(t) \tag{5.8}$$

If the acceleration is assumed constant for the time step, Δt, and is to be the average value, then for $t \leq \tau \leq t + \Delta t$

$$\{\ddot{u}(\tau)\} = \frac{\{\ddot{u}(t)\} + \{\ddot{u}(t+\Delta t)\}}{2} \tag{5.9}$$

$$\{\dot{u}(\tau)\} = \{\dot{u}(t)\} + \int_t^\tau \{\ddot{u}(\tau)\}\, d\tau \tag{5.10}$$

$$\{u(\tau)\} = \{u(t)\} + \int_t^\tau \{\dot{u}(\tau)\}\, d\tau \tag{5.11}$$

Carrying out the integration in Equations 5.10 and 5.11 for $\tau = t + \Delta t$, and rearranging

$$\begin{aligned} \{\Delta\dot{u}(t)\} &= \{\dot{u}(t+\Delta t)\} - \{\dot{u}(t)\} \\ &= \frac{\Delta t}{2}\left(2\{\ddot{u}(t)\} + \{\Delta\ddot{u}(t)\}\right) \end{aligned} \tag{5.12}$$

$$\begin{aligned} \{\Delta u(t)\} &= \{u(t+\Delta t)\} - \{u(t)\} \\ &= \Delta t\{\dot{u}(t)\} + \frac{\Delta t^2}{4}\left(\{\ddot{u}(t)\} + \{\ddot{u}(t+\Delta t)\}\right) \\ &= \Delta t\{\dot{u}(t)\} + \Delta t^2\left(\frac{\{\ddot{u}(t)\}}{2} + \frac{\{\Delta\ddot{u}(t)\}}{4}\right) \end{aligned} \tag{5.13}$$

Rewriting Equations 5.12 and 5.13,

$$\{\Delta\dot{u}(t)\} = \Delta t\{\ddot{u}(t)\} + \gamma\Delta t\{\Delta\ddot{u}(t)\} \tag{5.14}$$

and

$$\{\Delta u(t)\} = \Delta t\{\dot{u}(t)\} + (\Delta t)^2\left(\frac{\{\ddot{u}(t)\}}{2} + \beta\{\Delta\ddot{u}(t)\}\right) \tag{5.15}$$

where, $\gamma = \frac{1}{2}$ and $\beta = \frac{1}{4}$ This is the format commonly referred to as the Newmark–β method, and is an adaptation of the procedure derived by Newmark (1962).

If the variable $\{u(t)\}$ is kept as the basic variable of the analysis, Equation 5.15 can be rewritten as,

$$\{\Delta\ddot{u}(t)\} = \frac{\{\Delta u(t)\}}{\beta(\Delta t)^2} - \frac{\{\dot{u}(t)\}}{\beta\Delta t} - \frac{\{\ddot{u}(t)\}}{2\beta} \tag{5.16}$$

Substituting Equation 5.16 into Equation 5.14 and rearranging terms, results in

$$\{\Delta\dot{u}(t)\} = \Delta t\{\ddot{u}(t)\} + \frac{\gamma}{\beta\Delta t}\{\Delta u(t)\} - \frac{\gamma}{\beta}\{\dot{u}(t)\} - \frac{\gamma\Delta t}{2\beta}\{\ddot{u}(t)\} \tag{5.17}$$

Now, substituting Equations 5.16 and 5.17 into the incremental equation of motion, Equation 5.8,

$$\begin{aligned}
&[M]\left\{\frac{\{\Delta u(t)\}}{\beta(\Delta t)^2} - \frac{\{dotu(t)\}}{\beta\Delta t} - \frac{\{\ddot{u}(t)\}}{2\beta}\right\} \\
&+[C]\left\{\Delta t\{\ddot{u}(t)\} + \frac{\gamma}{\beta\Delta t}\{\Delta u(t)\} - \frac{\gamma}{\beta}\{\dot{u}(t)\} - \frac{\gamma\Delta t}{2\beta}\{\ddot{u}(t)\}\right\} \\
&+[K_t(t)]\{\Delta u(t)\} = -[M]\{I\}\Delta\ddot{u}_g(t)
\end{aligned} \tag{5.18}$$

Rearranging Equation 5.18,

$$\begin{aligned}
&\left[\frac{[M]}{\beta(\Delta t)^2} + \frac{[C]\gamma}{\beta\Delta t} + [K_t(t)]\right]\{\Delta u(t)\} = \\
&-[M]\{I\}\Delta\ddot{u}_g(t) + [M]\left(\frac{\{\ddot{u}(t)\}}{2\beta} + \frac{\{\dot{u}(t)\}}{\beta\Delta t}\right) \\
&+[C]\left(-\Delta t\{\ddot{u}(t)\} + \frac{\gamma}{2\beta}\Delta t\{\ddot{u}(t)\} + \frac{\gamma}{\beta}\{\dot{u}(t)\}\right)
\end{aligned} \tag{5.19}$$

This equation has the form of a linear system of equations,

$$\left[\tilde{K}(t)\right]\{\Delta u(t)\} = \left\{\tilde{P}(t)\right\} \tag{5.20}$$

where,

$$\left[\tilde{K}(t)\right] = \frac{[M]}{\beta(\Delta t)^2} + \frac{\gamma[C]}{\beta\Delta t} + [K_t(t)] \tag{5.21}$$

and

$$\left\{\tilde{P}(t)\right\} = [M]\left(-\{I\}\,\Delta\ddot{u}_g(t) + \frac{\{\ddot{u}(t)\}}{2\beta} + \frac{\{\dot{u}(t)\}}{\beta\Delta t}\right) + [C]\left(\left(\frac{\gamma}{2\beta} - 1\right)\Delta t\,\{\ddot{u}(t)\} + \frac{\gamma}{\beta}\{\dot{u}(t)\}\right) \tag{5.22}$$

Equation 5.20 can be used to solve for $\Delta u(t)$, which can then be substituted into Equation 5.17 to determine $\Delta\dot{u}(t)$. Finally, the displacements and velocities, at the end of the time step, can be found as,

$$\{u(t+\Delta t)\} = \{u(t)\} + \{\Delta u(t)\} \tag{5.23}$$

and

$$\{\dot{u}(t+\Delta t)\} = \{\dot{u}(t)\} + \{\Delta\dot{u}(t)\} \tag{5.24}$$

Because the tangent, rather than the secant stiffness matrix, is used in this derivation, errors are introduced at the end of each time step. These errors are prevented from accumulating during the analysis by imposing the requirement that the initial conditions for the accelerations at each time step be found by imposing dynamic equilibrium. This means that $\{\ddot{u}(t+\Delta t)\}$ must be found such that the equation,

$$[M]\{\ddot{u}(t+\Delta t)\} + [C]\{\dot{u}(t+\Delta t)\} + [K_t(t+\Delta t)]\{u(t+\Delta t)\} = -[M]\{I\}\,\ddot{u}_g(t+\Delta t) + \{P_{DL}\} \tag{5.25}$$

is satisfied. Solving Equation 5.25 for $\ddot{u}(t+\Delta t)$ results in the equation,

$$\{\ddot{u}(t+\Delta t)\} = [M]^{-1}\left[\{P_{DL}\} - [M]\{I\}\,\ddot{u}_g(t+\Delta t) - [C]\{\dot{u}(t+\Delta t)\} - [K_t(t+\Delta t)]\{u(t+\Delta t)\}\right] \tag{5.26}$$

5.4 Hysteretic Sheathing Connector Element Derivation

The sheathing connector element derived in Section 3.6 is able to accurately model the behavior of the connector for static one–directional loading. However, the connection experiences many random load reversals during an earthquake. The connection is also a major source of energy dissipation due to its hysteretic behavior. It is therefore important that characteristics of the sheathing connector be modeled as closely as possible.

Figure 5.3 shows the cyclic load–deflection curve for a shear wall, and Figure 6.14 shows the cyclic load–deflection curve for a single nail connection. In comparison, it is evident that the behavior of the entire shear wall is governed by the hysteretic behavior of the individual nail connections. The particular hysteretic behavior nail connections causes the pinching of the hysteresis, as shown in Figure 5.3. The reduction of the area enclosed in the hysteresis loops represents a loss of energy absorbing ability and is typical of nailed timber structures.

The dynamic, hysteretic connector has the same geometry and deflection calculations as the static one–directional connector. These parts of the derivation are given in Sections 3.6.1 and 3.6.2. The derivation used in the dynamic model differs from the static model in the method of calculating the connection force and stiffness. Load–deflection curves for the static connector are used as envelope values for the peak load, and as the virgin loading curve for the dynamic connector.

5.4.1 Connection Hysteresis Force

In addition to the equations used to define the load–deflection curves of the sheathing connector in the static program, four equations are used to define the hysteresis

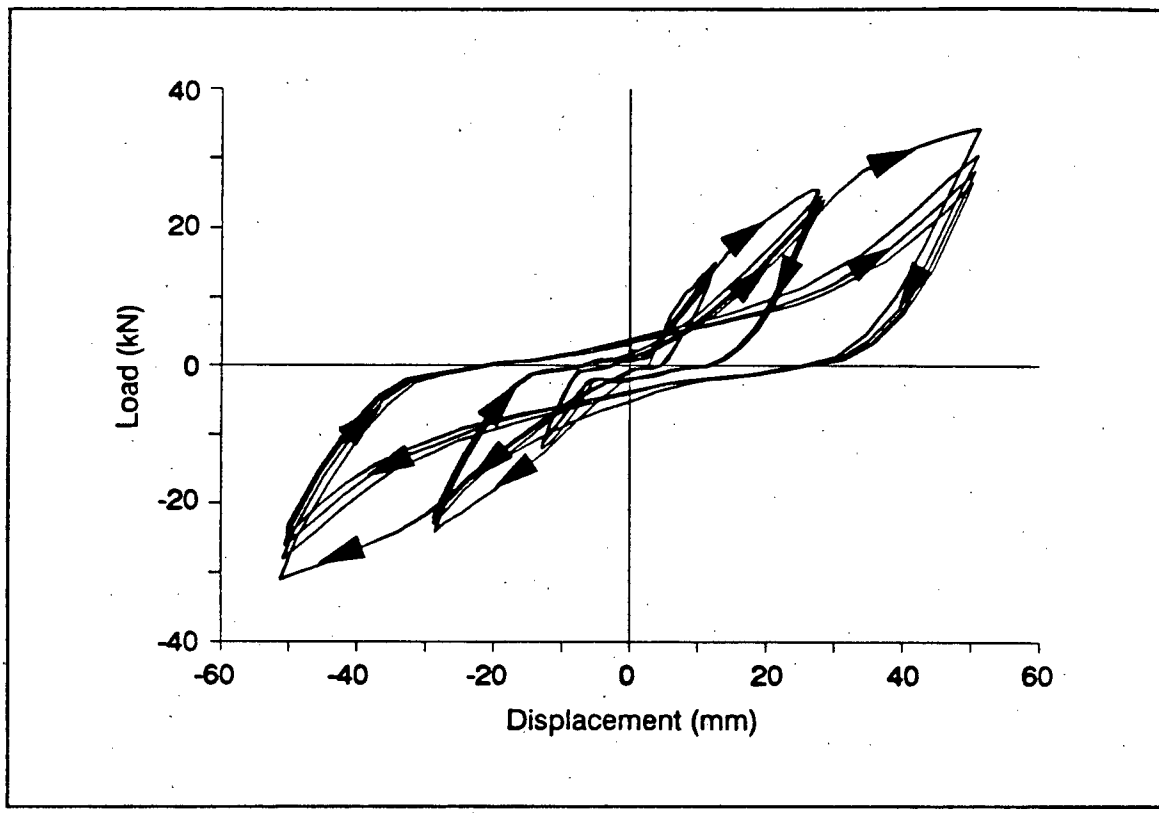

Figure 5.3: Typical Cyclic Load–Deflection Curve For a Timber Shear Wall.

for reversing loads. Figure 5.1 shows the hysteresis loops for the connector, with four segments defined. Each segment, 1–4, is defined by an exponential equation, each using four boundary conditions: the load–intercept P_1, the slope at zero displacement K_4, the maximum displacement reached in either direction, u_1 or u_2, and the corresponding maximum loads, F_1 or F_2. The first two boundary conditions ensure continuity and continuous differentiability for the region between the two end points of the hysteresis loop, Pt1 and Pt2.

The force for segment 1 of the hysteresis loop, shown in Figure 5.1, is modelled following the equation

$$F(u) = -P_1 + K_4 u + (\exp(a_1 u) - 1) \qquad \text{for} \qquad u \geq 0 \tag{5.27}$$

where,

$$a_1 = \frac{\ln(F_1 + P_1 - K_4 u + 1)}{u_1} \tag{5.28}$$

The slope of the curve for segment 1 is given by

$$F'(x) = K_4 + a_1 \exp(a_1 u) \tag{5.29}$$

Similar equations can be written for segments 2, 3 and 4. They are as follows,

For segment 2:

$$F(u) = -P_1 + K_4 u - (\exp(a_2 |u|) - 1) \qquad \text{for} \qquad u < 0 \tag{5.30}$$

where,

$$a_2 = \frac{(-P_1 - F_2 - K_4 u_2 + 1)}{|u_2|} \tag{5.31}$$

and

$$F'(x) = K_4 - a_2 \exp(a_2 |u|) \tag{5.32}$$

For segment 3:

$$F(u) = P_1 + K_4 u - (\exp(a_3 |u|) - 1) \qquad \text{for} \qquad u < 0 \tag{5.33}$$

where,

$$a_3 = \frac{(P_1 - F_2 + K_4 u_2 + 1)}{|u_2|} \tag{5.34}$$

and

$$F'(x) = K_4 + a_3 \exp(a_3 |u|) \tag{5.35}$$

For segment 4:

$$F(u) = P_1 + K_4 u + (\exp(a_4 u) - 1) \qquad \text{for} \qquad u \geq 0 \tag{5.36}$$

where,

$$a_4 = \frac{(P_1 - F_1 - K_4 u_1 + 1)}{u_1} \tag{5.37}$$

and

$$F' = K_4 + a_4 \exp(a_4 u) \tag{5.38}$$

5.4.2 Energy Formulation of Stiffness Matrix

The only change to the stiffness matrix formulation is the addition of the hysteresis equations. The same derivation process, as shown in Section 3.6.4, can be followed with the resulting tangent stiffness matrix being given by

$$[k_t]_{con} = \frac{nl}{2} \int_{-1}^{1} [L\,(P - P')]_{con}^{T}\, F'\,(u)\, [L\,(P - P')]_{con}\, d\tau \tag{5.39}$$

This matrix used in the same way as the other element tangent stiffness matrices, derived in Chapter 3, and are merged using the procedures outlined in Section 3.8 to form the global tangent stiffness matrix, $[K_t]$.

5.4.3 Error Checking

Due to the use of the tangent stiffness for the connector stiffness, errors are introduced into the solution. The effect of these errors can be minimized by requiring that dynamic equilibrium be satisfied at the beginning of each time–step, when the initial conditions for the accelerations are calculated, using Equation 5.7. Satisfying dynamic equilibrium prevents the accumulation of the incremental error. The error in the connector force is applied to the structure in the next time step as part of the structural spring force. This

residual has major effects in the analysis because the mass of the structure is placed primarily at the top of the framing elements in the wall. The plate elements representing the sheathing have very low mass when compared to the framing. The result is that the sheathing will have little inertial resistance compared to the framing. Therefore, the residual forces in the sheathing connectors will have a greater effect on the sheathing than on the framing displacements. Large displacements of the sheathing relative to the framing can result if the residual forces are too large. To prevent the residual forces in the sheathing connectors from becoming too large, the error in the calculated connector force is monitored.

Consider the load–deflection curve, shown in Figure 5.4. Assume the connector has the deflection, $u(t)$ force, $P(t)$, and stiffness, $K(t)$, at time, t, and an additional load, ΔP, is applied, increasing the applied load to $P_{Load}(t+\Delta t)$. The tangent stiffness method would determine the deflection of the connector to be $u(t+\Delta t)$, while calculating the connector force as $P_{Con}(t+\Delta t)$. The resulting error in force is P_{Error}, which is then incorporated into the calculation of initial conditions for the accelerations of the next time–step, when dynamic equilibrium is imposed. To minimize the residual force, two error conditions are checked, one for connectors with relatively low forces, and one for connectors with relatively high forces. The first condition is the error in force not be larger than a given percentage of the curve's intercept, P_{Int}. Written in equation form,

$$\frac{P_{Error}}{P_{Int}} \leq INTOL \tag{5.40}$$

where, $INTOL$ is the allowable tolerance, given as a percentage.

The second error condition is given as a ratio of the error, P_{Error}, and the calculated connector force, $P_{Con}(t+\Delta t)$, which must be less than a given tolerance. Written in equation form,

$$\frac{P_{Error}}{P_{Con}(t+\Delta t)} \leq ETOL2 \tag{5.41}$$

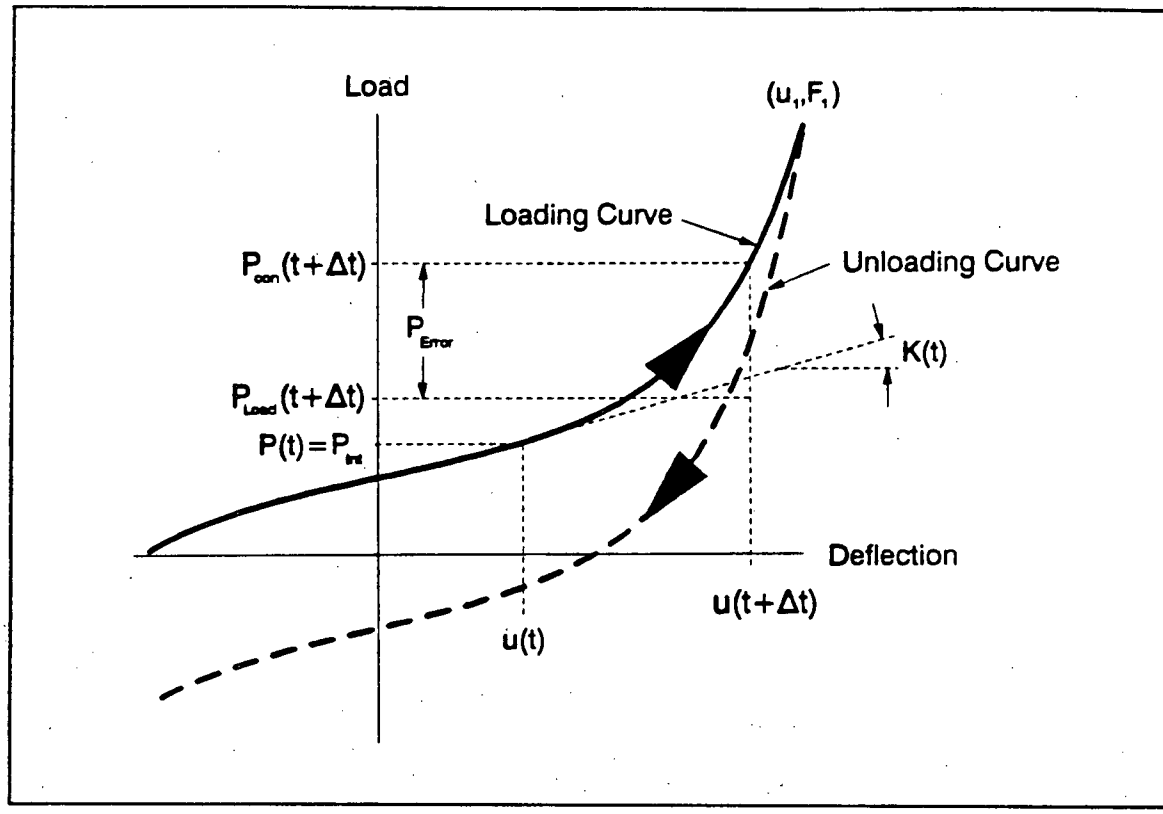

Figure 5.4: Error Checking Parameters for Sheathing Connector.

If both of the error conditions, given by Equations 5.40 and 5.41, are violated, the analysis is repeated for the time–step using a smaller time–step increment. The correction technique is repeated until either the error in the connector forces is within the tolerance, or the time increment reaches a minimum value. If the time increment is reduced to the minimum value, all error checking is ignored for one time–step. This is to prevent the round off error in the global equations from becoming too large.

5.5 Energy Calculations

Various authors, such as Belytschko (1978) and Mikkola, et al (1989), have described the usefulness of checking the energy balance as an indicator of the accuracy of the

solution.

At the end of each time–step, the various components energy are calculated in order to track the amounts of energy being dissipated by the viscous and hysteretic damping, as well as the accuracy of the solution.

Four energy components are calculated at the end of each time step in the program, **DYNWALL**. They are,

1. **Kinetic Energy,** which is energy stored in the mass of the structure.

2. **Energy Dissipated by Viscous Damping,** which is energy dissipated by material damping, and other sources not attributable to the hysteretic damping of the sheathing connectors. This is a continuously increasing value during the duration of motion.

3. **Strain Energy and Energy Dissipated by the Hysteretic Damping,** which is a combination of recoverable and non–recoverable energy in the structure. This is a continuously increasing value during the duration of the motion and accounts for the energy stored in the structure as strain energy, and the energy dissipated by the hysteretic effects of the sheathing connectors.

4. **Energy Input to the Structure,** which is energy input to the base of the wall due to motion of the base during the earthquake. This is also a continuously increasing value during the duration of motion.

These energy values are summed up at the end of each time–step to determine whether the error in energy for the solution is within a given error tolerance. The derivation of various expressions for the energy components begins with the equation of motion, given by Equation 5.6. Pre–multiplying Equation 5.6 by $\{\dot{u}(t)\}^T$, and integrating from time 0

to time t yields,

$$\begin{aligned} &\int_0^t \{\dot{u}(t)\}^T [M] \{\ddot{u}(t)\} dt \\ &+ \int_0^t \{\dot{u}(t)\}^T [C] \{\dot{u}(t)\} dt \\ &+ \int_0^t \{\dot{u}(t)\}^T [K] \{u(t)\} dt \;=\; -\int_0^t \{\dot{u}(t)\}^T [M] \{I\} \ddot{u}_g(t)\, dt \end{aligned} \tag{5.42}$$

Since,

$$\{\ddot{u}(t)\} = \frac{\{d\dot{u}(t)\}}{dt} \tag{5.43}$$

and

$$\{\dot{u}(t)\} = \frac{\{du(t)\}}{dt} \tag{5.44}$$

Equation 5.42 can be reformulated as

$$\begin{aligned} &\int_0^{\{\dot{u}\}(t)} \{\dot{u}(t)\}^T [M] \{d\dot{u}(t)\} \\ &+ \int_0^{\{u(t)\}} \{\dot{u}(t)\}^T [C] \{du(t)\} \\ &+ \int_0^{\{u(t)\}} \{du(t)\}^T [K] \{u(t)\} \;=\; -\int_0^{\{u(t)\}} \{du(t)\}^T [M] \{I\} \ddot{u}_g(t) \end{aligned} \tag{5.45}$$

integrating this equation,

$$\begin{aligned} &\frac{1}{2} \{\dot{u}(t)\}^T [M] \{\dot{u}(t)\} \\ &+ \int_0^{\{u(t)\}} \{\dot{u}(t)\}^T [C] \{du(t)\} \\ &+ \int_0^{\{u(t)\}} \{du(t)\}^T [K] \{u(t)\} \;=\; \int_0^{\{u(t)\}} \{du(t)\}^T [M] \{I\} \ddot{u}_g(t) \end{aligned} \tag{5.46}$$

This equation has the form,

$$\mathcal{K}(t) + \mathcal{D}(t) + \mathcal{U}(t) = \mathcal{I}(t) \tag{5.47}$$

where,

$\mathcal{K}(t) \;=\; \frac{1}{2} \{\dot{u}(t)\}^T [M] \{\dot{u}(t)\}$ = The kinetic energy of the system.

$$\mathcal{D}(t) = \int_0^{\{u(t)\}} \{\dot{u}(t)\}^T [C] \{du(t)\} = \text{The energy dissipated by viscous damping.}$$

$$\mathcal{U}(t) = \int_0^{\{u(t)\}} \{du(t)\}^T [K] \{u(t)\} = \text{The energy stored as strain energy in the system and the energy dissipated by hysteretic damping, combined. This term must be integrated from 0 displacement to } \{u(t)\} \text{ because the hysteretic behavior causes the results to be path–dependant.}$$

$$\mathcal{I}(t) = \int_0^{\{u(t)\}} \{du(t)\}^T [M] \{I\} \ddot{u}_g(t) = \text{The energy input to the structure.}$$

These equations account for all of the sources of energy input into the structure and dissipated by the structure. Equation 5.47 can be used to calculate the energy balance at the end of each time–step as described in the following section.

5.5.1 Energy Balance

The following equations are used in the program, **DYNWALL**, to calculate the different components of energy at the end of each time–step.

$$\begin{aligned} \mathcal{U}(t) &= \mathcal{U}(t-\Delta t) + \frac{1}{2}\left([K_s(t-\Delta t)]\{u(t-\Delta t)\}\right. \\ &\quad \left. + [K_s(t)]\{u(t)\}\right)\left(\{u(t)\} - \{u(t\Delta t)\}\right) \qquad (5.48) \\ &= \text{The strain energy, plus energy dissipated by the hysteretic sheathing connectors} \end{aligned}$$

$$\begin{aligned}\mathcal{D}(t) &= \mathcal{D}(t-\Delta t) \\ &\quad +\frac{1}{2}\{\{\dot{u}(t-\Delta t)\}+\{\dot{u}(t)\}\}^T[C]\{\{u(t)\}-\{u(t-\Delta t)\}\} \qquad (5.49) \\ &= \text{The energy dissipated by viscous damping}\end{aligned}$$

$$\begin{aligned}\mathcal{I}(t) &= \mathcal{I}(t-\Delta t) \\ &\quad +\frac{1}{2}\{\{u(t)\}-\{u(t-\Delta t)\}\}^T[M]\{I\}(\ddot{u}_g(t-\Delta t)+\ddot{u}_g(t)) \qquad (5.50) \\ &= \text{The energy input to structure by earthquake}\end{aligned}$$

These energy components are then added to calculate the error in the energy as,

$$EERROR = \mathcal{U}(t)+\mathcal{K}(t)+\mathcal{D}(t)-\mathcal{I}(t) \qquad (5.51)$$

This error is then checked against the acceptable error, which is a percentage of the system's energies, and is given by

$$TACEPT = ENTOL\,(\mathcal{U}(t)+\mathcal{K}(t)+\mathcal{D}(t)) \qquad (5.52)$$

If the error, $EERROR$, is greater than the acceptable error, $TACEPT$, the time–step increment for the analysis is reduced and the time–step repeated.

The calculations are based on equivalent lateral forces, being applied to a rigid base structure, where the forces are representative of the seismic forces in a real structure. This formulation eliminates the rigid body translation energies from the calculation, and therefore, has the advantage of eliminating the ground displacement from the calculations. Neglecting these displacements does not usually cause significant errors in the frequency range of most structures. Uang and Bertero (1988) investigated the difference between the energy formulations for absolute and relative displacements. They found that for very

short period structures, the absolute displacement energy formulation should be used, while the relative displacement formulation should be used for long structures. However, for structures with fundamental periods between 0.3 and 5.0 seconds, Uang and Bertero found no significant difference between the two energy formulations. Since the shear walls tested in the study had natural periods within the 0.3 to 5.0 sec range, the relative energy formulation can be used.

5.6 Summary of Time–Step Solution Process

The individual changes made to the static one–directional numerical model, **SHWALL**, have been outlined in the previous sections of this chapter. This section will outline the overall procedural steps used in my program, called **DYNWALL**, to solve the dynamic step–by–step integration problem. The steps followed in the program are:

1. Read the data giving the structural information for geometry, material properties, etc.
2. Calculate the mass matrix, $[M]$.
3. Calculate the solution to the static problem of dead load applied to the structure. This solution is used as the initial conditions for the dynamic analysis.
4. Calculate the damping matrix, $[C]$, given by Equation 5.5.
5. Calculate the tangent stiffness matrix, $[K_t]$, for the structure in its deformed shape.
6. Calculate the initial conditions for accelerations, $\{\ddot{u}(t)\}$, using Equation 5.26.
7. Calculate the apparent stiffness matrix, $\left[\tilde{K}\right]$, using Equation 5.21.

8. Calculate the apparent load vector, $\left\{\tilde{P}\right\}$, using Equation 5.22.

9. Solve Equation 5.20 for the incremental displacement vector, $\{\Delta u\,(t)\}$.

10. Using Equations 5.23 and 5.24, calculate the displacement vector, $\{u\,(t+\Delta t)\}$, and velocity vector, $\{\dot{u}\,(t+\Delta t)\}$, at the end of the time–step.

11. Using the conditions given in Equations 5.40 and 5.41, check to see that the error in the individual connector forces is not larger than an acceptable tolerance. If the error is too large, repeat steps 5 to 10, using a smaller time increment.

12. Calculate components of the energy balance and check against accuracy tolerance, using Equations 5.51 and 5.52. Reduce the time increment size or stop program if error in energy balance is too large.

13. Output results of time–step.

14. Check elapsed time for whether or not the analysis has progressed to the requested time. If not, repeat steps 5 to 13, otherwise end analysis.

The correlation with test data is examined in Chapter 9.

5.7 Summary

The non–linear, dynamic, numerical model, called **DYNWALL**, has been described, along with the assumptions on which the model is based. The changes required to convert the static, numerical model, **SHWALL**, to the dynamic model have been derived, along with the step–by–step integration procedures being outlined.

DYNWALL is a general finite element model, with the ability to predict the deflections of timber shear walls. By incorporating the model, **SHWALL**, all of the improvements made in Chapter 3 are also included in **DYNWALL**. These improvements include:

1. accounting for the ultimate load capacity,
2. the effects of bearing between adjacent sheathing panels,
3. the ability to model a variety of connectors,
4. representing the bearing and formation of gaps between framing elements, and
5. the capability of representing general random dynamic loads.

Possible improvements that could be made to the dynamic model, and the model's accuracy are examined in Chapter 9. The predicted displacements of the top of the wall, relative to the base is compared to dynamic shear wall test results, for both plywood and waferboard. The effects of the out–of–plane bending of the sheathing are also discussed in Chapter 9.

Chapter 6

Connection Tests

6.1 Introduction

The strength and stiffness of nailed timber shear walls are mainly governed by the strength and stiffness of the connections between the timber members, rather than the properties of the members themselves. This characteristic of timber shear walls has been investigated and described by several researchers, such as Toumi and McCutcheon (1977), and Foschi (1982). These investigations were primarily directed towards the one–directional static racking performance of the shear walls, with a few researchers, such as Falk and Itani (1988) studying the cyclic or dynamic performance. Virtually all of the experimental investigations have concentrated on the static, one–directional test for connections and shear walls, which does not adequately describe the structural behavior of shear walls.

A testing procedure, for determining wall stiffness and strength for various wall configurations, has been described in the ASTM Standard E72–77 (1986). This procedure involves full–sized 2.4 m × 2.4 m (8 × 8 ft) wall panels, which makes the testing time consuming and expensive. An inexpensive method would be to perform representative tests to determine the load–deflection curves for the connections between the timber components. The results of the connection tests could then be used along with computer models, such as the two described in Chapters 3 and 5, to predict the full-sized wall

performance.

This chapter describes procedures, equipment, specimens, data analysis procedures, and results for tests of nailed connections. The tests were conducted in order to determine the parameters defining the load-deflection curves for the sheathing and corner connections, which were used in constructing the timber shear walls described in Chapter 7. The results are presented in the form suitable for use in the programs **SHWALL** and **DYNWALL**.

6.2 Experimental Overview

6.2.1 Objectives

In order to obtain average load–deformation curves for use in modelling the full–sized shear walls, two types of connections were tested. Tests were performed on the connection between framing and sheathing materials, and on the connection between the two types of framing members used for the stud and sole plate, or stud and sill plate of the wall. Studs are defined as the vertical framing members. The sole and sill plates are defined as the horizontal framing members at the base and top of the wall, respectively. Figure 3.7, shown on page 54, shows an exploded view of a shear wall with the locations of the various connectors shown. The sheathing connection usually consists of nails spaced sufficiently close to provide resistance to the racking loads applied to the wall. The corner connection consists of a steel angle and is used to prevent the framing members from separating when loaded.

Three tests were performed to determine the characteristics of the sheathing connection. These were **1)** static one–directional tension, **2)** static cyclic, and **3)** "dynamic" cyclic tests. The procedure for each of these tests are described in Section 6.6. The

sheathing connection tests were repeated for each of the possible grain orientations and material combinations used in the full–sized wall tests described in Chapter 7.

The corner connection test was used to determine the configuration that would result in the highest stiffness and strength, using the minimum amount of steel and to obtain the average stiffness for the resulting connection. This connection is required to transmit the entire design force in the cord to the sole plate without failing. Failure of this connection has been described by the Applied Technology Council (1981), and Soltis (1984) as one of the predominate modes of failure for many timber shear walls and diaphragms during earthquakes. Observed failures in wood–sheathed diaphragms and shear walls have invariably been caused by inadequate connection detailing, or improper installation. The design of the diaphragm itself is not sufficient if the connections at the load transfer positions are inadequate. Shear walls transfer the overturning moment to the horizontal diaphragm or foundation at the corners where the end studs are connected to the sill and sole plates. Failure of this connection results in the shear wall's deformation, changing from a racking to a rigid body rotation. These two types of deformations are shown in Figure 6.1.

Table 6.1 gives a complete accounting of the type of tests performed and the number of replications used for each test.

6.3 Testing Equipment

The connection tests were performed using a hydraulic jack mounted to a Tinius Olson testing machine frame. The jack was controlled by an MTS 460 controller. This configuration is shown in Figures 6.2 and 6.3.

The data was acquired digitally using an IBM–AT and a Scientific Solutions Lab-Master 12 bit analog to digital converter. Displacements of the joint were measured

Table 6.1: Types of Connection Tests Performed and Number of Specimens.

Test Type	Sheathing Type	Grain Orientation to Load Sheathing	Grain Orientation to Load Framing	Number of Specimens
Sheathing Connections:				
Static 1–D	Plywood	Parallel	Parallel	5
		Parallel	Perpendicular	5
		Perpendicular	Parallel	3
		Perpendicular	Perpendicular	5
	Waferboard	Parallel	Parallel	4
		Parallel	Perpendicular	4
		Perpendicular	Parallel	5
		Perpendicular	Perpendicular	4
Static Cyclic	Plywood	Parallel	Parallel	5
		Parallel	Perpendicular	4
		Perpendicular	Parallel	3
		Perpendicular	Perpendicular	5
	Waferboard	Parallel	Parallel	5
		Parallel	Perpendicular	4
		Perpendicular	Parallel	4
		Perpendicular	Perpendicular	3
Dynamic Cyclic	Plywood	Parallel	Parallel	4
		Parallel	Perpendicular	4
		Perpendicular	Parallel	4
		Perpendicular	Perpendicular	4
	Waferboard	Parallel	Parallel	5
		Parallel	Perpendicular	4
		Perpendicular	Parallel	4
		Perpendicular	Perpendicular	3
Corner Connection	N/A	N/A	N/A	5

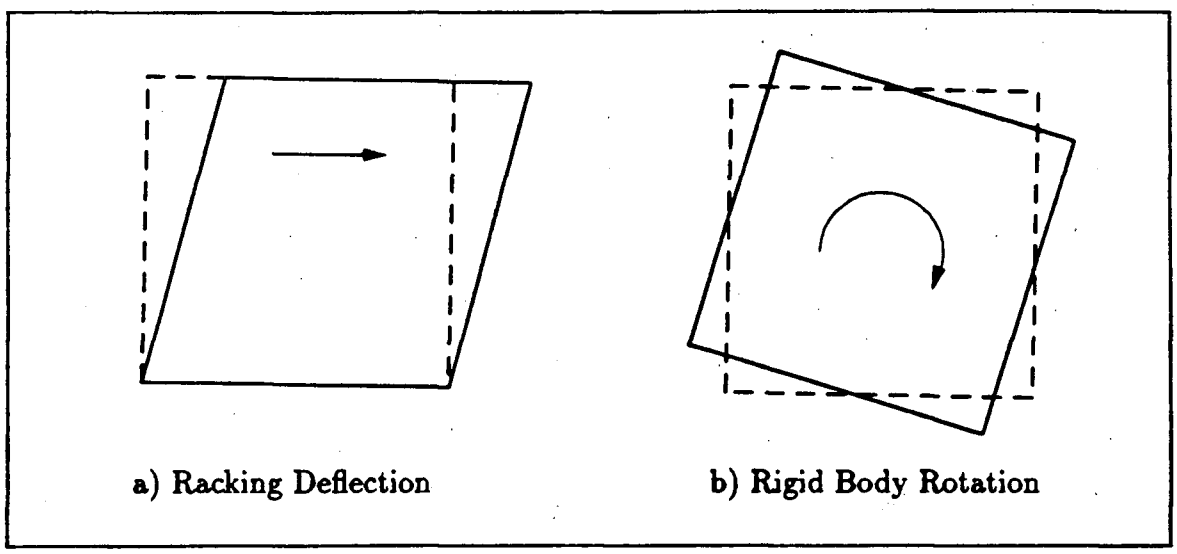

Figure 6.1: Racking Versus Rigid Body Rotation Deflection.

using Trans-Tek and Hewlett-Packard DC-DC displacement transducers. Loads were measured using a 5-metric ton MTS load cell. The data acquisition equipment is shown in Figure 6.4.

6.4 Test Material

The materials used in this study are employed in the construction of most timber residential structures in North America.

6.4.1 Framing

The framing material[1] consisted of 38 × 89 mm (2 × 4 in nominal) Spruce–Pine–Fir (SPF). The lumber, from Upper Fraser, British Columbia, was kiln dried, Standard and Better grade. The framing material was predominantly spruce.

The moisture content (MC) of the framing material ranged from 9–14% MC, with an

[1]Supplied by the Council of Forest Industries of British Columbia (COFI)

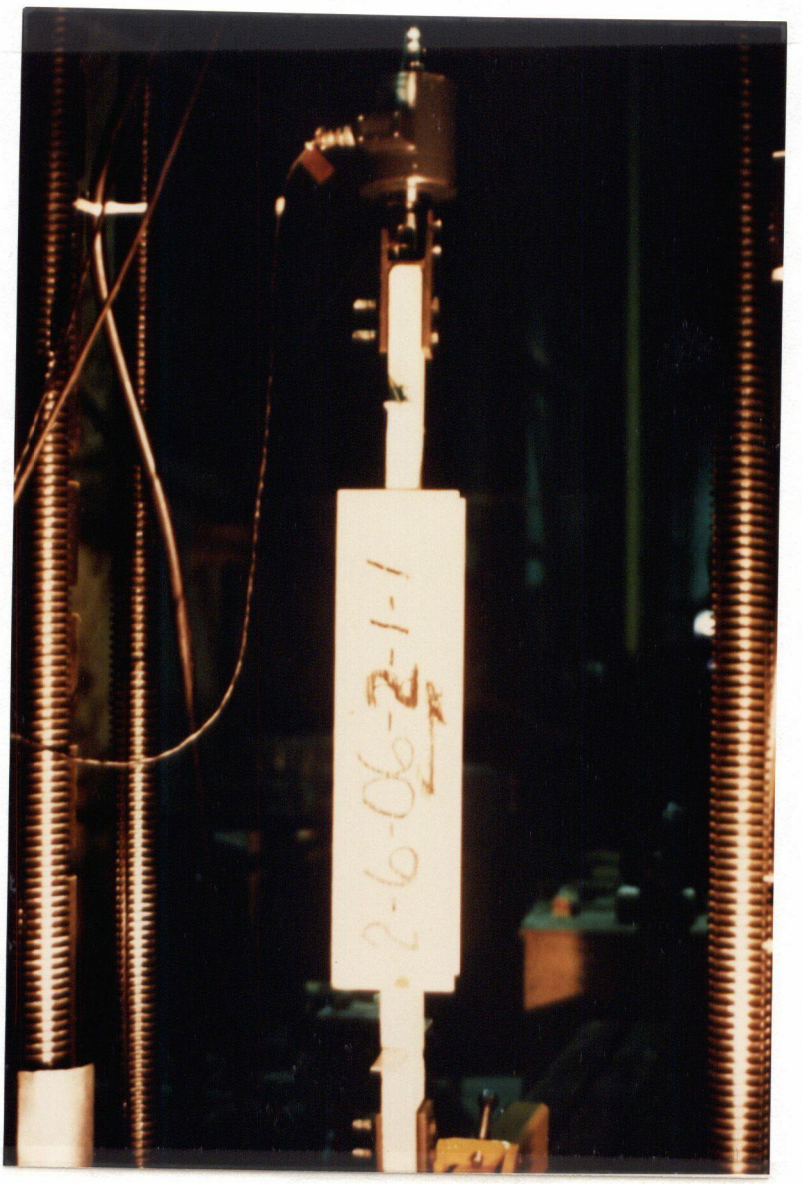

Figure 6.2: Test Frame With Hydraulic Jack.

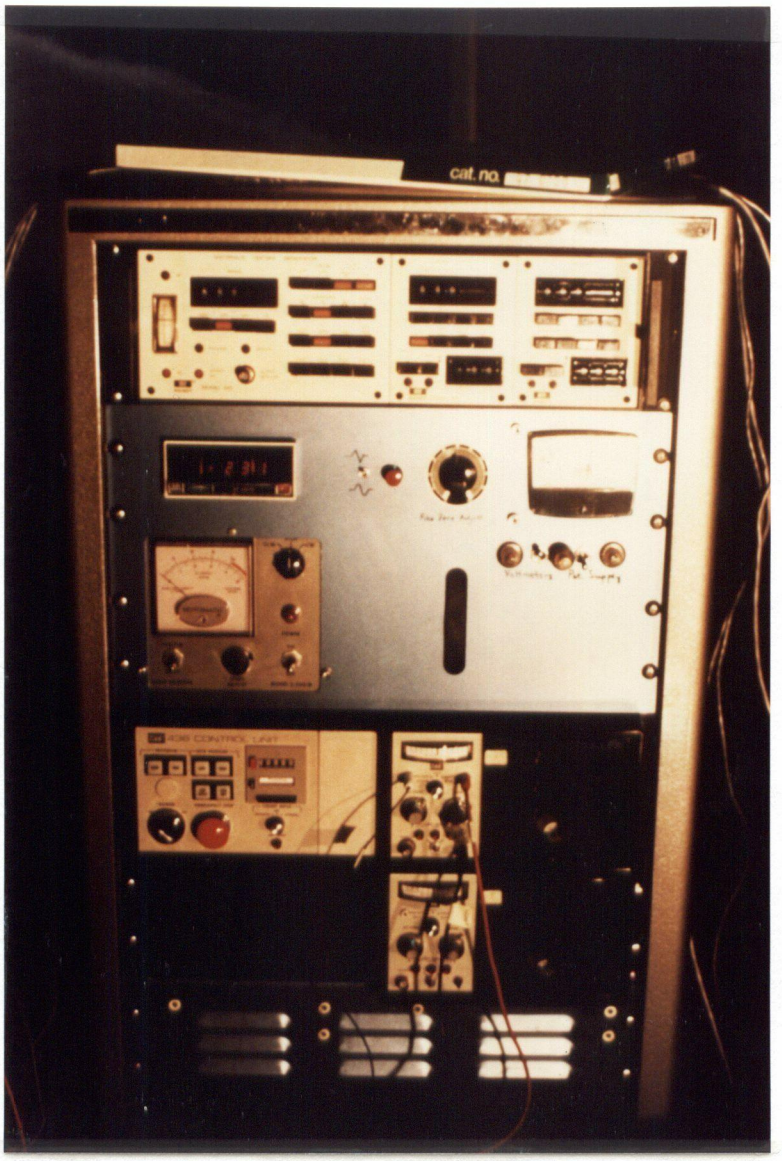

Figure 6.3: MTS Controller Used To Control The Hydraulic Jack.

Figure 6.4: Data Acquisition Equipment.

average value of 11% MC, and a standard deviation of 0.76% MC. The moisture content was measured using a Delmhorst moisture meter, and the meter readings were corrected to actual moisture contents using the tables published by Bramhall and Salamon (1978).

6.4.2 Sheathing

Two types of sheathing were used in this study, plywood[2] and waferboard[3]. The plywood used was 9.5 mm (3/8 in) A-5 Exterior CF BC 142 grade Canadian softwood plywood (CSP) sheathing[4] and, the waferboard, which was 9.5 mm (3/8 in) solid exterior grade[5] .

6.4.3 Nails

The nails used to make the sheathing connections were 8d or 63.5 mm (2.5 in) hot dipped galvanized common nails[6].

6.4.4 Screws

Screws were used to attach the steel angles for the corner connections. Several different types of screws were tried in various configurations, until one combination was found to change the failure mode from withdrawal of the screws to failure of the framing material. The final connection that was tested, used 4 × 38 mm (No. 8 × 1.5 in) drywall screws[7].

[2]Supplied by the Council of Forest Industries of British Columbia (COFI)
[3]Supplied by The Waferboard Association
[4]Produced by Crown Forest Industries Ltd. in Kelowna, British Columbia
[5]Produced by Weldwood Canada Ltd. in Vancouver, British Columbia
[6]Supplied by Titan Steel and Wire Co. Ltd., Surrey, British Columbia
[7]Supplied by Grabber Industrial Products Ltd., Vancouver, British Columbia

6.4.5 Steel Angles

Steel angles were used to make the corner connection. Figure 6.5 shows the location of the steel angle in a typical test specimen. The steel angle iron used in the connection tests was 101.6 × 76.2 × 6.4 mm (4 × 3 × 1/4 in) hot rolled, mild structural steel[8].

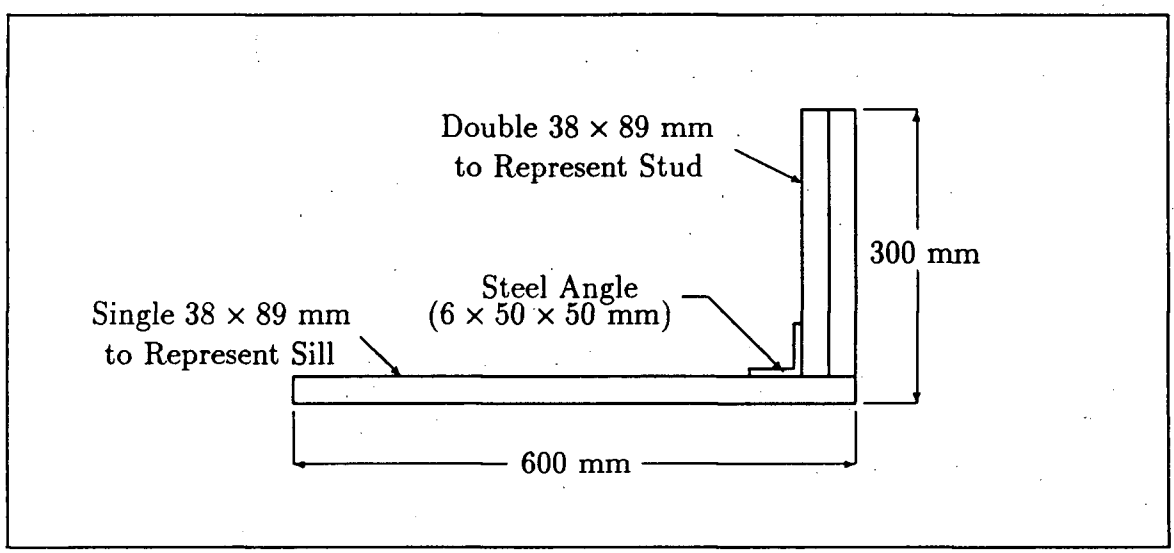

Figure 6.5: Corner Connection Test Specimen Configuration.

6.5 Specimen Description

6.5.1 Sheathing Connection Test Specimen

The sheathing connection test was performed to obtain seven parameters which were used to describe the load–deflection curve of the nail connection between the framing and sheathing. These parameters are shown in Figure 6.6a and 6.6b.

The sheathing connection specimens were constructed in four different configurations, as shown in Figure 6.7. The different configurations covered all possible combinations of

[8]Manufactured by Wilkinson Company Ltd., Vancouver, British Columbia

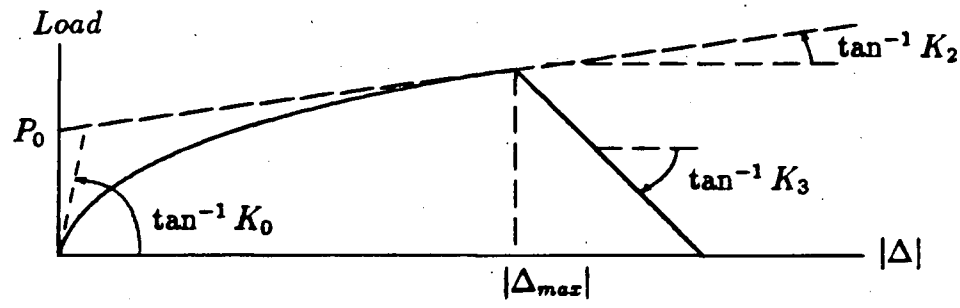

(a) Connector Load–Deflection Curve For Static One–Directional Movement And Envelope For The Hysteretic Curves.

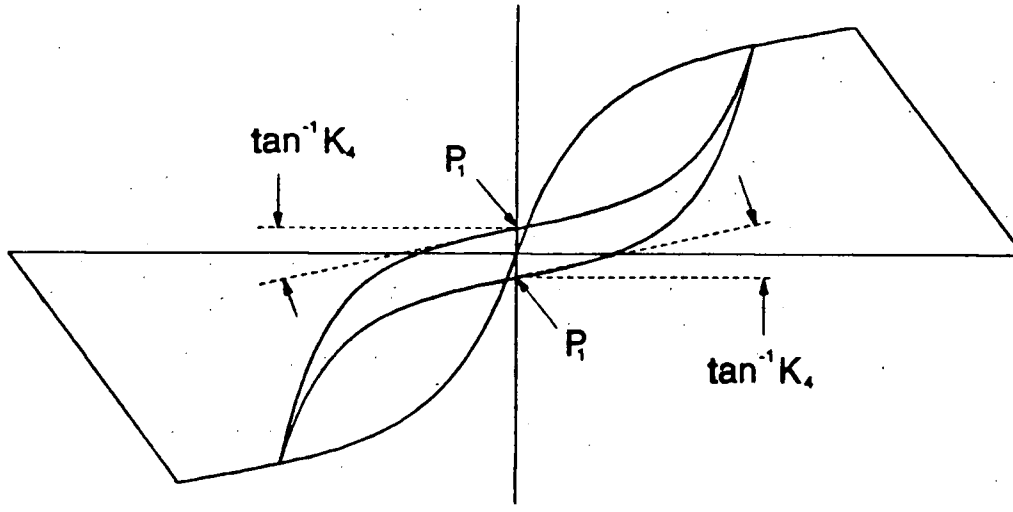

(b) Connector Hysteretic Load–Deflection Curve.

Figure 6.6: Sheathing Connector Load–Deflection Curve Parameters.

the sheathing face grain direction and framing grain direction. (While the waferboard does not have a predominant grain direction, the long dimension of the 2.4 m × 1.2 m (8 ft × 4 ft) panels was assumed to be the predominant grain direction for determining the specimen configuration so that comparisons could be made with the plywood sheathing.)

The nails were driven by hand until the nail head was flush with the sheathing surface. To prevent the variable of overdriven nails from entering the problem, care was taken to ensure the face veneer of the plywood specimens was not penetrated by the nail head. Two 25.4 × 12.2 mm (1 × 1/2 in) stiffeners were attached to the plywood specimens with the configuration shown in Figure 6.7a. These stiffeners were used in order to prevent the plywood from buckling in compression during the cyclic tests. Once the finite element models are verified, they can be used to investigate the effects of overdriven nails or the use of other fasteners on the behavior of shear walls. This would allow the data base of useful fasteners to be expanded without the expense of full size shear wall tests.

6.5.2 Corner Connection Test Specimen

The corner connection was tested to determine the stiffness of the joint in tension. This parameter is used as the stiffness of the beam–to–beam connection in the computer models, **SHWALL** and **DYNWALL**.

The test specimen configuration used for the corner connection test is shown in Figure 6.5. Some of the requirements for the corner connection were:

1. The anchor bolt in the sole plate could be located a maximum of 200 mm (8 in) away from the double stud member. This relaxes the accuracy required when positioning the anchor bolts in the foundation.

2. The connection would be assembled in a wall that had already been sheathed on one side. This allows less complicated construction methods to be used.

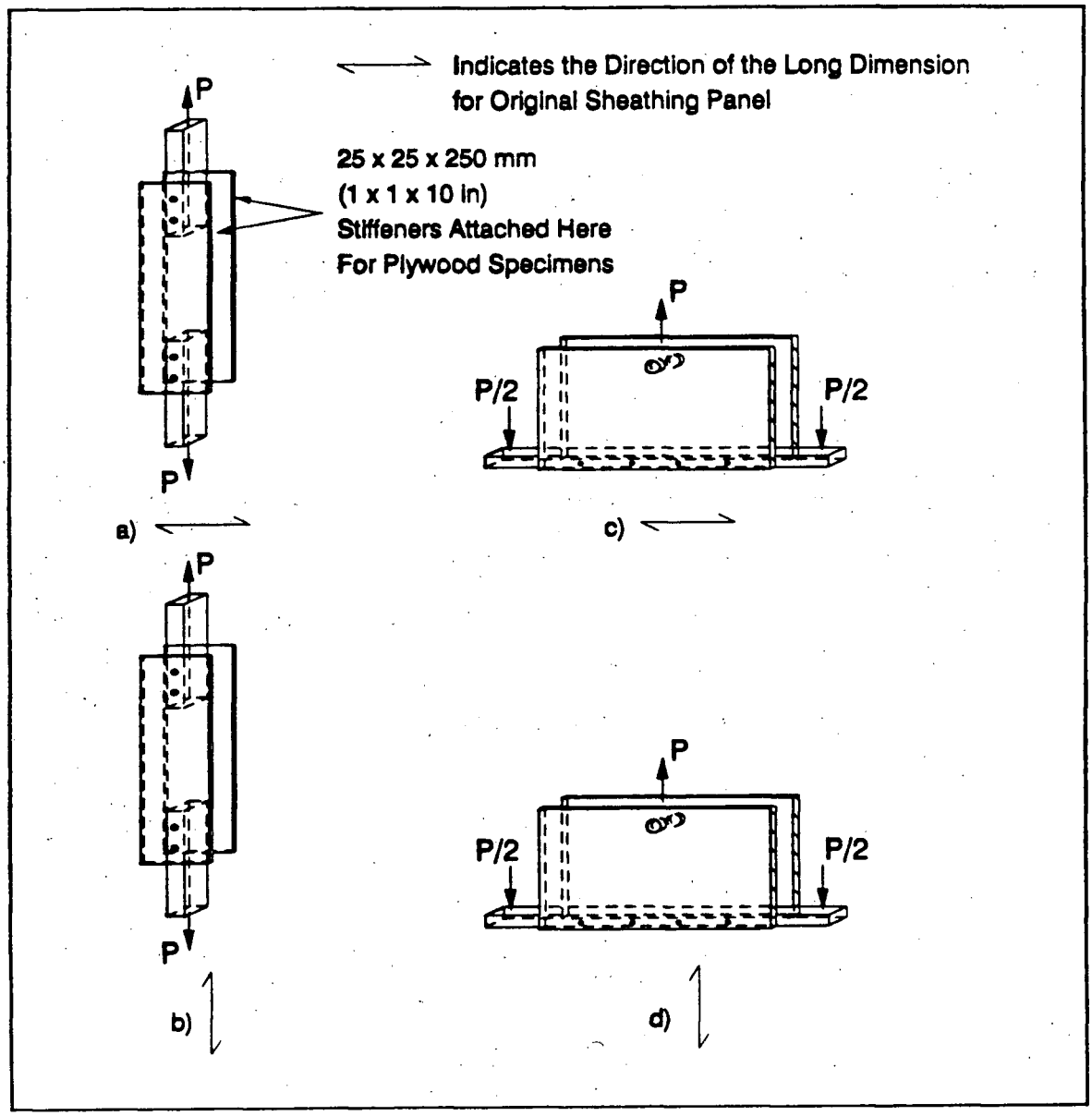

Figure 6.7: Sheathing Connection Test Specimen Configurations.

3. The connection must transmit the tension force in the stud framing element to the sole plate framing element. This requires the initial failure to occur in the framing.

6.6 Test Procedure

6.6.1 Sheathing Connection Tests

Each of the three tests used to determine the load–deflection parameters for sheathing connection are described separately. All the tests used a minimum of three specimens for each configuration of the sheathing connection.

6.6.2 Static One–Directional Tests

The static one–directional tests were performed to determine the five parameters that define the load–deflection curve, shown in Figure 6.6a. The loading was displacement controlled. The specimen were loaded in tension, following a ramp loading pattern. The rate of loading was such that the time to complete failure of the specimen was between 5 and 10 minutes. This is in between the loading rates specified by the ASTM Standards E72–77 and E564–76 used for shear walls, and allows the results of the tests to be compared to previous work with confidence, that the load rate will not affect the results. The displacement pattern used for this test is shown in Figure 6.8a.

Six signals were recorded during the testing; they were the load, jack displacement, and 4 DC displacement transducers (DCDT). The DCDT's were used to measure the displacement between the sheathing and the framing, and were positioned as shown in Figure 6.9.

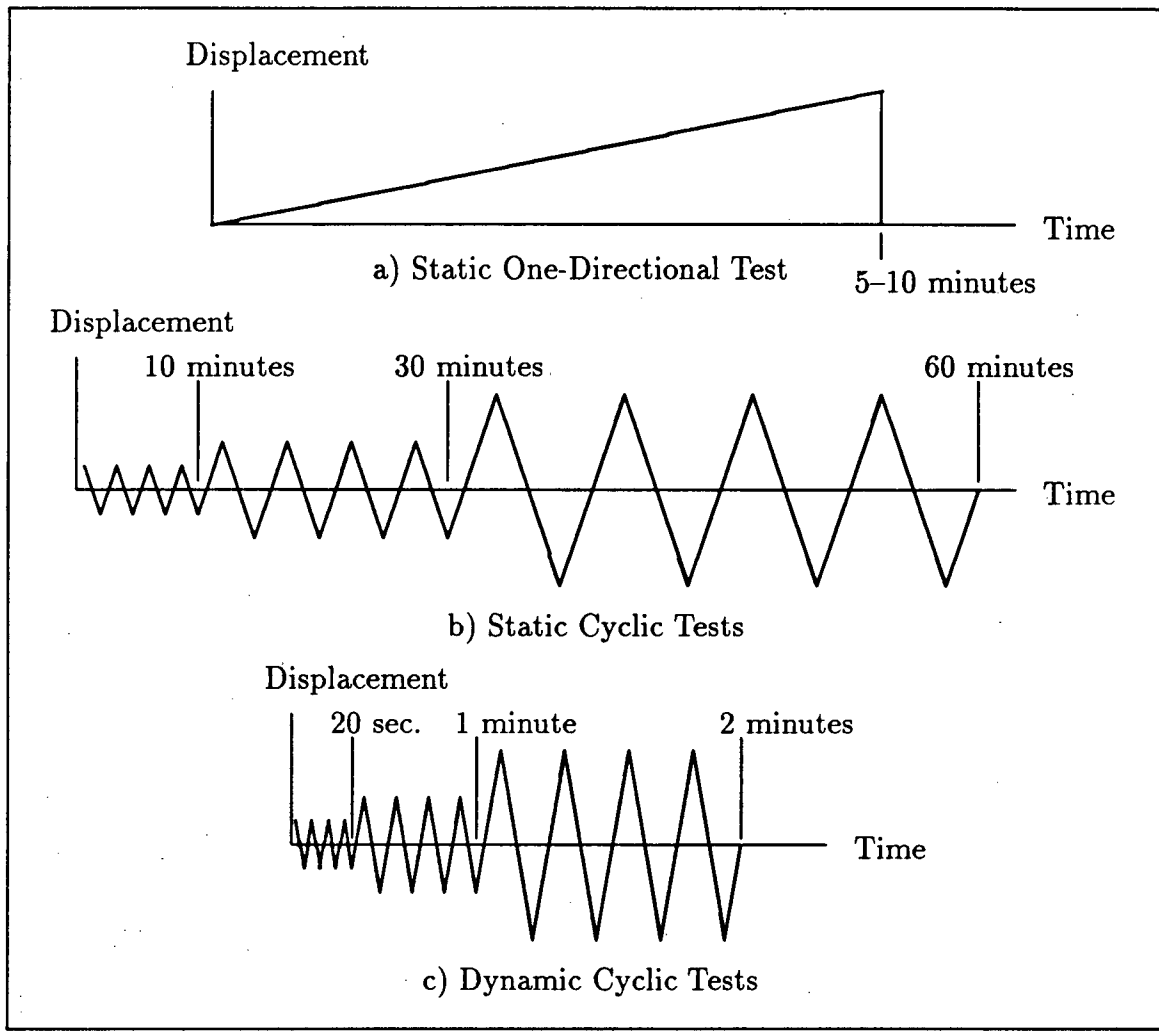

Figure 6.8: Typical Connection Test Displacement Patterns.

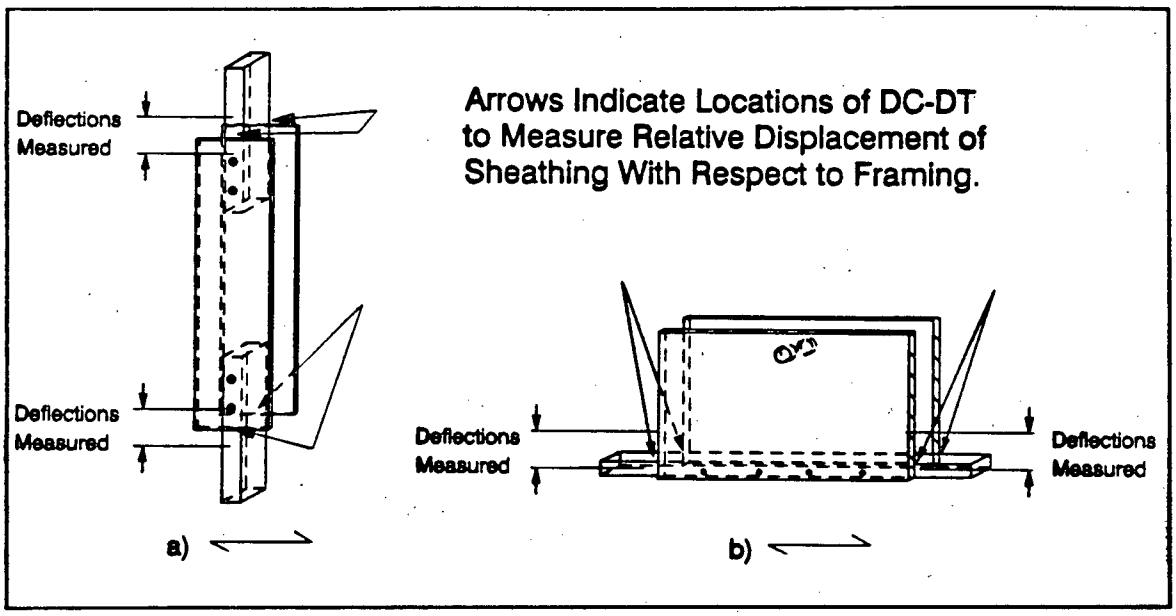

Figure 6.9: Locations of DC–DT's for Sheathing Connection Test Specimens.

6.6.3 Static Cyclic Tests

The two parameters of the hysteretic load–deflection curve, shown in Figure 6.6b were determined with the static cyclic test. These two parameters, the load intercept, P_1, and slope at zero displacement, K_4, are parameters required for the computer model, **DYNWALL**, described in Chapter 5.

The connection test used the same specimen configurations as those for the static one–directional test, and are shown in Figure 6.7. The loading, however, followed a triangular sine wave displacement pattern, which is shown in Figure 6.8b. The connection was tested by repeating the displacement pattern for four cycles, at three different maximum displacements. Each set of displacement cycles had a different period so as to maintain a uniform displacement rate equal to the rate used in static one–directional tests. Maintaining the same rate of displacement allows the results to be compared to previous work. Table 6.2 shows the displacements and respective settings used for this

Table 6.2: Sheathing Connection Test Displacements and Cycle Periods.

Test Type	Number of Cycles	Maximum Jack Displacement	Cycle Period
Static One-directional	1	N/A	5 – 10 minutes
Static Cyclic	4	+/- 6.4 mm (+/- 0.25 in)	150 seconds
	4	+/- 12.7 mm (+/- 0.5 in)	300 seconds
	4	+/- 19.0 mm (+/- 0.75 in)	450 seconds
"Dynamic" Cyclic	4	+/- 6.4 mm (+/- 0.25 in)	5 seconds
	4	+/- 12.7 mm (+/- 0.5 in)	10 seconds
	4	+/- 19.0 mm (+/- 0.75 in)	15 seconds

test.

6.6.4 "Dynamic" Cyclic Tests

The "dynamic" cyclic tests were performed to determine if any of the parameters that were chosen to define the connection load–deflection curves, were dependent on load rate. The "dynamic" cyclic test followed the same displacement patterns as those used for the static cyclic connection tests, but with higher displacement rates.

The term "dynamic" is used here to denote a loading rate 30 times faster than that used in the static test, as shown in Table 6.2. The displacements and respective cycle periods for this test are shown in Table 6.2.

6.6.5 Corner Connection Tests

The corner connection tests were conducted as static one–directional tests. The loading was displacement–controlled, and used a ramp displacement pattern similar to that shown in Figure 6.8a. The specimen were loaded in tension until failure, and the load, jack displacement, and uplift of the sole plate framing member were recorded. Displacements of the jack and sole plate uplift allow the load–displacement curve for joint separation to be calculated and, consequently, the joint stiffness in tension can be determined. The loading rate was such that the time to failure for each specimen was between 5 and 10 minutes. This is the same loading used for the static sheathing connection tests.

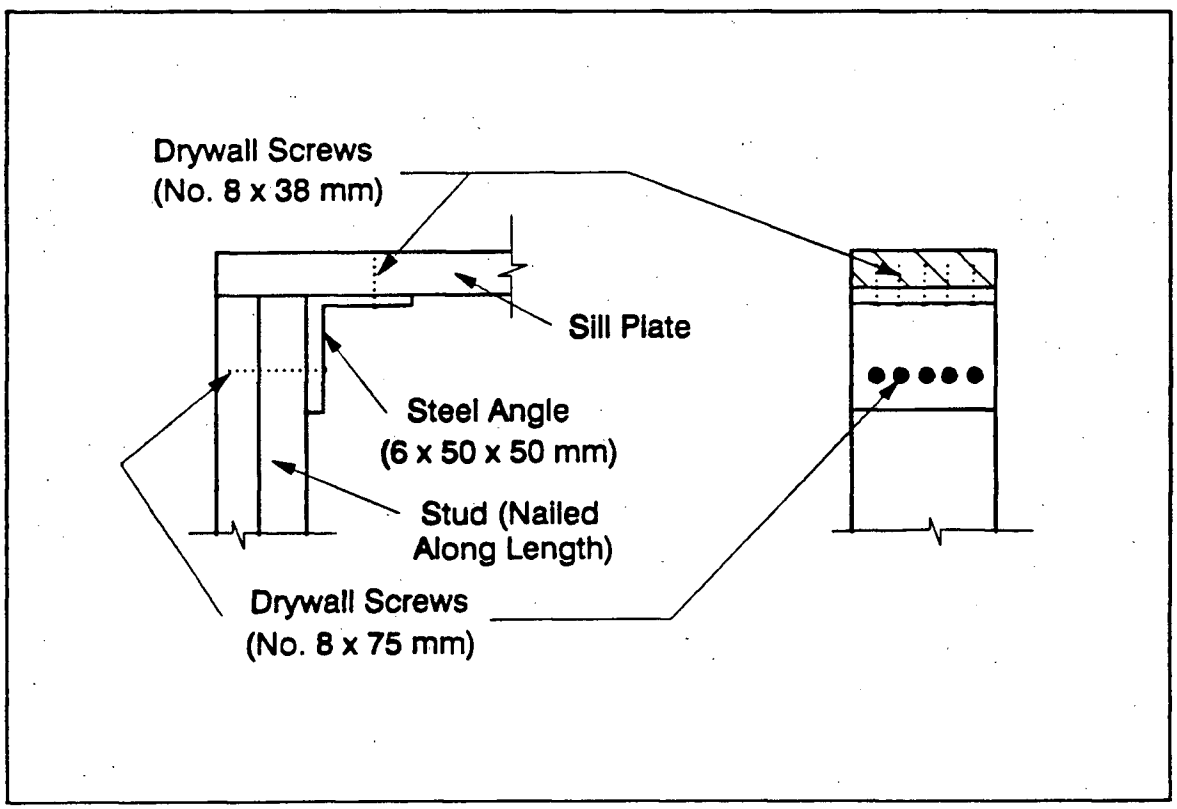

Figure 6.10: Detail of Corner Connection.

Various configurations were tested using different sizes and numbers of screws, and

different sized steel angles. The configuration was changed until the mode of failure in the specimen was failure of the sole plate framing member, rather than withdrawal of the screws or bending of the steel angle. The configuration chosen is shown is Figure 6.10 and, consisted of a 51 × 51 × 6 mm (2 × 2 × 1/4 in) steel angle which was attached, using five 4 × 38 mm (No. 8 × 1–1/2 in) drywall screws in each leg of the angle. Five connections, using this configuration, were then tested to determine the average stiffness of the connection.

6.7 Results and Discussion

The results of the connection tests are presented as average values and coefficients of variation (C.V.) for each specimen type. In some tables there are cells listed as N/A, to indicate that either the data was not intended for calculating this parameter or, there were to few specimens remaining in the sample for the results to be credible.

While using average values to draw conclusions helps smooth irregularities in the data, the C.V. values give an indication of the data's dispersion. Most of the coefficients of variation are 0.20 or lower, but a few have relatively high values. The higher C.V.'s indicate the parameter will have high variability and could be cause for concern. However, most of the high coefficients of variation pertain to parameters which are slopes that are affected by the failure mode of the specimen. A higher variability in these parameters is expected since the specimens could fail in more than one mode.

Another study conducted by Foschi (1982) used specimens of waferboard sheathing, Douglas–fir framing, an various nails, including 63 mm (3d or 2.5 in) galvanized nails. Foschi found no significant differences in the load–deflection parameters for different grain orientations. His findings add some credence to using average values for each of the parameters.

6.7.1 Sheathing Connection Tests

6.7.1.1 Static One–Directional

The static one–directional test data were analyzed using a least squares regression method to fit the equation,

$$F_{con} = (P_0 + K_2 |\Delta|) \left(1 - \exp(-\frac{K_0 |\Delta|}{P_0})\right) \tag{6.1}$$

to the data, up to the peak load. The connection force is represented by F_{con}, and Δ is the connection displacement. K_0, K_2, and P_0 are the parameters shown in Figure 6.6a.

The value, Δ_{max}, represents the displacement at peak load, and was obtained directly from the load–deflection data. The descending slope of the load–deflection curve, following the peak value, was found by performing a linear regression using the data following the peak value.

Figure 6.11 shows a typical load–deflection curve obtained from the static one–directional test. The figure also shows the segments of data used to determine each of the parameters. The negative displacements, with an increase in load, that can be seen in the load–deflection curve, are the result of the specimen configuration and the averaging of four displacement measurements. These vibrations in the load–deflection curve were considered to be noise and were eliminated by using a least squares regression of the data.

Tables 6.3 and 6.4 show average values and C.V.'s for the five parameters, K_0, K_2, K_3, P_0, and Δ_{max} for each configuration. The grain directions for the sheathing and framing are given with respect to the loading direction.

One conclusion that can be made from the static one–directional test results is that there is no obvious pattern to the average values with respect to grain orientation. While

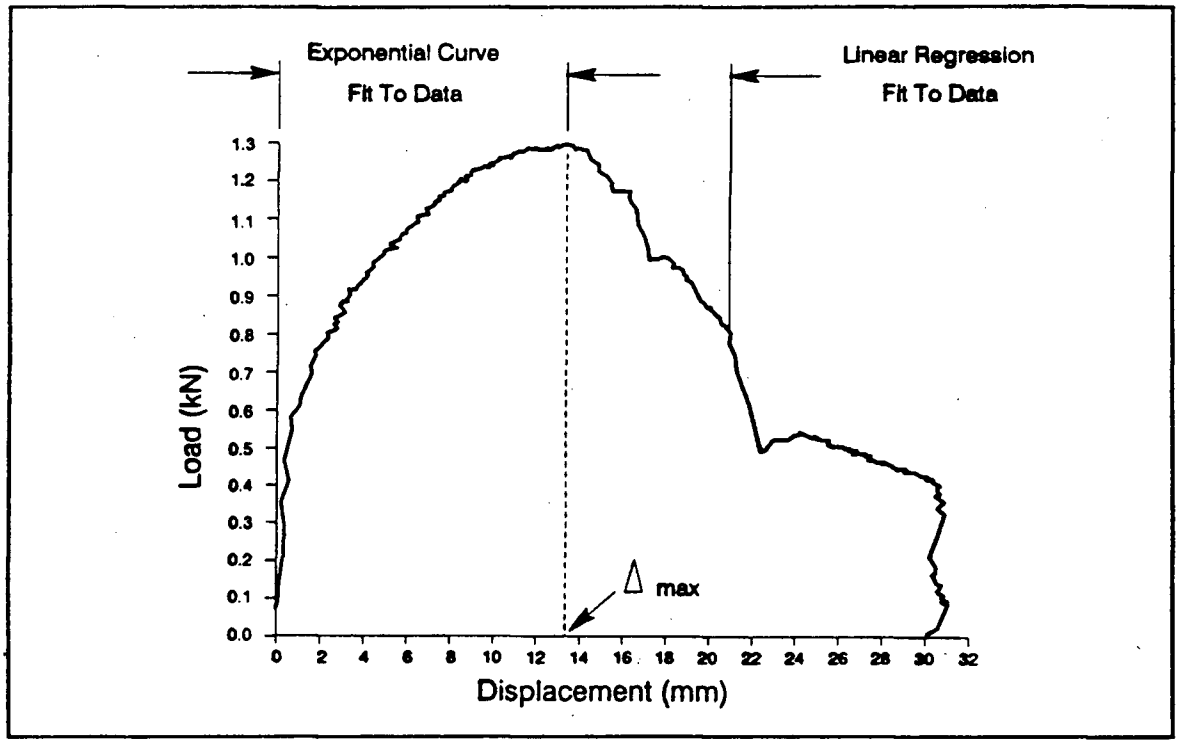

Figure 6.11: Typical Load–Deflection Curve Obtained From The Static One–Directional Connection Test.

this might be expected for waferboard, since it is more homogeneous in the way it is manufactured, plywood could have been expected to have a dependency on grain orientation. One reason plywood was expected to have this dependency is that it did tend to have different modes of failure, depending on the orientation of the face grain, with respect to the load direction. Plywood specimens with the configuration shown in Figure 6.7c, tended to fail either by the nail pulling out of the framing or tearing out sections near the edge of the plywood. When the face grain was oriented perpendicular to the load, the nail head usually broke through the first veneer, then pulled through the plywood, leaving a small hole. On the other hand, the waferboard specimens usually failed by pulling the nail out of the framing. Figures 6.12 and 6.13 show two of the typical failures that occurred in the sheathing connection tests.

Figure 6.12: Typical Failure of Sheathing Connection Test Specimen.

Figure 6.13: Typical Failure of Sheathing Connection Test Specimen.

Table 6.3: Load–Deflection Parameters Obtained From The Static One–Directional Sheathing Connection Tests Using Waferboard Sheathing.

Number	Framing Grain Orientation	Sheathing Grain Orientation	Value	K_0 N/mm (lb/in)	P_0 N (lbs)	K_2 N/mm (lb/in)	Δ_{max} mm (in)	K_3 N/mm (lb/in)
4	Parallel	Parallel	Ave.	875	989	31	9	–31
				(4994)	(222)	(177)	(0.4)	(–178)
			C.V.	0.11	0.08	0.34	0.18	0.21
4	Parallel	Perp.	Ave.	980	1127	22	8	–41
				(5599)	(253)	(127)	(0.3)	(–236)
			C.V.	0.24	0.10	0.41	0.14	0.56
5	Perp.	Parallel	Ave.	885	1062	44	9	–29
				(5056)	(239)	(250)	(0.4)	(–163)
			C.V.	0.19	0.11	0.68	0.10	0.44
4	Perp.	Perp.	Ave.	753	937	42	8	–33
				(4302)	(211)	(242)	(0.3)	(–189)
			C.V.	0.15	0.09	0.39	0.15	0.28
Overall Average Values			Ave.	874	1031	35	9	–33
				(4992)	(232)	(202)	(0.3)	(–190)
			C.V.	0.21	0.12	0.60	0.15	0.45

Since a dependency on face grain was expected, but was not obvious in the numerical results, the data for all the specimens were combined and ranked for each parameter. The results showed a slight dependency on the sheathing face grain orientation of plywood for only one of the parameters, K_0, the initial stiffness. As a result, the average value for each sheathing grain orientation of plywood is shown at the bottom of Table 6.4. The difference between the two initial stiffness values is minimal and therefore an overall average is also given.

There is little difference between the waferboard and plywood sheathing connections. The overall average values for K_0 and K_2 are higher for plywood than for waferboard, but the intercept value for waferboard is higher than for plywood. Figure 6.14 shows the average curves for plywood and waferboard sheathing connections, plotted on the same graph. The two curves show little difference in the initial deformations, but as

Table 6.4: Load–Deflection Parameters Obtained From The Static One–Directional Sheathing Connection Tests For Plywood Sheathing.

Number of Specimens	Framing Grain Direction	Sheathing Grain Direction	Value	K_0 N/mm (lb/in)	P_0 N (lbs)	K_2 N/mm (lb/in)	Δ_{max} mm (in)	K_3 N/mm (lb/in)
5	Parallel	Parallel	Ave.	794 (4531)	907 (204)	39 (224)	11 (0.4)	–41 (–234)
			C.V.	0.21	0.14	0.27	0.15	0.58
5	Parallel	Perp.	Ave.	1195 (6827)	910 (205)	26 (150)	7 (0.3)	–27 (–153)
			C.V.	0.25	0.23	0.84	0.41	0.61
3	Perp.	Parallel	Ave.	1436 (8201)	813 (183)	76 (432)	8 (0.3)	–36 (–204)
			C.V.	0.24	0.12	0.18	0.18	0.32
5	Perp.	Perp.	Ave.	832 (4750)	973 (219)	50 (285)	8 (0.3)	–54 (–308)
			C.V.	0.20	0.09	0.13	0.46	0.54
Overall One–Dimensional Tests Values								
	N/A	Parallel	Ave.	1034 (5907)				
			C.V.	0.38				
	N/A	Perp.	Ave.	1014 (5788)				
			C.V.	0.30				
	N/A	Overall	Ave.	1023 (5841)	910 (205)	45 (255)	9 (0.3)	–42 (–240)
			C.V.	0.34	0.17	0.49	0.35	0.70

the deflection increases the plywood connection stiffness decreases more quickly than the waferboard connection. Also, the plywood connection's ultimate load capacity is slightly lower, and the capacity decreases more rapidly for the plywood connection. The differences between the two connection types is probably due to some of the plywood connection specimens failing by the nail heads pulling through the sheathing, while none of the waferboard specimens failed in this manner.

The high coefficient of variation values shown for the parameter, K_3, are due to the different modes of failure that occurred. Some specimens failed by the nails breaking

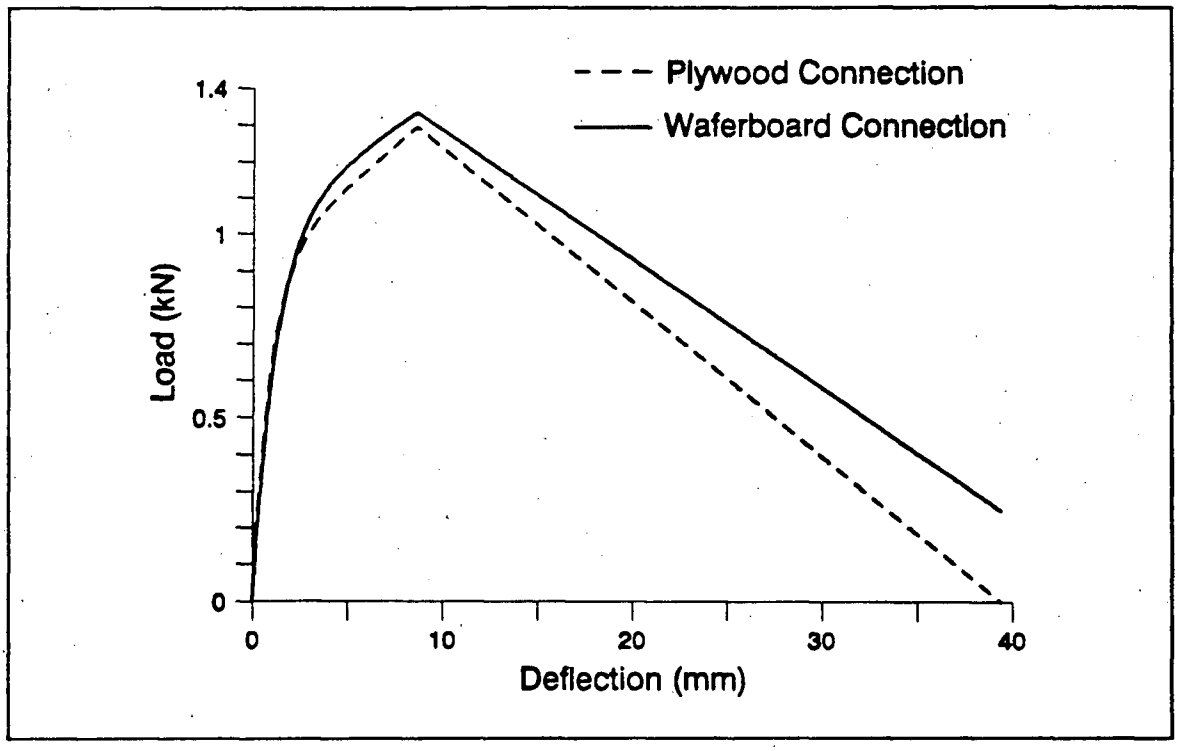

Figure 6.14: Average Load–Deflection Curves Using Exponential Curve Parameters.

while, others failed by the nails either pulling out of the framing or pulling through the sheathing. These differences do not appear in the data until after the peak load has been reached. Therefore, the C.V.'s for the parameters describing the load–deflection curve prior to the peak load are expected to be lower than for those after the peak load has been reached.

The discussion above shows that the connection properties are predominantly governed by the material properties of the nails rather than by the timber materials used. However, as the connection load approaches the load capacity of the connection, a slight dependency on the sheathing material exists.

The shape the nails have, after the test specimen has failed, is another piece of evidence that indicates the nail material properties are the predominate influence on the connection performance. Figure 6.15 shows a few of the nails after being tested.

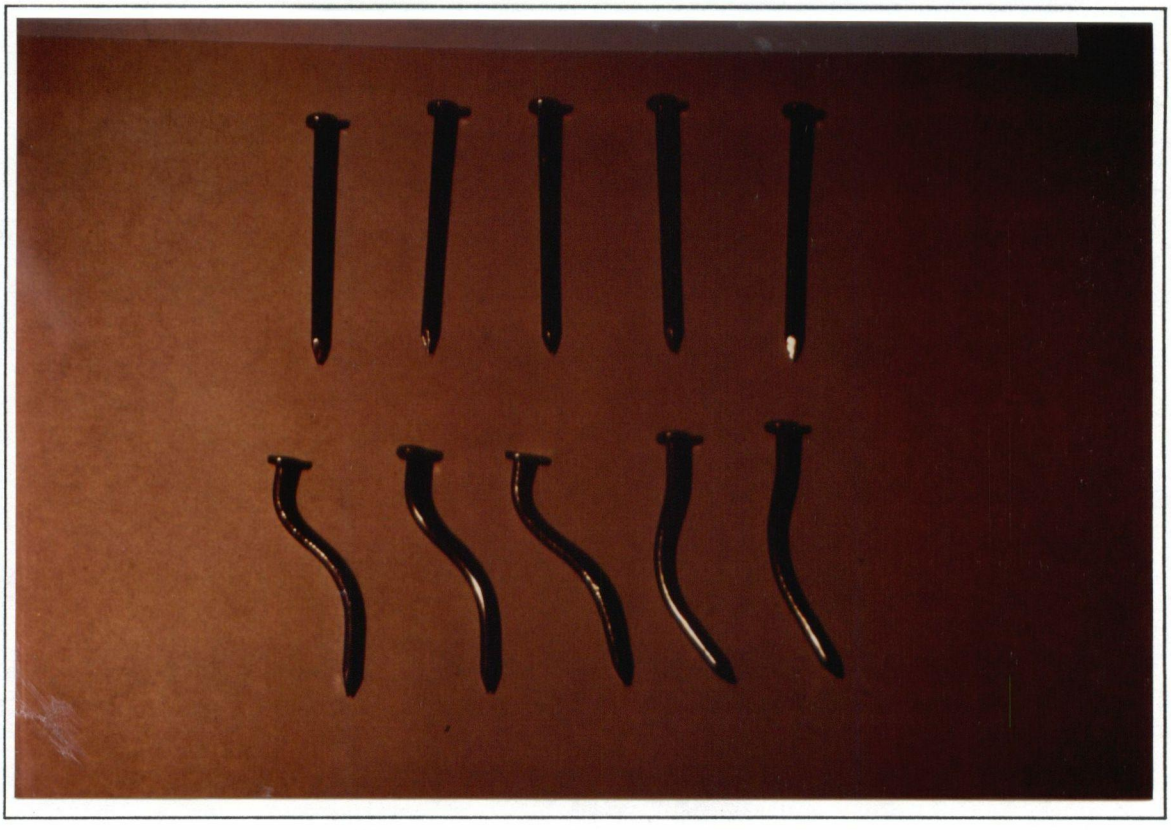

Figure 6.15: Nails After Connection Test Specimen Has Failed.

The S-shape that they are bent into, indicates that substantial yielding of the nail has occurred.

6.7.1.2 Static Cyclic

Five parameters were obtained from the static cyclic test of the sheathing connection. The parameters, K_0, K_2, and P_0 were obtained by extracting data points representing sections of the load–displacement curve that were being followed for the first time during the test. A least squares regression analysis was performed, then used to fit the function given by Equation 6.1 to the data, up to the peak load value. The parameters, P_1 and K_4, were found using a linear regression on the data between $\pm$ 2.5 mm ($\pm$ 0.1 in) for the second through fourth cycles at each displacement. A typical load-deflection curve

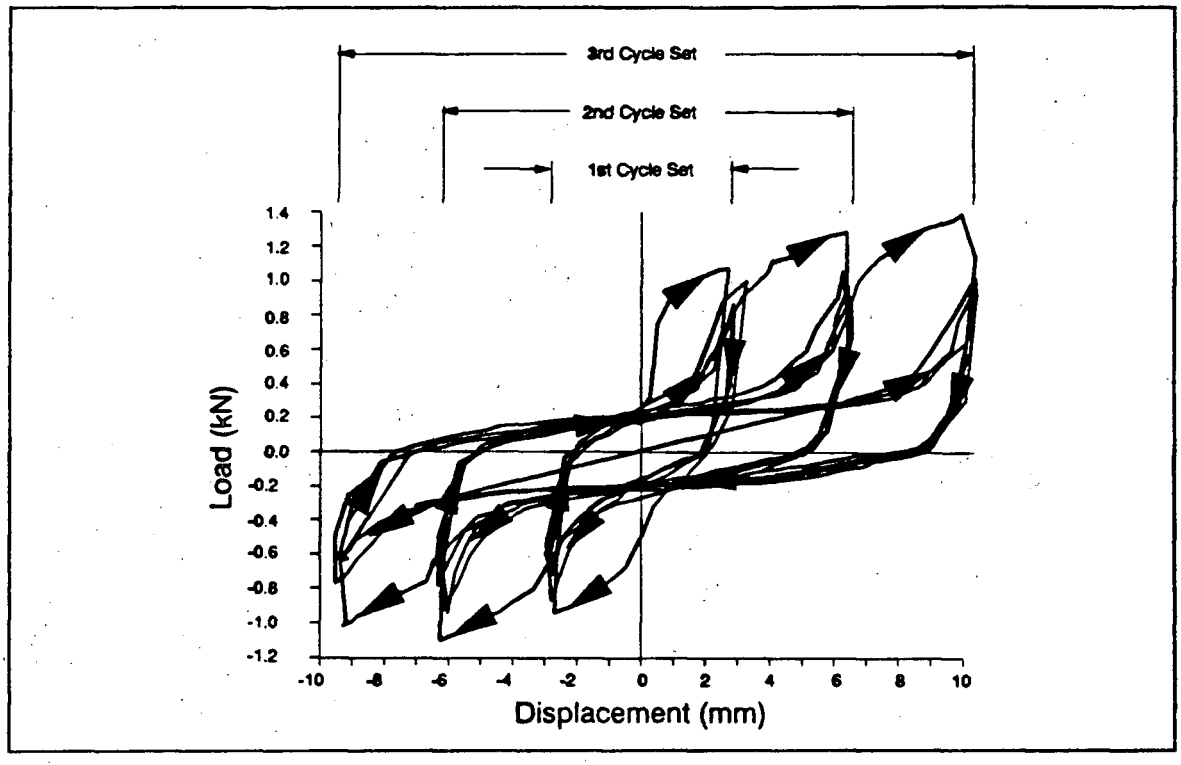

Figure 6.16: Typical Load–Deflection Curve Obtained From The Static Cyclic Sheathing Connection Test.

for a static cyclic test is shown in Figure 6.16.

The average values and C.V.'s for each of these five parameters are shown in Tables 6.5–6.12, for each configuration.

The envelope values shown in Tables 6.5–6.12 are less reliable than the ones from the static one–directional tests, shown in Tables 6.3 and 6.4. This is reflected in the higher values for the C.V.'s of each parameter and, is due in part to fewer data points being used to fit the exponential curve, given in Equation 6.1. The most significant effect of this lack of data is seen in the initial stiffness. The load–deflection curve had very few points in the initial section. In some cases, this was due to the specimen being preloaded when placed in the testing frame, but the main reason was the higher displacement per data point recorded. Fewer data points were recorded for a given displacement in this

test due to the length of the test and the limited memory available in the data acquisition equipment.

Despite these problems, similar conclusions to those drawn from the static one–directional test data can be made about the parameters K_0, P_0, and K_2. No information about the two parameters, Δ_{max} and K_3, can be found from the cyclic data due to the reversing of the displacements at locations that are different from Δ_{max}.

Tables 6.5–6.12 show a decrease in the value of K_4, with the increase in cycle number. This is expected since the load at zero displacement for the cyclic loops of the test curve, P_1, shown in Figure 6.16, remains fairly constant. Therefore, if the hysteresis loop is to remain smooth, as the displacements get larger, the slope at zero displacement must become flatter.

Table 6.5: Load-Deflection Parameters Obtained From The Static Cyclic Sheathing Connection Tests.

Waferboard Sheathing Connection Tests:									
Number	Framing Grain Orientation	Sheathing Grain Orientation	Cycle Set Number	Value	K_0 N/mm (lb/in)	P_0 N (lbs)	K_2 N/mm (lb/in)	P_1 N (lbs)	K_4 N/mm (lb/in)
5	Parallel	Parallel	Envelope	Ave.	1116 (6372)	848 (191)	32 (183)	N/A	N/A
				C.V.	0.38	0.15	0.37		
			1^{st}	Ave.	N/A	N/A	N/A	176 (40)	87 (497)
				C.V.				0.06	0.19
			2^{nd}	Ave.	N/A	N/A	N/A	181 (41)	28 (158)
				C.V.				0.12	0.24
			3^{rd}	Ave.	N/A	N/A	N/A	182 (41)	12 (67)
				C.V.				0.04	0.30
			Average	Ave.	N/A	N/A	N/A	177 (40)	28 (158)
				C.V.				0.08	0.35

Table 6.6: Load-Deflection Parameters Obtained From The Static Cyclic Sheathing Connection Tests (Continued).

Waferboard Sheathing Connection Tests (Continued):									
Number	Framing Grain Orientation	Sheathing Grain Orientation	Cycle Set Number	Value	K_0 N/mm (lb/in)	P_0 N (lbs)	K_2 N/mm (lb/in)	P_1 N (lbs)	K_4 N/mm (lb/in)
4	Parallel	Perp.	Envelope	Ave.	1280 (7310)	982 (221)	27 (154)	N/A	N/A
				C.V.	0.22	0.14	0.49		
			1st	Ave.	N/A	N/A	N/A	213 (48)	94 (540)
				C.V.				0.13	0.40
			2nd	Ave.	N/A	N/A	N/A	201 (45)	26 (147)
				C.V.				0.10	0.20
			3rd	Ave.	N/A	N/A	N/A	188 (42)	25 (143)
				C.V.				0.02	0.64
			Average	Ave.	N/A	N/A	N/A	195 (44)	37 (213)
				C.V.				0.02	0.19

Table 6.7: Load-Deflection Parameters Obtained From The Static Cyclic Sheathing Connection Tests (Continued).

Waferboard Sheathing Connection Tests (Continued):									
Number	Framing Grain Orientation	Sheathing Grain Orientation	Cycle Set Number	Value	K_0 N/mm (lb/in)	P_0 N (lbs)	K_2 N/mm (lb/in)	P_1 N (lbs)	K_4 N/mm (lb/in)
4	Perp.	Parallel	Envelope	Ave.	N/A	N/A	N/A	N/A	N/A
				C.V.					
			1st	Ave.	N/A	N/A	N/A	161	26
								(36)	(150)
				C.V.				0.09	0.53
			2nd	Ave.	N/A	N/A	N/A	174	14
								(39)	(79)
				C.V.				0.06	0.04
			3rd	Ave.	N/A	N/A	N/A	143	12
								(32)	(69)
				C.V.				0.04	0.29
			Average	Ave.	N/A	N/A	N/A	160	17
								(36)	(100)
				C.V.				0.04	0.25

Table 6.8: Load-Deflection Parameters Obtained From The Static Cyclic Sheathing Connection Tests (Continued).

Waferboard Sheathing Connection Tests (Continued):									
Number	Framing Grain Orientation	Sheathing Grain Orientation	Cycle Set Number	Value	K_0 N/mm (lb/in)	P_0 N (lbs)	K_2 N/mm (lb/in)	P_1 N (lbs)	K_4 N/mm (lb/in)
3	Perp.	Perp.	Envelope	Ave.	N/A	N/A	N/A	N/A	N/A
				C.V.					
			1^{st}	Ave.	N/A	N/A	N/A	133	44
								(30)	(250)
				C.V.				0.17	0.11
			2^{nd}	Ave.	N/A	N/A	N/A	133	18
								(30)	(105)
				C.V.				0.08	0.32
			3^{rd}	Ave.	N/A	N/A	N/A	121	18
								(27)	(105)
				C.V.				0.03	0.33
			Average	Ave.	N/A	N/A	N/A	133	20
								(30)	(116)
				C.V.				0.05	0.24

Table 6.9: Load-Deflection Parameters Obtained From The Static Cyclic Sheathing Connection Tests (Continued).

Plywood Sheathing Connection Tests (Continued):									
Number	Framing Grain Orientation	Sheathing Grain Orientation	Cycle Set Number	Value	K_0 N/mm (lb/in)	P_0 N (lbs)	K_2 N/mm (lb/in)	P_1 N (lbs)	K_4 N/mm (lb/in)
5	Parallel	Parallel	Envelope	Ave.	1553 (8868)	829 (186)	64 (367)	N/A	N/A
				C.V.	0.17	0.09	0.35		
			1^{st}	Ave.	N/A	N/A	N/A	216 (48)	108 (615)
				C.V.				0.14	0.09
			2^{nd}	Ave.	N/A	N/A	N/A	222 (50)	43 (245)
				C.V.				0.11	0.22
			3^{rd}	Ave.	N/A	N/A	N/A	215 (48)	22 (127)
				C.V.				0.05	0.60
			Average	Ave.	N/A	N/A	N/A	214 (48)	31 (178)
				C.V.				0.06	0.44

Table 6.10: Load-Deflection Parameters Obtained From The Static Cyclic Sheathing Connection Tests (Continued).

Plywood Sheathing Connection Tests (Continued):									
Number	Framing Grain Orientation	Sheathing Grain Orientation	Cycle Set Number	Value	K_0 N/mm (lb/in)	P_0 N (lbs)	K_2 N/mm (lb/in)	P_1 N (lbs)	K_4 N/mm (lb/in)
4	Parallel	Perp.	Envelope	Ave.	1408 (8040)	831 (187)	52 (295)	N/A	N/A
				C.V.	0.25	0.16	0.45		
			1st	Ave.	N/A	N/A	N/A	190 (43)	78 (443)
				C.V.				0.08	0.20
			2nd	Ave.	N/A	N/A	N/A	200 (45)	28 (159)
				C.V.				0.05	0.26
			3rd	Ave.	N/A	N/A	N/A	186 (42)	14 (81)
				C.V.				0.07	0.42
			Average	Ave.	N/A	N/A	N/A	191 (43)	20 (113)
				C.V.				0.06	0.37

Table 6.11: Load-Deflection Parameters Obtained From The Static Cyclic Sheathing Connection Tests (Continued).

Plywood Sheathing Connection Tests (Continued):									
Number	Framing Grain Orientation	Sheathing Grain Orientation	Cycle Set Number	Value	K_0 N/mm (lb/in)	P_0 N (lbs)	K_2 N/mm (lb/in)	P_1 N (lbs)	K_4 N/mm (lb/in)
3	Perp.	Parallel	Envelope	Ave.	N/A	N/A	N/A	N/A	N/A
				C.V.					
			1st	Ave.	N/A	N/A	N/A	162	38
								(36)	(220)
				C.V.				0.16	0.12
			2nd	Ave.	N/A	N/A	N/A	197	13
								(44)	(72)
				C.V.				0.14	0.15
			3rd	Ave.	N/A	N/A	N/A	N/A	N/A
				C.V.					
			Average	Ave.	N/A	N/A	N/A	177	22
								(40)	(123)
				C.V.				0.11	0.31

Table 6.12: Load-Deflection Parameters Obtained From The Static Cyclic Sheathing Connection Tests (Continued).

Plywood Sheathing Connection Tests (Continued):									
Number	Framing Grain Orientation	Sheathing Grain Orientation	Cycle Set Number	Value	K_0 N/mm (lb/in)	P_0 N (lbs)	K_2 N/mm (lb/in)	P_1 N (lbs)	K_4 N/mm (lb/in)
5	Perp.	Perp.	Envelope	Ave.	N/A	N/A	N/A	N/A	N/A
				C.V.					
			1^{st}	Ave.	N/A	N/A	N/A	178	37
								(40)	(211)
				C.V.				0.03	0.20
			2^{nd}	Ave.	N/A	N/A	N/A	197	13
								(44)	(72)
				C.V.				0.16	0.10
			3^{rd}	Ave.	N/A	N/A	N/A	N/A	N/A
				C.V.					
			Average	Ave.	N/A	N/A	N/A	177	14
								(40)	(78)
				C.V.				0.03	0.21

If the values of the parameters P_1 and K_4 for waferboard, shown in Tables 6.5–6.8, are compared to the same values for plywood, shown in Tables 6.9–6.12, three deductions can be made:

1. The plywood average values are slightly higher for P_1 and K_4, with the exception of the values for frame grain orientation parallel with sheathing grain orientation perpendicular.

2. Values for the two parameters are more consistent with respect to grain orientation changes for plywood than waferboard, as indicated by the values for the C.V.'s.

3. The lack of dependency on grain orientation again indicates that the performance of the connection is governed more by the nail material properties than by the timber material properties.

6.7.1.3 "Dynamic" Cyclic

The data reduction procedure of the "dynamic" cyclic connection investigation was identical to that used for the static cyclic tests. The results are summarized in Tables 6.13–6.20, and the load-deflection curves for the dynamic cyclic test are similar to the static cyclic load-deflection curve, shown in Figure 6.16.

Similar conclusions can be drawn from the "dynamic" cyclic test results, as those made for the static cyclic tests. The C.V.'s for each parameter are higher than the corresponding values for the static one–directional tests. This is again due to fewer data points being used to fit the exponential curve. There is little difference between nailed waferboard and plywood sheathing connections, as shown by the closeness of the values of the five parameters for each type of specimen. The exception is for the values of P_1 and K_4, which have higher values for plywood than for waferboard. An increase in the initial stiffness parameter, K_0, for the dynamic cyclic specimens is evident, and could be

Table 6.13: Load-Deflection Parameters Obtained From The Dynamic Cyclic Sheathing Connection Tests.

Waferboard Sheathing Connection Tests:									
Number	Framing Grain Orientation	Sheathing Grain Orientation	Cycle Set Number	Value	K_0 N/mm (lb/in)	P_0 N (lbs)	K_2 N/mm (lb/in)	P_1 N (lbs)	K_4 N/mm (lb/in)
5	Parallel	Parallel	Envelope	Ave.	1305 (7455)	1059 (238)	32 (182)	N/A	N/A
				C.V.	0.21	0.11	0.10		
			1st	Ave.	N/A	N/A	N/A	239 (54)	82 (471)
				C.V.				0.09	0.34
			2nd	Ave.	N/A	N/A	N/A	207 (46)	27 (157)
				C.V.				0.07	1.03
			3rd	Ave.	N/A	N/A	N/A	137 (31)	9 (53)
				C.V.				0.33	0.58
			Average	Ave.	N/A	N/A	N/A	192 (43)	31 (176)
				C.V.				0.15	0.55

Table 6.14: Load-Deflection Parameters Obtained From The Dynamic Cyclic Sheathing Connection Tests (Continued).

Waferboard Sheathing Connection Tests (Continued):									
Number	Framing Grain Orientation	Sheathing Grain Orientation	Cycle Set Number	Value	K_0 N/mm (lb/in)	P_0 N (lbs)	K_2 N/mm (lb/in)	P_1 N (lbs)	K_4 N/mm (lb/in)
4	Parallel	Perp.	Envelope	Ave.	1337 (7633)	1096 (246)	34 (194)	N/A	N/A
				C.V.	0.19	0.09	0.24		
			1st	Ave.	N/A	N/A	N/A	209 (47)	79 (453)
				C.V.				0.05	0.16
			2nd	Ave.	N/A	N/A	N/A	208 (47)	25 (141)
				C.V.				0.04	0.38
			3rd	Ave.	N/A	N/A	N/A	N/A	N/A
				C.V.					
			Average	Ave.	N/A	N/A	N/A	205 (46)	51 (289)
				C.V.				0.06	0.56

Table 6.15: Load-Deflection Parameters Obtained From The Dynamic Cyclic Sheathing Connection Tests (Continued).

Waferboard Sheathing Connection Tests (Continued):									
Number	Framing Grain Orientation	Sheathing Grain Orientation	Cycle Set Number	Value	K_0 N/mm (lb/in)	P_0 N (lbs)	K_2 N/mm (lb/in)	P_1 N (lbs)	K_4 N/mm (lb/in)
4	Perp.	Parallel	Envelope	Ave.	1111 (6346)	842 (189)	58 (330)	N/A	N/A
				C.V.	0.16	0.18	0.32		
			1st	Ave.	N/A	N/A	N/A	184 (41)	115 (658)
				C.V.				0.18	0.07
			2nd	Ave.	N/A	N/A	N/A	186 (42)	21 (123)
				C.V.				0.13	0.11
			3rd	Ave.	N/A	N/A	N/A	163 (37)	15 (85)
				C.V.				0.28	0.15
			Average	Ave.	N/A	N/A	N/A	175 (39)	23 (129)
				C.V.				0.19	0.14

Table 6.16: Load-Deflection Parameters Obtained From The Dynamic Cyclic Sheathing Connection Tests (Continued).

Waferboard Sheathing Connection Tests (Continued):									
Number	Framing Grain Orientation	Sheathing Grain Orientation	Cycle Set Number	Value	K_0 N/mm (lb/in)	P_0 N (lbs)	K_2 N/mm (lb/in)	P_1 N (lbs)	K_4 N/mm (lb/in)
3	Perp.	Perp.	Envelope	Ave.	971 (5545)	972 (219)	54 (308)	N/A	N/A
				C.V.	0.23	0.13	0.13		
			1st	Ave.	N/A	N/A	N/A	199 (45)	98 (577)
				C.V.				0.18	0.22
			2nd	Ave.	N/A	N/A	N/A	204 (46)	21 (117)
				C.V.				0.17	0.08
			3rd	Ave.	N/A	N/A	N/A	200 (45)	13 (75)
				C.V.				0.22	0.10
			Average	Ave.	N/A	N/A	N/A	195 (44)	22 (124)
				C.V.				0.20	0.14

Table 6.17: Load-Deflection Parameters Obtained From The Dynamic Cyclic Sheathing Connection Tests (Continued).

Plywood Sheathing Connection Tests:									
Number	Framing Grain Orientation	Sheathing Grain Orientation	Cycle Set Number	Value	K_0 N/mm (lb/in)	P_0 N (lbs)	K_2 N/mm (lb/in)	P_1 N (lbs)	K_4 N/mm (lb/in)
4	Parallel	Parallel	Envelope	Ave.	1332 (7607)	986 (222)	26 (146)	N/A	N/A
				C.V.	0.20	0.13	0.18		
			1st	Ave.	N/A	N/A	N/A	224 (50)	70 (400)
				C.V.				0.12	0.29
			2nd	Ave.	N/A	N/A	N/A	211 (48)	29 (163)
				C.V.				0.07	0.22
			3rd	Ave.	N/A	N/A	N/A	192 (43)	10 (59)
				C.V.				0.07	0.44
			Average	Ave.	N/A	N/A	N/A	206 (46)	28 (158)
				C.V.				0.10	0.40

Table 6.18: Load-Deflection Parameters Obtained From The Dynamic Cyclic Sheathing Connection Tests (Continued).

Plywood Sheathing Connection Tests (Continued):									
Number	Framing Grain Orientation	Sheathing Grain Orientation	Cycle Set Number	Value	K_0 N/mm (lb/in)	P_0 N (lbs)	K_2 N/mm (lb/in)	P_1 N (lbs)	K_4 N/mm (lb/in)
4	Parallel	Perp.	Envelope	Ave.	1214 (6930)	1006 (226)	38 (216)	N/A	N/A
				C.V.	0.23	0.12	0.52		
			1st	Ave.	N/A	N/A	N/A	187 (42)	89 (507)
				C.V.				0.12	0.34
			2nd	Ave.	N/A	N/A	N/A	177 (40)	36 (206)
				C.V.				0.18	0.79
			3rd	Ave.	N/A	N/A	N/A	138 (31)	9 (49)
				C.V.				0.51	0.51
			Average	Ave.	N/A	N/A	N/A	173 (39)	36 (203)
				C.V.				0.10	1.09

Table 6.19: Load-Deflection Parameters Obtained From The Dynamic Cyclic Sheathing Connection Tests (Continued).

Plywood Sheathing Connection Tests (Continued):									
Number	Framing Grain Orientation	Sheathing Grain Orientation	Cycle Set Number	Value	K_0 N/mm (lb/in)	P_0 N (lbs)	K_2 N/mm (lb/in)	P_1 N (lbs)	K_4 N/mm (lb/in)
4	Perp.	Parallel	Envelope	Ave.	923 (5273)	972 (218)	45 (255)	N/A	N/A
				C.V.	0.10	0.04	0.59		
			1st	Ave.	N/A	N/A	N/A	188 (42)	94 (535)
				C.V.				0.09	0.06
			2nd	Ave.	N/A	N/A	N/A	198 (45)	19 (111)
				C.V.				0.07	0.18
			3rd	Ave.	N/A	N/A	N/A	174 (39)	13 (76)
				C.V.				0.11	0.33
			Average	Ave.	N/A	N/A	N/A	187 (42)	24 (139)
				C.V.				0.09	0.11

Table 6.20: Load-Deflection Parameters Obtained From The Dynamic Cyclic Sheathing Connection Tests (Continued).

Plywood Sheathing Connection Tests (Continued):									
Number	Framing Grain Orientation	Sheathing Grain Orientation	Cycle Set Number	Value	K_0 N/mm (lb/in)	P_0 N (lbs)	K_2 N/mm (lb/in)	P_1 N (lbs)	K_4 N/mm (lb/in)
4	Perp.	Perp.	Envelope	Ave.	907 (5177)	1010 (227)	45 (259)	N/A	N/A
				C.V.	0.09	0.20	0.70		
			1st	Ave.	N/A	N/A	N/A	189 (42)	94 (535)
				C.V.				0.16	0.11
			2nd	Ave.	N/A	N/A	N/A	201 (45)	18 (104)
				C.V.				0.13	0.20
			3rd	Ave.	N/A	N/A	N/A	134 (30)	8 (46)
				C.V.				0.44	0.45
			Average	Ave.	N/A	N/A	N/A	182 (41)	24 (139)
				C.V.				0.15	0.42

attributed to the change in load rate but, there were also less data points to use in fitting the exponential curve. The lack of close data points to use in the curve fitting is a more likely cause for the higher values for K_0.

No pattern to the values for P_1 and K_4 is well defined, other than the decrease in the slope, K_4, with increase in cycle peak deflection. The same results were seen in the static cyclic test results. The lack of dependence on grain orientation for all of the parameters, again, indicates that the connection properties are more dependent on the nail properties than the sheathing or framing material properties.

6.7.1.4 Overall Comparison

With the exception of the initial stiffness, K_0, no significant difference in the values for the parameters is obvious, either with respect to grain orientation or load rate. The difference in the initial stiffness for load rate is probably due to the process of fitting the exponential curve, given by Equation 6.1, to very few data points. The reason for fewer data points being used is that the cyclic tests lasted a longer time than the static one–directional test. The longer time for testing dictated that fewer samplings of data points be taken for a given deflection because of the memory limitations of the data acquisition system.

Since there does not appear to be any significant difference in the results of the three tests, the data was averaged over all three tests. The results of this averaging is given in Tables 6.21 and 6.22.

There appears to be a trend for the initial stiffness, K_0, to be slightly higher for loading parallel to the grain than for loading perpendicular to the grain of the framing. At the same time,the slope, K_2,seems to be lower for the same grain orientation. As shown in Figure 6.14, there is no significant difference in the exponential increasing section of the load–deflection curve. The variables, K_0 and K_2, are asymptotes for the exponential

Table 6.22: Overall Average Load-Deflection Parameters Obtained From The Sheathing Connection Tests For Plywood Sheathing.

Plywood Sheathing Connection Test Overall Average Values:										
Number	Framing Grain Orientation	Sheathing Grain Orientation	Value	K_0 N/mm (lb/in)	P_0 N (lbs)	K_2 N/mm (lb/in)	Δ_{max} N (in)	K_3 N/mm (lb/in)	P_1 N (lbs)	K_4 N/mm (lb/in)
	Parallel	Parallel	Ave.	1219	901	44	11	-41	207	48
				(6959)	(203)	(253)	(0.4)	(-234)	(46)	(272)
			C.V.	0.33	0.14	0.50	0.15	0.58	0.23	0.75
	Parallel	Perp.	Ave.	1320	915	39	8	-27	180	42
				(7536)	(206)	(220)	(0.3)	(-153)	(40)	(241)
			C.V.	0.30	0.19	0.62	0.41	0.61	0.22	0.85
	Perp.	Parallel	Ave.	1039	904	58	8	-36	183	38
				(5932)	(203)	(330)	(0.3)	(-204)	(41)	(215)
			C.V.	0.24	0.12	0.46	0.18	0.32	0.13	0.87
	Perp.	Perp.	Ave.	853	983	49	8	-54	182	34
				(4872)	(221)	(277)	(0.3)	(-308)	(41)	(196)
			C.V.	0.18	0.13	0.37	0.46	0.54	0.18	0.92
Overall Average Values			Ave.	1182	920	50	9	-42	193	41
				(6750)	(207)	(258)	(0.3)	(-240)	(42)	(236)
			C.V.	0.33	0.16	0.53	0.35	0.70	0.21	0.84

Table 6.21: Overall Average Load-Deflection Parameters Obtained From The Sheathing Connection Tests For Waferboard Sheathing.

Waferboard Sheathing Connection Test Overall Average Values:										
Number	Framing Grain Orientation	Sheathing Grain Orientation	Value	K_0 N/mm (lb/in)	P_0 N (lbs)	K_2 N/mm (lb/in)	Δ_{max} N (in)	K_3 N/mm (lb/in)	P_1 N (lbs)	K_4 N/mm (lb/in)
	Parallel	Parallel	Ave.	1102	939	30	9	-31	191	47
				(6292)	(211)	(172)	(0.3)	(-178)	(43)	(270)
			C.V.	0.30	0.16	0.30	0.18	0.21	0.19	0.80
	Parallel	Perp.	Ave.	1199	1068	28	8	-41	205	51
				(6847)	(240)	(158)	(0.3)	(-236)	(46)	(290)
			C.V.	0.25	0.12	0.41	0.14	0.56	0.04	0.35
	Perp.	Parallel	Ave.	992	943	56	9	-29	171	38
				(5665)	(212)	(320)	(0.3)	(-163)	(38)	(218)
			C.V.	0.22	0.18	0.38	0.10	0.44	0.19	1.03
	Perp.	Perp.	Ave.	847	952	47	8	-33	184	45
				(4835)	(214)	(270)	(0.3)	(-189)	(41)	(255)
			C.V.	0.24	0.11	0.29	0.15	0.28	0.25	0.81
Overall Average Values			Ave.	1062	983	38	9	-33	189	46
				(6067)	(221)	(217)	(0.3)	(-190)	(42)	(260)
			C.V.	0.29	0.15	0.48	0.15	0.45	0.19	0.82

curve and therefore, interact to form the full curve. When two curves have the same values for K_0 and P_0, but different values for K_2, the curve with the lower value of K_2 would change slope at a lower value and, more quickly than the other. If the curves have different initial stiffnesses and their values of K_2 differ in the opposite direction, the two curves could be very similar when compared overall, as shown in Figure 6.14.

There does not appear to be any significant difference in the values of P_0, P_1, or K_4. Therefore, all the values have been averaged to obtain values for each of the parameters irrespective of grain orientation. These overall average values, are shown at the bottom of Tables 6.21 and 6.22, will be used in the computer programs, **SHWALL** and **DYNWALL**.

The initial stiffness, K_0, and slope, K_2, of the plywood connection are slightly higher than for a waferboard connection, but the C.V.'s for each of the values indicate the difference may not truly exist. There is no significant difference in any of the other parameters.

6.7.2 Corner Connection Tests

The programs, **SHWALL** and **DYNWALL**, model the corner connection with a linear elastic element. Only the average stiffness of the connection in tension is required from the test results. This variable will be used as the stiffness of the model's element. Therefore, a linear regression analysis was performed, using the data up to the peak load value. The reason the linear regression can be used for all the data, up to the peak value, is that the load–deflection curve for a typical test shows little non–linearity up to the ultimate load capacity of the connection, as shown in Figure 6.17.

The five values obtained for the connection stiffness in tension have an average value of 1244.37 N/mm (7105.88 lb/in) and a coefficient of variation of 0.22. Noise in the

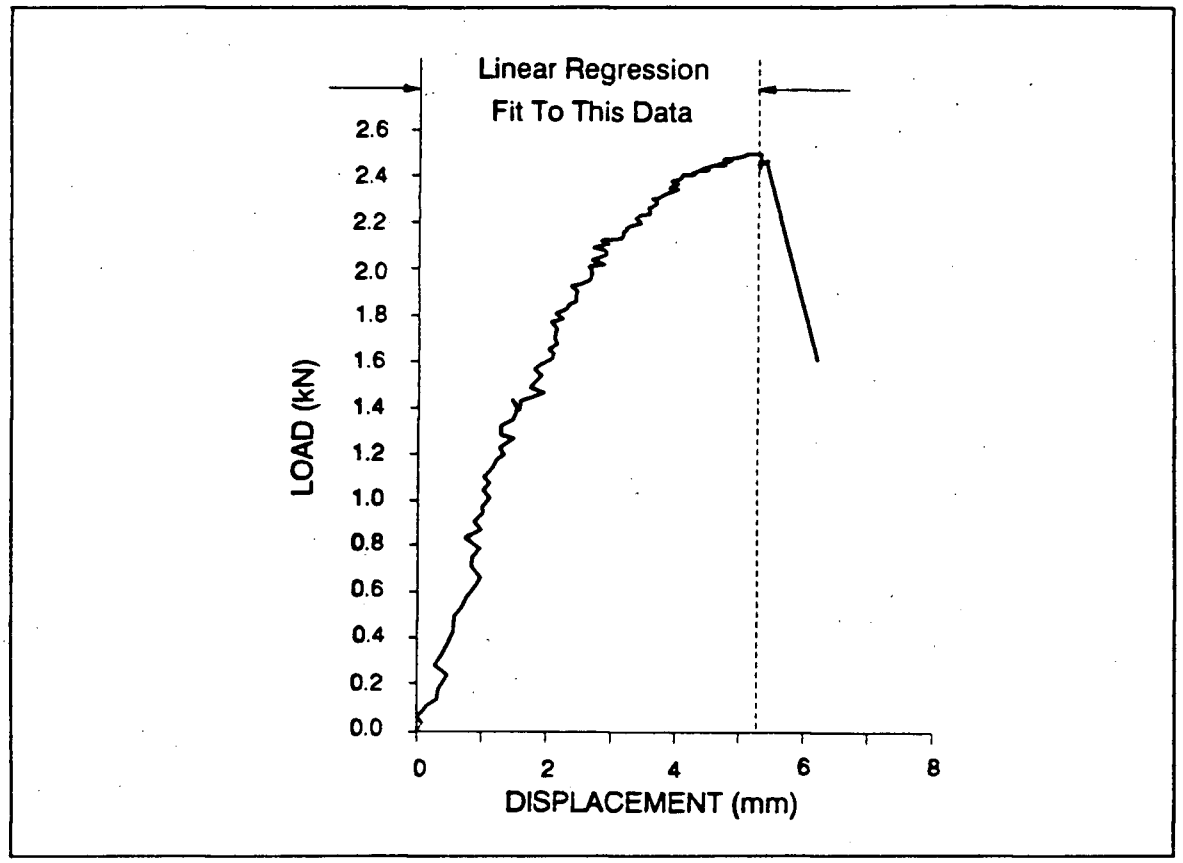

Figure 6.17: Typical Load–Deflection Curve Obtained From The Corner Connection Test.

displacement transducer signal, at times, caused the deflection to decrease for an increase in load. The linear regression analysis smooths the curve and minimizes the effect of the noise in the signal.

6.8 Summary

The test equipment, procedures, specimen configurations, analysis procedures, and results for the connection tests have been presented in this chapter. The average values for the parameters defining the load–deflection curves for the sheathing connection and

the corner connections are given in a form readily usable in the programs **SHWALL** and **DYNWALL**. It has been shown that the sheathing connection parameters are not dependent on the grain orientation of either the framing or the sheathing components of the connection. This is due to the connection performance being primarily governed by the nail properties, rather than the timber properties.

Chapter 7

Full-Size Shear Wall Test Descriptions and Procedures

7.1 Introduction

The design procedures for timber shear walls, specified by the current design codes for Canada and the United States, are based on the results of static one–directional racking tests of 2.4 × 2.4 m (8 × 8 ft) shear walls (described in the ASTM E72–77 (1986) test procedure). However, these tests are expensive, and they do not load the specimen in a manner representative of an earthquake. Therefore, a different test is proposed that loads the test specimen in a fashion representative of earthquakes.

This chapter describes **a)** the test equipment, materials used to construct the specimens, and the procedures followed in performing five different tests of full–size shear walls, and **b)** the methods used to analyze the test data. The tests performed were:

1. Static one–directional racking (similar to the ASTM E72–77 test),
2. Static cyclic racking,
3. Sinewave frequency sweeps,

4. Free vibration, and

5. Dynamic earthquake simulation tests.

The results of these tests will be correlated with predictions from the three numerical models developed in this thesis. Conclusions about the behavior of timber shear walls subjected to dynamic loads will be drawn, and the results of these tests will be discussed in greater detail in Chapter 8.

7.2 Test Equipment

7.2.1 Earthquake Table

An earthquake simulation table was used to load the walls in all but the free vibration test. This equipment consists of a 3 × 3 m (10 × 10 ft) aluminum table, supported on four pin–pin columns. The table is moved back and forth in one horizontal direction by a hydraulic jack, which is controlled by an MTS controller and Digital Equipment PDP–11/04 computer. Any one–directional displacement or acceleration record can be reproduced, allowing for a large variety of tests.

7.2.2 Steel Four–Hinged Frame

A steel frame was built to provide the vertical support for an inertial mass of 4,545 kg (311.3 slugs), but was designed so that it had no lateral resistance. The frame, shown in Figures 7.1 and 7.2, did not restrict lateral movement of the inertial mass in the vertical plane of the wall. Figure 7.1 shows the frame being raised into the vertical position. The figure shows how the frame is hinged in each corner to allow free lateral movement. In Figure 7.2, a shear wall is shown mounted in the frame and ready to be tested. The wall

is required to provide full lateral support to the frame and concrete mass at the top of the frame during the tests.

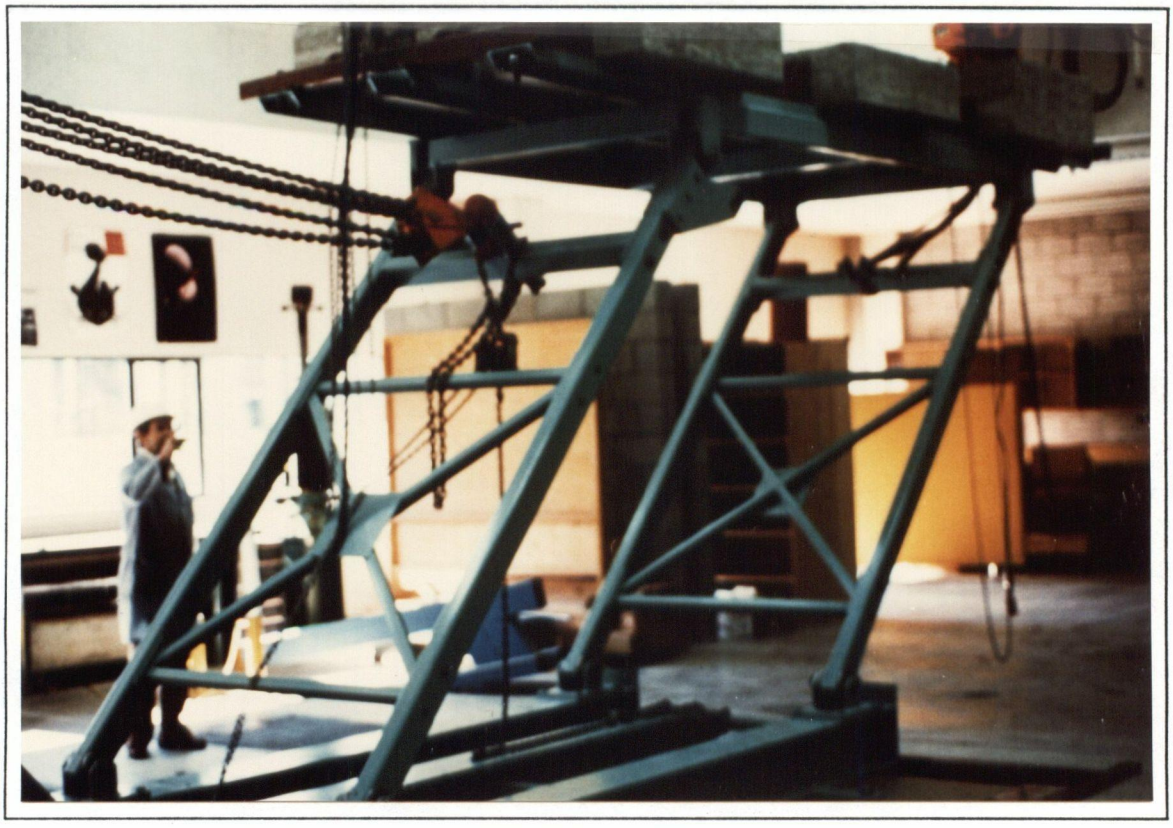

Figure 7.1: Test Frame being Raised into Vertical Position.

The testing frame was also designed so that vertical loads could be applied to the wall specimens representing structural dead load. Figure 7.3 shows a wall with a full dead load applied. Vertical loads are applied by suspending two weights over pulleys at the top of the wall and a structural steel tube, attached to the top of the wall, spreads the vertical load along the wall. These weights are free in the vertical direction, but are restrained from swinging. The vertical load can be easily varied, allowing shear walls representing either partition or bearing walls to be tested. Any ratio of vertical load to inertial load can be used.

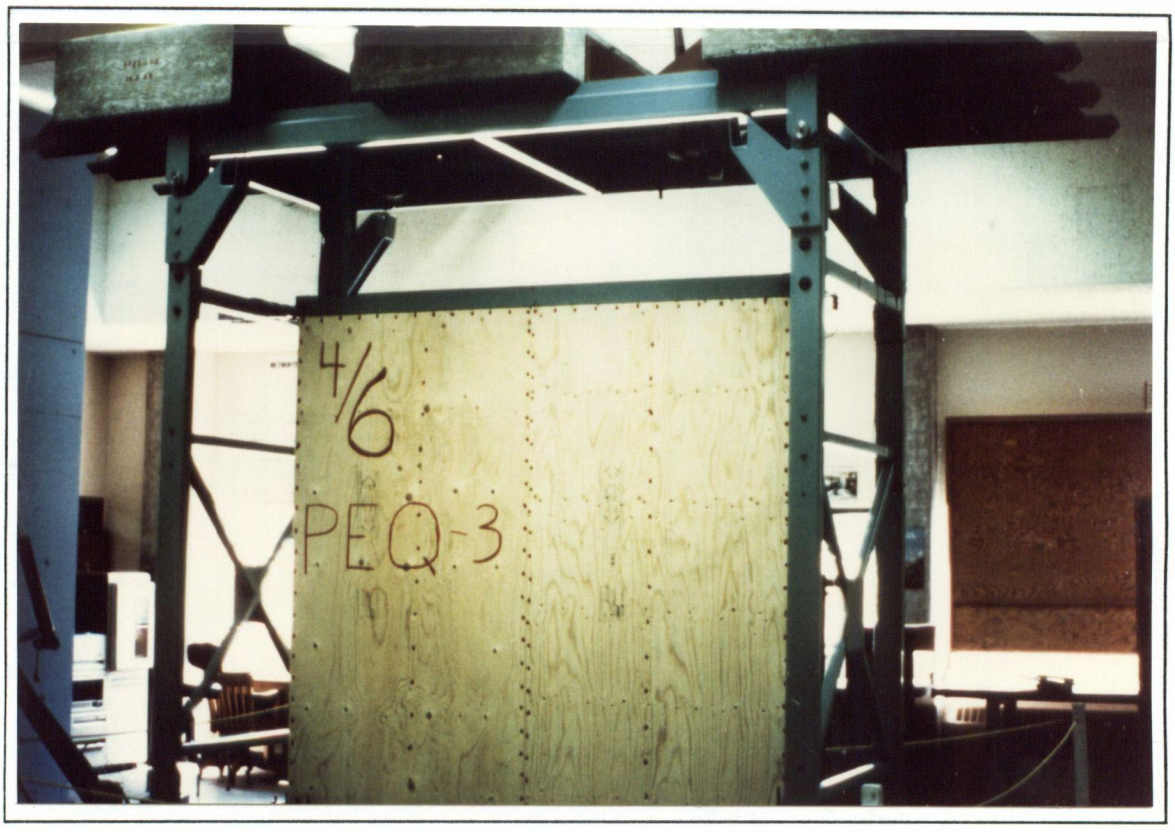

Figure 7.2: Test Frame with Wall Specimen in Place for Testing.

The inertial mass used in these tests represented the upper two stories of a three-storey, North American–style apartment building. The intent was to test the wall specimens in a manner where the loading was representative of that which the ground floor wall of an apartment building would experience during an earthquake. Framing plans for various apartment buildings were reviewed, and the average mass and tributary area was determined for the top two stories of the structures. The mass[9] used in these tests was approximately the equivalent mass found for a 2.4 m (8 ft) length of shear wall.

[9]The amount of mass required was determined using the advise of C.Y. Loh Associates Ltd., an engineering firm that has designed many apartment buildings in the Greater Vancouver area, British Columbia.

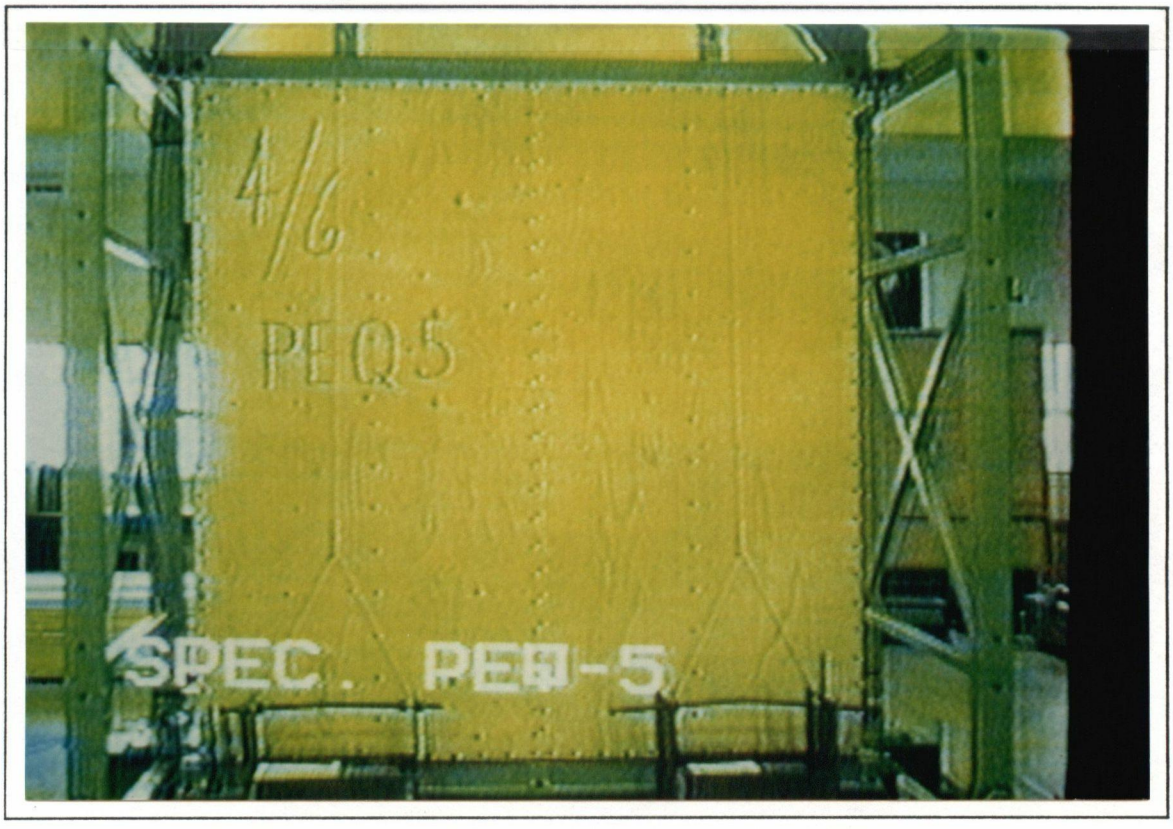

Figure 7.3: Wall Specimen with Dead Load Applied.

7.2.3 Reaction Column

A column was erected at one side of the four–hinged test frame, as shown in Figure 7.4. The "reaction" column was used to restrain the top of the wall during static one–directional and static–cyclic racking tests. As shown in Figure 7.4, an arm, consisting of structural tubing and a load cell, was attached to the reaction column, at one end, and attached to the test frame at the other end. This arm was attached to the test frame at the same height as the top of the wall. Pinned connections were used at both ends of the arm, to prevent bending stresses from affecting the load cell readings.

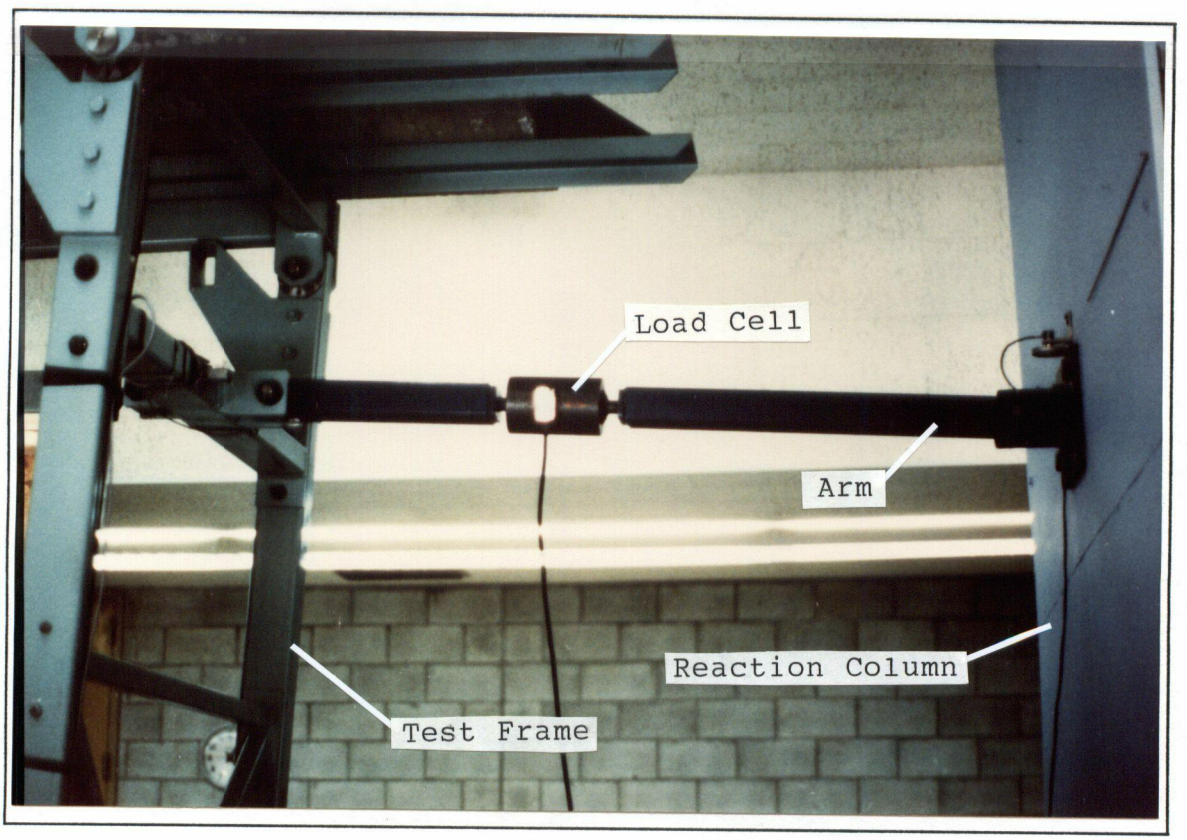

Figure 7.4: Reaction Column with Arm Including Load Cell Attached to Testing Frame.

7.3 Data Acquisition

Two computers, an IBM compatible AT computer and a Digital PDP–11/04, were used simultaneously to record data during the experiments. The AT computer used a Techmar analog–to–digital converter, and the PDP–11 used a custom–designed analog–to–digital converter to record the data. A common trigger switch started both data acquisition systems, and the earthquake table simultaneously. Between 1 and 21 signals were recorded during each of the shear wall tests. Details of the variables monitored during each test, are given in Section 7.6.

A variety of instruments were used to measure the variables of interest during the tests. The instruments were used as follows:

- Trans–tek and Hewlett–Packard DC–DC displacement transducers were used to measure the in–plane displacements of wall components, both absolute and relative.
- Bourne and Ohmite Type–A potentiometers were used to measure the in–plane displacements of the top of the wall, and out–of–plain movement of the sheathing, mid–span between the studs.
- The displacement transducer, located inside the hydraulic jack, that moved the table was used to measure the displacement of the base of the wall, i.e. earthquake table.
- A 20,000–lb Baldwin–Lima–Hamilton load cell was used to record the racking loads at the top of during static tests.
- Statham accelerometers were used to measure the accelerations at the base of the wall, top of wall, and inertial mass locations.

7.4 Test Specimen Materials

7.4.1 General

The materials used to construct the shear wall specimens were the same as those used to construct the connection test specimens described in Chapter 6. The detailed descriptions for the framing, sheathing, nails, screws, and steel angles are given in Section 6.4.

7.4.2 Steel Hold–Down Connections

One connection was required to anchor the bottom of the end studs (cords) to the base of the test frame, described in Section 7.2.2. Figure 7.5 shows one of these connections, and how it was used to anchor the corner of the wall to the base. These connections were required for the wall to perform in a racking fashion. If the hold–down connections, or something similar, are not used the shear wall will deform by rotating essentially as a rigid body. When loaded, the sole plate usually separates from the end stud and causes the forces, due to the overturning moment, to be concentrated in the corner of the sheathing. The tension force in the end stud must be transferred across the framing joint at the base of the stud by the few nails in the corner area of the sheathing. Finally, nails connecting the sheathing to the framing begin to fail in the lower corner of the wall, and failure progresses along the row of nails attaching the sheathing to the sole plate. This will continue until the wall fails, by either collapsing due to high deflection at the top, or breaking into two parts along the sole plate.

The connection used in these tests consists of a 75 × 200 × 6 mm ($3 \times 4\frac{7}{8} \times \frac{1}{4}$ in) mild steel plate, welded to a 12 mm (0.5 in) mild steel rod. The plate is attached to the bottom of the double end stud, using 26 - 4 × 76 mm (No. 8 × 3.0 in) drywall screws. The rod passed through the inside of a structural tube at the base of the wall, and a

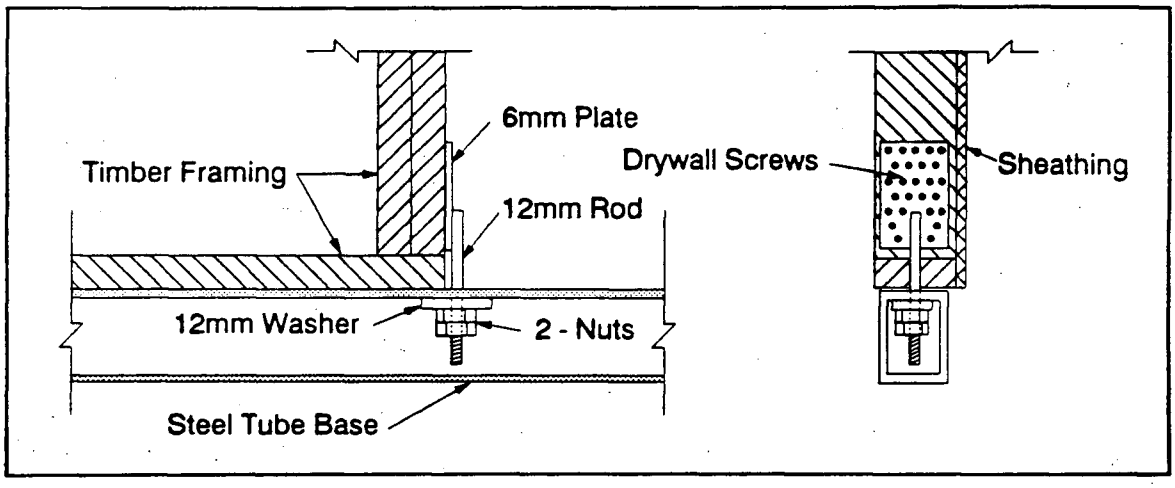

Figure 7.5: Hold-Down Connection Configuration.

$\frac{1}{2}$–in thick steel washer and double nut were then threaded onto the steel rod. The nuts were tightened to anchor the corners of the wall's framing to the base of the test frame. This connection was used only to resist the tension forces in the studs due to the overturning moment. An additional four $\frac{5}{8}$–in diameter bolts were used to transfer the shear forces along the bottom and top of the wall. The uplift forces, due to the overturning moment in the end studs, will be smaller for longer walls. The hold–down connections, therefore, would not be as important a consideration for longer walls, as it would be in the short walls used in the test.

7.5 Wall Specimen Configuration

All the shear wall specimens tested were 2.4 × 2.4 m (8 × 8 ft). The sheathing was attached, using 63 mm (8d or 2.5 in) galvanized common nails spaced from 50 mm (2 in) to 152 mm (6 in) on the perimeter of each sheathing panel, and either 152 mm (6 in) or 305 mm (12 in) along the interior studs of each sheathing panel. **Figure 7.6** shows the configuration used for most of the specimens. The framing is shown using dashed lines,

while the sheathing is shown with solid lines. The locations of the corner, and hold–down connectors are also indicated. These two types of connectors are attached to the framing only and did not restrict the movement of the sheathing panels.

All wall specimens were sheathed on one side only, and the studs were attached to the header and sill framing members by nailing through the header or sill plate into the end–grain of the stud, using 2 – 76 mm (10d or 3 in) common nails. The asymmetry, due to the sheathing being applied on one side, did not cause any problems because the wall was restrained by steel tubes at the top and bottom of the wall. These steel tubes prevented any twisting of the wall. The parameters that were changed in various specimens were the sheathing nail spacing, sheathing type, and sheathing panel orientation. Each of these variables are discussed, together with the results, in Chapter 8.

7.6 Test Procedures

7.6.1 Static One–Directional Tests

The static one–directional tests were conducted according to the ASTM E564–76 Standard (1986). The test consisted of displacing the base of the wall 130 mm (5 in) relative to the top of the wall in one direction. The steel frame was anchored to the reaction wall, at the same height as the top of the wall specimen. Movement of the top of the wall was prevented, causing the wall specimen to be forced into a racking configuration. The duration of each test was 5 minutes, which is between the load rates specified for the ASTM E72–77 and E564–76 shear wall tests, with the data being sampled every 0.5 seconds. The displacement pattern used in the static one–directional tests is shown in Figure 7.7a.

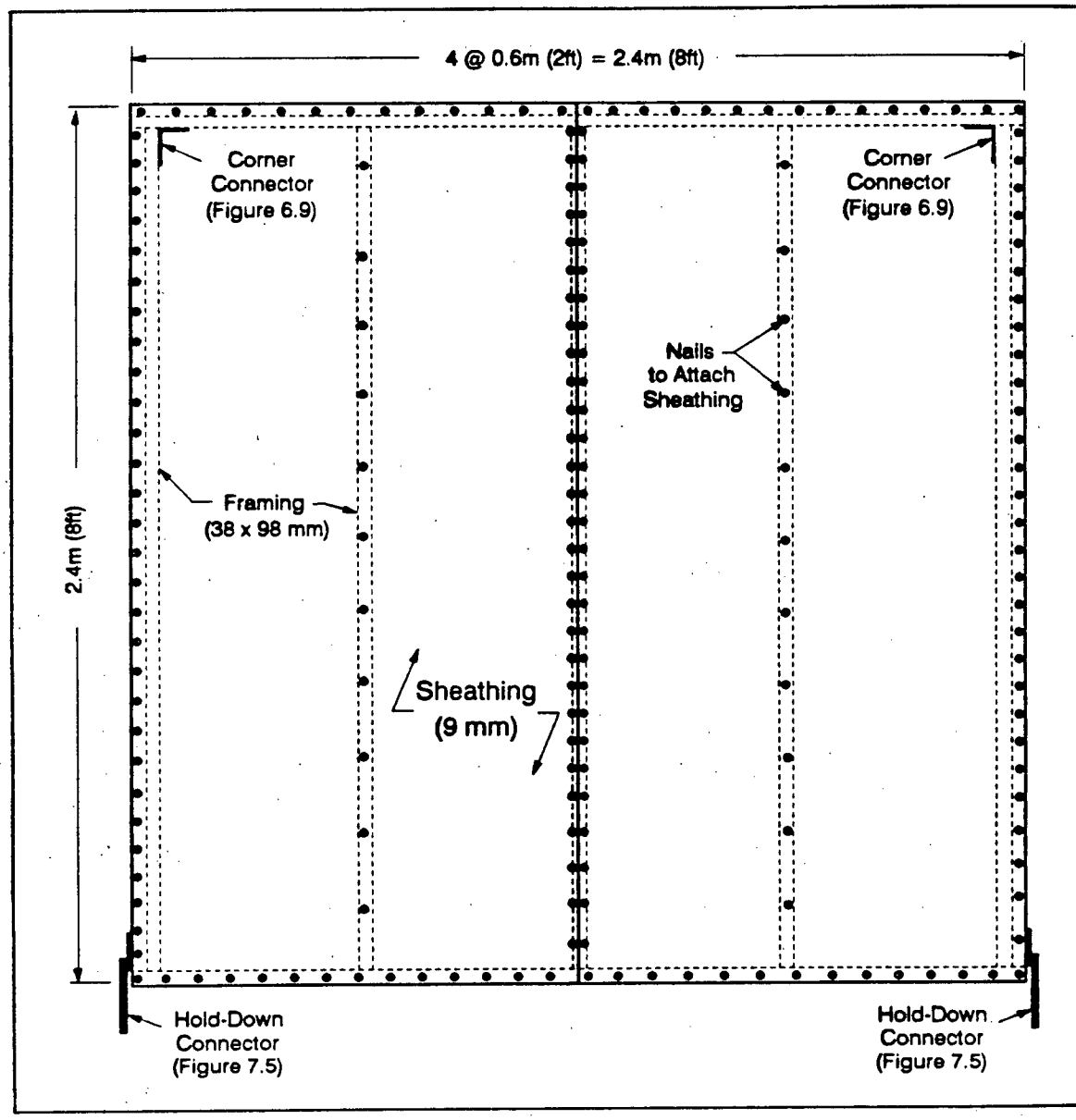

Figure 7.6: Typical Configuration of Framing, Sheathing, and Connections Used in Full-Size Shear Wall Tests.

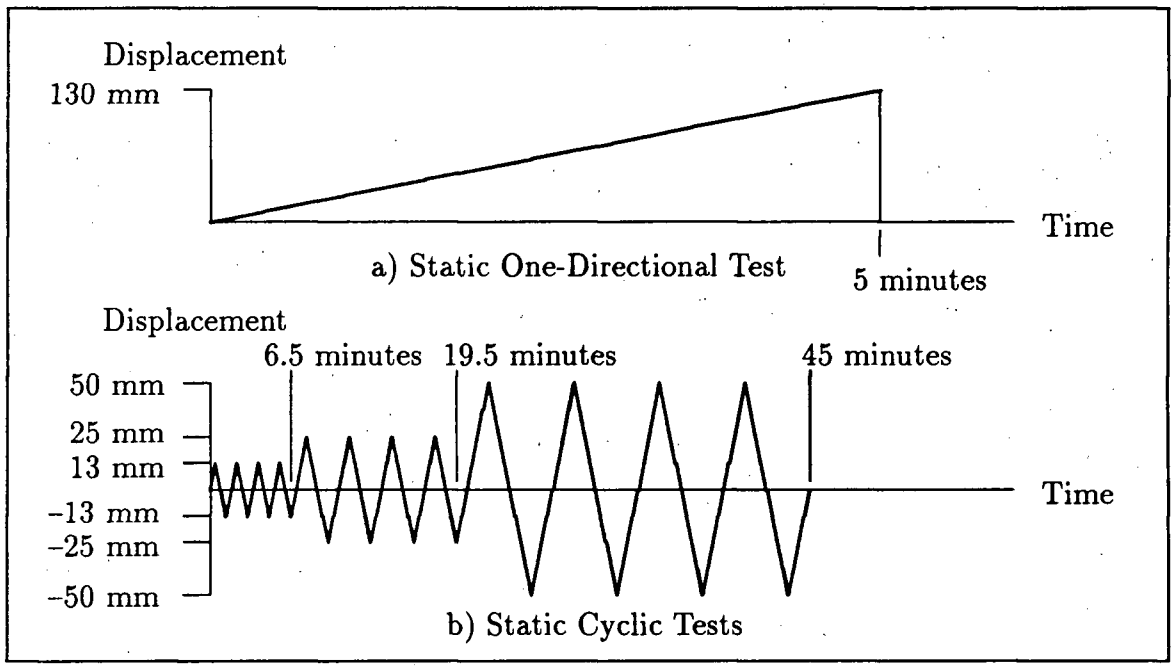

Figure 7.7: Displacement Patterns Used in Static Shear Wall Tests.

The wall is loaded in racking, similar to both the ASTM E72–77 or ASTM E564–76 tests. Like the ASTM E564–76 Standard, these tests do not require a tie rod to prevent uplift of the framing. The tie rod used in the ASTM E72–77 test forces the wall framing to deform as a parallelogram; this is how a section from a long wall would perform. Walls that are short in the horizontal direction must resist the relatively high overturning moments prevented by use of the tie rod. Therefore, the decision was made to eliminate the tie rod during this study and force the test specimen to perform as a short, high shear wall. This requires the hold–down connections to resist the entire overturning moment as would be the case for a wall that is part of a building.

The hold–down connections used in these tests would also be required if a shear wall of similar dimensions were used in an apartment building. The overturning moment must be resisted in addition to the lateral shear force, and in order for the tension force developed in the end studs to be effectively transferred to the foundation of the structure

(or to the floor in the case of upper stories), the steel connectors must be used. The elimination of these anchors renders the shear wall incapable of effectively resisting the lateral loads experienced during an earthquake because the wall will no longer deform in a racking manner. Rather, a rigid body rotation will be the predominant motion and little or none of the lateral or overturning loading will be transferred to the foundation.

A total of 16 signals were recorded during the static one–directional racking experiments. Eight of these measurements pertained to variables oriented in the plane of the wall, while the other 8 pertained to variables oriented out of the plane of the wall. Figure 7.8 shows a shear wall specimen with the locations of the various measurements taken.

The in–plane variables monitored were:

1. The load at the top of the wall.
2. Displacement of the base of the wall.
3. Uplift of the sheathing at each bottom corner of the wall.
4. Uplift of each of the doubled end studs.
5. Uplift of each end of the sole plate.
6. Separation of each of the top corners of the framing.

The following out–of–plane variables were monitored:

7. The sheathing deflection at each of the four corners of the wall specimen.
8. The sheathing deflection at each mid–span location between the studs, at mid–height levels on the wall.

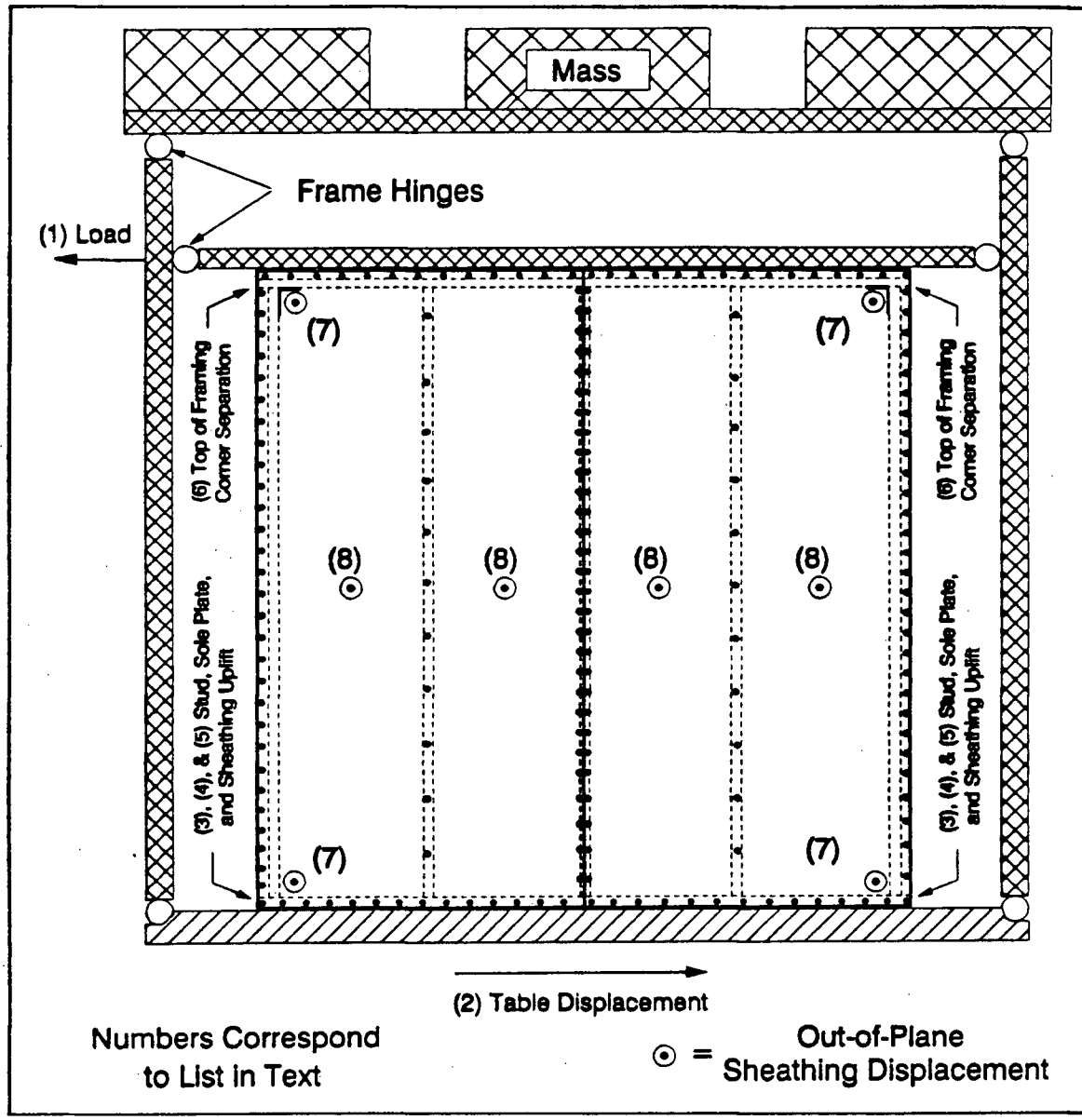

Figure 7.8: Location of Variables Measured During Static One–Directional Tests.

In order to correct the load reading for the P–delta effects of the inertial mass, a test without a wall specimen was conducted for the static one–directional test. The resulting correction curve can then be subtracted from the test load–deflection curves to find the true load applied to the wall at any deflection, as shown in Figure 7.9. The P–delta effect causes an error in the load recorded because, as the columns of the test frame are moved out of plumb, the horizontal component of the force in the column is measured by the load cell. The correction curve, shown in Figure 7.9b, begins with a load at zero deflection due to the load cell having an offset to the reading. The load is actually zero but, the load cell is reading a load. All of the loads must be corrected by the value of the offset.

7.6.2 Static Cyclic Tests

The static cyclic tests were used to determine the hysteretic behavior of shear walls. The tests were similar to the static one–directional tests, in that the wall was loaded in a slow racking fashion. The top of the frame was attached to the reaction wall, and the base of the wall was then displaced following a triangular sinewave pattern, as shown in Figure 7.7b. The displacement rate used for these tests was the same as that used in the static one–directional tests. This resulted in a test duration of 45 minutes, where the data was sampled every 6 seconds.

Four signals were recorded during the static cyclic tests. The variables measured are shown in Figure 7.10. All of the variables monitored pertained to the in–plane motion of the wall.

A test was performed without a wall specimen to correct the load readings for the P-delta effects of the inertial mass. The resulting curve correction was then subtracted from the test load–deflection curves, as was done for the static one–directional tests.

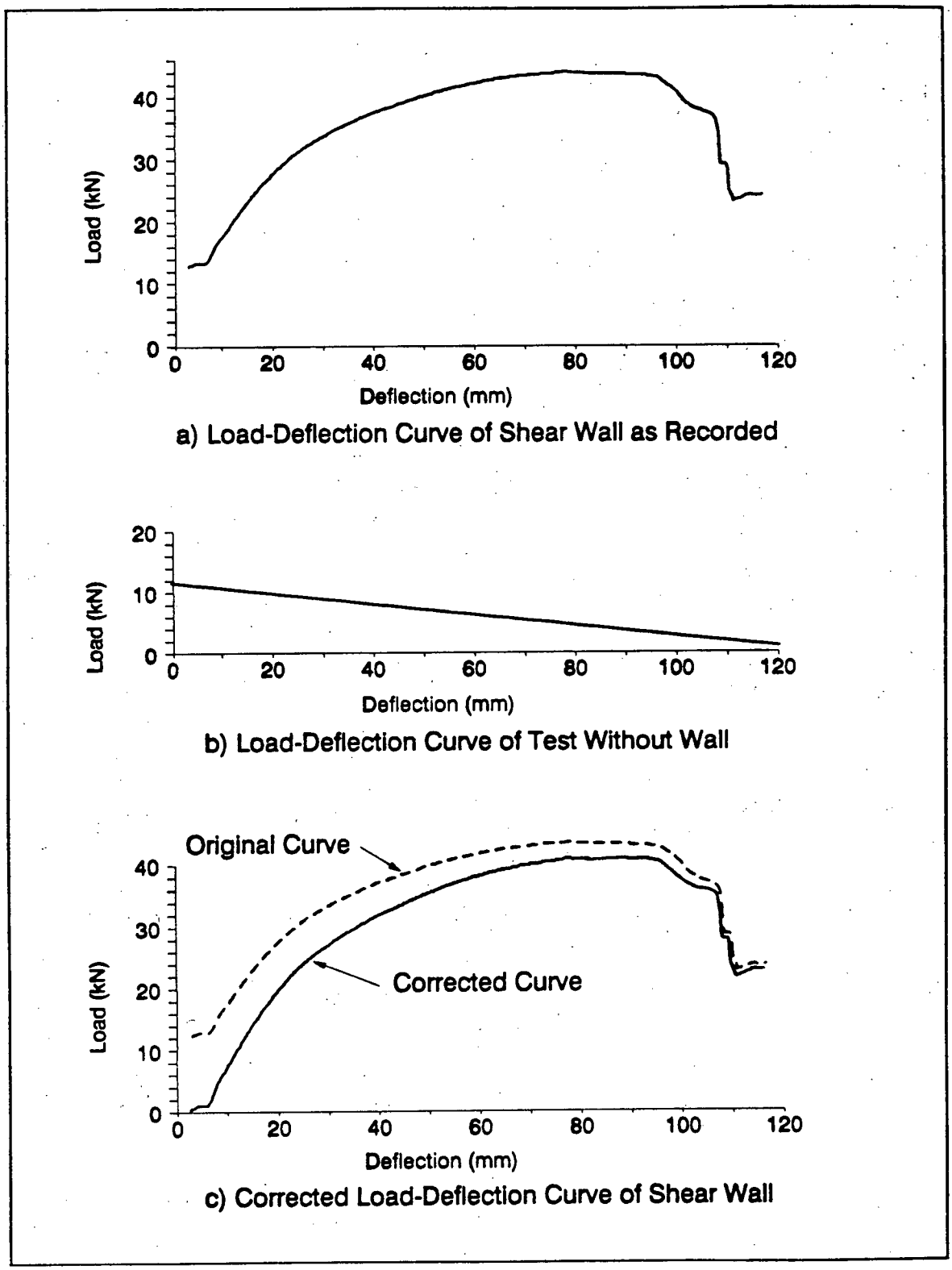

Figure 7.9: Steps Used to Correct the Load–Deflection Curves for the Static Tests.

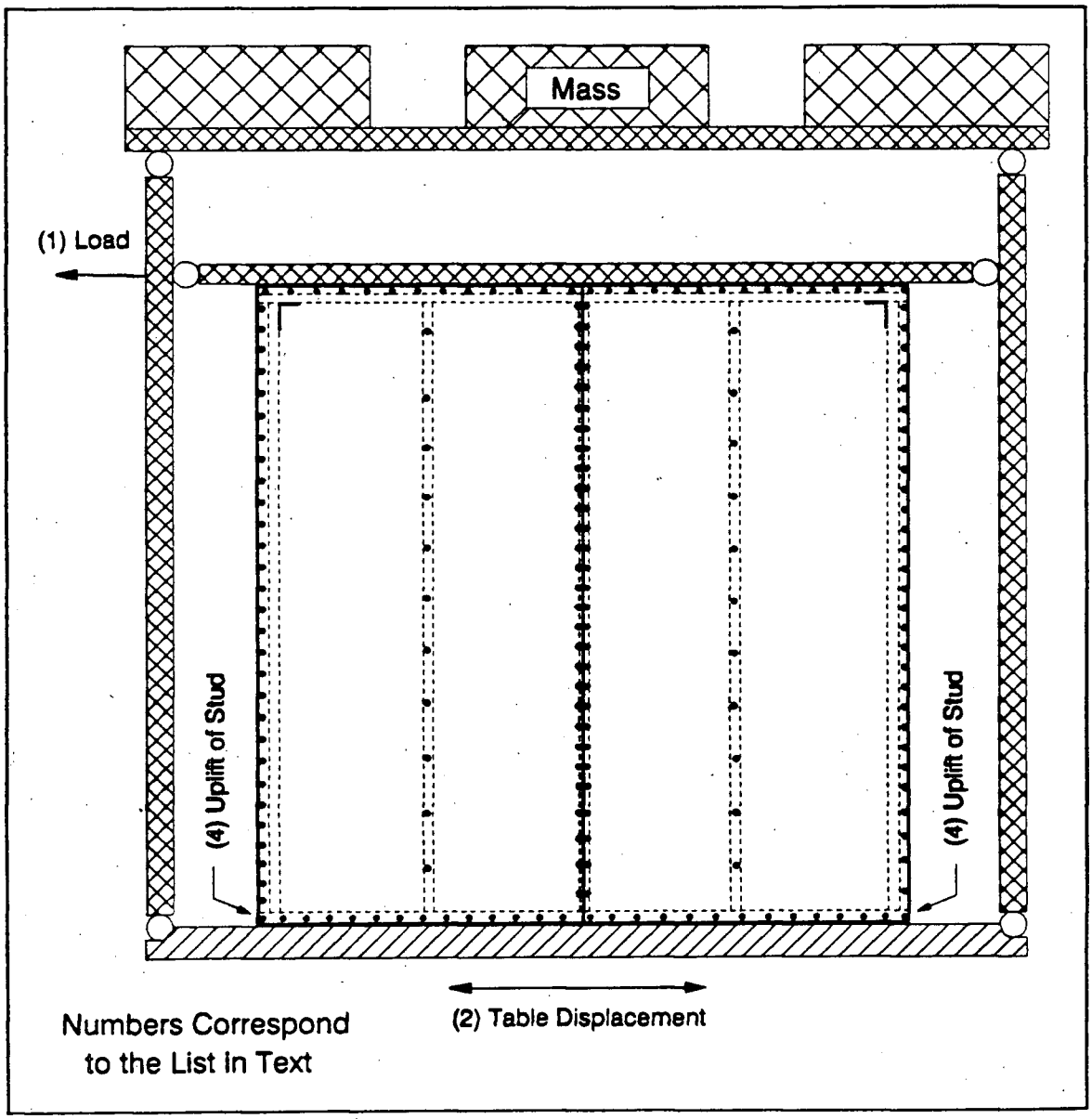

Figure 7.10: Location of Variables Measured During Static Cyclic Tests.

7.6.3 Free Vibration Tests

Free vibration tests were conducted to determine the initial and final fundamental periods of the overall structure. Other authors, such as Falk and Itani (1986), have investigated the natural frequencies of wall, floor and ceiling diaphragms. However, most of these investigations concentrated on the natural period for the diaphragms themselves. While this information is helpful, the results have little bearing on the performance of the diaphragm when the mass of the supported structure is involved, because of the combined effect that determines the natural period of a structure.

After the wall specimen had been mounted in the test frame, the free vibration tests were conducted . The fundamental period determined included the effects of the lateral stiffness of the wall, and full inertial mass of the testing frame. It is believed that the results of this test are representative of the behavior of shear walls when they are integral parts of the larger structures.

The procedure followed for the free vibration tests consisted of disconnecting the restraining arm to the reaction column, and then allowing a 95 kg (6.5 slug) mass impact the testing frame at the same height as the top of the wall. The natural frequency for the wall and test frame system was determined from the accelerations that were recorded during and after the impact. The accelerometer, used to measure the pertinent accelerations, was located at the top of the wall, at the opposite end from where the impact mass hit the frame. The testing frame was not attached to the reaction column, thereby requiring the wall specimen to provide full lateral stiffness for the test frame.

The results of this test give an indication of how much the shear wall stiffness deteriorates when damaged during an earthquake. The future response could also change significantly. If the natural period shows a large shift in natural period, due to damage, the future response could also change significantly.

7.6.4 Sine Wave, Frequency Sweep Tests

The sine wave frequency sweep tests were performed to get an indication of the steady–state response of timber shear walls. The test results are used to verify the closed form analytical model derived in Chapter 5, which in turn can be used to investigate the steady–state response of the walls for different wall configurations.

Table 7.1: Frequency and Corresponding Base Accelerations for Sine Wave Tests.

Specimen # 1		Specimen # 2	
Frequency (Hz)	Base Acceleration (g)	Frequency (Hz)	Base Acceleration (g)
1.00	0.100	3.50	0.099
1.25	0.100	3.20	0.101
1.60	0.103	2.85	0.101
1.90	0.101	2.50	0.097
2.00	0.101	2.20	0.101
2.20	0.101	2.00	0.101
2.50	0.097	1.90	0.100

During the sine wave tests, the frame was not attached to the reaction wall, thereby requiring the wall specimen to provide all the lateral support to the test frame and inertial mass. The base of the wall was then displaced in a sine wave pattern, with peak base accelerations being approximately 0.1 g. Accelerations at the top of the wall were monitored and the test was stopped as soon as a steady state condition was reached and maintained for three to five cycles, to prevent the nails from failing due to fatigue. The test was repeated for each of the frequencies, shown in Table 7.1, with the displacements being adjusted in order to maintain the peak base acceleration at 0.1 g.

Using one wall specimen for more than one test can cause problems. The wall will be damaged during the first test and would give erroneous results for the subsequent experiment. The damage of the wall is not always visible. Nails can be loosened or

broken without damaging the sheathing surrounding the nail, which makes detection almost impossible. However, these problems are unlikely to have affected the results of the tests conducted as part of this thesis. Each wall specimen was first tested, using low amplitude displacements. Higher amplitude displacements were used for each subsequent test. The results for tests conducted after resonance had been achieved were not used. Also, the steady state behavior is governed by the maximum displacement achieved. Therefore, the first tests would not adversely affect the subsequent tests, because the specimen was subjected to increasing displacements with each test.

Five signals were recorded during the sine wave tests, each being sampled at 0.01 sec intervals. Figure 7.11 shows the location of the various instruments used to measure each variable. The measurements recorded were:

1. Displacement of the top of the wall.
2. Displacement of the base of the wall.
3. Accelerations at the top of the test frame, i.e. inertial mass.
4. Accelerations at the top of the wall.
5. Accelerations at the base of the wall.

Two walls of each sheathing material were tested, for a total of four walls. The two wall specimens of each type were required in order to trace the response curves accurately. A typical set of frequency response curves, predicted by the closed–form model, is shown in Figure 4.5 on page 85. The deflection increases, as the frequency of base accelerations approaches the resonance frequency for the structure. Timber shear walls do not behave elastically, and therefore, the stiffness and response of timber shear walls are governed by the largest previous deflection. The resonance frequency of the shear walls must be

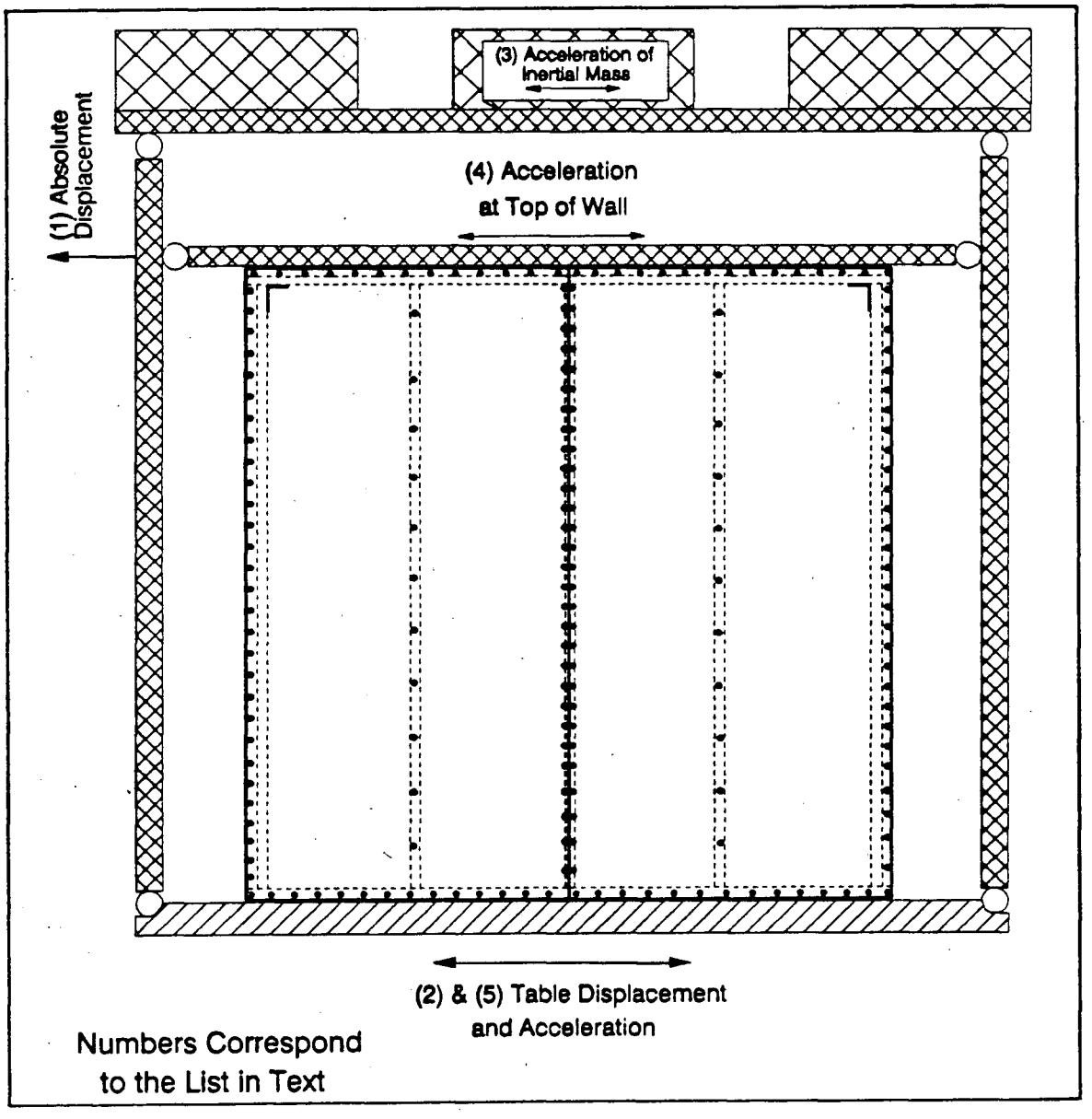

Figure 7.11: Location of Variables Measured During Sinewave, Frequency Sweep Tests.

approached from both lower and higher frequencies in order to follow the true response curve. For this reason, two walls for each sheathing type were tested, as shown in Table 7.1. Specimen #1 was tested starting with a frequency of 1.00 Hz and increased to 2.50 Hz, while Specimen #2 started with a frequency of 3.50 Hz and decreased to 1.90 Hz. If the entire frequency range were to be used to test one wall specimen, the response of the wall after resonance has occurred would not be indicative of steady state conditions in an undamaged wall, due to the large displacements incurred during resonance. The results of this test are presented in Section 9.3.

7.6.5 Earthquake Tests

7.6.5.1 Background

The earthquake tests used in this study were designed to investigate the accuracy of the predictions made by the numerical model, **DYNWALL**. All numerical models should be verified with experimental tests to ensure the predictions are correct. Without these verifications, the subsequent use of the model could be highly suspect. Therefore, a variety of tests were used to compare predictions of the model with test results. The test specimens used were varied by changing the sheathing type and nail spacing to represent different wall strengths. The numerical model, **DYNWALL**, was used to predict the dynamic response of test specimen, and test results were then compared to the prediction of the program in order to check the accuracy of the prediction.

In addition to verification of the model, the earthquake tests were used to investigate the following seven topics:

1. Response of timber shear walls to dynamic loadings, similar to those expected in a structure during an earthquake.

2. The appropriateness of allowing equivalent design values for shear walls using waferboard and plywood, as is done in the United States.

3. The accuracy of the design loads used in the building codes for Canada and the United States.

4. Effects of nail spacing on stiffness and strength.

5. The strength and stiffness of a timber shear wall after being damaged during an earthquake.

6. The effect of dead load on the dynamic response.

7. The effect of the orientation of the sheathing.

The earthquake test used an inertial mass at the top of the frame to load shear walls in the same way the mass of the top two floors of an apartment building would load the ground floor walls. The base of the wall was displaced according to the acceleration records of actual earthquakes. The accelerations were transmitted by the wall to the mass at the top of the frame, just as the accelerations of the ground are transmitted to the upper stories of a building during an earthquake. The load experienced by the wall is directly proportional to the accelerations transmitted to the inertial mass. Therefore, this test includes the effects of the damage received by the wall. The effects of the damage include the degrading stiffness, lengthening natural period, and possibly loss of strength for the wall specimen.

In previous investigations, the effects of change in stiffness and natural period on the loading, experienced by the wall during a test, have been neglected. Most of the tests have required shear wall specimens to react at the frequency of loading by attaching the loading device to the top of a wall specimen, while the bottom is rigidly anchored. This

may lead to erroneous findings, since the fundamental frequency of timber shear walls will change as they are damaged. The effect of changes in natural frequency could be to lower the load requirements of the wall by effectively insulating the inertial mass from high accelerations.

The earthquake test used in this study includes all of the effects of change in stiffness, natural frequency, and possibly, strength. The test is, therefore, representative of the loading shear wall elements experience in structures subjected to earthquakes. The results will be more representative of the response of timber shear walls to earthquake loading, than if some other tests were used.

7.6.6 Procedure

The walls were subjected to two earthquake events. In the first, the base of the wall was displaced according to the acceleration record of an earthquake, with the peak base acceleration equal to the full amplitude originally recorded. Since most of the wall specimens survived the first earthquake without being significantly damaged, the test was repeated after scaling the base acceleration record to 150% of the amplitude of the original record. The higher amplitude acceleration was used in an effort to subject more of the specimens to their ultimate capacity. The higher intensity earthquake had a peak acceleration of 0.3 g, which was the largest acceleration that the test frame could safely be used for. The scaling of the acceleration amplitude was accomplished by simply multiplying the magnitudes of recorded earthquake record by a scalar number, such that the peak acceleration of the resulting record equalled the desired value. The time parameter of the acceleration was not changed, only the magnitude of the accelerations. No repairs were made to the shear wall specimens between earthquakes, but each wall was inspected to note any visual damage sustained.

Two earthquake records used were:

1. The S69E component of the July 21, 1952 Kern County, California earthquake, recorded in the basement of the Taft High School, was used for most of the tests. The decision to use this earthquake record was made after consulting with various authorities in the field of earthquake engineering. This earthquake includes a wide band of frequencies, and would therefore be capable of exciting many frequencies in the wall. The earthquake's duration is almost quite long compared to most earthquakes, which makes it potentially more damaging. It is understood that no future earthquake will be the same as any of the ones from the past, but in an effort to give the reader some reference to reality, a significant earthquake from the past was used.

2. The other earthquake used was the N21E component of the February 9, 1971 San Fernando earthquake. This earthquake record was chosen so the numerical model, **DYNWALL**, could be verified using two earthquakes having different frequency contents. The San Fernando earthquake is a relatively short earthquake, containing a narrow band of frequencies.

Twenty–one signals were recorded, and each channel was sampled at 0.01 sec intervals for the duration of each earthquake. The locations where each of these variables were measured on a typical wall specimen are shown in Figure 7.12. The variables monitored in the plane of the wall were:

1. The Displacement at the top of the wall.

2. Displacement at the base of the wall.

3. Separation of the framing joint at each of the top corners of the wall.

4. Sheathing uplift at each of the bottom corners of the wall.

5. Uplift of each of the end studs.

6. Uplift of each end of the sole plate framing number.

7. Acceleration at the base of the wall.

8. Acceleration at the top of the wall.

9. Acceleration at the top of the frame where the inertial mass is located.

Variables monitored perpendicular to the plane of the wall were:

10. The sheathing displacement at each of the corners of the wall.

11. Sheathing displacement at mid–span between the studs, mid–height on the wall.

A minimum of two specimens and a maximum of four were tested for each configuration of sheathing type and nail density. An overview of the different tests is presented in Section 8.1.

7.7 Data Analysis Procedures

7.7.1 Static Tests

The static one–directional and the static cyclic test data were recorded using analog filters before it was converted to digital form. A few signals did not show significant noise levels, and consequently the raw data could be used. Analog filters, with a cut–off frequency of 60 Hz were used for the static tests. These filters were required to essentially eliminate the noise from the electrical supply and did not shift or damp the signal, since the sampling rate was slow enough to allow the signal intensity, being recorded, to settle.

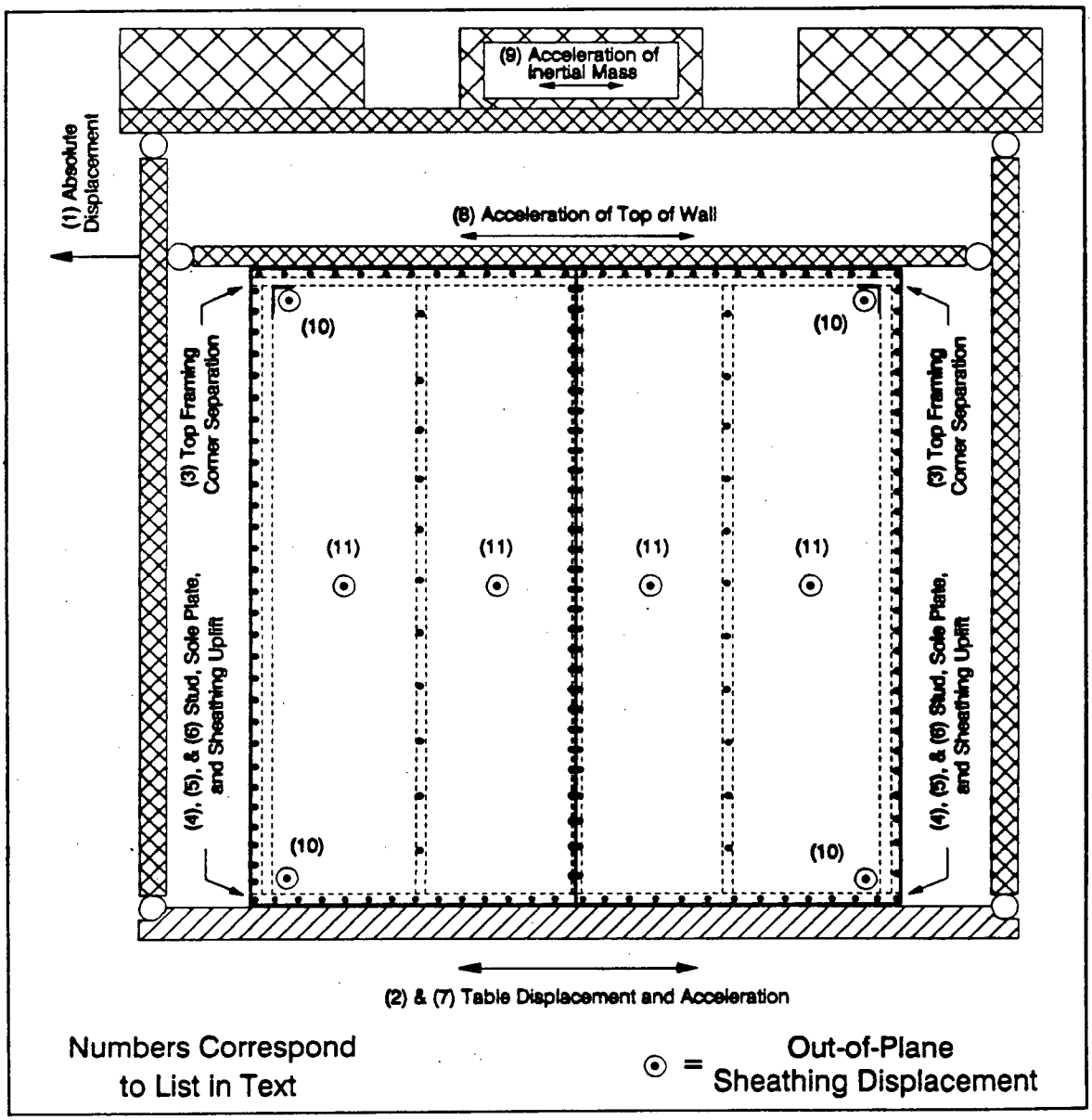

Figure 7.12: Location of Variables Measured During Earthquake Tests.

Two relations were used to verify the numerical model, **SHWALL**: **(a)** load versus racking deflection of the wall's framing, and **(b)** the out–of–plane defection of sheathing versus racking deflection of the framing. The deflection of the base is equivalent to racking deflection because the top of the wall was restrained by the reaction column and, therefore, did not move. Figure 7.13 shows a typical load–deflection curve obtained in this manner. The load–deflection curve was corrected in order to eliminate the P–delta effects, by subtracting the curve obtained from the test run without a wall specimen. Figure 7.9 shows the steps used to correct the load–deflection curve. Figure 7.9a shows a typical load–deflection curve as originally recorded. Figure 7.9b shows the load–deflection curve of the test run without a wall specimen. To obtain the correct load–deflection curve, the curve in Figure 7.9b is subtracted from the curve in Figure 7.9a. The resulting corrected curve is shown in Figure 7.9c.

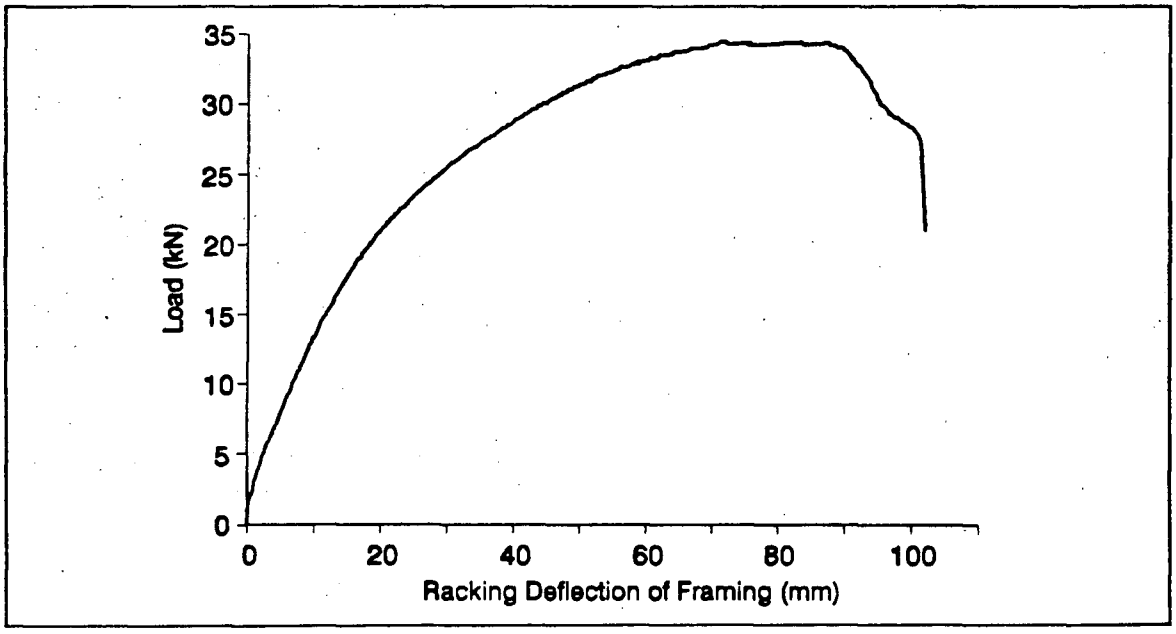

Figure 7.13: Typical Load Versus Racking Deflection Curve for a Static One–Directional Test.

A curve representing the out–of–plane deflection of sheathing versus racking deflection

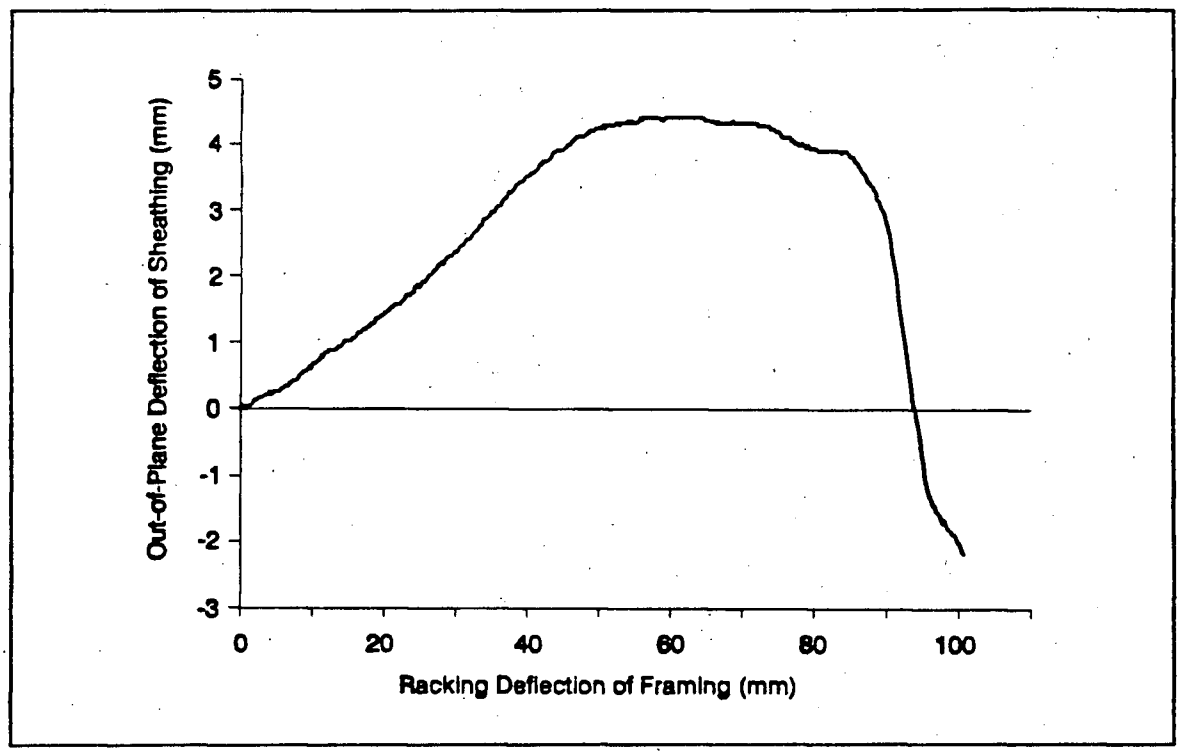

Figure 7.14: Typical Out–of–Plane Deflection Versus Racking Deflection Curve for a Static One–Directional Test.

of the framing can be obtained by plotting data for one of the potentiometers, used to measure the sheathing out–of–plane deflection, against data record for the base of the wall deflection. Figure 7.14 shows a typical out–of–plane deflection versus racking deflection curve obtained from test data. The negative deflection shown in the curve is due to the nails used to attach the sheathing to the framing, failing towards the end of the particular test used for this example, and the sheathing deflection changing from moving away from the framing to bearing on the framing. The particular point of measuring was located midway between the studs and, therefore, negative displacements are possible. Positive deflections represent separation of the framing and sheathing.

The results of the static one–directional and static cyclic tests are presented, and discussed in Sections 8.2 and 8.3, respectively.

7.7.2 Digital Filtering Method

Due to the higher sampling rate used to record data during the dynamic tests, the digital signal had to be filtered to eliminate background noise in the signal. This was accomplished using digital filtering techniques. Various techniques for digital filtering are available, and detailed theories can be found in many books such as those by Bendat (1971) and Kanasewich (1975). The method used for this study utilized the Fast Fourier Transform (FFT) to transform data records into the frequency domain and filter the data using a low pass filter to eliminate the high frequency noise.

The procedure used to eliminate the noise is illustrated in Figure 7.15. Figure 7.15a shows a typical record for the displacement at the top of the wall, as it was originally recorded. The recorded signal was then transformed from the time domain, into the frequency domain, as shown in Figure 7.15b, using a FFT. A low pass filtering window was made to have an amplitude of 1.0 for all frequencies below a cut–off frequency, and 0 above the cut–off frequency. The cut–off frequency used was twice the highest frequency of significant peaks of transformed data signal, determined from Figure 7.15b. To avoid a numerical problem known as a ripple effect, a cosine bell curve was used to smooth the transition from a value of 1.0 to 0 in the filtering window. The resulting filter window is shown in Figure 7.15c.

The frequency signal of the data (Figure 7.15b) was then multiplied by the filter (Figure 7.15c) to produce the filtered signal in the frequency domain, shown in Figure 7.15d. This frequency signal is finally transformed back into the time domain, using the Inverse Fast Fourier Transform (IFFT). The resulting record is the filtered record of displacements.

Figure 7.16 shows the effect of the filtering process. In Figures 7.16a and 7.16b, respectively, 10–second portions of the raw and filtered data records are shown. The filtered

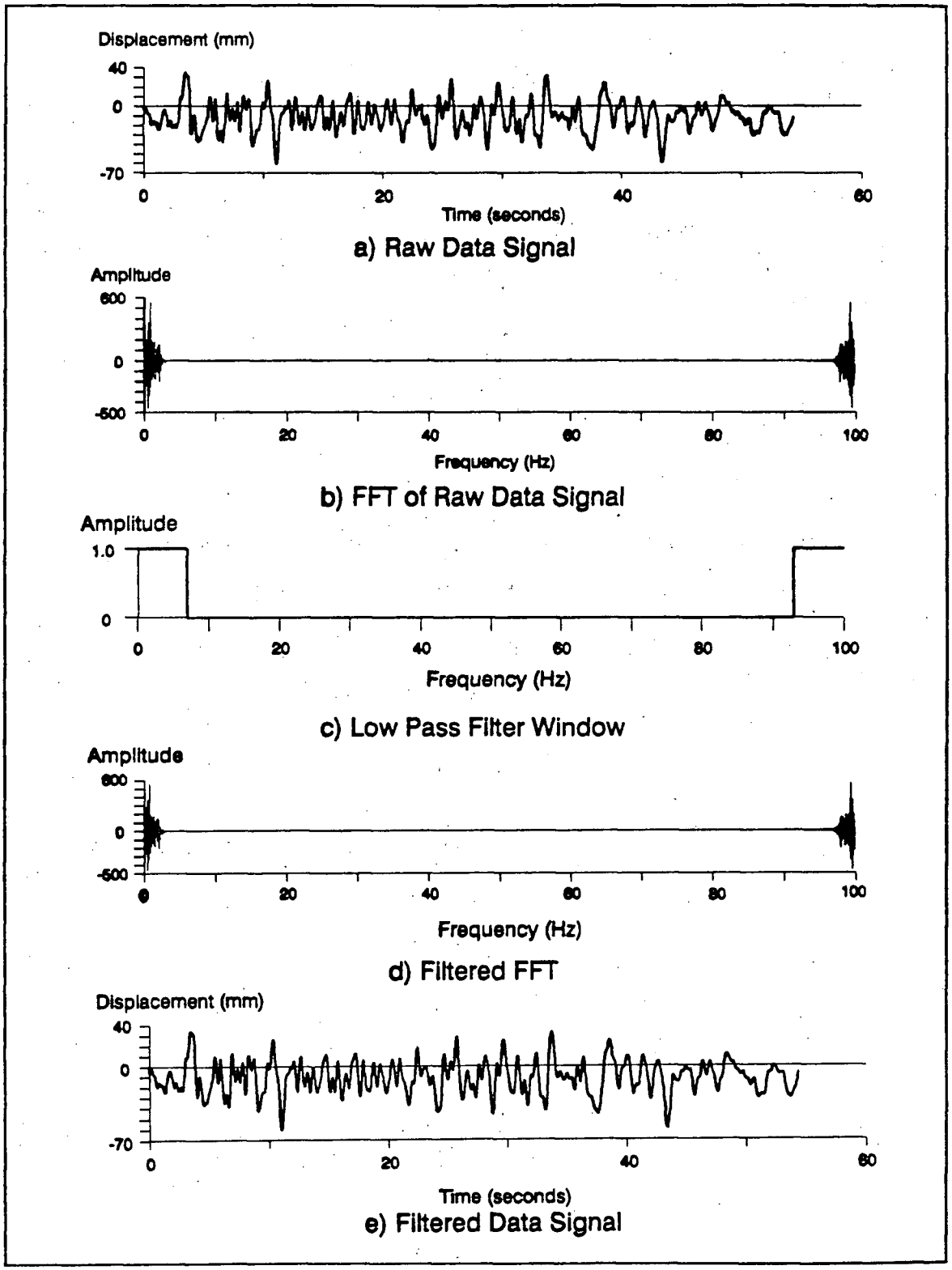

Figure 7.15: Digital Filtering Procedure.

displacement signal plotted over the unfiltered signal is also shown in Figure 7.16c. As demonstrated by Figure 7.16, the filtering process smooths the data signal by eliminating the higher frequency oscillations, which are considered to be noise introduced into the recorded signal by a variety of unrelated sources. It is also important to note that the filtered data does not show any phase shift due to the filtering process. All of the dynamic test data was filtered using this method.

7.7.3 Free Vibration Tests

The free vibration data was analyzed to obtain only the initial and final natural periods. This was accomplished by reading the times for acceleration record periods, which would be equal to the natural period of the testing system, including the wall and inertial mass. Figure 7.17 shows a typical filtered acceleration record for the free vibration test. The period of this wall is approximately 0.6 seconds (frequency of 1.67 Hz). The results of these tests are presented and discussed in Section 8.4.

7.7.4 Sine Wave Tests

The sine wave tests yielded, as a parameter of interest, the steady state amplitude of the deflection at the top of the wall relative to the base of the wall, i.e. racking deflection of the shear wall. This is obtained by subtracting the base deflection data, from the record for deflection at the top of the wall.

The steady–state deflection is defined as the peak relative displacement that is repeated after the accelerations at the top show a steady–state behavior. The accelerations at the top of the wall were monitored during the tests, and when the amplitude of the acceleration record was repeated for at least three successive cycles, it was assumed that

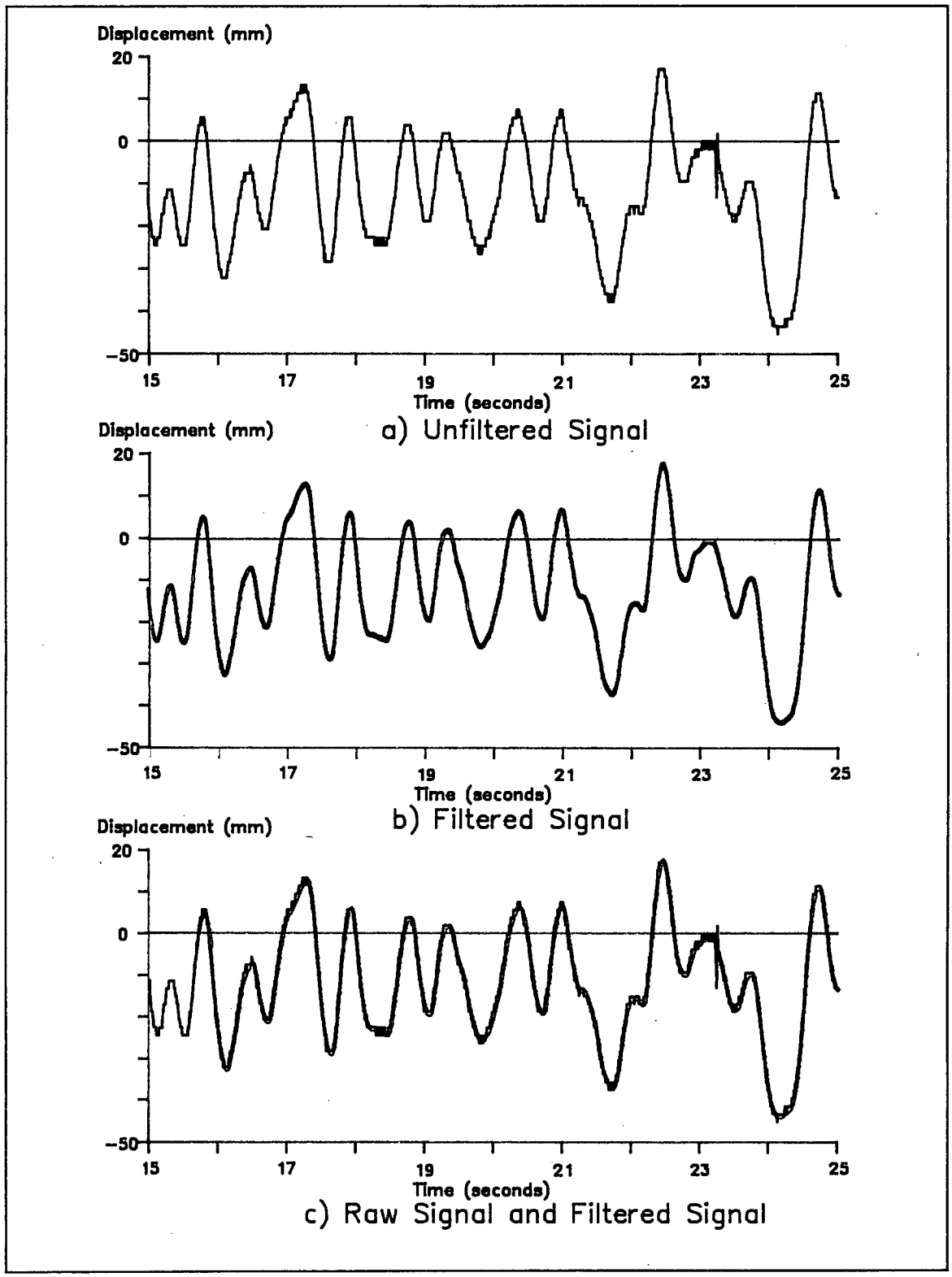

Figure 7.16: Comparison of a Filtered and Unfiltered Displacement Record.

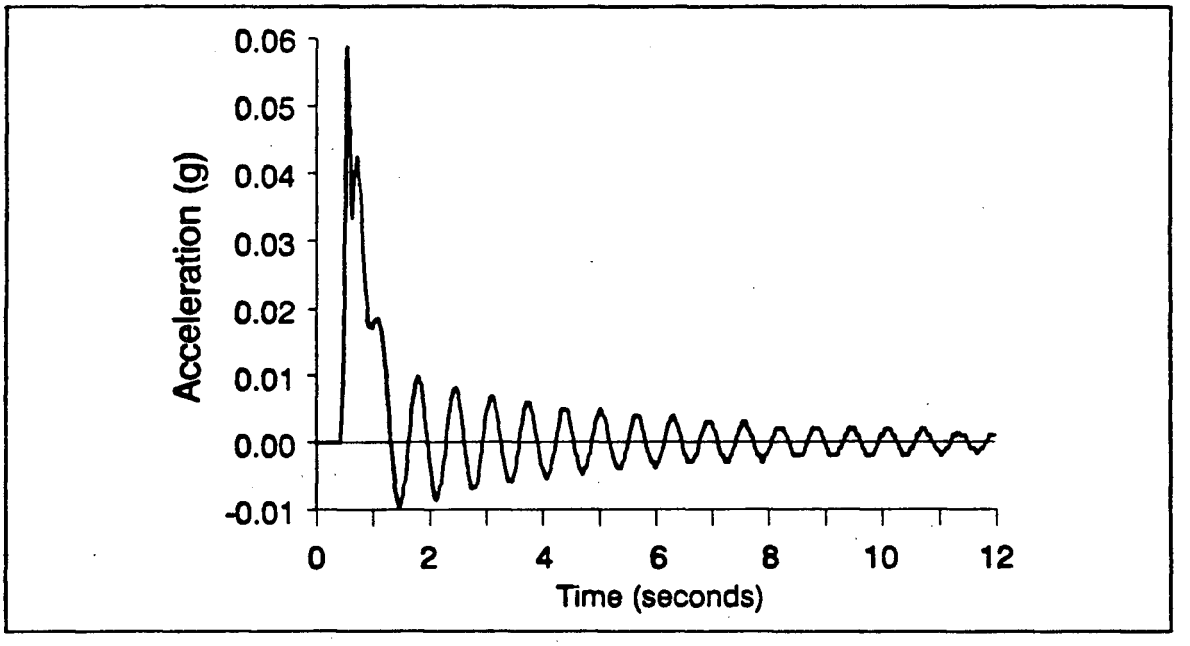

Figure 7.17: Typical Acceleration Record for a Free Vibration Test of an Undamaged Shear Wall.

a steady–state condition had been reached. Figure 7.18 shows a typical displacement record for the sine wave tests, with the steady–state deflection indicated.

7.7.5 Earthquake Tests

Three topics investigated, using data recorded during the earthquake tests were:

1. Conclusions were made based on relative deflections, which required the difference between two data records be determined. The two recorded signals involved were first filtered, using the procedure described in Section 7.7.2, then one signal was subtracted from the other to determine deflections at the top of the wall relative to the base. The separation of framing joints at the bottom of the wall was also

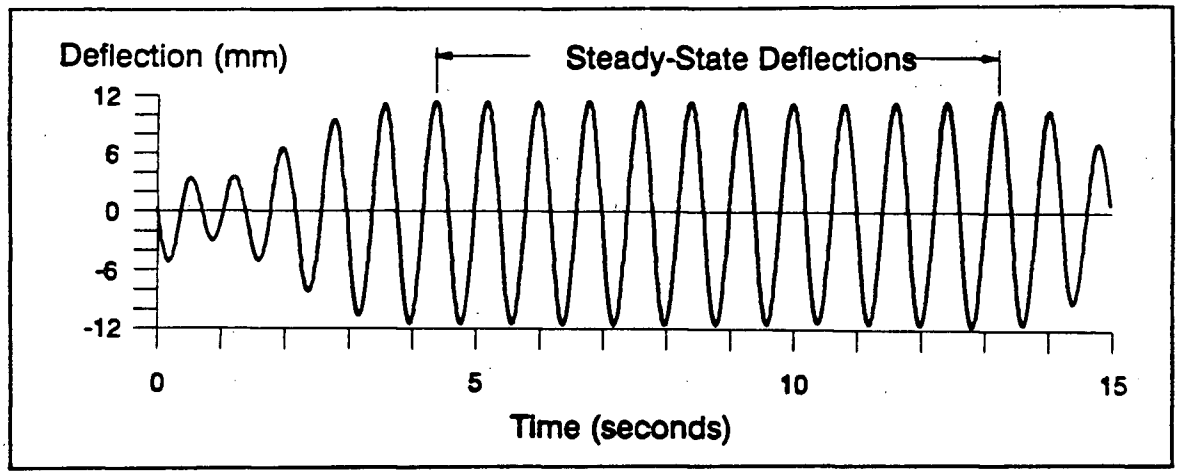

Figure 7.18: A Typical Racking Displacement Curve for a Sine Wave Test.

determined in this way.

2. The time histories measured and derived variables were investigated. The measured time history of a variable was obtained by filtering the recorded signal to eliminate high frequency noise. These variables included uplift of the end studs and out–of–plane displacement of the sheathing.

   The time history of the load was obtained by filtering the acceleration record for the top of the frame, where the inertial mass is located. This signal was then multiplied by the value of mass to determine the load history. The load at the top of the wall could then be found using statics. Figure 7.19 shows a free–body diagram of a column for the testing frame. If moments are summed about the base of the column, the resulting equation is

$$\sum M = 2.9 * P_{\mathrm{H}} - 2.4 * P_{\mathrm{TOP\ OF\ WALL}} = 0 \qquad (7.1)$$

   where, P_{H} is the horizontal load at the top of the column and $P_{\mathrm{TOP\ OF\ WALL}}$ is the load resisted by the wall.

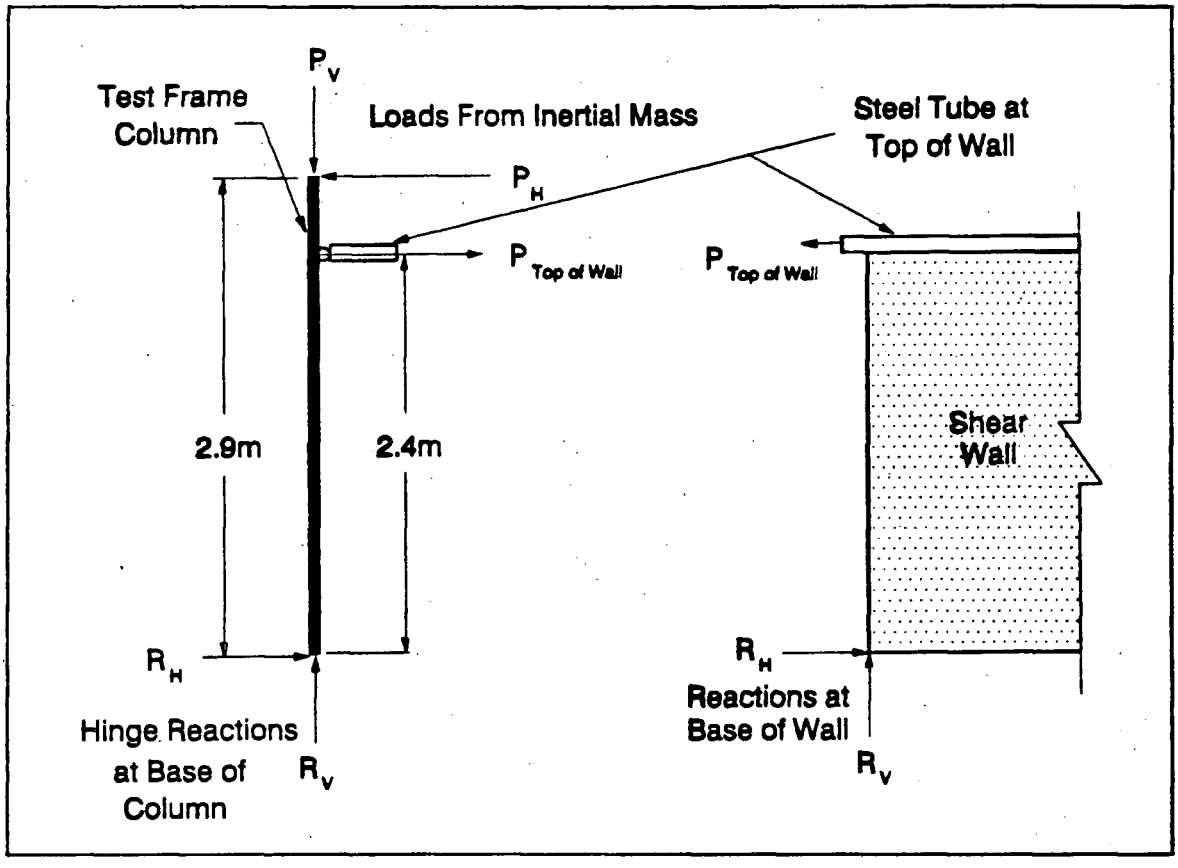

Figure 7.19: Free–Body Diagram of Testing Frame Column.

Solving for $P_{\text{TOP OF WALL}}$,

$$P_{\text{TOP OF WALL}} = \frac{2.9}{2.4} * P_{\text{H}} \tag{7.2}$$

Using Equation 7.2 and the desired time history of the load at the top of the frame, the time history of load applied to the top of wall can be obtained.

3. Peak values of one or more of the measured or derived variables were also examined. These are obtained directly from filtered or derived data records.

The results of the earthquake tests are presented and discussed in **Section 8.6.**

7.8 Summary

The test equipment, materials used to construct the shear wall specimens, and the procedures followed in performing each of five test types of full–size shear wall specimens have been described. The tests included were:

1. Static one–directional racking,
2. Static cyclic racking,
3. Free vibration,
4. Sine wave frequency sweep, and
5. Earthquake.

The shear wall specimens were 2.4 × 2.4 m (8 × 8 ft) in size, and were considered to be full scale specimens.

The methods used to analyze data obtained from each test were also described, to allow the reader to compare the different methods. However, no conclusion about the performance of shear walls has been attempted in this chapter. The results of the analysis and subsequent discussion are given in Chapter 8.

Chapter 8

Full–Size Shear Wall Test Results

8.1 Introduction

The test results for the five types of shear wall tests, described in Chapter 7, are analyzed and discussed in this Chapter. "Full–size" shear walls, 2.4×2.4 m (8×8 ft), were used for all of the tests, and the construction techniques used are described in Sections 7.4 and 7.5. Each test will be presented separately, along with pertinent discussion. Some of these results are used, in Chapter 9, to verify the numerical accuracy of the three models derived in Chapters 3, 4, and 5.

A section of general discussion on the behavior of timber shear walls follows the last individual test discussion. This section is intended to correlate the results of individual tests together, and to try to draw conclusions on the usefulness and deficiencies of each type of test. The discussion also relates to the overall performance of shear walls, rather than to just one type of loading.

A total of 20 waferboard and 22 plywood sheathed shear walls were tested in conjunction with this thesis. Table 8.1 presents an overview of the tests, including what tests were performed, how many specimens were used for each test, and their configurations. The table also shows whether dead load was applied or not, and which earthquake record was used.

Table 8.1: Overview of Full Size Shear Wall Tests.

Sheathing Type	Sheathing Orientation	Nail Spacing Perimeter/Field mm / mm	(in / in)	Dead Load Applied kN	(lb)	Earthquake Record Used	Number of Specimens
Static One-Directional:							
Waferboard	Vertical	100/150	(4/6)	0	0	N/A	3
Waferboard	Vertical	100/150	(4/6)	44.5	10,000	N/A	1
Plywood	Vertical	100/150	(4/6)	0	0	N/A	3
Static Cyclic:							
Waferboard	Vertical	100/150	(4/6)	0	0	N/A	2
Plywood	Vertical	100/150	(4/6)	0	0	N/A	2
Sinewave:							
Waferboard	Vertical	100/150	(4/6)	0	0	N/A	2
Plywood	Vertical	100/150	(4/6)	0	0	N/A	2
Earthquake:							
Waferboard	Vertical	100/150	(4/6)	0	0	Kern Cnty.	4
		100/150	(4/6)	44.5	10,000	Kern Cnty.	3
		50/150	(2/6)	0	0	Kern Cnty.	2
		150/150	(6/6)	0	0	Kern Cnty.	2
		300/300	(12/12)	0	0	Kern Cnty.	1
Plywood	Vertical	100/150	(4/6)	0	0	Kern Cnty.	4
		100/150	(4/6)	44.5	10,000	Kern Cnty.	2
		50/150	(2/6)	0	0	Kern Cnty.	2
		150/150	(6/6)	0	0	Kern Cnty.	2
		300/300	(12/12)	0	0	Kern Cnty.	1
	Horizontal	100/150	(4/6)	0	0	Kern Cnty.	2
	Vertical	100/150	(4/6)	0	0	San Fernando	2
Free Vibration: The free vibration tests were performed on test specimens for other tests before and after the test was complete.							

8.2 Static One–Directional Tests

A total of seven shear walls were tested, according to the static one–directional procedures presented in Section 7.6.1. Four of the walls were sheathed with waferboard and three walls were sheathed with plywood. All the specimens were constructed with their sheathing panels oriented with the long dimension of the panels in the vertical direction (parallel to the studs). The nails used to attach the sheathing were spaced at 100 mm (4 in) on the perimeter, and 150 mm (6 in) along the interior stud.

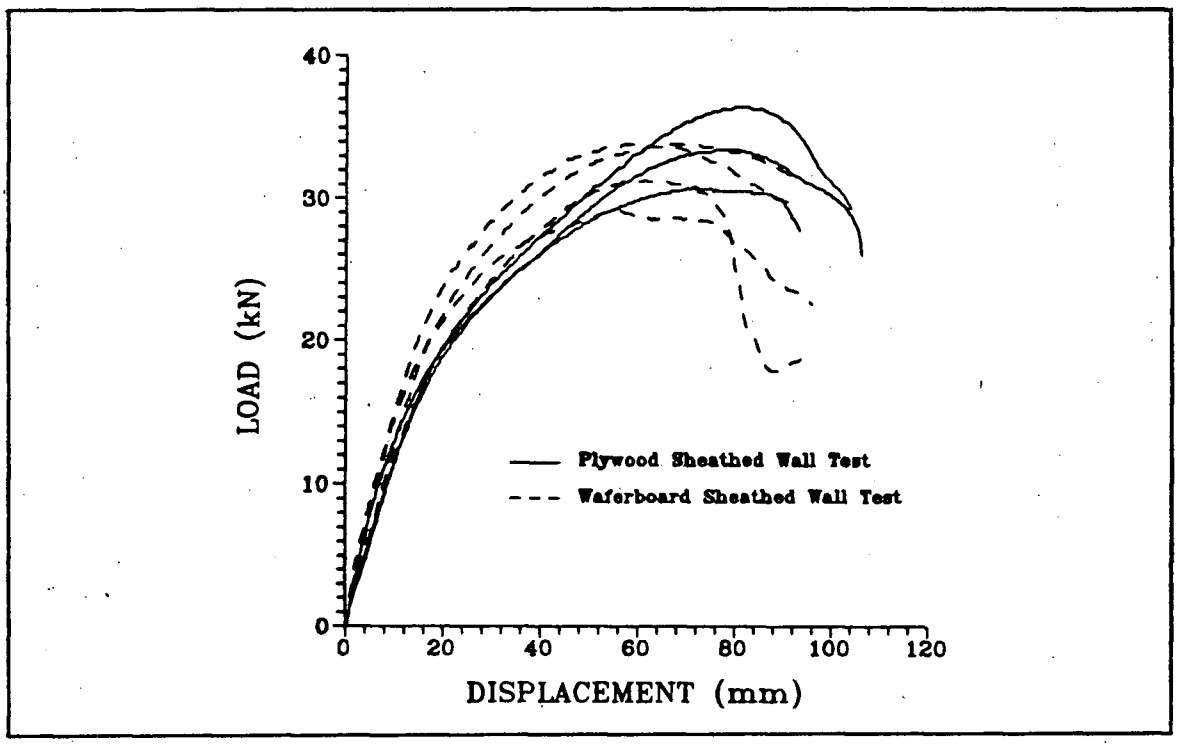

Figure 8.1: Load–Deflection Curves Obtained From The Static One–Directional Shear Wall Tests.

Figure 8.1 shows the load–deflection curves for the seven test specimens. The peak loads and corresponding displacements of each of the walls are shown in Table 8.2. Figure 8.1 shows the initial stiffness of the waferboard sheathed walls (dashed lines) was marginally higher than the initial stiffness of the plywood sheathed walls (solid lines).

This is due to the higher stiffness and density of the waferboard panels. The plywood sheathing panels were significantly more flexible than the waferboard, especially in the direction perpendicular to the face grain of the panel (the 1.2 m (4 ft) direction of the panel). This difference in flexibility, between the two types of sheathing, is also evident for the out–of–plane deflection.

Figure 8.1 and Table 8.2 show that the average peak load for plywood walls is higher than the average peak load for waferboard walls. It can also be seen that the corresponding displacement for plywood walls is higher than that for waferboard walls. However, if the coefficients of variation for peak load of each type of shear wall are considered, it is found that the difference in load capacity between the two types of construction is not significant. Therefore, it can be concluded that there is little difference in load capacity between plywood and waferboard sheathed walls, while the stiffness of waferboard sheathed walls is marginally higher than that of plywood sheathed walls.

Out–of–plane displacements of the sheathing panels were monitored in eight locations; the four corners of the wall and between each of the studs (at center of span and mid–height of the wall). There was virtually no movement of the corners of sheathing. This lack of movement was expected since the number of nails in the corners of each sheathing panel was quite high, and the framing would support the sheathing in both directions. The peak displacement recorded in any one of the out–of–plane corners was 0.25 mm (0.01 in). The out–of–plane movement of sheathing between the studs was higher than in the corners, but the amount of displacement was not significant. Table 8.3 shows peak values for the displacements between studs, recorded during the tests. As Table 8.3 shows, the plywood sheathing deflections are higher than the corresponding waferboard deflections. Also, it can be seen that these deflections are all less than the thickness of sheathing. It can be concluded that buckling of sheathing is not a major factor in determining the strength or stiffness of shear walls, when using plywood or waferboard

Table 8.2: Peak Load and Corresponding Deflection for Static One-Directional Shear Wall Tests.

Specimen	Peak Load		Corresponding Displacement		Dead Load Applied	
	kN	(lbs)	mm	(in)	kN	(lb)
Waferboard Sheathed Specimens:						
WS-11	28.6	(6430)	62	(2.5)	0	(0)
WS-12	33.8	(7598)	77	(3.0)	44.48	(10000)
WS-13	31.2	(7014)	74	(2.9)	0	(0)
WS-14	33.8	(7600)	81	(3.2)	0	(0)
Average	31.8	(7160)	74	(2.9)		
C.V.	0.07		0.10			
Plywood Sheathed Specimens:						
PS-1	30.4	(6835)	78	(3.07)	0	(0)
PS-2	33.5	(7531)	86	(3.37)	0	(0)
PS-3	36.5	(8206)	89	(3.52)	0	(0)
Average	33.5	(7524)	84	(3.32)		
C.V.	0.07		0.06			

Note: WS indicates waferboard specimen and static one-dimensional test.

PS indicates plywood specimen and static one-directional test.

sheathing of 9.5 mm (3/8 in) thickness or more.

The rest of the variables monitored showed that the framing joints did not separate, and that the framing was anchored securely to the base. The largest displacement measured for the separation of either of the top corner framing joints was 0.6 mm (0.02 in). This displacement occurred in the joint at the top of the wall nearest the restraining arm on the frame. This joint was loaded in tension during all the tests, and would therefore be the location expected to have the largest separation of the two top corners. The average displacement of this joint was 0.4 mm (0.016 in), which is negligible.

The sole plate uplift (both sides) were all, essentially, zero. However, the compression end stud uplift did show significant displacements during the static one–directional tests. In every test, the sole plate was crushed underneath the end stud that was in compression. The largest displacement recorded for the downward movement of the end stud was 4.1 mm (0.16 in), with an average displacement of 2.8 mm (0.11 in). Although this displacement does not seem large, it was significant in that the hold–down anchor at this location was loosened. These connections may become slack during the dynamic reversing loading during an earthquake, which would affect the overall stiffness of the wall. The dynamic behavior of the wall would also be affected significantly.

Finally, if the shape of the curves shown in Figure 8.1 are compared to the shape of load–deflection curves for the individual nail connection, shown in Figure 6.11, it can be seen that the two types of curves are very similar. The exponential equation,

$$F = (P_0 + K_2\Delta)\left(1 - \exp\left(-\frac{K_0\Delta}{P_0}\right)\right) \tag{8.1}$$

was fit to the load–deflection data for each wall specimen, as has been done for the connection tests. Table 8.4 shows the resulting parameters K_0, K_2, and P_0 for each wall. As shown in Table 8.4, the initial stiffness for waferboard sheathed walls is higher than that for plywood sheathed walls. This information supports the conclusion that the

Table 8.3: Out–of–Plane Displacements of Sheathing, Mid–height and Midway Between Studs.

Specimen	Location and Displacement							
	East Edge		East Inside		West Inside		West Edge	
	mm	(in)	mm	(in)	mm	(in)	mm	(in)
Waferboard Sheathed Walls:								
WS–11	2	(0.1)	-2	(-0.1)	-2	(-0.1)	2	(0.1)
WS–12	2	(0.1)	-1	(-0.0)	-2	(-0.1)	0	(0.0)
WS–13	1	(0.0)	-0	(-0.0)	2	(0.1)	-2	(-0.1)
WS–14	1	(0.0)	-0	(-0.0)	-3	(-0.1)	3	(0.1)
Average[1]	1	(0.1)	1	(0.0)	2	(0.1)	2	(0.1)
Plywood Sheathed Walls:								
PS–1	-1	(-0.0)	1	(0.0)	-5	(-0.2)	5	(0.2)
PS–2	5	(0.2)	3	(-0.1)	7	(0.3)	-3	(-0.1)
PS–3	-1	(-0.0)	0	(0.0)	-9	(-0.4)	10	(0.4)
Average[1]	2	(0.1)	2	(0.1)	7	(0.3)	6	(0.2)

NOTE: Positive displacements indicate the sheathing displacing away from framing. Negative displacements indicate the sheathing displacing into the framing.

1. The average is calculated on absolute values of peaks since the direction of the displacement is random and does not change the effect.

Table 8.4: Exponential Curve Parameters Fit to Static One–Directional Test Data.

Specimen	Envelope Values					
	K_0		P_0		K_2	
	kN/mm	(lbs/in)	kN	(lbs)	kN/mm	(lbs/in)
Waferboard:						
WS–11	2.0	(11600)	22.7	(5100)	0.1	(400)
WS–12	2.1	(11900)	18.7	(4200)	0.2	(1400)
WS–13	1.6	(9400)	15.1	(3400)	0.3	(1600)
WS–14	1.7	(9800)	13.3	(3000)	0.3	(1700)
Plywood:						
PS–1	1.1	(6400)	16.9	(3800)	0.3	(1700)
PS–2	2.1	(12000)	11.6	(2600)	0.2	(1200)
PS–3	1.2	(6600)	14.2	(3200)	0.2	(1400)

waferboard panel's higher density and stiffness provide higher initial stiffness to the wall.

8.3 Static Cyclic Tests

The static cyclic tests were conducted to obtain information about the hysteretic behavior of shear walls. The procedure followed, and the locations of the various variables monitored during the test, are described in Section 7.6.2.

Figure 8.2 shows a typical load–deflection curve obtained from the static cyclic test of a shear wall. A few observations can be made from Figure 8.2. The first observation is that the curves seem to be contained within an envelope of similar shape to the static one–directional curves, shown in Figure 8.1. When the sections of the curve, where the wall is being loaded for the first time (the proposed envelope) are extracted, and then

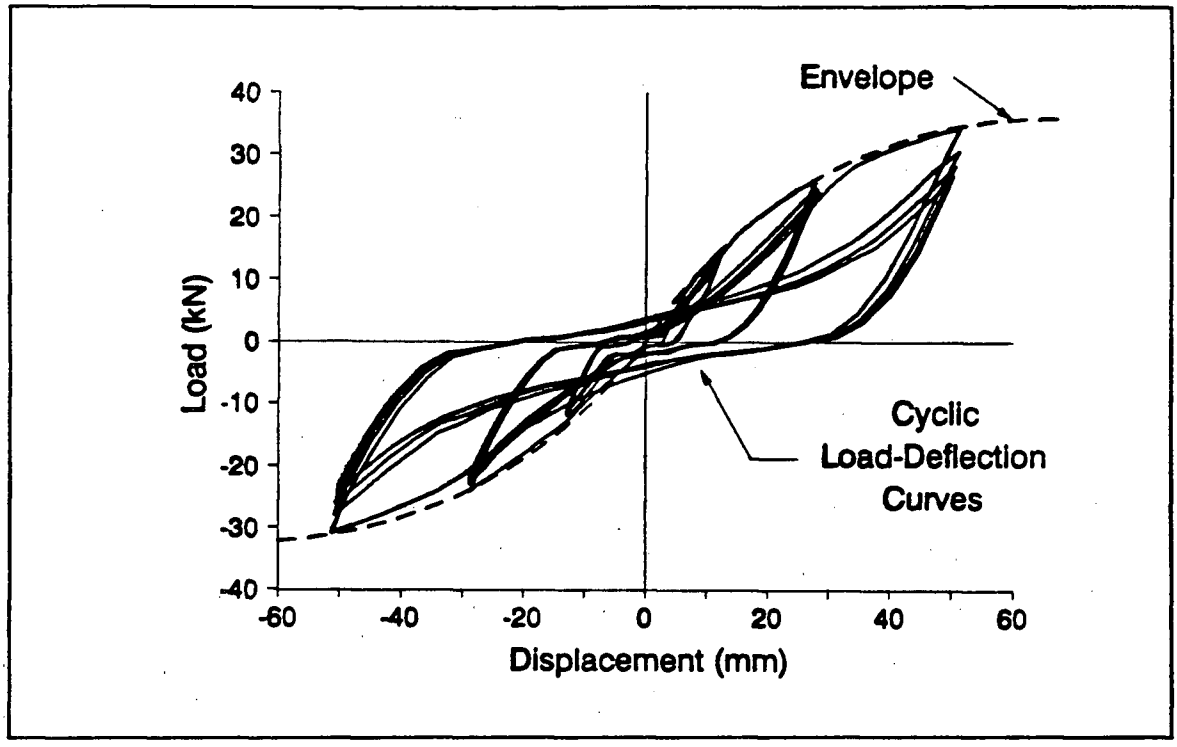

Figure 8.2: Typical Load–Deflection Curves Obtained From The Static Cyclic Shear Wall Tests.

used to fit parameters for the exponential curve (shown in Equation 8.1), the resulting parameter values are close to those found for the static one–directional shear wall tests. The calculated values for the three parameters for each wall are shown in Table 8.5. When these values are compared to those found for the static one–directional test, shown in Table 8.4, it can be seen that there is little difference in the parameters. The value of P_0, for specimen WC–2, is higher than the corresponding value for the other three specimens. This is due to the shape of the envelope curve for this specimen being flatter near the top of the curve than the other three specimens. However, the overall shape of the envelope curve for WC–2 was similar to the curves for the other three specimens. It can be concluded that the static one–directional racking test gives a good indication of the envelope of maximum load capacities for timber shear walls. It is also noted that

the characteristic of plywood walls having a lower initial stiffness, K_0, than waferboard walls, is again borne out by these results.

Table 8.5: Exponential Curve Parameters, Fit to Static Cyclic Test Data

Specimen	Envelope Values					
	K_0		P_0		K_2	
	kN/mm	(kips/in)	kN	(kips)	kN/mm	(kips/in)
Waferboard:						
WC–1	2.1	(11800)	18.7	(4200)	0.3	(1700)
WC–2	2.1	(11800)	29.4	(6600)	0.1	(700)
Plywood:						
PC–1	1.8	(10100)	18.2	(4100)	0.3	(1800)
PC–2	1.8	(10200)	17.8	(4000)	0.3	(1700)

NOTE: WC indicates waferboard specimen and static cyclic test.

PC indicates plywood specimen and static cyclic test.

The load capacity of shear walls decreases as the number of cycles increases for a given displacement. Table 8.6 shows the peak load values for each of the cycles in SI units, while Table 8.7 contains the same information in Imperial units. As can be seen in Tables 8.6 and 8.7, the load capacity for the wall does not decrease much for the ±12.7 mm (±0.50 in) displacements. However, the load capacity of the wall decreases an average of 7% during the cycles to ±25 mm (±1.0 in), and 18% during the cycles to ±51 mm (±2.0 in). The drop in load capacity is believed to be due to a number of related factors. As the wall is racked in a cyclic fashion, the galvanized nails tend to damage the

wood surrounding it, causing a lower contact pressure between the nail and the wood on successive cycles to the same displacement. During the larger displacement cycles, the galvanized nails were observed to work their way out of the framing in an incremental fashion. The nails almost seemed to be pulled out a set amount during each cycle. As the nails were being withdrawn, there would be less length of the nail in the framing to resist the applied forces. Some of the nails that experienced large deformations, broke towards the end of the test. This left fewer nails to resist the loading. These three factors are the major causes of loss in load capacity of the wall for cyclic loading.

Another observation is that the load intercept values of the curve, shown in Figure 8.2, increase as the peak displacement of the cycles increase. It is also noted that the load at zero displacement (intercept) remains fairly constant during the cycles at any given peak displacement. The characteristic of having a constant intercept at any given displacement is expected since the same behavior was observed during the cyclic connection tests, described in Chapter 6. However, the increase in the intercept value was not expected. When the deformation of shear walls is investigated further, the increase can be accounted for. As a shear wall deforms, nails located in the corners of sheathing panels deform more than nails at the mid–point, along the edges of the sheathing panel, as shown in Figure 8.3. For small racking deformations, only the nails located in the corners of each sheathing panel are deformed enough to force the nails into hysteretic behavior. The nails away from the sheathing panel corners would behave more or less elastically during small racking deformations. As racking deformations increase, more nails along the edges of the panel, close to the corners, become deformed enough to cause inelastic behavior. This means more nails would follow the hysteresis curves and would have a non–zero load intercept. The sum of all the individual nail load intercepts would equal the load intercept of the wall. Therefore, even though individual nails have a constant intercept value, the wall would have a load intercept that would depend on the magnitude of

Table 8.6: Peak Loads for Each Cycle of Static Cyclic Tests (SI Units)

Specimen	Peak Loads at ±13mm		Peak Loads at ±25mm		Peak Loads at ±51mm	
	Positive (kN)	Negative (kN)	Positive (kN)	Negative (kN)	Positive (kN)	Negative (kN)
Waferboard:						
WC–1	13.6	-13.5	24.3	-25.2	33.0	-32.2
	13.2	-12.8	24.4	-24.0	29.2	-29.2
	12.9	-13.1	23.5	-23.3	26.9	-27.3
	12.9	-13.3	23.0	-22.6	25.4	-25.8
WC–2	11.1	-12.3	25.9	-26.2	31.8	-32.6
	12.3	-12.3	23.8	-25.4	29.6	-28.7
	12.8	-12.7	24.2	-23.3	25.9	-27.7
	12.5	-11.4	24.6	-23.7	26.1	-24.5
Plywood:						
PC–1	11.2	-11.0	21.7	-22.1	(See	-30.5
	10.9	-11.3	21.2	-21.6	Note	-25.9
	11.0	-10.8	21.4	-20.5	Below)	-24.7
	11.4	-10.9	20.0	-20.0		-24.9
PC–2	11.4	-10.8	22.4	-22.1	30.9	-30.3
	11.2	-11.3	21.9	-22.0	28.8	-28.8
	10.7	-10.8	20.2	-20.4	25.9	-26.7
	10.9	-11.3	21.2	-21.2	26.9	-26.7

NOTE: The ±51mm values for specimen PC–1 have been omitted because the tension cord for the wall failed during the second cycle. This caused the loads to be very small in the positive direction.

Table 8.7: Peak Loads for Each Cycle of Static Cyclic Tests (Imperial Units).

Specimen	Peak Loads at ±0.5in		Peak Loads at ±1.0in		Peak Loads at ±2.0in	
	Positive (lbs)	Negative (lbs)	Positive (lbs)	Negative (lbs)	Positive (lbs)	Negative (lbs)
Waferboard:						
WC–1	3057	-3026	5474	-5671	7426	-7240
	2978	-2870	5476	-5400	6566	-6575
	2899	-2949	5286	-5244	6057	-6145
	2900	-2988	5168	-5086	5703	-5792
WC–2	2496	-2767	5833	-5901	7157	-7337
	2769	-2769	5361	-5705	6657	-6450
	2887	-2848	5445	-5235	5828	-6219
	2807	-2573	5520	-5318	5874	-5509
Plywood:						
PC–1	2522	-2469	4880	-4972	(See	-6851
	2443	-2548	4769	-4857	Note in	-5828
	2483	-2430	4808	-4617	Table	-5561
	2561	-2456	4490	-4503	8.6)	-5602
PC–2	2564	-2426	5039	-4973	6941	-6819
	2526	-2545	4929	-4935	6481	-6467
	2407	-2527	4532	-4584	5812	-6001
	2449	-2546	4771	-4778	6050	-5998

racking displacement.

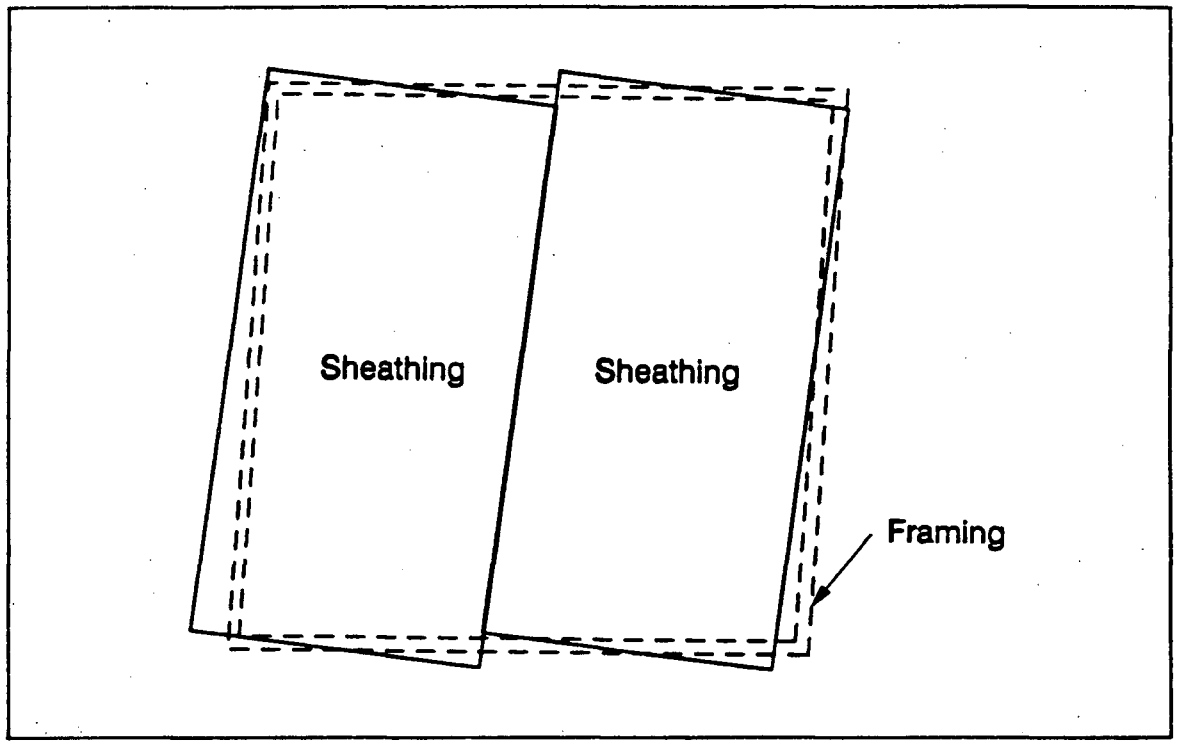

Figure 8.3: Deformation Patterns for Racking Displacement of Typical Shear Wall.

Finally, it should be noted that the shape of the load–deflection curves for cyclic shear wall tests, shown in Figure 8.2, resemble the cyclic connection test load–deflection curves, shown in Figure 6.14. This indicates that the nail connection characteristics govern the wall's load–deformation characteristics.

8.4 Free–Vibration Tests

A free–vibration test was conducted on nineteen wall specimens to find the change in natural frequency of the wall and test frame system during other tests. The test was performed before and after each wall was tested using either the sinewave, frequency sweep or earthquake tests. Table 8.8 shows the results of the free–vibration tests. All of

Table 8.8: Initial and Final Fundamental Frequencies for Shear Walls

Specimen	Nail Density[1] (mm / mm)	Fundamental Frequency Initial (Hz)	Fundamental Frequency Final (Hz)	Percent Change (%)	Comments
Plywood Sinewave Tests:					
PSI-1	100 / 150	3.5	N/A		
PSI-2	100 / 150	3.5	1.4	59	
Waferboard Sinewave Tests:					
WSI-1	100 / 150	3.7	1.8	51	
WSI-2	100 / 150	3.6	3.3	8	
Plywood Earthquake Tests:					
PEQ-8	50 / 150	3.1	N/A		
PEQ-9	50 / 150	2.9	2.1	28	
PEQ-10	150 / 150	3.0	2.6	13	
PEQ-12	150 / 150	3.1	2.8	10	
PEQ-13	300 / 300	1.9	N/A		
PEQ-14	100 / 150	3.5	2.9	17	(2)
PEQ-15	100 / 150	3.5	2.7	23	(2)
PEQ-16	100 / 150	3.4	3.0	12	(3)
PEQ-17	100 / 150	3.2	2.5	22	(3)
Waferboard Earthquake Tests:					
WEQ-7	100 / 150	4.3	3.0	30	
WEQ-8	100 / 150	4.1	1.9	54	
WEQ-9	50 / 150	3.5	2.7	22	
WEQ-10	50 / 150	3.2	1.3	59	
WEQ-12	150 / 150	3.1	N/A	N/A	
WEQ-13	300 / 300	3.2	N/A	N/A	

1) The nail spacing is given as (Perimeter / Field Spacing).
2) All the sheathing was attached to the walls with the long direction of the panels oriented in the vertical direction (parallel to the studs) except these. These two specimens had the sheathing applied horizontally with blocking at the panel edges.
3) All the tests used the 1952 Kern County, California earthquake except these two. The 1971 San Fernando earthquake was used for these two specimens.

NOTE: PSI = plywood specimen and sinewave test
WSI = waferboard specimen and sinewave test.
PEQ = plywood specimen and earthquake test.
WEQ = waferboard specimen and earthquake test.
N/A = indicates that the test results were not available.

the walls had sheathing applied with the long dimension of the panel oriented vertically (parallel to the studs), except for two plywood specimens. The two exceptions, specimens PEQ-14 and PEQ-15, had the sheathing applied horizontally and were fully blocked. The 1952 Kern County, California earthquake record was used in all but two of the earthquake tests. The two exceptions were tested using the 1971 San Fernando, California earthquake record to briefly investigate if different earthquake records would significantly affect the response of the shear walls.

As can be seen in Table 8.8, the fundamental frequency of the wall specimens changes substantially during the various tests. While these tests are very limited in the number of specimens, and construction of walls that were used varied significantly, the premise that timber shear walls are ductile structural elements is confirmed. The minimum change in the fundamental frequency was 10% and the maximum change is about 60%. The walls with N/A for the final fundamental frequency are walls that totally collapsed during testing and, therefore, would not have a final fundamental frequency.

Historically, timber buildings have performed very well, and these results are an indication of why they have been able to perform as well as they have. Timber shear walls behave in a ductile manner and should, therefore, perform well when subjected to earthquakes and other dynamic loading. The shift of the fundamental frequency is an indication of the ductile behavior. As the wall yields during an earthquake, it's stiffness is reduced. The reduction in stiffness translates to a lower fundamental frequency. Lower fundamental frequencies will help reduce the loading experienced by the upper stories of a timber structure because fewer frequencies contained in the base acceleration record will be transmitted to the upper floors by the wall. Table 8.8 also shows that the shift in the fundamental frequency is not influenced by the nail density.

8.5 Sinewave Frequency Sweep Tests

The sine wave frequency sweep test was conducted on four shear wall specimens. The results were used exclusively to verify the accuracy of the steady state model, therefore, the results are included in Section 9.3, rather than here. The reader is referred to Section 9.3, the Numerical Verification of the Closed Form, Steady State Model, for the results and discussion of the test results.

8.6 Earthquake Tests

A total of 25 walls were tested using the earthquake simulation test procedure, described in Section 7.6.5. Eleven of the specimens were sheathed with waferboard and 14 of the walls were sheathed with plywood. The first topic to be investigated during this test was to see if the hold–down connections, located at the base of each of the end studs, prevented the overturning moment from lifting the bottom corners of the wall away from the base. Tables 8.9 and 8.10 show the peak values of the uplift recorded during the tests. The maximum value of uplift for any type of wall, on either end stud, and during any magnitude earthquake was 1.6 mm (0.06 in). This deflection has negligible effect on the relative deflection of the top of the shear wall compared to the base, and it can therefore be concluded that the connections used to anchor end studs to the base performed adequately.

Another deflection that indicates whether the wall specimens deformed in a racking fashion or not, is the separation of the framing joints at the top corners of the wall. As shown in Tables 8.9 and 8.10, the largest top corner joint separation measured during any of the tests was 0.5 mm (0.02 in) which indicates that the steel angles performed well. Together, the end stud uplift and top corner joint separation measurements, give

Table 8.9: Peak Values of Measured Displacements.

Table for Kern County Earthquake with Peak Base Acceleration = 0.18g

Sheathing Type and Orientation	Dead Load Applied	Nail Density Perimeter/Field		East End Stud Uplift		West End Stud Uplift		East Top Corner Seperation		West Top Corner Seperation		Sheathing Out-of-Plane Deflection	
		mm/mm	(in/in)	mm	(in)	mm	(in)	mm	(in)	mm	(in)	mm	(in)
Waferboard													
Vertical	No	50/150	(2/6)	1	(0.0)	1	(0.0)	0	(0.0)	0	(0.0)	1	(0.0)
Vertical	No	100/150	(4/6)	1	(0.1)	1	(0.0)	1	(0.0)	0	(0.0)	1	(0.1)
Vertical	Yes	100/150	(4/6)	1	(0.1)	1	(0.0)	0	(0.0)	0	(0.0)	1	(0.1)
Vertical	No	150/150	(6/6)	0	(0.0)	0	(0.0)	0	(0.0)	0	(0.0)	2	(0.1)
Vertical	No	300/300	(12/12)	0	(0.0)	0	(0.0)	0	(0.0)	0	(0.0)	2	(0.1)
Plywood													
Vertical	No	50/150	(2/6)	1	(0.0)	1	(0.0)	0	(0.0)	0	(0.0)	4	(0.1)
Vertical	No	100/150	(4/6)	0	(0.0)	0	(0.0)	0	(0.0)	0	(0.0)	4	(0.2)
Vertical	Yes	100/150	(4/6)	1	(0.0)	1	(0.0)	0.0	(0.00)	0.0	(0.00)	4	(0.2)
Horizontal	No	100/150	(4/6)	0	(0.0)	0	(0.0)	0	(0.0)	0	(0.0)	Not Measured	
Vertical	No	150/150	(6/6)	0	(0.0)	0	(0.0)	0	(0.0)	0	(0.1)	3	(0.1)
Vertical	No	300/300	(12/12)	0	(0.0)	0.6	(0.0)	0	(0.0)	1	(0.0)	2	(0.1)

Table 8.10: Peak Values of Measured Displacements.

Table for Kern County Earthquake with Peak Base Acceleration = 0.30g

Sheathing Type and Orientation	Dead Load Applied	Nail Density Perimeter/Field		East End Stud Uplift		West End Stud Uplift		East Top Corner Seperation		West Top Corner Seperation		Sheathing Out-of-Plane Deflection	
		mm/mm	(in/in)	mm	(in)	mm	(in)	mm	(in)	mm	(in)	mm	(in)
Waferboard Vertical	No	50/150	(2/6)	1	(0.0)	2	(0.1)	1	(0.0)	0	(0.0)	1	(0.0)
Vertical	No	100/150	(4/6)	2	(0.1)	1	(0.0)	1	(0.0)	0	(0.0)	1	(0.1)
Vertical	Yes	100/150	(4/6)	1	(0.0)	1	(0.0)	0	(0.0)	0	(0.0)	2	(0.1)
Vertical	No	150/150	(6/6)	Colapsed									
Vertical	No	300/300	(12/12)	Colapsed									
Plywood Vertical	No	50/150	(2/6)	1	(0.1)	2	(0.1)	0	(0.0)	0	(0.0)	3	(0.1)
Vertical	No	100/150	(4/6)	1	(0.0)	1	(0.0)	0	(0.0)	0	(0.0)	4	(0.1)
Vertical	Yes	100/150	(4/6)	1	(0.1)	1	(0.0)	0	(0.0)	0	(0.0)	3	(0.1)
Horizontal	No	100/150	(4/6)	1	(0.0)	1	(0.0)	0	(0.0)	0	(0.0)	Not Measured	
Vertical	No	150/150	(6/6)	Colapsed									
Vertical	No	300/300	(12/12)	Colapsed									

a clear indication that the displacements of the top of the wall relative to the base can be considered as racking deformations. This is the desired deformation pattern for shear walls since rigid body rotations are eliminated, and the maximum energy dissipation will occur. Shear walls in most timber buildings in North America will deform in a manner somewhere in between the desired racking deformations and rigid body rotation. This is due to hold–down anchors often not being used, and the floor, ceilings, and adjacent walls are relied on to provide anchorage for the end studs.

One of the variables that was initially thought to be an important factor in describing the dynamic behavior of timber shear walls was the out–of–plane deflections of sheathing. During some of the tests, the sheathing appeared to be moving in the out–of–plane direction. Which led to the question of out–of–plane bending causing a loss of stiffness or strength in the wall, as is the case in some other structural stability problems. These tests have shown that this is not the case for timber shear walls that are sheathed with 9 mm (3/8 in) plywood or waferboard. Tables 8.9 and 8.10 show the peak out–of–plane displacements measured for each type of wall construction. As can be seen from the two tables, the plywood sheathing deflected more than the corresponding waferboard sheathing. This is due to the stiffness perpendicular to the face grain of the plywood being so much lower than for waferboard. However, as can be seen from Tables 8.9 and 8.10, the largest peak out–of–plane displacement measured was 4.3 mm (0.17 in). This displacement is equivalent to approximately half the sheathing thickness which can be considered small, and does not significantly affect the in–plane performance of the wall. It can, therefore, be concluded that out–of–plane deflections of 9 mm (3/8 in) and thicker sheathing is not an important consideration for design purposes.

It should be noted that for the three variables, end stud uplift, top corner separation, and out–of–plane deflection of the sheathing, there does not appear to be any dependency on intensity of the earthquake. There also does not appear to be any dependency on

sheathing type, except for the out–of–plane deflection of sheathing as was discussed above. Finally, neither the orientation of sheathing nor the application of vertical dead loading to the frame had any effect on any of the displacements measured.

Since virtually all previous studies of shear walls that have been carried out by other researchers have recorded the racking load applied to the shear wall specimens, a method for calculating the load that each wall specimen was subjected to during these tests was desired. In order to accomplish this, the acceleration record at the top of the frame, where the inertial mass was located, was analyzed to determine the peak acceleration recorded. Tables 8.11 and 8.12 show the peak accelerations recorded for each type of wall construction. As can be seen, the walls with the higher nail densities produce higher peak accelerations of the inertial mass for both types of sheathing.

The higher accelerations experienced by the densely nailed walls are due to a direct correlation of wall stiffness with the nail density. The walls, with a perimeter nail spacing of 51 mm (2 in), are much stiffer than the walls with a spacing of 300 mm (12 in) and, therefore, attract higher loads. The correlation between nail density and wall stiffness is shown in Tables 8.13 to 8.16. As can be seen in Tables 8.13 and 8.14, the peak deflection of the top of the wall relative to the base, for walls with a nail spacing of 300 mm (2 in) around the perimeter is between $2\frac{1}{2}$ to 3 times higher than for walls with a nail spacing of 51 mm (2 in) around the perimeter. As the intensity of the earthquake is increased from 0.18 g to 0.30 g, the effect of the nail spacing becomes more evident. As can be seen in Tables 8.15 and 8.16, walls with a 300 mm (12 in) perimeter nail spacing deflect approximately 7 times as far as the walls with a 51 mm (2 in) perimeter nail spacing.

Peak accelerations can be converted to the load applied to the top of the wall using the method described in Section 7.7.5. The loads that correspond to the peak acceleration recorded for each wall specimen configuration are shown in Tables 8.11 and 8.12. As can be seen, in Tables 8.11 and 8.12, these loads are also dependent on nail density, with

Table 8.11: Peak Acceleration of Top of Frame and Force at Top of Wall.

Table for Kern County Earthquake with Peak Base Acceleration = 0.18g

Sheathing Type and Orientation	Nail Density Perimeter/feild mm/mm	in/in	Dead Load Applied	Peak Acceleration Max. g	Min. g	Ave. g	Coeficient of Variation	Load at Top of Wall kN	(lbs)	Failure Occur
Waferboard: Vertical	50/150	2/6	No	0.44	0.33	0.40	0.11	26.2	(5901)	No
Vertical	100/150	4/6	No	0.37	0.29	0.34	0.05	22.1	(4961)	No
Vertical	100/150	4/6	Yes	0.36	0.29	0.33	0.08	21.5	(4828)	No
Vertical	100/150	4/6	Yes/No	0.37	0.29	0.34	0.07	22.1	(4961)	No
Vertical	150/150	6/6	No	0.27	0.22	0.24	0.08	15.7	(3538)	No
Vertical	300/300	12/12	No	0.18	0.15	Only 1 Specimen		10.7	(2404)	Yes
Plywood: Vertical	50/150	2/6	No	0.43	0.35	0.39	0.07	25.4	(5716)	No
Vertical	100/150	4/6	No	0.36	0.28	0.31	0.08	21.5	(4840)	No
Vertical	100/150	4/6	Yes	0.32	0.31	Only 1 Specimen		19.0	(4276)	No
Horizontal	100/150	4/6	No	0.32	0.28	0.30	0.04	18.7	(4215)	No
Vertical	100/150	4/6	Yes/No	0.36	0.28	0.31	0.07	21.5	(4840)	No
Vertical	150/150	6/6	No	0.26	0.24	0.24	0.04	15.3	(3450)	No
Vertical	300/300	12/12	No	0.18	0.15	Only 1 Specimen		10.9	(2442)	Yes

Table 8.12: Peak Acceleration of Top of Frame and Force at Top of Wall.

Table for Kern County Earthquake with Peak Base Acceleration = 0.30g

Sheathing Type and Orientation	Nail Density Perimeter/feild mm/mm	in/in	Dead Load Applied	Peak Acceleration Max. g	Min. g	Ave. g	Coeficient of Variation	Load at Top of Wall kN	(lbs)	Failure Occur
Waferboard:										
Vertical	50/150	2/6	No	0.58	0.45	0.53	0.10	34.5	(7765)	No
Vertical	100/150	4/6	No	0.42	0.35	0.40	0.08	25.0	(5628)	No
Vertical	100/150	4/6	Yes	0.41	0.34	0.39	0.07	24.1	(5415)	No
Vertical	100/150	4/6	Yes/No	0.42	0.34	0.39	0.07	25.0	(5628)	No
Vertical	150/150	6/6	No	0.35	0.26	0.30	0.13	20.8	(4670)	No
Vertical	300/300	12/12	No	0.11	0.05		Only 1 Specimen	6.3	(1418)	Yes
Plywood:										
Vertical	50/150	2/6	No	0.49	0.29	0.38	0.23	28.7	(6457)	No
Vertical	100/150	4/6	No	0.42	0.35	0.39	0.06	24.9	(5606)	No
Vertical	100/150	4/6	Yes	0.41	0.40		Only 1 Specimen	24.1	(5425)	No
Horizontal	100/150	4/6	No	0.41	0.37	0.38	0.04	24.2	(5434)	No
Vertical	100/150	4/6	Yes/No	0.42	0.35	0.39	0.05	24.9	(5606)	No
Vertical	150/150	6/6	No	0.37	0.28		Only 1 Specimen not Failed	21.6	(4862)	Yes
Vertical	300/300	12/12	No	0.13	0.06		Only 1 Specimen	7.4	(1673)	Yes

Table 8.13: Peak Displacement of Top of Wall Relative to the Base (SI).

Table for Kern County Earthquake with Peak Base Acceleration = 0.18g

Sheathing Type and Orientation	Nail Density Perimeter/field mm/mm	Dead Load Applied	Peak Displacement Max. mm	Min. mm	Ave. mm	Coefficient of Variation	Failure Occur
Waferboard:							
Vertical	51/150	No	19	9	13	0.27	No
Vertical	100/150	No	18	14	16	0.09	No
Vertical	100/150	Yes	17	14	15	0.07	No
Vertical	100/150	Yes/No	18	14	15	0.09	No
Vertical	150/150	No	21	13	18	0.17	No
Vertical	300/300	No	49	40	Only 1 Specimen		Yes
Plywood:							
Vertical	51/150	No	19	18	18	0.02	No
Vertical	100/150	No	18	12	15	0.10	No
Vertical	100/150	Yes	17	15	Only 1 Specimen		No
Horizontal	100/150	No	18	14	16	0.08	No
Vertical	100/150	Yes/No	18	12	15	0.09	No
Vertical	150/150	No	20	14	18	0.14	No
Vertical	300/300	No	57	40	Only 1 Specimen		Yes

Table 8.14: Peak Displacement of Top of Wall Relative to the Base (Imperial).

Table for Kern County Earthquake with Peak Base Acceleration = 0.18g

Sheathing Type and Orientation	Nail Density Perimeter/field (in/in)	Dead Load Applied	Peak Displacement Max. (in)	Min. (in)	Ave. (in)	Coefficient of Variation	Failure Occur
Waferboard:							
Vertical	(2/6)	No	(0.7)	(0.3)	(0.5)	0.27	No
Vertical	(4/6)	No	(0.7)	(0.5)	(0.6)	0.09	No
Vertical	(4/6)	Yes	(0.7)	(0.5)	(0.6)	0.09	No
Vertical	(4/6)	Yes/No	(0.7)	(0.5)	(0.6)	0.07	No
Vertical	(6/6)	No	(0.8)	(0.5)	(0.7)	0.17	No
Vertical	(12/12)	No	(1.9)	(1.6)	Only 1 Specimen		Yes
Plywood:							
Vertical	(2/6)	No	(0.7)	(0.7)	(0.7)	0.02	No
Vertical	(4/6)	No	(0.7)	(0.5)	(0.6)	0.10	No
Vertical	(4/6)	Yes	(0.7)	(0.6)	Only 1 Specimen		No
Horizontal	(4/6)	No	(0.7)	(0.6)	(0.6)	0.08	No
Vertical	(4/6)	Yes/No	(0.7)	(0.5)	(0.6)	0.09	No
Vertical	(6/6)	No	(0.8)	(0.6)	(0.7)	0.14	No
Vertical	(12/12)	No	(2.2)	(1.6)	Only 1 Specimen		Yes

Table 8.15: Peak Displacement of Top of Wall Relative to the Base (SI).

Table for Kern County Earthquake with Peak Base Acceleration = 0.30g

Sheathing Type and Orientation	Nail Density Perimeter/field mm/mm	Dead Load Applied	Peak Displacement Max. mm	Min. mm	Ave. mm	Coefficient of Variation	Failure Occur
Waferboard:							
Vertical	51/150	No	27	22	24	0.09	No
Vertical	100/15Q	No	28	23	25	0.09	No
Vertical	100/150	Yes	26	20	22	0.09	No
Vertical	100/150	Yes/No	28	20	24	0.11	No
Vertical	150/150	No	212	57	97	0.67	Yes
Vertical	300/300	No	190	36	Only 1 Specimen		Yes
Plywood:							
Vertical	51/150	No	28	21	24	0.14	No
Vertical	100/150	No	38	22	28	0.21	No
Vertical	100/150	Yes	37	33	Only 1 Specimen		No
Horizontal	100/150	No	31	25	28	0.07	No
Vertical	100/150	Yes/No	38	22	29	0.18	No
Vertical	150/150	No	146	74	103	0.27	No
Vertical	300/300	No	200	36	Only 1 Specimen		Yes

Table 8.16: Peak Displacement of Top of Wall Relative to the Base (Imperial).

Table for Kern County Earthquake with Peak Base Acceleration = 0.30g

Sheathing Type and Orientation	Nail Density Perimeter/field (in/in)	Dead Load Applied	Peak Displacement Max. (in)	Min. (in)	Ave. (in)	Coefficient of Variation	Failure Occur
Waferboard:							
Vertical	(2/6)	No	(1.1)	(0.9)	(1.0)	0.09	No
Vertical	(4/6)	No	(1.1)	(0.9)	(1.0)	0.09	No
Vertical	(4/6)	Yes	(1.0)	(0.8)	(0.9)	0.09	No
Vertical	(4/6)	Yes/No	(1.1)	(0.8)	(0.9)	0.11	No
Vertical	(6/6)	No	(8.4)	(2.2)	(3.9)	0.67	Yes
Vertical	(12/12)	No	(7.6)	(1.4)	Only 1 Specimen		Yes
Plywood:							
Vertical	(2/6)	No	(1.1)	(0.8)	(1.0)	0.14	No
Vertical	(4/6)	No	(1.5)	(0.9)	(1.1)	0.21	No
Vertical	(4/6)	Yes	(1.5)	(1.3)	Only 1 Specimen		No
Horizontal	(4/6)	No	(1.2)	(1.0)	(1.1)	0.07	No
Vertical	(4/6)	Yes/No	(1.5)	(0.9)	(1.1)	0.18	No
Vertical	(6/6)	No	(5.7)	(2.9)	(4.1)	0.27	No
Vertical	(12/12)	No	(7.9)	(1.4)	Only 1 Specimen		Yes

higher nail densities producing higher loads. This can also be attributed to the concept of ductility that is used in earthquake engineering.

Ductility is the ability to yield and sustain load. This leads to reduced loads during earthquakes, i.e., the more a structure is able to yield, the lower the loads it will experience. It is, therefore, not surprising that the more ductile wall specimens experienced lower loads than the stiff ones that had high yield strengths. The idea of ductility also accounts for failure in that a structure is supposed to yield, but not fail. As can be seen in Tables 8.11 and 8.12, some wall specimens with 300 mm (12 mm) nail spacing did not survive the 0.18 g earthquake, and none of the walls with a perimeter nail spacing of 150 mm (6 in) or greater survived the 0.30 g earthquake. This validates the concept that while timber shear walls are ductile, they must be designed to have a minimum load capacity. This concept is one of the primary criteria that is used in formulating structural design codes for earthquakes.

There are a couple more observations that should be made regarding the information shown in Tables 8.11 to 8.16. The orientation of the sheathing (vertical or horizontal) does not appear to affect the performance of the shear walls, as long as the wall is fully blocked and nailed uniformly on the perimeter of each sheathing panel. (Unblocked shear walls were not investigated in this study.)

There appears to be no difference in the performance of shear walls sheathed with waferboard or plywood. While the maximum peak displacement for each of the sheathing types show some difference during a 0.30 g earthquake, the average peak displacements are essentially the same.

These results imply that any panel material could be used for sheathing as long as it can prevent the nail head from pulling through the sheathing. The sheathing material also must have a minimum rigidity so as to transmit and develop the full shear capacity of the nails or other connectors. This leads to the possibility of products utilizing plastics

or composites of various materials being used as panel products, as long as they meet the minimum performance criteria of being able to transfer the shear loads in the nails.

It should be noted that all of the wall specimens tested had deflections that would cause substantial architectural damage. However, as will be discussed in Chapter 10, all but the walls with a perimeter nail spacing of 300 mm (12 mm) performed within the standards set by the American Uniform Building Code (UBC) for a 0.18 g earthquake. All of the walls with a perimeter nail spacing fo 100 mm (4 in) or smaller performed within the UBC standard for a 0.3 g earthquake.

The peak acceleration of inertial mass (i.e. load at the top of the wall) and the displacement of the top of the wall relative to the base, were essentially the same for both walls tested using the San Fernando earthquake, as those observed for the specimens tested using the Kern County earthquake. The maximum peak relative displacement of the top of the wall was 22.0 mm (0.87 in) and the peak acceleration at the top of the frame was 0.37 g for tests using the San Fernando earthquake. The corresponding peak load applied to the wall was 22 kN (4971 lb). Even though the peak base acceleration for the San Fernando earthquake was 0.35 g, and the peak base acceleration for the Kern County earthquake was 0.18 g, the relative deflection of the top of the wall and peak acceleration at the top of the frame were only slightly higher for the San Fernando tests. This illustrates that peak ground acceleration is not the only factor that influences the effects of earthquakes. The duration and frequency contents also affect how buildings will respond. The San Fernando earthquake had a duration of 35 seconds with the strong motion essentially finishing after 15 seconds, while the Kern County earthquake had a duration of 54 seconds with the strong motion finishing after approximately 35 seconds. Also, the frequency content of the San Fernando earthquake is concentrated between 4.0 and 7.0Hz, while the Kern County earthquake has strong motion in a frequency range from about 1.5 Hz to 5.0 Hz. These two factors make an earthquake, similar to the one

in Kern County, capable of causing more damage for a given intensity. The frequency content of the Kern County earthquake includes the range of natural frequencies of the timber shear wall system so that the resonance frequencies will be excited, and the duration of strong motion is longer, which means the structure must resist the motion longer.

The final topic to be discussed is the change in natural frequency of the wall system. It was shown by the free vibration test that the natural frequency, or fundamental period, of the shear wall changed during any given test. Shear walls were observed to have lower stiffnesses at the end of the tests than they had at the beginning. The change was due to the shear walls sustaining damage during the test. The shift in the wall's stiffness affects the frequency content of the accelerations transmitted to the upper stories of a building. In order to illustrate this, 5–second sections of the acceleration records for the base and top of the wall, as shown in Figure 8.4, were used. The Fourier spectrum of each section of the records was calculated as shown in Figure 8.5. The two spectra are plotted on the same axis in order to show that the accelerations are amplified for the frequencies close to the natural frequency of the wall specimen (2-4 Hz), while all the frequencies above and below this range are not transmitted from the base of the wall to the upper stories well. A series of these plots, using 5–second successive sections of time, illustrates the effect of the change in the natural frequency of the wall.

A different method to show the effect of the wall's natural period, would be to plot the ratio of the amplitudes at each frequency in the spectrum. This type of plot, shown in Figure 8.6, shows how much the accelerations at each frequency are amplified or de-amplified. Any frequency with an amplification factor greater than one is amplified, while an amplification factor less than one indicates that the particular frequency is not transmitted by the wall to the upper stories well. The bounds of amplified frequencies for each 5–second segment of time are plotted in Figure 8.7. Figure 8.7 shows the effect

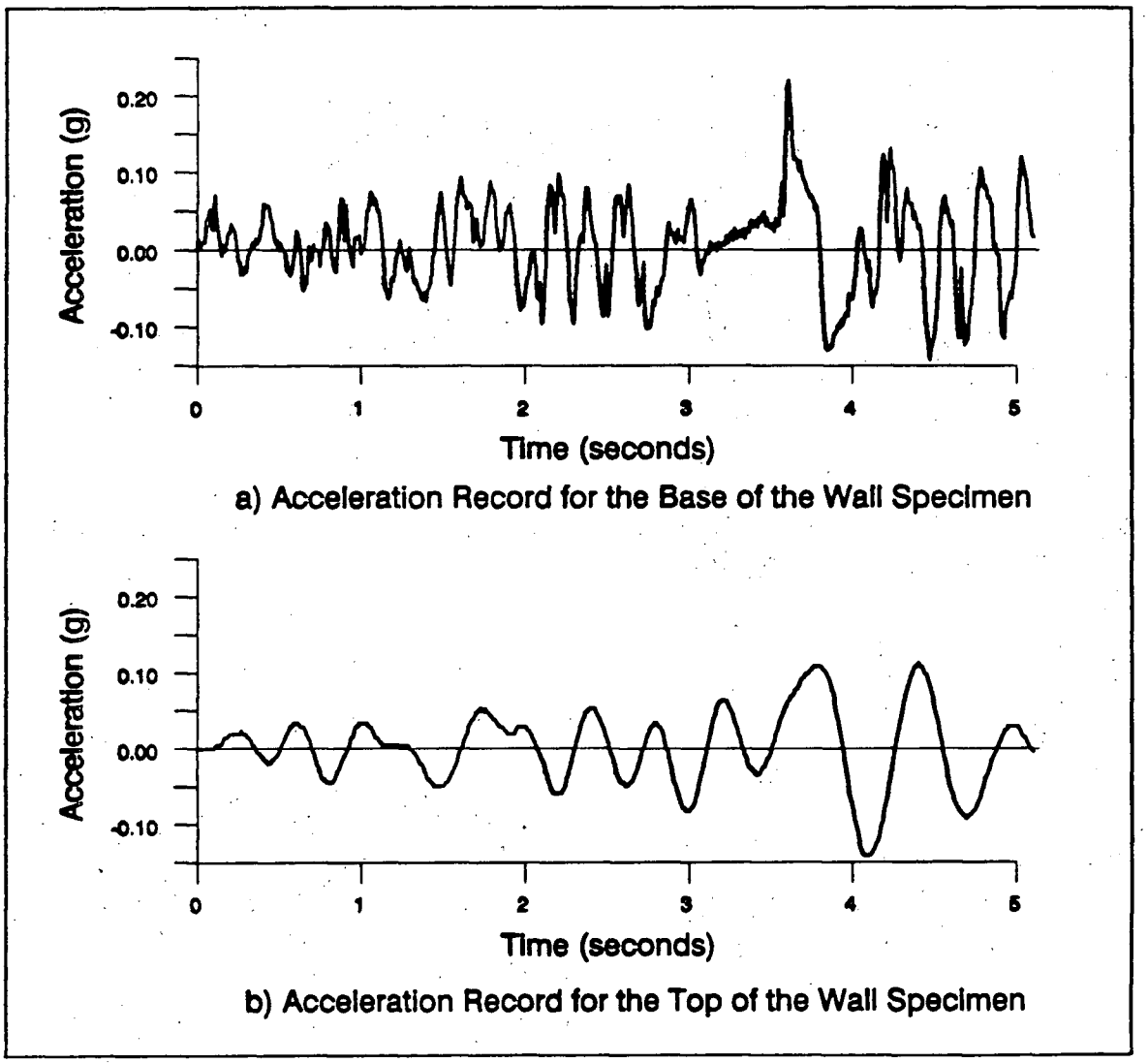

Figure 8.4: Typical Acceleration Records for the Base and Top of Wall.

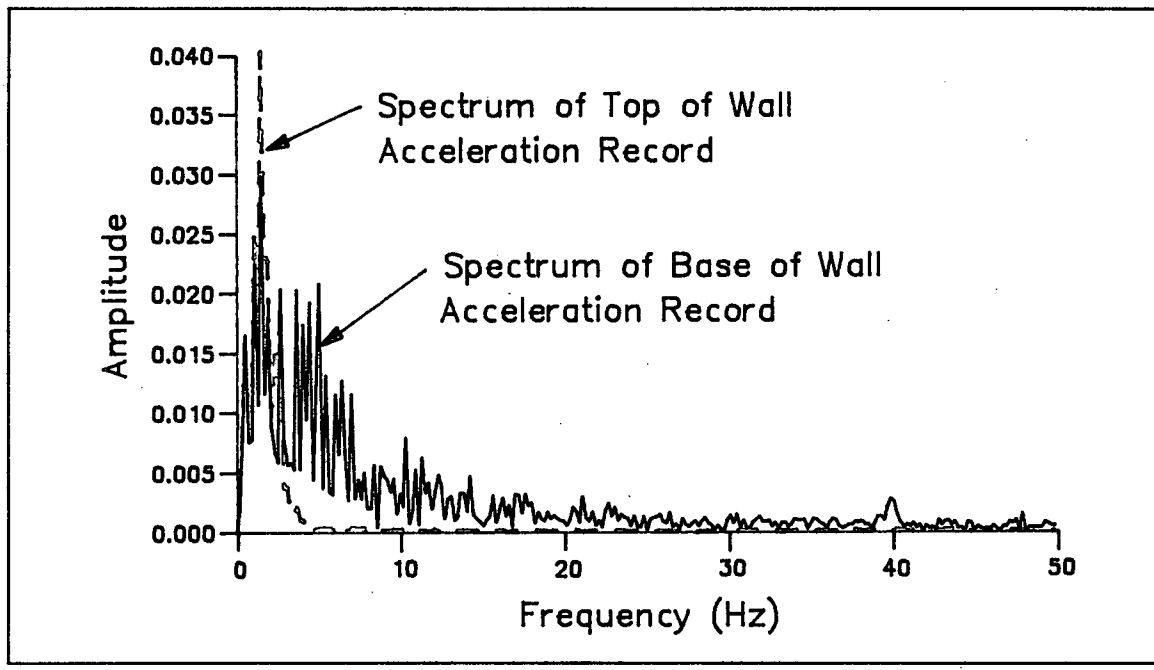

Figure 8.5: Fourier Spectra for Acceleration Records Shown in Figure 8.4.

of change in natural frequency of the wall on the frequency content of accelerations transmitted to the upper stories. Notice that the band of frequencies transmitted and amplified by the wall system becomes narrower as the upper bound changes. This is due to the natural period of the wall becoming longer as the wall is damaged. All of the wall specimens exhibited this behavior with the stiffer walls (ones with higher nail densities) showing less change, and the softer walls (walls with lower nail densities) showing more of the effect.

While the effect of the narrowing band width for transmitted and amplified frequencies is described here in qualitative terms only, the behavior is important. As the first floor shear walls are damaged, the fundamental frequency of the structure lengthens and the building is subjected to fewer and fewer high frequency accelerations. This indicates that if the upper stories of the building can be designed such that they are not severely damaged during the first part of the earthquake, they should experience lower loads as

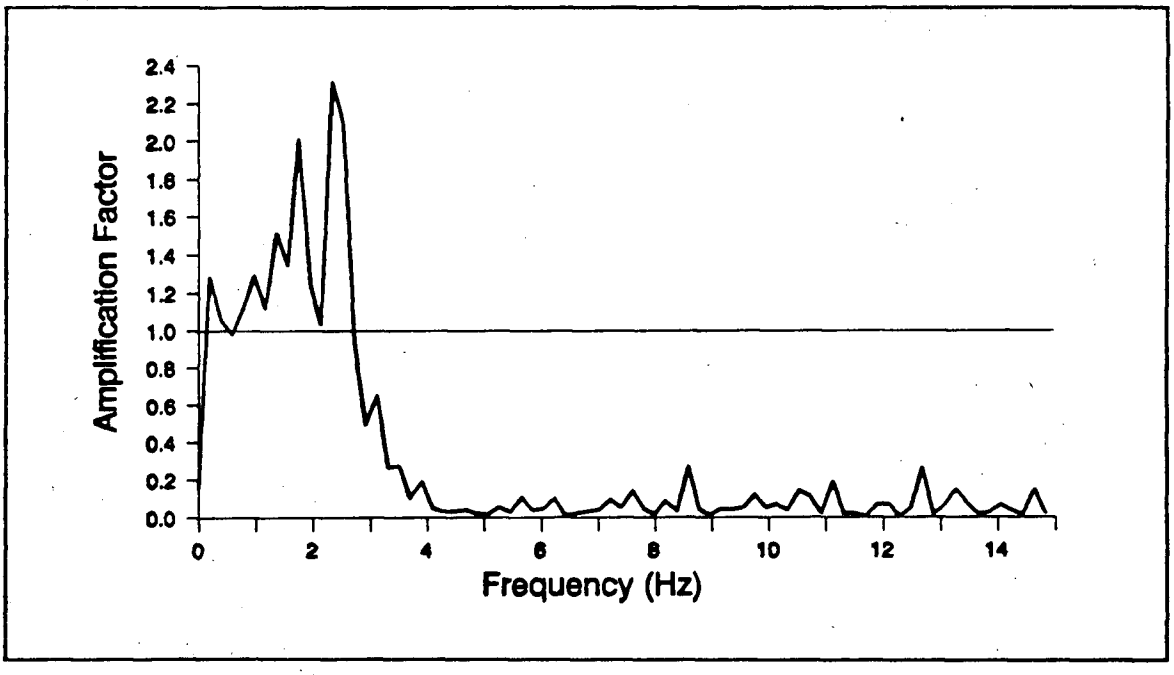

Figure 8.6: Plot of Amplification Factors versus Frequency.

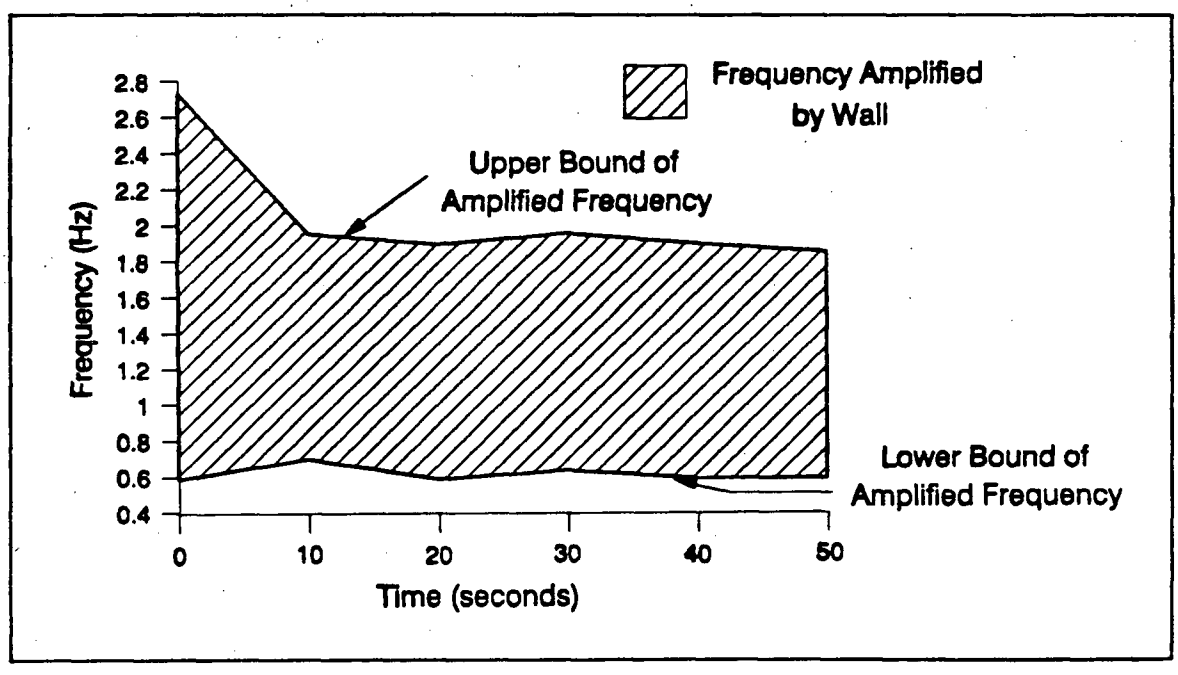

Figure 8.7: Plot of Amplified Frequencies versus Time.

the earthquake progresses. Caution should be exercised in extrapolating this conclusion too far. While the concept does occur to some extent, one should also realize that the excitation is random in nature. This means that the structure is being excited in many frequencies simultaneously. Resonance, meanwhile, is a phenomena that usually occurs at one frequency. Therefore, catastrophic events that lead to failure are not likely to occur. The deflections would be larger if the natural period was excited, than if the natural period of the structure was either higher or lower than the frequency range containing the majority of the acceleration activity.

8.7 General Discussion of Results

This section is intended to tie the information gained from each of the shear wall tests together in an effort to understand the overall behavior of timber shear walls. Each test is also discussed in order to point out the pros and cons. Hopefully, with this information, future studies will better utilize the different tests.

Two variables, previously thought to be important, have been shown to not affect the behavior of shear walls significantly. The experimental investigation showed that there is little or no difference between shear walls sheathed with plywood or waferboard. Both the static and dynamic deflections were essentially equivalent for loads in the range expected during earthquakes. The small differences between the two types of walls became evident only when loads close to the ultimate capacity of the walls were applied. While plywood sheathing did show higher out–of–plane deflections than waferboard sheathing, the peak displacements were not significant and the out–of–plane deflection had no effect on the in–plane performance of the shear walls.

The earthquake test results, and the predictions made with **DYNWALL**, show that the density of the sheathing nails is the number one variable governing the behavior

of shear walls. The more densely the sheathing was nailed, the stiffer the wall became. Walls with higher nail densities also experienced higher loads during the earthquake. The correlation between stiffness and load magnitude is similar to other types of structures, where the more ductile structures are designed for lower earthquake loads.

Each test was useful in investigating the behavior of shear walls, which were subjected to a particular type of loading. However, none of the tests give enough information to predict the behavior of shear walls subjected to a variety of loads. The static one–directional test was useful for comparing the maximum capacity and initial stiffness of shear walls. Results of the static test are useful when comparing different sheathing materials or methods of attaching the sheathing to the framing. However, the static one–directional test does **not** give any information about the dynamic or cyclic behavior of shear walls.

The static cyclic test conducted as part of this study provided information about the hysteretic behavior of shear walls. The energy dissipating ability of timber shear walls is dependent on the shape and size of the hysteresis, since the area enclosed by the loops is a representation of the energy dissipated. Therefore, information on the shape of the hysteresis is helpful in determining the damping characteristics of the walls. If the pinching of the hysteresis for nailed shear walls could be changed so that the hysteresis loop was larger in size, the response of overall structure to earthquakes would be improved, due to the increased energy dissipation. The hysteresis would also be helpful for comparing various sheathing connectors for their ability to sustain large loads and deflections, while dissipating energy. The loops of the cyclic load–deflection curves are contained within the envelope of the static load–deflection curve, therefore, the combination of the static cyclic and static one–directional tests would be useful. Some of the problems associated with the static cyclic test are associated with the deflection pattern used. An accurate indication of the maximum load capacity of shear walls cannot be obtained, because the

deflections used for each set of cycles may not correspond to the ultimate load capacity. The static cyclic test is also less severe than the earthquake or sinewave tests, because the maximum load is reached only once, on the first cycle to each displacement. The subsequent cycles do not load the wall as high because of the damage done to the nails.

The free-vibration tests provided information about the natural frequency of the wall system being tested. It could also be used to give an indication of how much the wall was damaged during one of the other shear wall tests. As the wall was damaged, the natural frequency changed to a lower and lower frequency. The natural frequency can be used as an indication of the wall's stiffness because the frequency is directly proportional to the square root of the wall stiffness. This test was not useful for any other purpose, however, and would be dependent on the amount of mass used as inertial mass. Therefore, the free vibration test can only supplement the other shear wall tests.

The sine wave frequency sweep test, while not presented in this chapter, did provide an indication of the natural frequency of the wall test system. Information about the wall's response to excitations at frequencies different from the natural frequency is also obtained. If the test were repeated for different amplitude excitations, the load capacity of the wall could also be found since the load is directly proportional to the inertial mass and accelerations. The one topic not covered by this test is the effect of random excitations, such as those experienced in an earthquake.

Finally, the earthquake test used in this study was a representative test that could be used to gain information about the response of timber shear walls to earthquakes. The shear wall was loaded in a fashion representative of the loading walls of a timber structure would experience during an earthquake. The test allowed the inertial mass to be adjusted to represent any type of structure. Vertical loads could also be adjusted to represent any type of wall. Wall specimens were also loaded to high loads multiple times during the test, rather than once or twice as would be the case in the other tests, because

inertial mass is free to move. It is believed that this test was useful in studying the true response of shear walls to the random dynamic loads of earthquakes.

There are, however, some shortcomings to the earthquake test. First, the ultimate load capacity of the shear walls was not usually reached during full–scale earthquakes. The walls, if designed properly for the earthquake, will have a strength sufficient to withstand the loads experienced. Second, because of the random nature of the loading it was hard to gain any detailed information about the natural frequency of wall, hysteresis, etc.. The energy dissipation could be calculated using the various displacements and accelerations measured, but it would be difficult to get any reliable information about the strength or stiffness of shear walls.

As can be seen from this discussion, each test procedure has its good and bad points. Each test is useful for investigating particular aspects of shear walls. However, no one test can be considered to be the "best" test, and researchers will have to continue to pick which of the tests will reveal the most information pertinent to their particular study.

8.8 Summary

The results of four different types of shear wall tests for full–size specimens have been presented and discussed. It has been shown that each test gives information about the behavior of timber shear walls, but none of the tests provide enough information to completely describe the behavior of shear walls subjected to a variety of loadings.

Static one–directional test results showed that there is little or no difference in the behavior of shear walls sheathed with plywood or waferboard. The out–of–plane deflection of the sheathing was also shown not to adversely affect the in–plane performance of timber shear walls of 9.5 mm (3/8 in) thickness and higher.

The static cyclic shear wall tests showed that the hysteresis for the nailed shear walls

was contained in an envelope, represented by the static one–directional load–deflection curve. Free–vibration tests were used to monitor the change in natural period, due to damage received during loading.

The results of earthquake tests show that there is little difference between plywood and waferboard sheathed shear walls. The earthquake results also indicated that the orientation of the sheathing has no effect on the wall's performance, as long as it is fully blocked. Evidence was presented to illustrate that the peak ground acceleration was not the only factor affecting the potential damage due to earthquakes. The earthquake's frequency content and duration also were important.

The discussion of each test was followed by a general overview of the useful points and failures of each type of test. No attempt was made to compare the test results with the model predictions in this chapter. A discussion of the accuracy of the three models is presented in Chapter 9.

Chapter 9

Verification of Mathematical Models

9.1 Introduction

Verification of the numerical accuracy of all finite element or closed–form mathematical models is required before the predictions can be used with confidence. To ensure that the three models presented in this thesis accurately predict the behavior of timber shear walls, comparisons with other models and test results have been made. These comparisons are presented in this chapter.

The individual models are investigated separately, beginning with the static one–directional finite element model, **SHWALL**. The closed form model, **FREWALL**, is then presented, followed by the dynamic finite element model, **DYNWALL**. Comparisons between the derived models and other mathematical models were made when possible. Predictions for full–size shear walls are then compared to the test results presented in Chapter 8.

9.2 Static One-Directional Model

The numerical accuracy of the static one–directional finite element model was checked in two ways. First, the beam and plate elements, used in this model, were checked for their accuracy in predicting the deformations of framing and plates. The accuracy of the entire model was subsequently checked by comparing the predicted racking behavior of shear walls with the results of the full size shear wall tests, presented in Section 8.2.

9.2.1 Plate Element Accuracy

In addition to the usual checks made to verify the correctness of the plate element (such as Eigenvalue checks of the stiffness matrix, patch tests, cantilever plate problems, etc.), the element was checked for accuracy using a problem presented by Timoshenko (1968) and Brebbia and Connor (1969). The problem consists of a square plate, supported on all four edges by fixed supports, and loaded out–of–plane with a distributed load. Symmetry boundary conditions, as shown in Figure 9.1, were used to model the problem as a quarter plate. The results presented by Brebbia are for a quarter plate model using 9 elements instead of 4. The comparison between the three solutions is shown in Figure 9.2. As can be seen from Figure 9.2 the plate element used in the program, **SHWALL** predicts the behavior of the plate quite well. The difference between the prediction by Brebbia's model and the plate element used in **SHWALL** can be attributed to the difference in the number of degrees–of–freedom and displacement fields used for the two elements. The prediction from Timoshenko is a closed form mathematical solution and should be closer to the exact solution. Based on this comparison, the plate element derived in Section 3.5 was deemed to be acceptable for use in modeling the plywood and waferboard sheathing panels used for timber shear walls.

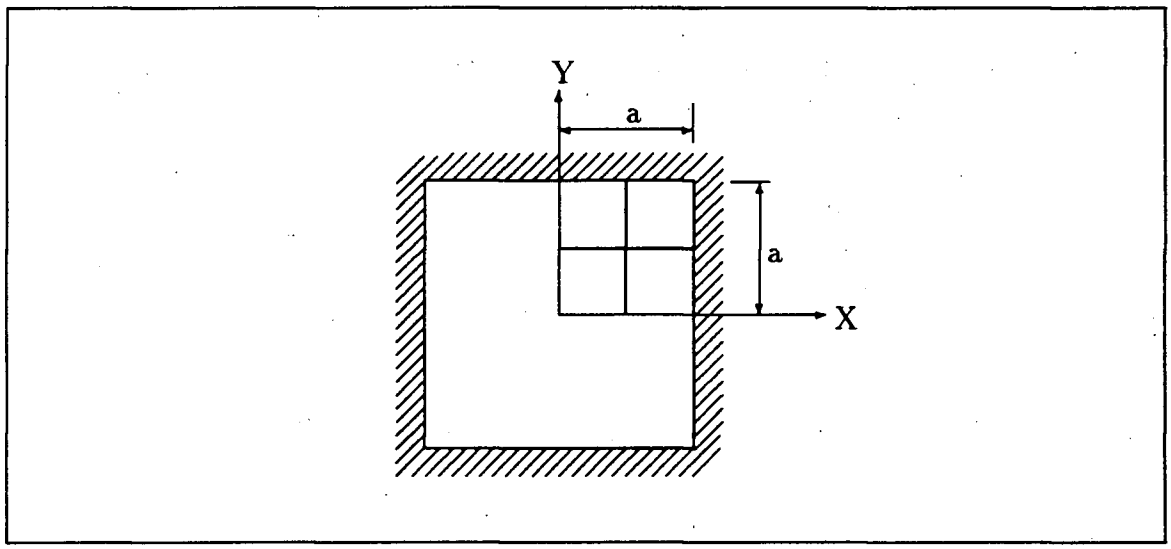

Figure 9.1: Finite Element Mesh used to Model a Fixed–Fixed Plate.

9.2.2 Comparison to Test Results.

The final check on the accuracy of the model, **SHWALL**, was made by comparing the predicted load–deflection behavior of the shear walls to the results of the full size shear wall tests presented in Section 8.2. The in–plane load–deflection curves of the framing were compared for both plywood and waferboard sheathed walls. The results presented in Figure 8.1 are again shown in Figure 9.3, along with the model's prediction of the wall behavior. As can be seen from Figure 9.3, the model predicts the average of load deflection curves for each type of sheathing quite well. The difference in the stiffness between the plywood and waferboard sheathed walls is again shown in the predictions made by the model. One will also notice that the model's predictions are more stiff than the test results. The higher stiffness can be attributed to the models failure to account for the crushing of the framing sole plate under the end stud in compression. The boundary conditions used to model the effects of the hold–down anchors, at the base of each of the end studs, interfered with the bi–linear corner connector element used to model the crushing effects. In every one of the static shear wall tests, the framing sole

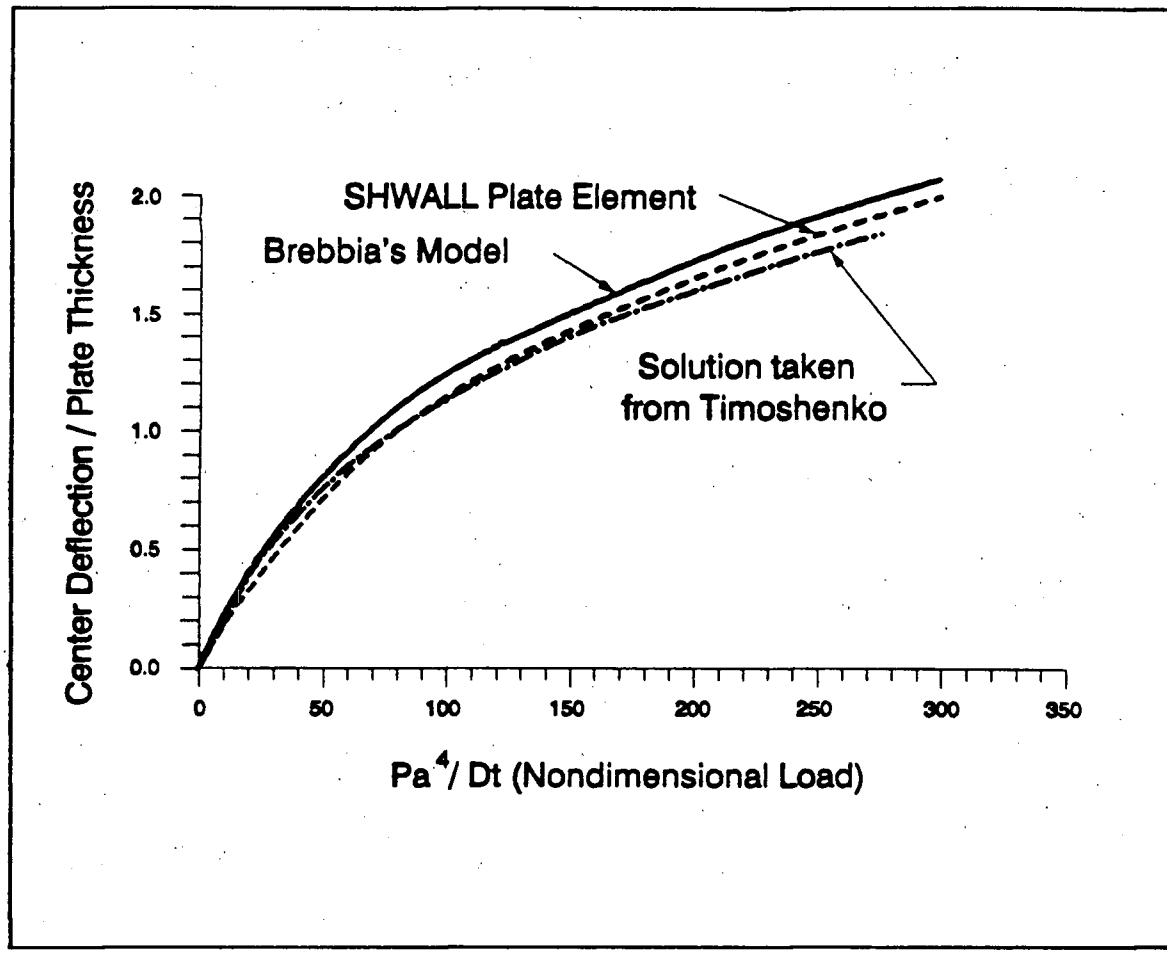

Figure 9.2: Comparison of Predicted Center Deflection of Plate with Distributed Load.

plate was crushed under the end stud that was loaded in compression. Failure to model this deflection causes the deflections at any load to be under estimated.

A second important prediction that must be checked is the ultimate load capacity of the two shear walls. Table 9.1 shows the ultimate load capacity, for plywood and waferboard sheathed shear walls, as predicted using **SHWALL**. The average ultimate load capacities for the static one–directional shear wall tests are also shown in Table 9.1. As shown, the model underpredicts the average load capacity of plywood sheathed shear walls by 6%, and overpredicts the load capacity of waferboard sheathed walls by 4%.

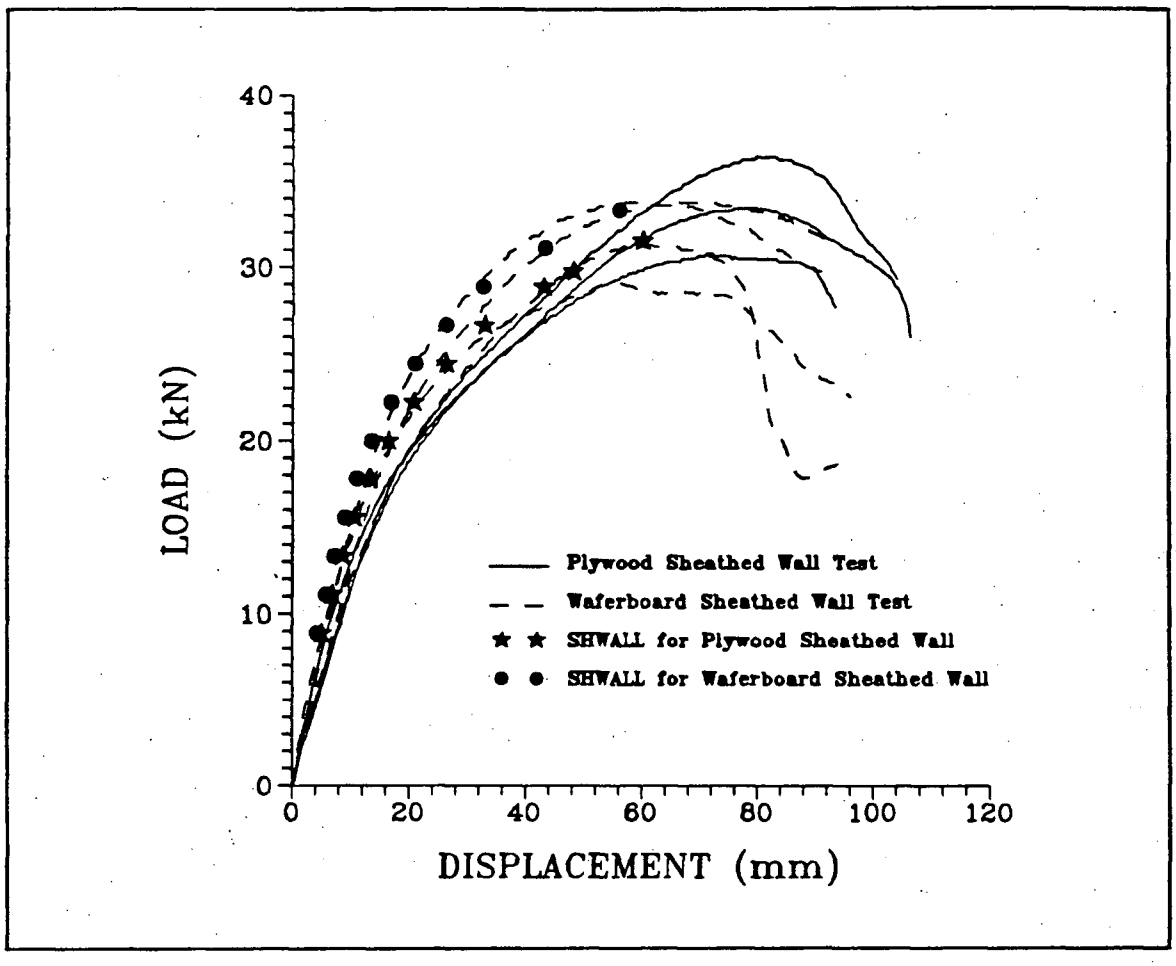

Figure 9.3: Comparison of Model's Predicted Load-Deflection Curves with Test Results.

Considering the variability in the ultimate load capacity of the test walls, the predictions made by **SHWALL** were accepted as being accurate.

The final check on the model's accuracy was made by comparing the predicted out–of–plane deflection of the sheathing with those measured during the tests. **SHWALL** was not able to predict these deflections very well. Due to the finite element used to model the sheathing, not including an initial imperfection, a "small" out–of-plane load had to be applied to the sheathing element. The out–of–plane force was used to cause an initial curvature in the sheathing element. The resulting P–delta effects make the in–plane forces

Table 9.1: Comparison of Predicted Versus Test Ultimate Load Capacity

SHEATHING TYPE	PREDICTED LOAD		AVERAGE TEST LOAD		PERCENT ERROR
	kN	(lbs)	kN	(lbs)	
PLYWOOD	31.6	(7100)	33.6	(7560)	6
WAFERBOARD	33.4	(7500)	32.0	(7200)	4

produce out–of–plane deflections. The out–of–plane deflections were, therefore, highly dependent on the magnitude of the "small" initial loading and would vary significantly, depending on the amplitude of the applied load. The out–of–plane deflections were shown to be insignificant during the testing, therefore, failure to accurately predict the out–of–plane deflection of the sheathing was not considered to be serious.

In light of the above discussion, the finite element model, **SHWALL**, is considered to be capable of accurately predicting the in–plane behavior of timber shear walls. While the out–of–plane behavior is not predicted well by the model, it is not considered to be a serious failure. The model is general in its formulation and, can therefore be used to model virtually any type of shear wall configuration. However, to increase the efficiency, the model should be simplified to eliminate the out–of–plane degrees–of–freedom. Simplifications should increase the speed of the simulation by a factor of 2, or more. Removing the out–of–plane deflections of the sheathing will eliminate one-third of the number of equations. The speed of the solution is approximately proportional to the number of equations squared, therefore, the speed of the simulation should increase by more than a factor of 2.

9.3 Closed Form Steady State Model

Four wall specimens were tested to verify the numerical accuracy of the closed form mathematical model for steady state response, derived in Chapter 4. Four walls were required so that the resonance frequency could be approached from both higher and lower frequencies. The response of timber shear walls is dependent on the maximum previous deflection, and since the maximum deflection occurs at resonance, the resonant frequency must be approached from both higher and lower frequencies. The walls were not used after the resonance condition had been reached because the damage sustained during resonance would affect the subsequent tests. Results from the tests are shown in Table 9.2. The steady state response shown in Table 9.2 is the relative deflection of the top of the wall specimen with respect to the base of the wall. Values shown in the column headed κ, are calculated values of the non–dimensional frequency response ratio, defined by Equation 4.4. Finally, the values shown in the column, with the heading, $\frac{K_0 R_0}{P_0}$, are the non–dimensional amplitude ratios.

If the non–dimensional results, shown in Table 9.2, are plotted against each other, along with the model's predicted frequency response function, it can be seen that the model predicts the steady state behavior of shear walls quite well. Figure 9.4 shows a comparison between the steady state response predicted by the model and the response recorded during the tests using plywood sheathing. The agreement between the model and the test results is good for frequency ratios near resonance. However, for the frequency ratios below 0.5 and above 1.2 the model is not as accurate. The discrepancies between the model and the test at low and high frequency ratios is probably caused by errors in measuring the low amplitude displacements. Displacements of the top–of–the–wall were measured using a potentiometer, with a measurement range of ± 1505 mm (± 6 in). Therefore, the resolution of the device is not high enough to measure small

Table 9.2: Steady State Response of Shear Walls

Specimen	Base Acceleration Frequency (Hz)	Steady State Response (mm)	Steady State Response (in)	κ	$\frac{K_0 R_0}{P_0}$
Plywood: PSI–1	1.00	6	0.3	0.34	1.54
	1.25	6	0.2	0.43	1.45
	1.60	6	0.2	0.55	1.38
	1.90	10	0.4	0.65	2.40
	2.00	24	1.0	0.69	4.99
	2.20	14	0.6	0.76	3.27
	2.50	8	0.3	0.86	1.81
PSI–2	3.50	8	0.3	1.20	1.85
	2.85	10	0.4	0.99	2.26
	2.50	13	0.5	0.86	3.01
	2.20	17	0.7	0.76	3.99
	2.00	19	0.8	0.69	4.45
	1.90	28	1.1	0.65	6.61
Waferboard: WSI–1	1.00	3	0.1	0.32	0.85
	1.25	3	0.1	0.40	0.84
	1.60	4	0.1	0.51	1.21
	1.90	4	0.2	0.61	1.31
	2.00	4	0.2	0.64	1.37
	2.20	14	0.6	0.70	4.80
	2.50	7	0.3	0.80	2.26
WSI–2	3.50	3	0.1	1.12	1.13
	3.20	6	0.2	1.02	1.93
	2.80	8	0.3	0.89	2.91
	2.50	14	0.5	0.80	4.72
	2.20	18	0.7	0.70	6.16
	2.00	19	0.7	0.64	6.45
	1.90	19	0.7	0.61	6.39

displacements accurately.

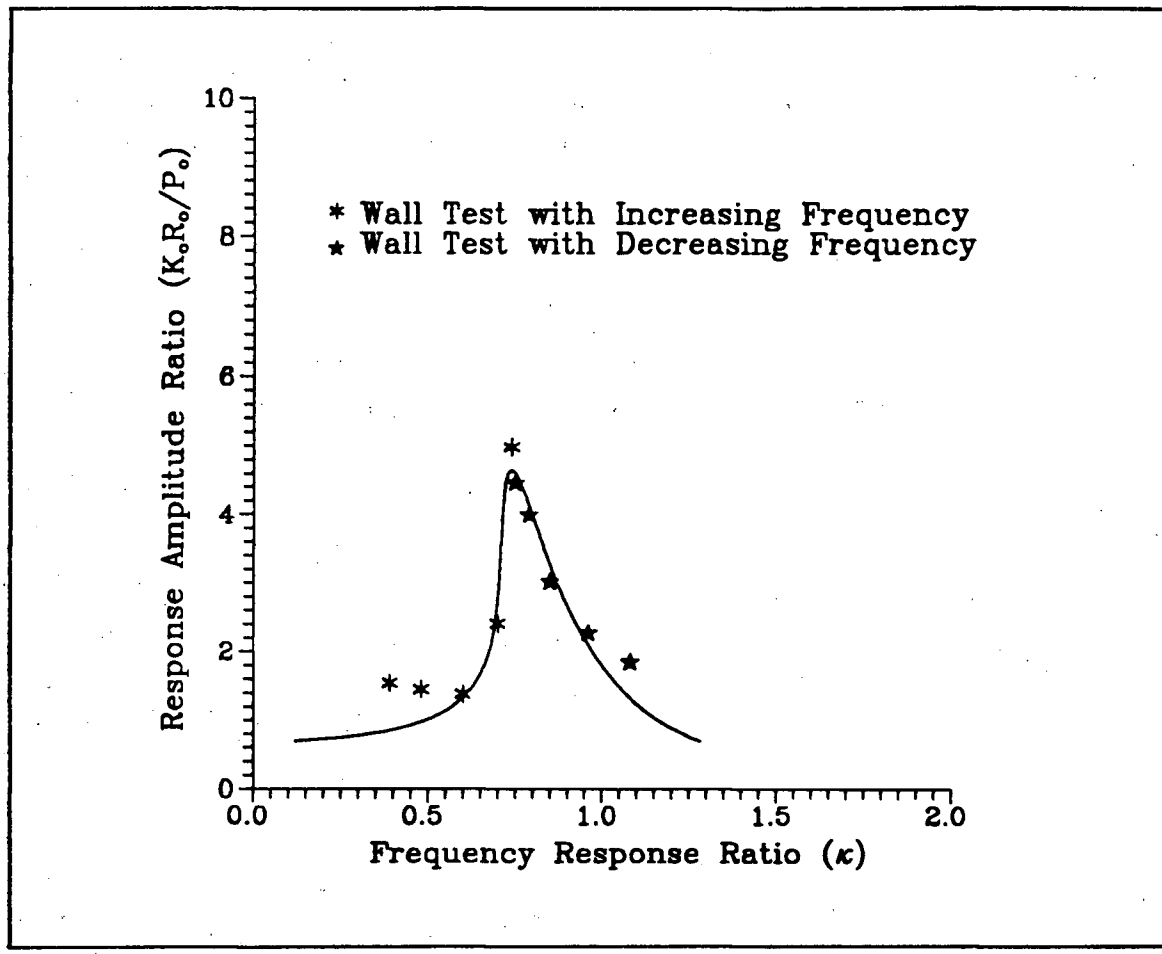

Figure 9.4: Comparison of Steady State Model's Prediction and Test Results for Plywood Sheathed Walls.

Figure 9.5 shows a comparison between the model's predicted frequency response and test results for waferboard sheathed walls. As can be seen, the agreement between the model's prediction and the test results is quite good for the entire range of test frequencies. The improved agreement between the low and high frequency ratio tests for the waferboard tests is due to a higher excitation voltage being used for the potentiometer. The higher excitation voltage increased the change in voltage output for a given deflection, thereby, increasing the effective resolution of the instrument.

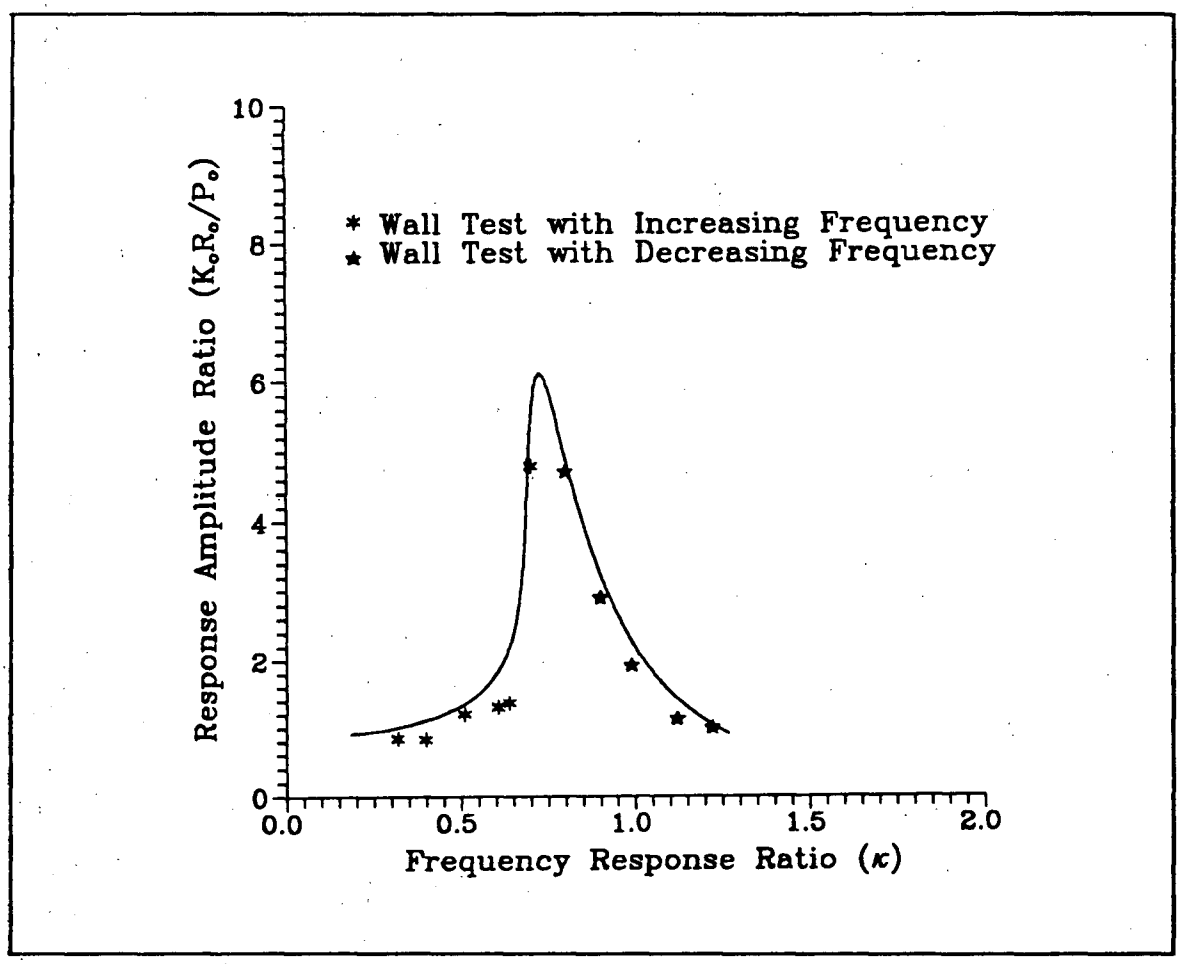

Figure 9.5: Comparison of Steady State Model's Prediction and Test Results for Waferboard Sheathed Walls.

If the two types of walls are to be compared, the response amplitude, R_0, must be used rather than the response amplitude ratio, K_0R_0/P_0. The load–deflection curves for plywood and waferboard sheathed walls have different values for the parameters, K_0 and P_0, therefore the response amplitude ratio cannot be used for comparisons. Figure 9.6 shows the predicted steady state response of plywood and waferboard sheathed walls for various amplitude base accelerations. The curves are shown for acceleration amplitude increments of 0.5 g, from 0.05 g to 0.35 g. As can be seen, for low amplitude accelerations, the response of the walls is essentially the same, with the plywood sheathed

wall having a slightly higher resonance frequency ratio. As the amplitude of the base acceleration increases, the plywood wall begins to have a higher response amplitude than the waferboard sheathed walls, and the resonant frequency response ratios approach the same value. The difference in the predicted resonance response between plywood and waferboard sheathed walls at 0.35 g is 16 mm (0.64 in) or 20%.

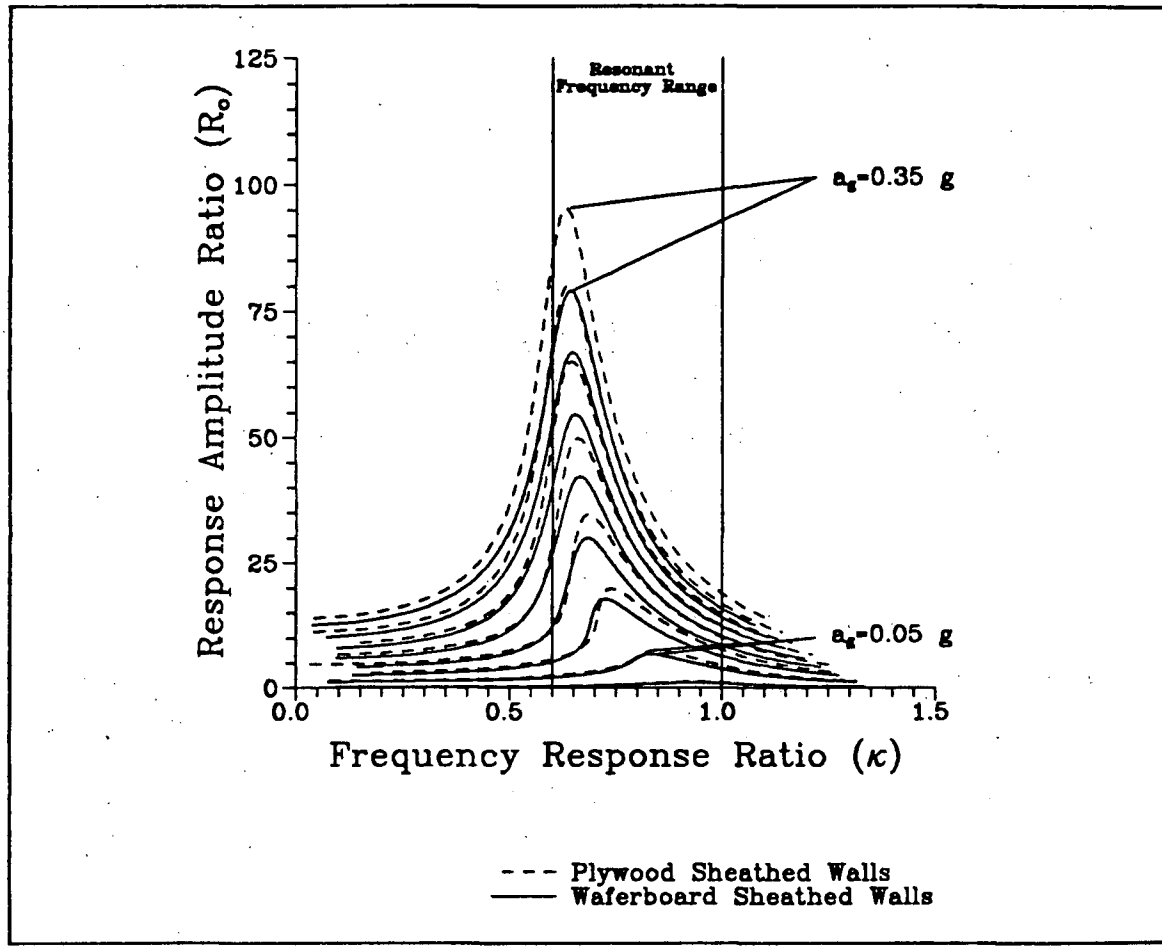

Figure 9.6: Comparison of the Predicted Steady State Responses for Plywood and Waferboard Sheathed Walls.

The difference in the response between the plywood and waferboard sheathed walls can be explained by their difference in stiffness. The loading frequency used for these

predictions is assumed to be constant, while the wall's natural frequency changes depending on the amplitude of the displacement. Once a steady state condition has been reached, for a particular loading, all the parameters describing the wall's response remain constant. Now, if Figure 9.3 is considered, it can be seen that for any given load, the plywood walls deflect further than the waferboard walls. The same behavior is shown in the predicted steady state response, because plywood walls are less stiff than waferboard walls.

Finally, **FREWALL** assumes the walls can sustain both infinite deflections and infinite loads. The predicted deflections of 75 mm (3 in) and more could not be sustained in reality and are shown for theoretical considerations only.

9.4 Dynamic Shear Wall Model

Three accuracy checks were performed to verify the numerical model, **DYNWALL**'s ability to predict the dynamic behavior of timber shear walls. The program was checked against the static model and another dynamic finite element analysis model to verify that the deflections were being predicted correctly. The hysteretic connector loops were checked to verify that the shape of the hysteresis was correct. Finally, the model's predictions were compared to the test results of full size shear walls, subjected to earthquakes, in order to ensure that the model could predict the deflections of a real structure accurately.

9.4.1 Comparison with Static Model

Since the static finite element model, **SHWALL**, is essentially contained within the dynamic model, **DYNWALL**. The dynamic finite element model was used to predict the static load–deflection curves for plywood and waferboard sheathed shear walls. The deflections for two configurations, used in the static model's verification, shown in

Figure 9.3, were again predicted using **DYNWALL**. Comparing the predictions made by the two models showed no differences in the load–deflection curves. It was therefore concluded that the changes made to the sheathing connector, for modeling the hysteretic behavior, did not alter the model's ability to predict the static behavior of timber shear walls.

9.4.2 Time–Step Integration Accuracy Check

Two comparisons were made to check the accuracy of the time–step integration scheme used in **DYNWALL**. First, a predicted time history for deflection made with **DYNWALL** was compared with the one from the program **DRAIN2D**. **DRAIN2D** is a well known and tested dynamic finite element analysis program, which was written at the University of California, Berkeley. The program, **DRAIN2D**, was used as a benchmark because of its wide acceptance in the field of dynamic structural analysis. The three member frame, shown in Figure 9.7, was used to compare the predicted displacements from the two programs. A harmonic base acceleration was used to excite the structure. When the predictions from each of the models were compared, there was no difference in the predicted displacement time histories. This was expected, since both programs used the same finite element representation for the beam elements. Based on the results of this comparison, the accuracy of the beam element was judged acceptable for both **SHWALL** and **DYNWALL**.

The second check that was made on the accuracy of the time–step integration scheme was to compare **DYNWALL**'s prediction of the fundamental period for a cantilevered plate with the Eigenvalue solution for the same problem. The model's prediction of the fundamental period was calculated using the predicted time history of deflections for a three element cantilevered plate after being subjected to a short duration step function

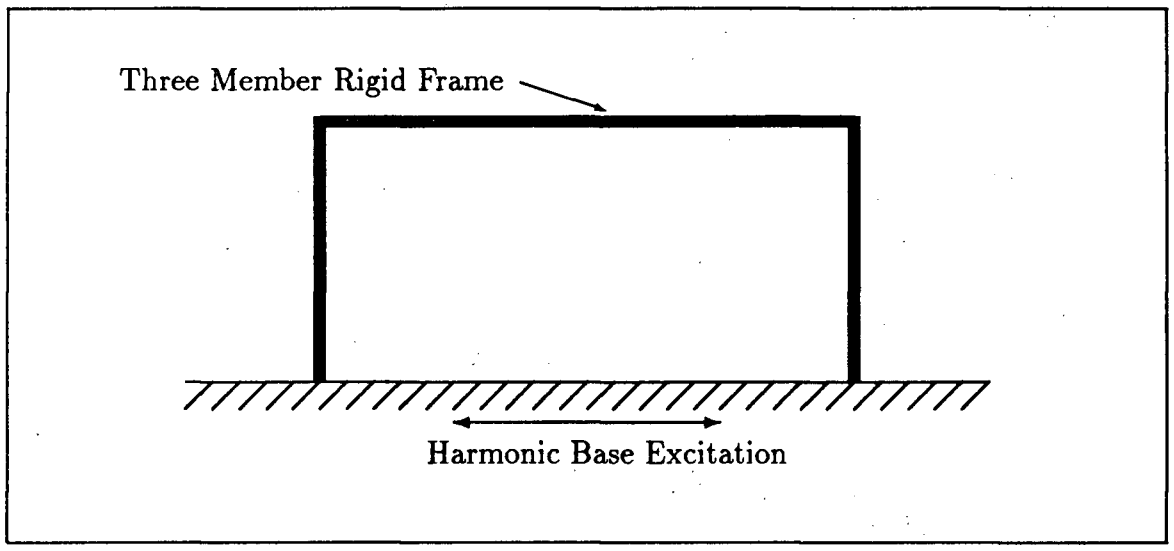

Figure 9.7: Three Member Frame Used to Check Time–Step Integration.

as a base acceleration. The average period of ten successive deflection cycles was used as the predicted fundamental period, which was compared to the lowest Eigenvalue for the problem. The model's prediction of the fundamental period was 1.69×10^{-2} seconds and the Eigenvalue solution resulted in an fundamental period of 1.66×10^{-2} seconds. the difference between the two predictions is 1.8% which was judged to be an acceptable error for numerical modeling.

9.4.3 Hysteretic Sheathing Connector

The hysteretic behavior of the sheathing connector was checked by monitoring the load and deflection of one connector during the analysis of a shear wall subjected to a harmonic base excitation. The load deflection curves for the connector were then plotted to see if the shapes of the hysteresis loops were similar to the ones used to derive the connector element, shown in Figure 6.1. The hysteresis of the connection monitored is shown in Figure 9.8. As can be seen in Figure 9.8, the dynamic model's representation of the hysteresis loops results in the desired pinched shape typical of nailed connections.

Therefore, it was assumed that the model of the hysteretic connector was correct.

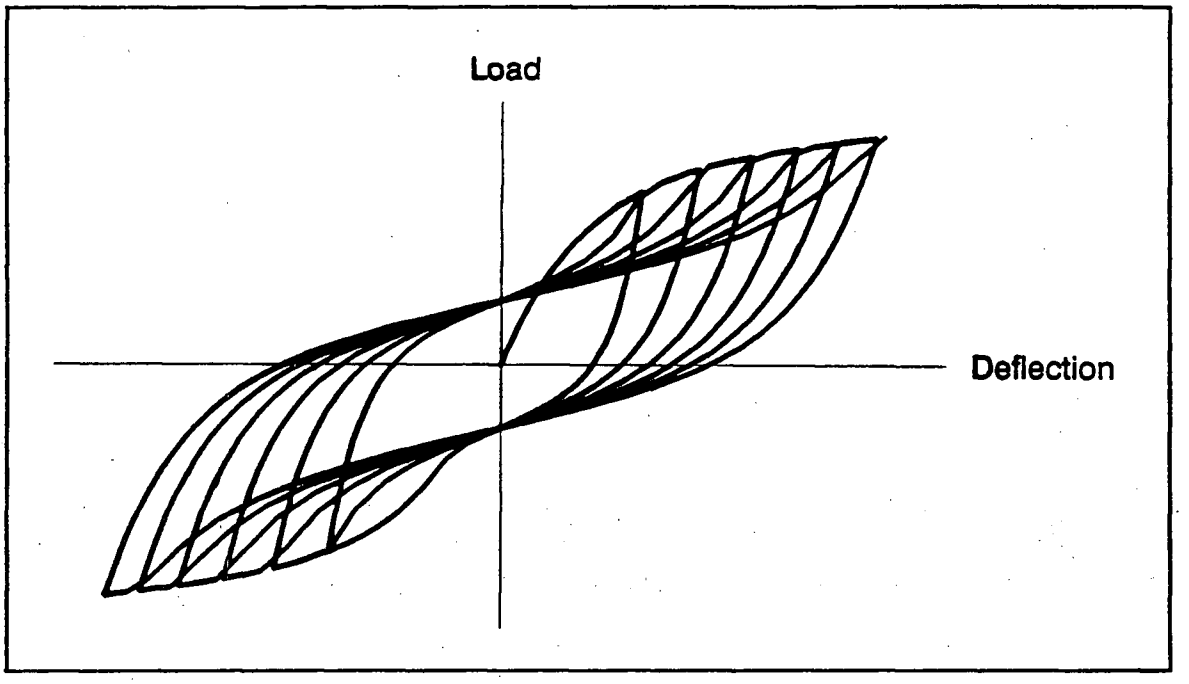

Figure 9.8: Hysteresis Loops for Connector in Shear Wall.

9.4.4 Comparison with Test Results

The final check on the accuracy of the dynamic model's predictions was made by checking the predictions with the results of the earthquake tests presented in Section 8.6. The program, **DYNWALL**, was used to predict the time history for the in-plane deflection of the top of the wall relative to the base for 10 wall specimens. These predictions were then compared with the test results for each of the specimens simulated. The base acceleration record used for each simulation was the base acceleration record that was recorded during the shear wall test.

Two comparisons were made between the predictions made with **DYNWALL** and the test results. The frequency content of the deflections was compared to ensure that

they were predicted correctly. The technique that was used is described by Ewins (1984), is used for checking models using modal analysis methods. The Fourier spectrum of the prediction and test displacement records was calculated, then a linear regression was performed using the frequency value of each major peak in the predicted deflection spectrum as an X–value, and the frequency value of each major peak in the spectrum of the test results as a Y–value. If the prediction of the frequency content were perfect, the linear regression would result in a slope of 1:1 and a coefficient of fit of 1.0. Figure 9.9 shows a typical comparison of the frequency contents for two displacement records. The results for the comparisons are shown in Table 9.3. As can be seen, the program predicts the frequency content of the deflections very well with an average slope of the linear regression analysis equal to 0.997 and an average coefficient of variation of 0.999.

The accuracy of the predicted displacement time–histories was checked by comparing the prediction with the earthquake test results. Figure 9.10 shows the displacement time histories for the first 10 seconds of one of the earthquake tests. The model's predictions of the time–history is shown in Figure 9.10a, and the corresponding experimental time–history is shown in Figure 9.10b. The two records are plotted on the same axes in Figure 9.10c. As can be seen, the model predicts the peaks in the displacement record quite well. In order to evaluate the model's ability to predict the deflections, a quantitative method of comparing the two time–histories was employed. The correlation coefficient for the amplitudes of each of the peaks in the time–histories was used for this purpose, with the results of this comparison being shown in Table 9.3 . While the correlation between the predicted displacements and the measured displacements is not perfect, an average correlation coefficient of 0.907 is considered to be quite good. The use of average load–deflection parameters for the nails and the neglecting of the crushing of the sole plate accounts for most of the error in the prediction. Some additional sources of error are: **1)** the residual error of the connector force, resulting from using the tangent

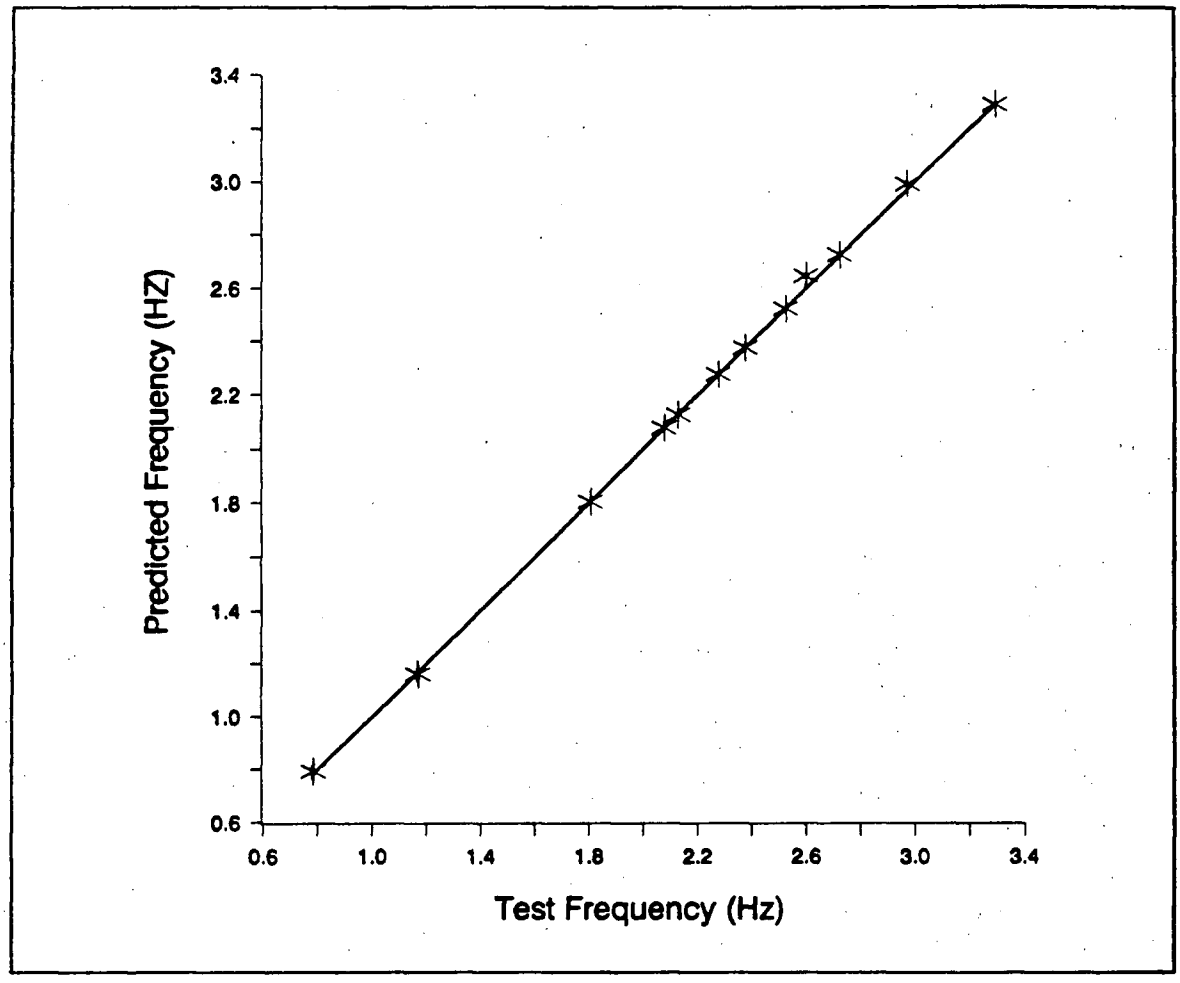

Figure 9.9: Test versus Predicted Frequencies in the Displacement Records.

stiffness as was discussed in Section 5.4.3, **2)** the unavoidable round–off error that occurs in all numerical calculations, and **3)** the errors due to the approximate nature of the finite element method.

In light of the above discussion, it was concluded that the dynamic finite element model, **DYNWALL**, predicted the in–plane dynamic behavior of timber shear walls quite well. The problems encountered in modeling the out–of–plane sheathing deflections using the model, **SHWALL**, were also encountered using **DYNWALL** because the same plate element is used to model the sheathing in both programs. Since the out–of–plane

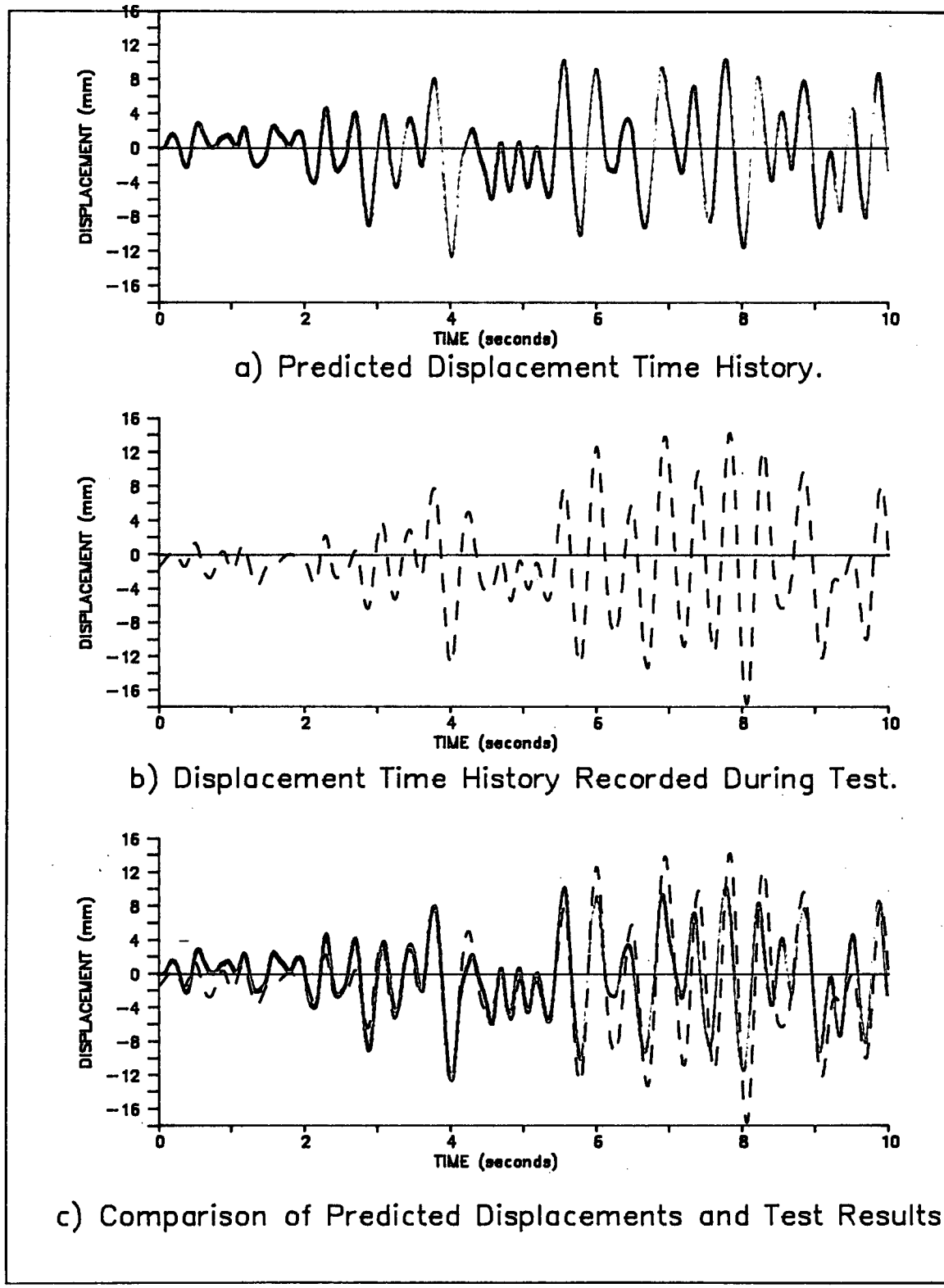

Figure 9.10: Time–Histories for Test and Model.

Table 9.3: Results of Accuracy Verification for **DYNWALL**

Specimen	Nail Spacing (Perimeter/Field)		Frequency Content Linear Regression		Peak Displ. Time–Histories Correlation Coefficient	Earthquake Record Used
	mm/mm	(in/in)	Slope	C.V.		
Plywood:						
PEQ–8	51/152	2/6	0.99	0.969	0.887	0.18g[1]
PEQ–3	101/152	4/6	1.00	0.999	0.894	0.18g[1]
PEQ–3	101/152	4/6	1.00	0.999	0.927	0.30g[1]
PEQ–16	101/152	4/6	1.00	0.999	0.919	0.35g[2]
PEQ–10	152/152	6/6	1.00	1.000	0.922	0.18g[1]
Waferboard:						
WEQ–8	51/152	2/6	1.00	0.999	0.888	0.18g[1]
WEQ–4	101/152	4/6	1.00	0.997	0.869	0.18g[1]
WEQ–4	101/152	4/6	1.00	0.999	0.877	0.30g[1]
WEQ–10	152/152	6/6	1.00	1.000	0.943	0.18g[1]
WEQ–10	152/152	6/6	0.99	0.995	0.994	0.30g[1]
AVERAGE			1.00	0.999	0.907	

1) Kern County, California Earthquake Record was Used.
2) San Fernando, California Earthquake Record was Used.

deflection of the sheathing has been shown by the full size wall tests to not be important, the failure to predict these deflections was not seen as a significant failure.

9.5 Proposed Simplifications and Improvements to Models.

The programs, **SHWALL** and **DYNWALL**, have been used to show that many of the variables they model do not significantly influence the behavior of timber shear walls. Eliminating these variables will reduce the computation time and memory required to simulate the behavior of the walls. Reducing the memory required to simulate the displacement will also allow the models' capabilities to be expanded. The following simplifications and improvements are recommended:

1. Eliminate the modeling of the out–of–plane deflections of the sheathing. It has been shown that the out–of–plane deflections do not significantly affect the in–plane behavior of nailed timber shear walls. Therefore, this simplification will not affect the models' abilities to predict the racking behavior of shear walls. The number of equations required to model the shear wall will be reduced by more than 30%, which will increase the execution of the program by more than a factor of 2.

2. Simplify the shape functions used to model the sheathing. The cubic displacement field used for the element derived in this thesis was used because the bearing between adjacent elements was modeled as a line of spring connectors. If the bearing connectors were located only at the nodes, the plate element could be modeled as a quadratic, or even a linear element. While this simplification would further reduce the execution time and memory requirements, the effect of the substitution would have to be investigated to ensure that the true in–plane behavior of the plates is modeled accurately. For example, some sheathing materials may have a low in–plane shear modulus, which would require that the shear deformation be modeled accurately.

3. The extreme simplification would be to model the sheathing as rigid plate elements, and the framing as rigid beam elements, with pinned ends. This extreme simplification would neglect any deformations other than the yielding of the sheathing connectors, and would therefore be limited to predicting the overall wall response.

4. The ability to calculate the member forces can be added to the program. The force calculation was not included in these models, because the memory requirements would have exceeded the computer's available memory. The simplifications, given above, would eliminate the memory problem. The ability to predict the member forces would provide an economical method of investigating the connections used in shear walls, eventually leading to a rational design process. The possible change in failure modes, due to the use of adhesives or other new fasteners, can also be studied.

5. After the above simplifications have been made, the new model can be used to perform reliability studies for the dynamic behavior of shear walls, by adding such algorithms as the Rachwitz and Fiessler algorithm.

Each of the above simplifications and improvements will have to be checked to ensure that they will not cause unacceptable errors in the predictions made. This can be accomplished by either comparing the predictions with those made, by using either **SHWALL** or **DYNWALL**, or by making comparisons directly with test results.

9.6 Summary

The accuracy of the three numerical models derived in this thesis has been verified using a number of comparisons to other models, and the results of full size shear wall tests. Each of the models was shown to predict the in–plane behavior of timber shear

walls quite well. However, none of the model's were able to predict the out–of–plane deflection of the sheathing well. This was not seen as a significant failure, since the test results presented in Chapter 8 indicated that the out–of–plane deflection of the sheathing was not an important factor, in either the static or dynamic behavior of timber shear walls.

Simplifications and improvements to the models presented in this thesis are proposed. The proposed simplifications will reduce the memory requirements, and the execution time for the programs. The improvements will expand the capabilities of each of the programs and make them useful for investigating a wide variety of topics.

Chapter 10

Design and Construction of Timber Shear Walls

10.1 Introduction

The Canadian and American earthquake design codes for timber structures are currently being scrutinized and changed. In some cases, the earthquake design of timber structures is being given serious consideration for the first time. The number of timber buildings that are being designed by engineers is increasing. The resulting structures have changed to the point that the historical record of the good performance can no longer be justly expected to continue. This chapter is intended to give an overview of the design requirements for three of the current or recent design codes for North America, along with the proposed 1990 National Building Code of Canada.

The discussion of the various design codes, and comparisons between the requirements of these codes and the performance observed during tests, or predicted by the model, **DYNWALL**, are presented. **DYNWALL** is used to compare the performance of three wall configurations. The three walls considered are:

1. The 2.4 × 2.4 m (8 × 8 ft) wall specimen used for the shear wall experimental study.

2. A hypothetical 4.8 × 2.4 m (16 × 8 ft) wall.

3. A hypothetical 2.4 × 4.8 m (8 × 16 ft) shear wall.

Comparing these three walls provides information about the effect the dimensions have on the response of the wall.

Three construction details that are considered to be critical to the performance of timber shear walls are also discussed. These are: **1)** the hold-down connection, **2)** corner connection, and **3)** sheathing nails.

10.2 Present Design Procedures

10.2.1 Overview of Codes

This study is oriented toward the type of timber structure commonly used for apartments in North America, and the three prominent design codes used in North America are included in this section. These are:

1. The 1985 National Building Code of Canada (1985 NBCC), In addition, the proposed 1990 NBCC and accompanying Canadian Standards Association CAN/CSA-086.1-M89, Engineering Design in Wood (Limit States Design) (1990 NBCC/CSA) are investigated.

2. The 1976 Uniform Building Code (UBC), and

3. The 1988 Recommended Lateral Force Requirements and Tentative Commentary by the Seismology Committee, Structural Engineers Association of California (SEAOC).

The ASTM E-72 static racking test for shear walls, and the idea of ductility are two subjects the design codes reviewed in this section have in common. When the

design codes were originally written, the technology required to perform dynamic tests was not available and numerical models for shear walls had not been developed. Static racking tests were used to obtain as much information as possible about the wall system. The response of timber buildings during earthquakes was deduced from the racking test results, along with engineering experience. The codes that are currently followed for designing timber buildings in North America were written to include the information obtained from this process.

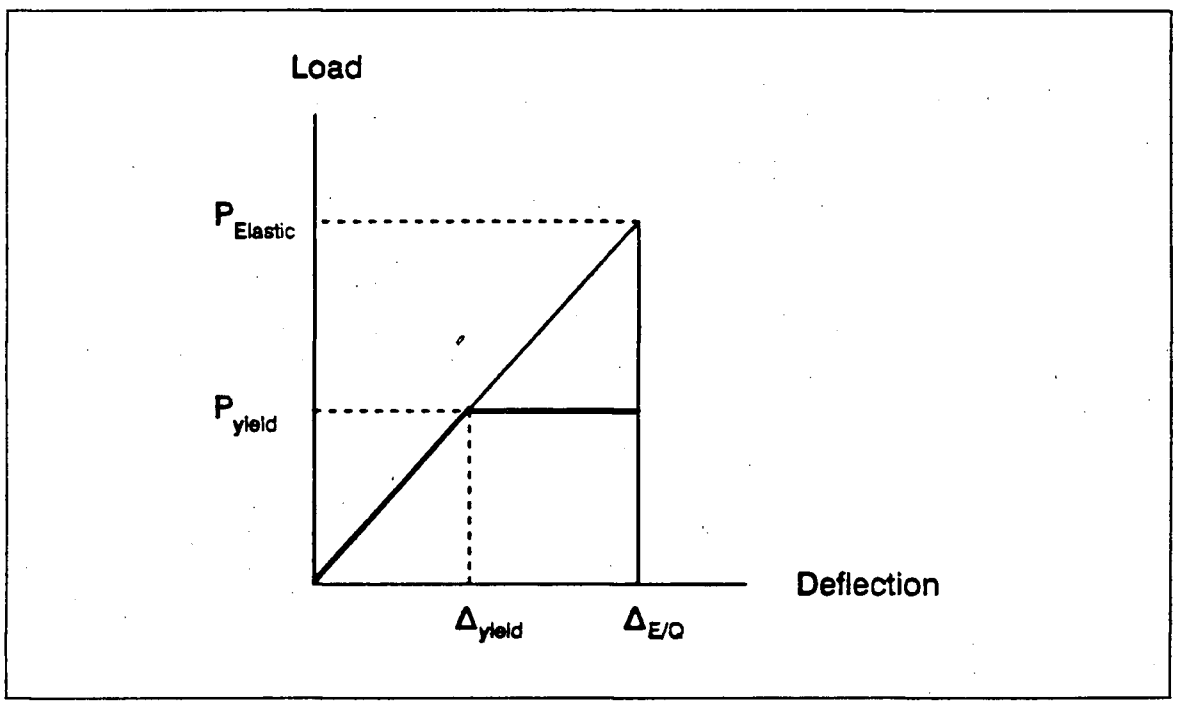

Figure 10.1: Illustration of Ductility Concept.

The important concept included in the building codes is that a structure that is designed and built, according to the requirements of the code, should be able to resist moderate earthquakes without major damage and severe earthquakes without collapsing. To achieve this, the idea of ductility is incorporated into the building codes. Ductility is defined as the deflection of a structure at ultimate load divided by the structure's

deflection at yield. The concept of ductility, as used in earthquake design is illustrated in Figure 10.1. It is assumed in earthquake design that the structure will deflect an amount, $\Delta_{E/Q}$, which depends on the initial natural period and the design spectrum, but is independent of the yield strength of the structure. A stiff structure will have a lower $\Delta_{E/Q}$ than a less stiff structure. The structure could be designed to sustain this deflection and not yield, but it would have to resist very large loads, and the resulting design would be uneconomical to construct. Structures are designed, instead, to yield at a lower load, P_{yield}, and have the reserve ability to deflect enough to sustain the required deflections. The ductility demand for the structure is $\frac{\Delta_{E/Q}}{\Delta_{yield}}$. Design codes recognize that different building materials and structural systems have differing abilities to sustain large deflections after yielding. Therefore, a ductility factor is used to determine the design load. This factor varies from high values for ductile structures, such as steel frames, to low values for nonductile structures, as is unreinforced masonry. Nailed timber shear walls are considered ductile structures, and deserve fairly high ductility factors as has been done in the 1990 NBCC/CSA codes.

All of the design codes included in this investigation indirectly incorporate the concept of ductility by calculating the seismic force, using equations of the general form,

$$V = vSKIFW \tag{10.1}$$

where,

V = the lateral seismic force at the base of the structure.

v = a velocity ratio that represents the magnitude of the peak acceleration of the earthquake.

S = a seismic response factor which accounts for the effect the natural period of the structure has on the response.

K = a coefficient that accounts for different types of structures, their associated ductility, and energy damping.

I = a coefficient that accounts for the importance of a structure. Important structures, such as hospitals are given a higher value than others because they will be required to survive most earthquakes and remain functional.

F = a coefficient that accounts for the variability of the soil conditions and how the soil transmits the earthquake accelerations.

W = the weight of the structure.

Some of the newer codes, such as 1990 NBCC/CSA, have rearranged the terms to use a different factor instead of the coefficient, K. The new factor overtly embodies the ductility associated with the structure type and becomes a denominator in calculating the seismic force. All of the codes basically calculate the design loads in the same manner, as will be seen in the following discussion.

When designing for other loads, such as wind or gravity, the objective is to reduce the probability that the actions (moment, shear, etc.), resulting from the loads will exceed the structural resistance or capacity. This is achieved by multiplying the design loads, V (generally a large load with a high return period) by a load factor, λ, to account for the variation in load as well as other uncertainties; and by multiplying the structural resistance, R, by a capacity reduction factor, ϱ, which accounts for the variation in the resistance. The design earthquake specified by the Canadian code has been chosen so that the probability of excedience is 10% in the 50 year expected life of the structure. The structural resistance specified by the code will depend on the material used to construct the structure. The load factor, λ, is greater than one while the resistance factor, ϱ, is less than one. If $\varrho R \geq \lambda V$, the desired result is achieved. This is illustrated by Figure 10.2.

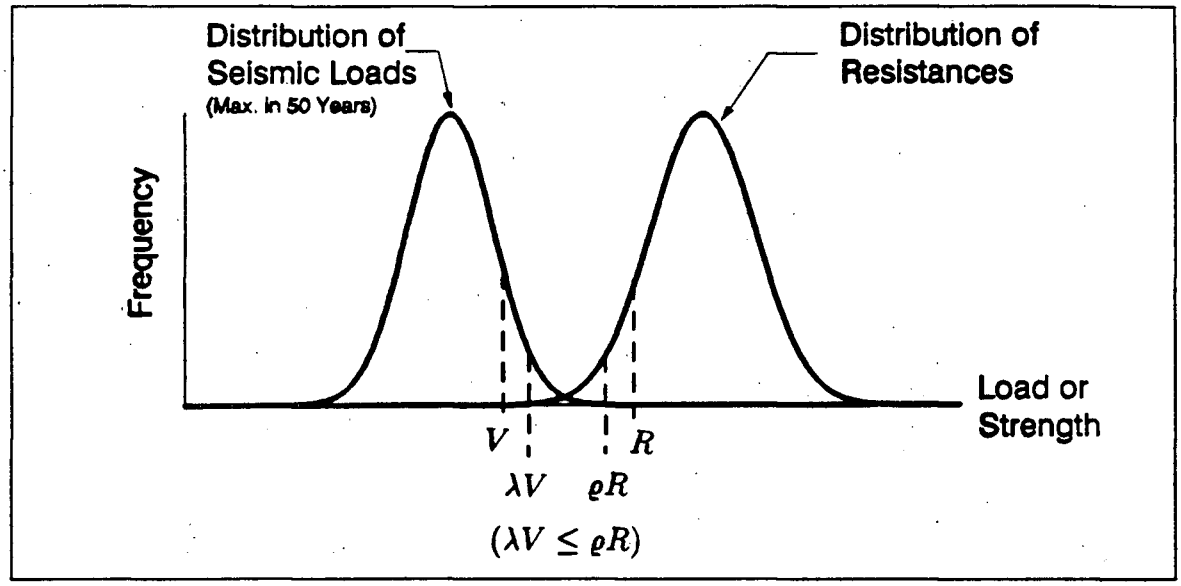

Figure 10.2: Load and Strength Distributions.

The value of ϱ used by the newer design codes was obtained by numerical conversions of the allowable stress design codes. When Foschi's (1982) investigation of shear walls and diaphragms was used as part of the evidence to allow waferboard sheathing to be considered, as an equivalent to plywood sheathing for the United States design codes, a factor of safety of 3 was incorporated into the design tables. (The ultimate load capacity for shear walls was divided by 3 to determine the allowable design capacity presented in the code.) As reported by Adams (1987), the original plywood design tables also incorporate a minimum factor of safety of 3.0. When the codes changed from working stress design format to the limit states design format, the value used for ϱ was calibrated so that structures designed using either code would be expected to have approximately equal performance. The resistance factor, ϱ, that has been derived for timber shear walls, in 1990 NBCC/CSA is 0.7. However, this value does not have any reliability analysis as a basis, and it is purely a numerical conversion of the previous deterministic design code.

Seismic design deals with an entirely different set of objectives. As was shown in the discussion of Figure 10.1, the structural resistance is *always* reached in a major earthquake. The structure will yield and the question is no longer how strong the structure is, but rather what will the ductility demand be. The design codes used in Canada and the United States specify a level of base shear which already includes a probability of excedience corresponding to probability of exceeding the specified ground motion. If the structural resistance is inadvertently made low, the ductility demand will be higher than expected. Conversely, if the resistance is too high, the ductility demand will be lower, but the higher "yield" load of the structure will always be reached.

For reasons of convenience when combining the seismic probabilities with those of other loads, as well as to conform with the past practices in design, the seismic loads have generally been reduced by the load factor before being presented in the design code. When using the previous design codes, the designer multiplied the seismic load presented by the code by the factor $\lambda = 1.5$, along with the other types of loads involved in the design. Therefore, the designer would simply convert the design load back to the average value of the design earthquake, rather than the correct value being presented in the first place.

The proposed 1990 NBCC/CSA will be one of the first codes to abandon this approach, and present the actual yield level base shears in the codes. The value for λ, for seismic design, will also be reduced to a value of 1.0 to indicate the average design base shear is being presented as the characteristic load.

To reiterate, the base shear experienced by the structure during an earthquake will be equal to the average value of the yield resistance. If the design is properly executed,

$$\lambda V = \varrho R \tag{10.2}$$

or

$$R = \frac{\lambda V}{\varrho} = P_{yield} \tag{10.3}$$

where, $\lambda = 1$ for the 1990 NBCC.

How does R relate to the average value of the yield resistance? For some structural materials and systems, the characteristic value of resistance, R, is the average strength. For concrete the characteristic strength is the average strength, while steel design uses a value based on the minimum strength of coupon tests. For most aspects of timber design, the characteristic resistance is the 5th percentile strength. Thus, the average value of yield resistance, Y, for timber engineering would be given by

$$Y = \mathcal{L}R = \frac{\mathcal{L}\lambda V}{\varrho} \tag{10.4}$$

For most materials, $\mathcal{L} = 1.0$, and for most aspects of timber design, $\mathcal{L} > 1.0$. The higher value of $\mathcal{L}$ used for timber construction accounts for the different characteristic strength presented. For shear walls $\mathcal{L} = 1.0$, since their characteristic resistance is the average resistance.

Equation 10.4 would be sufficient if timber shear walls behaved in the elastic–plastic manner assumed by the design code. However, timber shear walls begin to behave non-linearly at very low loads when compared to other structures. The actual behavior is as shown in Figure 10.3. Another factor, $\mathcal{F}$, is required to convert the nominal yield resistance, P_{yield}, to the resistance at the expected ductility demand, P_{wall}. Multiplying $\mathcal{L}R$ by $\mathcal{F}$ essentially changes P_{yield} to a value equal to the true load the wall experiences. The new value of P_{yield} will result in the design load–deflection curve shown in Figure 10.4. The factors, $\mathcal{L}$, ϱ, and $\mathcal{F}$ can be combined into the single resistance factor, ϕ, for use in design, but have been kept separate until now for illustrative purposes. The following discussion will assume the factors are combined and will be called ϕ, and Equation 10.2

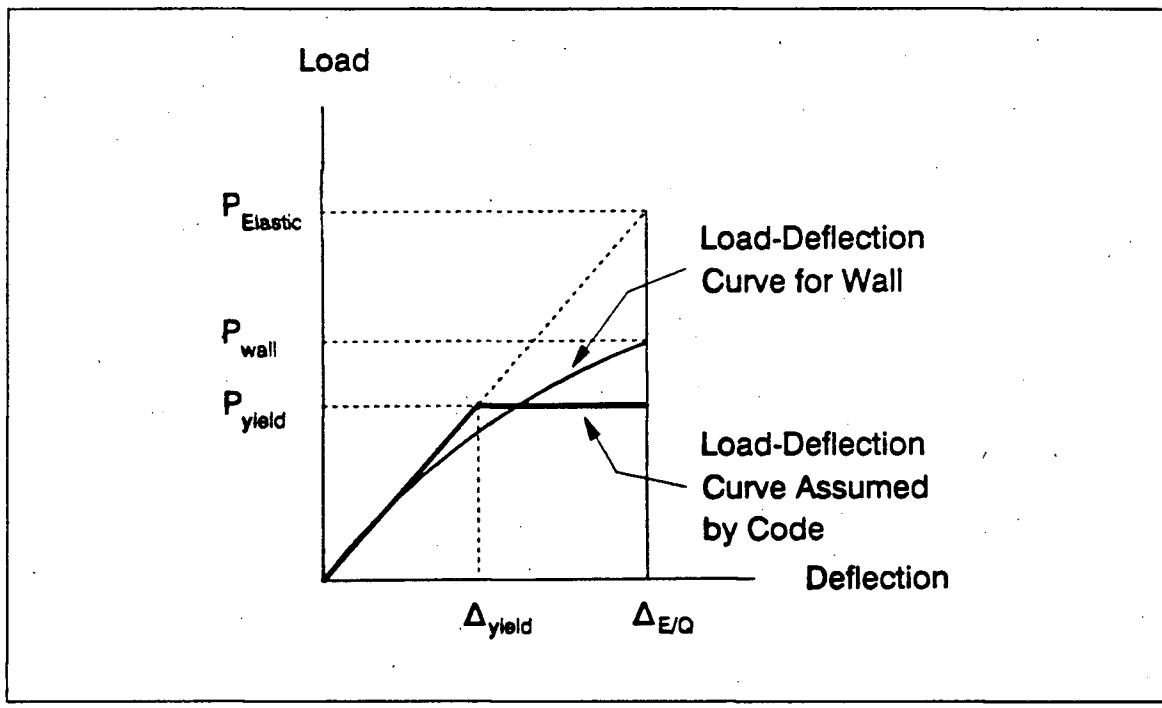

Figure 10.3: Load–Deflection Curves for Design Code and Shear Wall.

will be assumed to have the form,

$$\lambda V = \phi R \tag{10.5}$$

All of the design codes use tables to determine the load capacity of the shear walls. Design tables for the United States were produced by the American Plywood Association (APA) (revised, 1978). Equivalent tables for Canada were produced by the Council of Forest Industries (1979), these are essentially soft conversions of the APA tables to metric units. The APA tables are based on the ASTM E-72 shear wall test, and therefore, present the design capacity of shear walls for various sheathing thicknesses, nail sizes, and nail spacing that were obtained from the static racking test. As discussed earlier, the shear strengths presented in the APA tables, incorporate a minimum factor of safety of 3.0. One reason Foschi (1982) chose 3.0 as the factor of safety for the waferboard studies, was to prevent the deflections from becoming large. The high factor of safety effectively

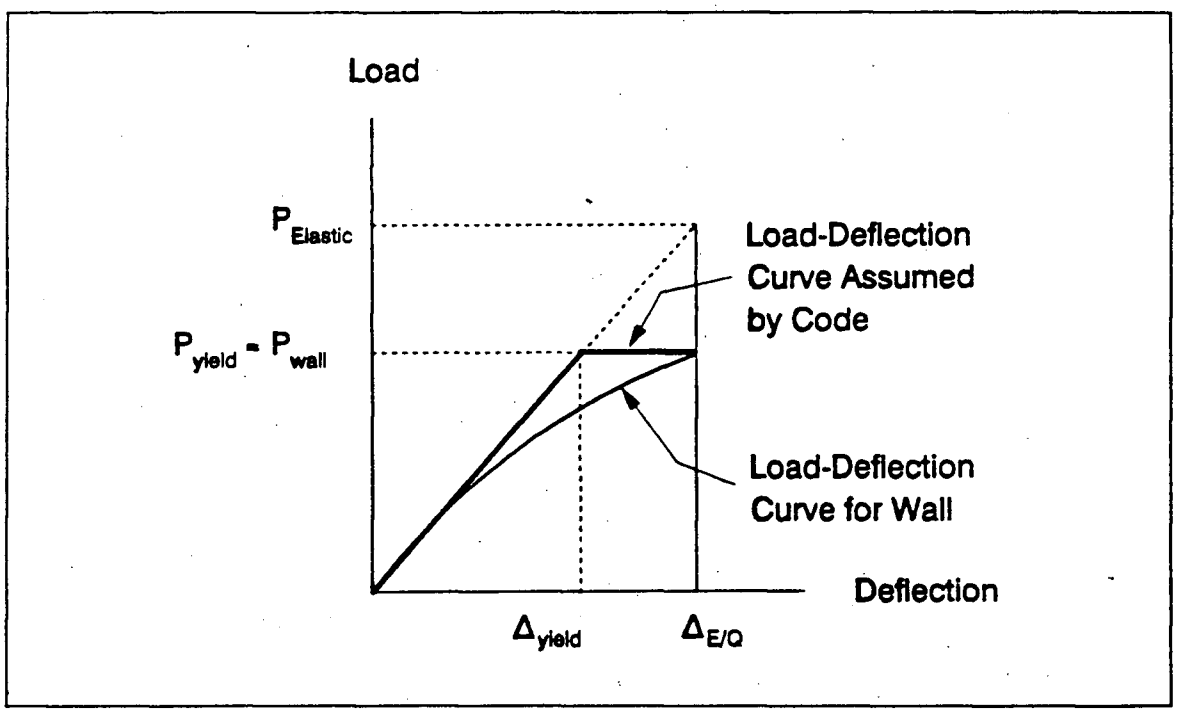

Figure 10.4: Correct Load–Deflection Curves for Design Code.

reduces the walls ductility demand, and thereby requires the wall to resist larger loads.

The final design of shear walls for all of the codes, is essentially determined by calculating the design shear per length of wall, then consulting tables to determine the nail and sheathing thickness requirements to resist the load. The design capacity of shear walls is assumed to be directly proportional to the length of the wall in all four design codes. This assumption has been shown to be valid for static loads by tests performed by Patton–Mallory, et. al. 1984).

10.2.2 Comparison of Codes to Model Predictions and Test Results

A shear wall of the same dimensions as the test specimens used in this study (2.4 × 2.4 m (8 × 8 ft)) was designed using each of the four design codes. The design

peak base acceleration used was 0.2 g (the same as the 1952 Kern County earthquake used for the shear wall tests), which is also the design acceleration for the Vancouver area of British Columbia. A structural weight of 53kN (12,000 lbs.) was used so that the design would represent a wall equivalent to those studied during the experimental and analytical section of this thesis.

All four design codes, investigated in this thesis, required the same shear wall configuration for the given design parameters. The shear wall designed, consisted of 9.5 mm ($\frac{3}{8}$ in) sheathing with 62 mm ($2\frac{1}{2}$ in or 8 d) common nails spaced at 100 mm (4 in) around the perimeter and 152 mm (6 in) along the interior studs of each sheathing panel. While it is interesting that all four design codes require the same final design, it should not be surprising. All of the codes have some tie to the Uniform Building Code and the design tables published by APA. The resulting design corresponds to one of the test specimen configurations used, both in the static and earthquake shear wall tests. The response expected by the design codes can therefore be compared to the test results to see if the design is conservative or not.

10.2.2.1 Seismic Loads

The seismic forces, assumed to be acting on the structure by the design codes, ranged from 6.7 N to 9.6 kN (1510 lb to 2160 lb), as shown in Table 10.1. Peak shear loads imposed on the walls during the earthquake tests are also shown in Table 10.1. As can be seen, the loads recorded during the tests are much higher than the design loads. The average peak load recorded for the 100 mm (4 in) perimeter, 150 mm (6 in) field nail spacing was between 2.2 and 3.2 times the design loads required by the codes. However, the design load , V, is not the value that should be compared to the test results because, the factors λ and ϕ have not been included.

Table 10.1: Comparison of Design Loads and Deflections with Test Results.

Design Code	Minimum Seismic Force	Peak Shear Load for Earthquake Tests		Factored Yield Load	Test/Factored Load		Design Drift	Peak Displacement for Earthquake Tests	
		Waferboard	Plywood		Waferboard	Plywood		Waferboard	Plywood
SI Units									
	kN	kN	kN	kN			mm	mm	mm
1985 NBC	6.7	22.1	21.5	10.1	2.19	2.13	12	18	18
1976 UBC	7.5			11.3	1.96	1.90	12		
1988 SEAOC	7.3			11.0	2.01	1.95	12		
1990 NBC/CSA	9.6			13.7	1.61	1.57	48		
Imperial Units									
	lb	lb	lb	lb			in	in	in
1985 NBC	(1510)	(4961)	(4840)	(2265)	2.19	2.13	(.48)	(0.69)	(0.70)
1976 UBC	(1680)			(2520)	1.96	1.90	(.48)		
1988 SEAOC	(1650)			(2475)	2.01	1.95	(.48)		
1990 NBC/CSA	(2160)			(3090)	1.61	1.57	(1.92)		

Equation 10.3 shows that the value, $\frac{\lambda V}{\phi}$, would be the average yield resistance, P_{yield}, shown in Figure 10.1. (The variable, ϕ, has been substituted for ϱ.) The load, P_{yield} would be expected during an earthquake. The value of $\frac{\lambda V}{\phi}$ for the 1990 NBCC/CSA design code is shown in Table 10.1 as the factored yield load. The factored yield loads shown for the 1985 NBCC, 1976 UBC, and 1988 SEAOC are the values of λV, since, an allowable load was used for these codes. Loads experienced during the earthquake should not exceed the factored yield load. As can be seen in Table 10.1, the loads recorded during the earthquake tests were 1.9–2.19 times higher than the factored yield load for the working stress design codes. The factored yield load for the 1990 NBCC/CSA was also exceeded by a factor of 1.57–1.61. While the recorded loads are higher than the expected design loads, they are not so high as to cause failure of the wall. The factor of safety for the walls can be calculated by dividing the peak loads obtained for the static one–directional test, shown in Table 8.1, by the peak shear loads obtained from the earthquake tests. The factor of safety, calculated in this manner, is about 1.6 rather that the 3.0 assumed in the APA design tables. As can be seen from Table 10.1 and the above discussion, the shear walls may be over loaded but, at the same time they do have sufficient reserve strength to avoid collapse. What is desired is to have the walls yield while, the rest of the structure remains elastic. This can be accomplished with the present design code if the design procedure for connections would be addressed separately.

The difference between the load expected by the codes, and those observed during the experimental study, can be explained by the fact that nailed connections in timber do not behave elastically. As discussed above, the earthquake code is based on the assumption that the structure will behave perfectly elastic up to the yield load, P_{yield}, then change to be perfectly plastic. The difference in the behavior is illustrated in Figure 10.3. The load–deflection curve on which the design codes are based, is again shown in Figure 10.3, as it was in Figure 10.1. The shape of a load–deflection curve for a timber shear wall is

also shown in Figure 10.3. As can be seen, the timber shear wall starts to yield at very low deflections and continues to follow this non-linear load-deflection curve to higher loads than the P_{yield} expected by the design codes.

Underestimation of the expected forces by the design code will have a serious implication on how timber structures perform during earthquakes. The objective of the earthquake engineering is to design for the capacity of the structure, and the design code assumes that this capacity will be realized during the earthquake. If the stiffness and forces in one or more of the structural elements are underestimated, the adjoining structural elements will not be designed for the correct loads. This is because the design of the adjoining elements assumes the low loads used to design the shear wall. In turn, these adjacent elements may be required to resist much higher loads than they were designed for and as a consequence will fail. Many of the failures observed in timber structures after earthquakes are anchorage failures. The anchoring connections are designed to resist the loads expected by the design code, while the loads experienced by the structure are much higher. This suggests that the value used for the resistance factor, ϕ, should be decreased to account for the loads being higher. If the 1990 NBCC/CSA code is used, and Equation 10.1 is rearranged to the form,

$$\phi \geq \frac{\lambda V}{R} \tag{10.6}$$

then the proper value of ϕ can be determined. Using values for λ, V, and R, of 1.5, 9.6 kN, and 21.8 kN, respectively, the value of ϕ would be 0.66. The value of R used in this calculation is the average of the peak loads recorded during the earthquake tests for the waferboard and plywood sheathed walls combined, The proper value of ϕ would change the assumed load-deflection curve to that shown in Figure 10.4 which would more representative of the loads experienced in structures during an earthquake. In turn, this would produce more reliable designs for connections and more compatibility between the

design codes for the different materials.

To account for the weak walls that will be constructed from time to time, the proposed value of 0.7 could be used for ϕ as long as a different value of ϕ were used for the design of connections. Different values of ϕ are used in the design of concrete where, the beams are designed to yield and the columns remain elastic. The same process could be used in timber where, a value of 0.7 or higher would be used when designing shear walls and a low value of ϕ would be used for designing connections. This would make the shear walls the weak link in the structure which would yield while, the rest of the structure remains elastic.

The factor of safety and how it is incorporated into the above analysis can be examined by rearranging Equation 10.5 into the form,

$$R = \frac{\lambda V}{\phi} \tag{10.7}$$

The ultimate capacity of the wall, R_{ULT}, must be greater than R for the wall to be capable of sustaining the loads generated during an earthquake. The wall will always yield, and will always have to resist a force of magnitude R. In equation form, the safe design would be,

$$R = \frac{\lambda V}{\phi} \leq R_{ULT} \tag{10.8}$$

Incorporating the factor of safety into Equation 10.8 results in,

$$R_{ULT} = f_s(R) = f_s\left(\frac{\lambda V}{\phi}\right) \tag{10.9}$$

Recall that the APA design tables use a minimum factor of safety of 3.0. Therefore,

$$R_{ULT} = 3.0 R_{APA} \tag{10.10}$$

where, R_{APA} is the design shear strength of the wall as presented in the design tables. Combining Equations 10.9 and 10.10, and rearranging the terms results in the following

equation.

$$R_{APA} = \left(\frac{f_s}{3.0}\right)\frac{\lambda V}{\phi} \tag{10.11}$$

Equation 10.11 shows how the factor of safety could be adjusted to any desired value. If the value of f_s is chosen as 3.0, the resulting design shear, R_{APA}, would be the value currently presented in the APA tables. Any value of f_s can be chosen, depending on the level of safety desired. The resulting value for R_{APA} will also change.

The variable, ϕ, is not effected by the factor of safety. The yield load for the wall will remain $\frac{\lambda V}{\phi}$, and the value of ϕ should be determined using experimental and analytical results. The connections used to attach the shear wall to the adjacent structural elements should be designed to resist the yield load R not the factored design load, λV. One reason the connection between the shear wall and the adjacent structural elements fail could be that they are designed to resist the design shear load rather than the yield load for the wall. In addition to using 0.70 for ϕ, it is recommended that a discussion of the proper design procedure for the connections be included in the commentary of the design code.

10.2.2.2 Deflections

A second check on the design codes was made to see if the inter-storey drift requirements of the various design codes were met by the design wall. The purpose of this requirement is to prevent excessive architectural damage during moderate earthquakes. The deflection requirements of the NBCC and both codes for the United States are more restrictive than the proposed 1990 NBCC/CSA, with the maximum allowable drift being 0.005 times the wall height. The UBC code, however, makes an exception in that it allows higher drifts, provided it can be shown that the larger deflections do not adversely affect the structural integrity of the building. Exceeding the maximum drift requirement necessitates that the designer check to ensure that the P–Δ effects at the higher deflections will not cause

the structure to collapse. The 1990 NBCC/CSA code is the most liberal in its requirements, with the maximum drift being limited to 0.02 times the wall height. Allowable design drifts are shown in Table 10.1 for each of the design codes. Designers will have more leeway in designing for higher ductilities with the higher allowable drift for the 1990 NBCC/CSA.

Peak displacements recorded during the earthquake tests are shown in Table 10.1 for the walls with 100/150 mm (4/6 in) nail spacing. If these deflections are compared to the maximum allowable drifts for each design code, it can be seen that only the 1990 NBCC/CSA code is strictly adhered to. The UBC and SEAOC codes would also accept these deflections since, the wall is still able to sustain the shear loads. The deflection required for the 1985 Canadian code was exceeded by 50%, and the code makes no allowance for accepting the higher deflections. While the deflections recorded during the experimental study may seem quite large, a visual inspection of the shear wall specimens, after the tests were finished, revealed little or no visual damage. It is, therefore, believed that the only architectural damage would be in the form of cracks in the wall finishes, broken windows, etc., and the change in the proposed 1990 NBCC/CSA to accept the larger deflections is justified.

As can be seen from the above discussion, the design codes investigated in this chapter assume seismic lateral loads that are unconservative. The loads observed during the earthquake shear wall tests and predicted by the finite element model, **DYNWALL**, were significantly higher than those used for design purposes. The resistance factor proposed for the 1990 NBCC/CBC code is acceptable if a new design procedure for connections is presented. A high resistance factor for designing shear walls and a low resistance factor for designing connections would help guarantee that the shear wall would yield and the connections would remain elastic. The deflection requirement of the 1985 NBCC is the only deflection requirement exceeded by the test specimens. However, since this

requirement is to be relaxed in the 1990 NBCC/CSA code, it is not a significant problem.

10.3 Other Investigations

10.3.1 Effects of Using Adhesives

The model, **DYNWALL**, was used to check the effect of using adhesives to attach the sheathing to the framing. Recently, there has been an increase in interest for using adhesives to reduce the deflections and increase the strength of timber shear walls. However, none of the North American design codes have addressed this issue. Adhesives will significantly reduce the ductility of timber shear walls, but will also increase the load requirements. The New Zealand (1976) design code did address the use of adhesives by increasing the factor for ductility by 20%, i.e. reducing the ductility demand, which effectively increases the design loads by 20%.

To investigate the effects of adhesives, the same earthquake record was used, as in all of the material parameters for the sheathing and framing were the same as that used to model a waferboard sheathed wall in Chapter 9. Only the load–deflection parameters used for the sheathing connectors were changed to represent adhesives. The connector parameters were obtained from tests conducted by Dr. T. P. Cunningham Jr. (1988) at the APA Testing Laboratory in Tacoma, Washington. The parameters used to model the adhesive connection were, K_0 = 11628 N/mm (66400 lb/in), P_0 = 10230 N (2300 lb), K_2 = 4728 N/mm (27000 lb/in), Δ_{max} = 3.2 mm (0.125 in), K_3 = −6830 N/mm (-3900 lb/in), P_1 = 330 N (75 lb), and K_4 = 5810 N/mm (33200 lb/in).

The maximum displacement predicted for a 0.2 g earthquake was 13 mm (0.50 in) which is approximately equal to the maximum drift allowed by the current design codes. Predicted peak acceleration at the top of the wall was calculated by differentiating the

predicted displacement time history twice, and the base shear was be calculated by multiplying the peak acceleration by the mass. The predicted peak base shear was 34 kN (7640 lb), which is close to the average ultimate strength of 35.5 kN (7990 lb) for the waferboard shear walls, tested in the static one-directional tests. Excedience of the strength for framing or sheathing was not checked because the model does not predict forces. As the shear wall loads become higher, there is a distinct possibility of the failure mode changing from the ductile failure of the nails to a brittle failure of the framing or sheathing material. The change in predicted loads are also much higher than the 20% increase incorporated in the New Zealand code.

Adhesives were investigated to show that their use has a significant influence on the resulting structures performance. These results should be reviewed with the following in mind:

1. **DYNWALL** uses an exponential curve to model the load-deflection curve of the adhesive, which in fact is almost linear until very high loads are reached. Therefore, the parameters for the exponential curve were difficult to fit to the connection test data, and the resulting prediction is close to the limit of the theory. The adhesive may be better modelled by a quadratic or even a linear equation.

2. The differentiation of the displacement record to find the peak acceleration and corresponding forces, introduces some error in the results.

Before adhesives can be included in the design codes, a few full size shear wall tests should be conducted to verify that the predictions made using either of the models, **SHWALL** or **DYNWALL**, are accurate. Once the models are verified, they can be used to determine the strengths and ductility for the various construction configurations. The appropriate ductility factors and design tables could also be determined.

10.3.2 Effects of Aspect Ratio

Three walls are compared in this section to show the effect of changing the dimensions of the wall on the response. **DYNWALL** was used to model the following walls:

1. A 2.4 × 2.4 m (8 × 8 ft) wall which was identical to one of the walls modeled in Chapter 9 ("standard" wall).

2. A 2.4 × 4.8 m (8 × 16 ft), (2.4 m long by 4.8 m high) wall ("high" wall).

3. A 4.8 × 2.4 m (16 × 8 ft), (4.8 m long by 2.4 m high) wall ("long" wall).

All of the walls were modeled as having 38 × 89 mm (12 × 4 in) studs, spaced at 600 mm (24 in) centers and waferboard sheathing. The walls were modeled as being blocked and having a nail spacing of 100 mm (4 in) around the perimeter of the sheathing panels and 150 mm (6 in) along the interior studs. The mass for all three walls was 21.9 kN/m (1500 lb/ft) and the Kern County earthquake was used as the base acceleration record.

Figure 10.5 shows the displacements of the "high" wall during the first 8.0 seconds of the earthquake. As can be seen, the displacement is not proportional to height. The peak displacements of the top of the wall (4.8 m height) is greater than twice the displacement at the mid-height (2.4 m level). When the peak displacements are considered, the top of the wall displaces an average of 2.2 times what the mid-height displacements. When the vertical displacements of the end studs at the same two heights and at the same times are investigated, the vertical displacement of the top of the wall is found to be an average of 1.3 times the mid-height deflection. Together, these two deflections show that the "high" shear wall begins to deflect in bending, as well as shear. The bending effects are negligible in the 2.4 m (8 ft) high walls. Figure 10.6 shows the difference in the two deflected shapes.

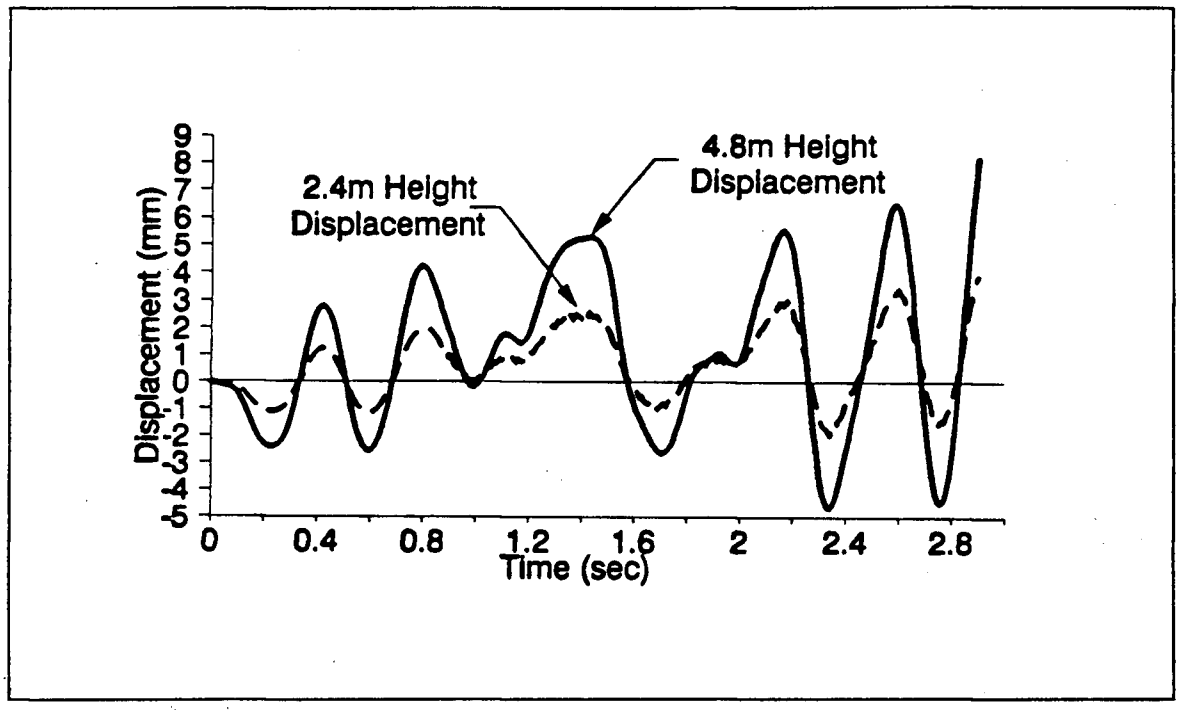

Figure 10.5: Displacement Records for 4.8 m (16 ft) High Wall.

The effect of constructing a long horizontal wall was also investigated using **DYNWALL**. Figure 10.7 show the displacement records for the first nine seconds of the earthquake. All of the displacement predictions are for a height of 2.4 m (8 ft). Comparing the deflection for the standard and long walls reveals that the two displacements follow approximately the same frequency pattern, with the displacements of the long wall usually being smaller than for the standard wall. The frequency content for the two records would be expected to be close if the equation for the fundamental frequency is examined. The fundamental frequency, ω, is given by,

$$\omega = \sqrt{\frac{K}{m}} \tag{10.12}$$

where, K is the structural stiffness and m is the mass. The long wall has twice the mass and approximately twice the stiffness of the standard wall, since it is two times as long as the standard wall. If both the stiffness and mass of Equation 10.12 are doubled,

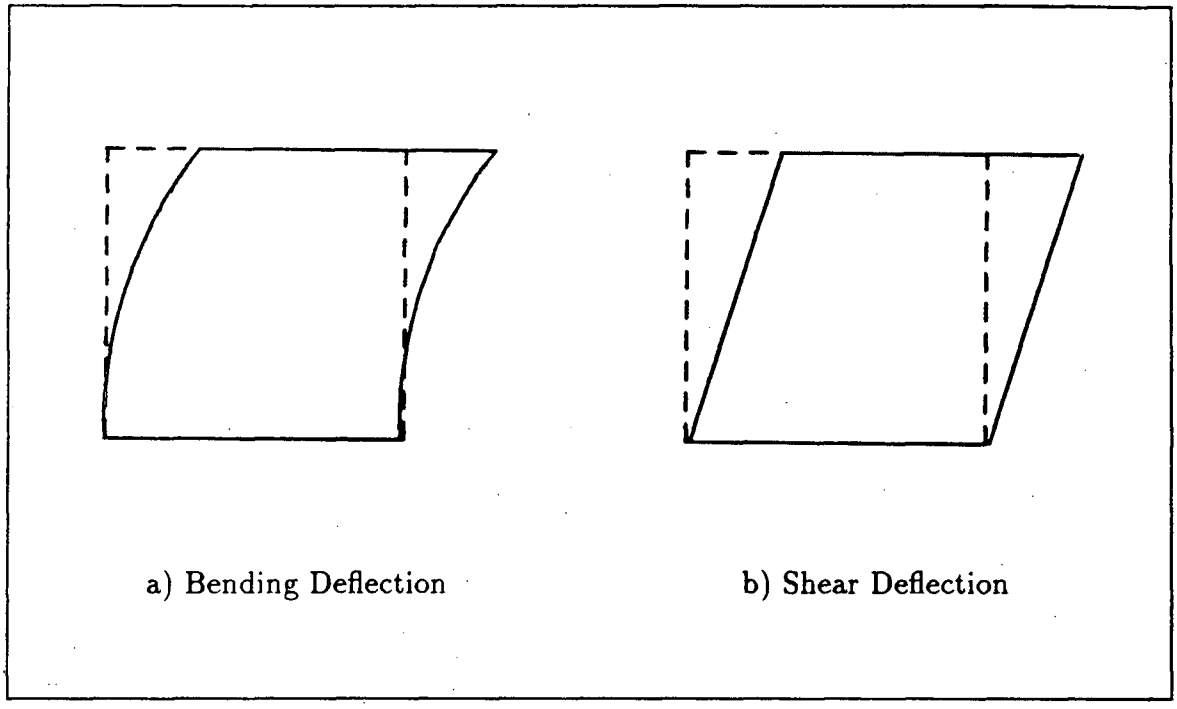

Figure 10.6: Bending versus Shear Deflection.

the natural frequency, ω remains the same. The natural frequencies calculated for the two walls by **DYNWALL** were 2.95 Hz for the standard wall and 3.2 Hz for the long wall. The increase in the natural frequency of long wall indicates that the stiffness is not directly proportional to length, but rather increases at a rate faster than the length. The additional stiffness is due to adjacent sheathing panels bearing on each other.

The phase shift that is evident towards the end of the record is partly due to the difference in fundamental frequencies for the two walls. The higher deflections that the standard wall experiences will also cause it to accumulate more damage, which will in turn cause the fundamental frequency to change more for the standard wall than for the long wall. The combination of beginning with a lower natural frequency and accumulating more damage during the earthquake will make the standard and long walls' natural frequencies move farther apart.

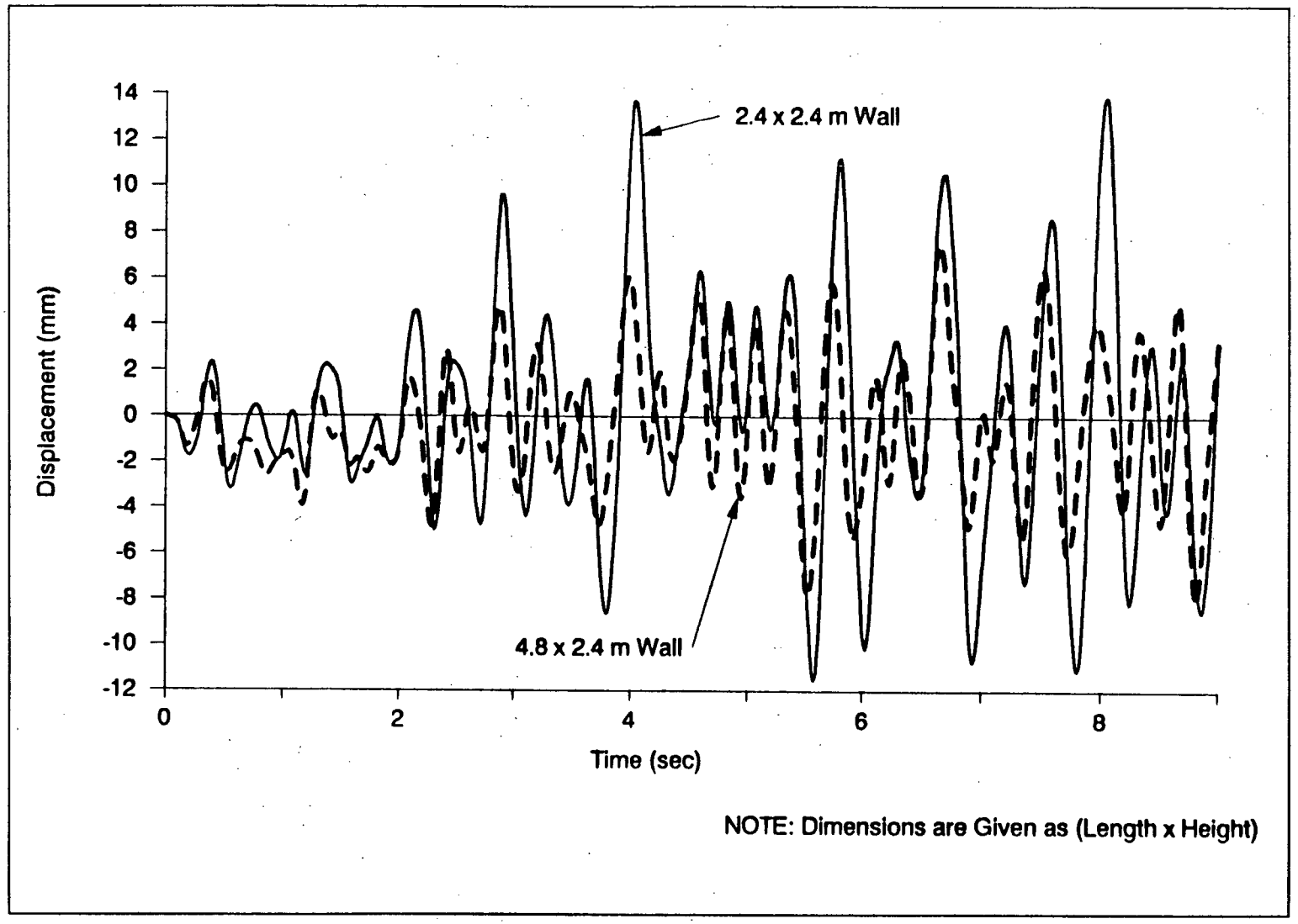

Figure 10.7: Displacement Records for Standard and Long Walls.

10.4 Construction Details

Problems associated with the individual details of timber shear wall construction have been neglected by researchers in the past. Design codes have attempted to provide the designer with methods that ensure the problems will be addressed. The experience gained through the modelling and testing of the shear walls during this study have highlighted three main details of shear walls that merit special discussion. In addition, the above discussion has shown that the loads experienced by the connections are probably higher than the design code expects. Therefore, it is important that the design of timber shear walls include special consideration of the following three details.

10.4.1 Hold-Down Connection

One of the most important construction details in timber shear walls is the hold–down connection used to anchor the end studs of the wall and resist the overturning moment. The earthquake tests of full size shear walls showed how important these connections can be. The first couple of trial shear wall specimens did not have any anchorage for the end studs, only bolts located between the studs were used to resist the base shear. As a result, localized failures occurred at the bottom corners of the walls and the end studs separated from the sole plate. The wall then tried to resist the earthquake by rigid body rocking rather than racking and deflections of the top of the wall relative to the base were 2.5 to 4 times larger than those measured for equivalent walls with hold–down anchors.

One of the few people that has investigated this detail was Polensek (1986). He showed that by increasing the sheathing nail density in the corners of shear walls, the overall deflection of the walls could be reduced for static one–directional loadings. To the knowledge of the author, no research has been performed to investigate the effects of load

reversal on the connection. However, the importance of the connection has been shown in other investigations, such as the ones on shear walls by Stewart (1987) and braced frames by Dean (1987). This connection is also considered to be one of the important details for shear walls by Dean et. al. (1989).

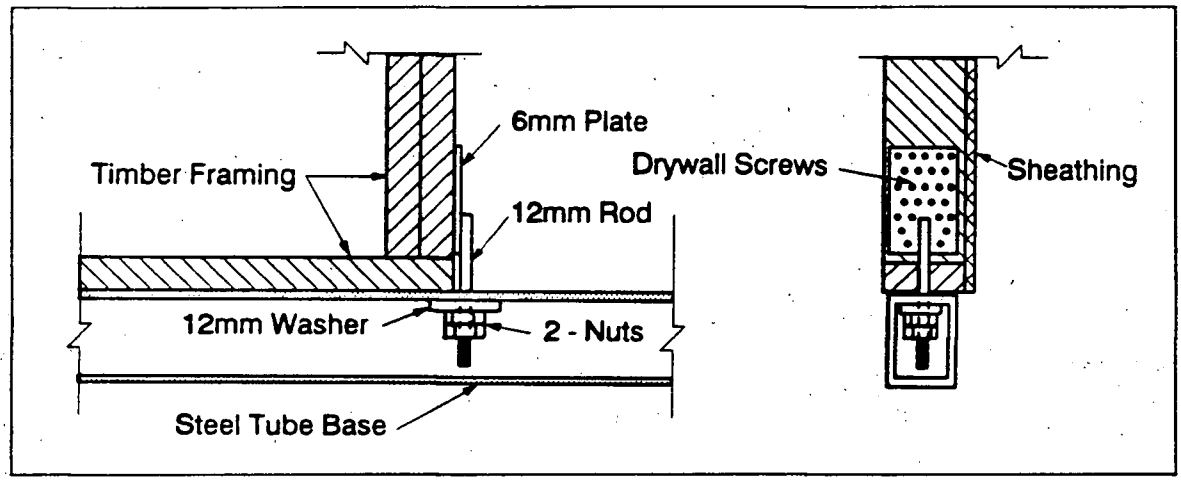

Figure 10.8: Hold-Down Connection Configuration.

The connection used in this study is shown in Figure 10.8. This is probably one of an infinite number of possible solutions for anchoring the end stud to the foundation (or floor system for walls not at ground level). Whatever the designer decides to use for anchoring the end studs, the connection must be strong enough to transfer the tensile forces to the next structural component, be it the floor system or foundation. It must also be stiff in order to prevent the end stud from lifting away from the foundation. The importance of this connection decreases as the length of the shear wall increases. In long walls, the forces in the end studs are separated by a greater distance, thereby reducing force required to generate an equivalent couple. Also, as the length of the wall increases, the dead weight of the structure will help counter the overturning moment.

10.4.2 Corner Connection

Like the hold-down connection discussed in the previous section, the connection used to tie the end studs to the sill plate in the framing, has not been given much consideration. The most common solution used to ensure the top corners in the framing members remain connected is to count on the sheathing to transfer the loads across the joint. While this might be sufficient for longer walls, where the forces due to the overturning moment are not as high, the sheathing cannot usually restrain the joint from separating in shorter walls. Some form of strap or angle iron is usually required for this joint, but many designers neglect checking the connection to see if extra strength is required. The connection used in the tests, performed as part of this study, is shown in Figure 10.9. The angle iron was sufficient for the loads experienced in these tests and the joint integrity was maintained.

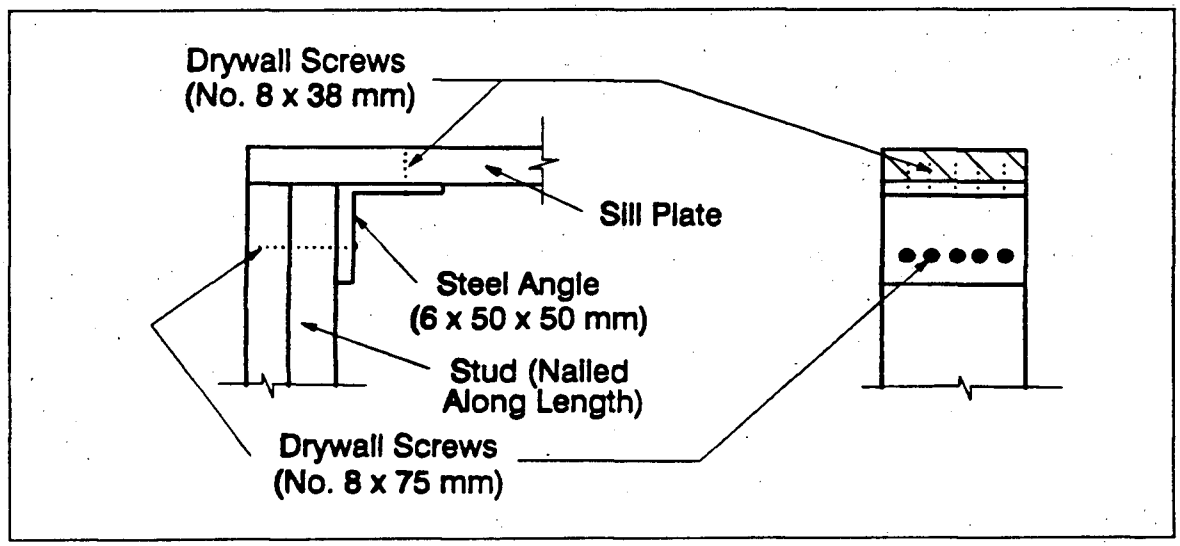

Figure 10.9: Corner Connection Configuration.

10.4.3 Sheathing Connectors

As discussed in Chapters 3 and 6, the fasteners used to attach the sheathing to the framing are an important detail that governs the strength and stiffness of timber shear walls. Nails are the most common fastener, but screws, staples, and adhesives are also used. Many of the fasteners are being used in shear walls without relevant tests being performed to verify their suitability for resisting dynamic loads. The fasteners supplied for this purpose also show a wide variability in their yield strengths for each type and, because of the large number of different fasteners, the strength and stiffness of shear walls can also show a large variability.

All of the design codes investigated in this study recognized the relation between strength and the nails used to attach the sheathing, by specifying the required nail size and spacing required to achieve the design load capacity. However, according to Dean et. al. (1989), the current New Zealand code goes one step further by restricting the length of the nail allowed to a maximum of 5 times the sheathing thickness. This is because it has been observed that partial withdrawal of the nails enhances the ductility of the wall.

While many carpenters and contractors will argue against what they consider to be too many nails in shear walls, it is important that inspectors ensure the design nail spacing is adhered to and that the nails are not overdriven. Overdriving the nails damages the sheathing by forcing the head of the nail to penetrate the face of the sheathing, thereby, reducing the strength of the connections. Lower nail densities and overdriving of the nails translate directly to lower load capacities and stiffness. Another observation that has been made is that the nails must be spaced in a uniform pattern around the perimeter of each sheathing panel. If the nails are spaced more closely on one side of a panel, the center of rotation for that particular panel is shifted toward the denser nail pattern. This

leads to premature failures along the less dense nail line.

With the introduction of new methods for fastening the sheathing in shear walls, the load–deformation characteristics of walls might be altered significantly. Adhesives reduce the ductility of the shear walls, which will require the walls to withstand higher loads. Other fasteners, such as staples, may increase the ductility or reduce the strength of shear walls when compared to nails. As additional methods of fastening the sheathing are introduced, continued use of the ASTM racking test for determining the design capacities of the various fastener systems becomes not only unrealistic and expensive, but could also provide incorrect information about the dynamic performance of the resulting walls. The hysteretic characteristics and ductility under reversing loads must be determined in order to obtain a reasonable prediction of the dynamic characteristics. Only after this information is found can values be assigned to the pertinent factors in design code, with confidence that the resulting designs will be safe.

The previous discussion of these three construction details illustrates that designing a shear wall is more than a simple matter of finding the load capacity for the shear wall in a design table. To ensure the final structure will perform properly, the connection details must be given sufficient attention, both in design and construction. The discussion also illustrates the need for further research to improve the understanding of the effects that changes to the construction of shear walls will have.

10.5 Summary

The design requirements of four design codes were investigated in this chapter, with the results indicating that the design loads required by these codes are lower than those observed in tests. This could cause failures in timber structures, especially in the adjoining structural elements since they will be designed assuming the lower loads. The shear

walls have been shown to have the reserve capacity required, but connections and other structural components may not. When compared to the loads recorded during tests and predicted using the model, **DYNWALL**, the peak loads were found to be between 1.6 and 3.2 times higher than the design loads. The assumption of perfectly elastic–plastic behavior made by the codes when shear walls exhibit non–linear behavior throughout the load range is the main reason for the difference. A reduced factor of safety is calculated for the allowable stress design codes, based on the static racking test results presented in Chapter 8. The resistance factor, ϕ, proposed for 1990 National Building Code of Canada, and accompanying CSA–086.1–M89 Standard was found to be acceptable. However, it is also recommended that the new code specify a design procedure for the hold–down connections that would guarantee the connections remain elastic. The allowable inter–storey drift for the 1985 NBCC was also exceeded by the tests but, since the deflection requirement is being relaxed in the 1990 code, and the other two design codes allow for higher deflections, it was not considered to be important.

The effects of underestimating the design load on the resulting structure's performance were discussed. It was shown that, while the timber shear wall will be capable of resisting the higher loads observed in tests, the adjoining elements, such as anchor connections to the foundation, could fail because the design codes allow these connections and structural elements to be designed for the lower loads. This could be one of the reasons why many of the observed failures of timber structures occur at the anchorage connections during earthquakes.

Different sized walls were investigated to determine the effect of length and height on the response of timber shear walls to earthquakes. It was found that the natural frequency of shear walls increases with the length of the wall at a rate higher than the linear relation for strength. It was also shown that the shorter wall will experience higher deflections and be damaged more than the long wall, and leads to a widening

of the difference in natural frequencies for the two walls. Relatively high, narrow walls were shown to be influenced by bending, as well as shear deformations. The bending deformations resulted in peak deflections at the top of a 4.8 m (8 ft) wall to be 2.3 times as large as the deflections at mid-height.

Three of the most important construction details were also discussed. These were: **1)** the hold-down anchor, **2)** the corner connection, and **3)** the sheathing fasteners. In all three cases, it is believed that further research is required to develop sound design procedures for the two framing connections and for any new sheathing fastener system. It should also be pointed out that all of the present design codes are primarily based on experiments that used one type of nail (bright common), manufactured by one manufacturer. Considering that this connector is the most important item governing the load capacity, stiffness, and ductility of shear walls, and the high variability between manufacturers, it is important that a simplified model be developed to allow the current test results to be expanded to include the other manufacturers and types of nails.

Chapter 11

Conclusion

11.1 Summary and Conclusions

This thesis has addressed the topic of timber shear walls from several perspectives, using experiments and numerical modelling. The background to the topic was discussed and the pertinent research to-date reviewed, then three numerical models were developed. The three numerical models were:

1. **SHWALL**, a general finite element model capable of describing the static load-deflection behavior of timber shear walls.

2. **FREWALL**, a closed form mathematical model capable of describing the steady state dynamic behavior of shear walls.

3. **DYNWALL**, a general finite element model which uses a time-integration procedure to predict the load-deflection behavior of timber shear walls, subjected to random base accelerations, such as those experienced during earthquakes.

Following the derivations of the numerical models, the procedures used and the results from tests of connections and full size shear walls were presented. Results from the connection tests were used as data for the two finite element models. Results from the full size shear wall tests were used to verify the accuracy of the numerical models and to

gain an understanding of the dynamic behavior of shear walls. Finally, the design and construction methods that are currently used in North America were discussed. Results of the full size shear wall tests and predictions from the numerical model were used to check the adequacy of the design codes.

The conclusions and accomplishments of this study are as follows:

1. The numerical model, **SHWALL**, is capable of accurately predicting the load–deflection behavior of general timber shear walls, subjected to static one–directional loads in the plane of the wall. The model is capable of predicting the ultimate load capacity of waferboard and plywood sheathed walls within 4% and 6%, respectively.

2. The closed form mathematical model, **FREWALL**, predicts the steady state response of timber shear walls loaded by harmonic base excitations. When compared to test results for a qualitative assessment of its accuracy, the prediction of the steady state response of nailed shear walls is quite accurate.

3. The numerical model, **DYNWALL**, is capable of predicting the time–history of the dynamic displacements for timber shear walls subjected to random dynamic base accelerations. Predictions of the frequency content of the displacement time–history, and the displacement records have average correlation coefficients of 0.99 and 0.91, respectively when compared to test results.

These three models can be used to predict the general behavior of shear walls. Simplified models can eventually be used to design the shear walls as components of buildings, investigate the design codes in detail, and conduct reliability studies. The model does not restrict the shear wall configuration to be investigated, as long as the load–deflection characteristics of the various connections and material properties for the sheathing and framing can be determined.

Some additional observations and conclusions are:

1. The results from all of the shear wall tests indicated that out–of–plane deflections of sheathing are insignificant for 9.5 mm (3/8 in) and higher thickness. This result provides direction for the first simplifications to be made to the two finite element models developed in this thesis. The elimination of the out–of–plane DOF will reduce the required computation time by more than 50%.

2. Comparisons between the results from sheathing connection tests, and full size shear wall tests, along with experience from modelling, indicate that the fasteners used to attach the sheathing to the framing govern the load capacity, stiffness, and ductility of timber shear walls. The literature review revealed very little research has been done to investigate the effects of different fasteners on the overall response of timber shear walls to different loadings.

3. It was shown that the deflections would be significantly lowered by using adhesives and, the loads experienced by the walls during an earthquake would be significantly increased. It is also postulated that the use of adhesives may be detrimental to the dynamic response of shear walls because of the

   (a) loss in ductility,

   (b) increase in accelerations transmitted to other parts of the structure, and

   (c) the possibility of shifting the failure mechanism from the ductile failure of the nails, to a brittle failure in the framing or shear through the thickness of the sheathing.

4. Since a major portion of the test results, on which the design codes of North America are based, is from test specimens constructed using nails that are no

longer manufactured, the two finite element models presented in this thesis provide a practical method of extending the current data base to include nails manufactured by other companies. Also, shear walls constructed with other methods of attaching the sheathing, such as adhesives, screws, or staples can be investigated.

5. The current North American design codes and proposed 1990 National Building Code of Canada, have been shown to underestimate the design shear load for a 0.2 g earthquake. A detailed investigation of the design code is beyond the scope of this study, but the results of comparisons made indicate that the design codes specify design shears significantly lower than those recorded during earthquake tests of full size shear walls. The resistance factor of 0.70 is recommended for nailed timber shear walls, and should be included in the 1990 National Building Code of Canada. However, it is also recommended that a design procedure for the hold–down connections be specified. The resistance factor for connections should be low to ensure that they will remain elastic.

6. The factor of safety for the working stress design codes for North America has been shown to be approximately 1.6 rather than the 3.0 previously assumed.

7. It was found that 1985 NBC code restrictions for inter–storey drift were exceeded during the earthquake tests of full size shear walls. The other three North American design codes requirements were met by the shear wall specimens tested and the numerical model predictions.

8. Deflections of high, short walls were shown to be influenced by bending behavior as well as shear. Shear deformations were shown to be governing deflected shape for short, long walls.

9. Longer walls were shown to deflect less than shorter walls, which indicates that shorter walls would receive more damage during an earthquake.

10. The hold-down connections used to anchor the end studs of shear walls have been shown to be one of the critical details. These connections decrease in importance as the length of the wall increases, because the overturning moment will be higher, leading to large tensile forces in the end studs of shorter walls. It is recommended that these connections be designed to remain elastic.

11. The corner connections used to keep the top corners of the framing from separating are required for shorter walls and become less important as the length of the wall increases. Like the hold-down anchors, this is because the overturing moment has less effect on a long wall than a short wall.

12. The larger deflections observed during shear wall tests using the Taft earthquake, then observed during tests using the San Fernando earthquake, showed that peak acceleration alone is not a good indicator of the damage potential of earthquakes. Rather, the duration and frequency content of the earthquake must also be considered.

13. No significant difference was observed in the dynamic response to earthquakes for waferboard and plywood sheathed walls. Both test results and the predictions of the dynamic model indicated that the dynamic response of walls sheathed with these two sheathing materials are essentially the same.

14. The steady state resonance response of plywood sheathed walls was predicted to be significantly higher than waferboard sheathed walls for accelerations of 0.15 g and higher. The two types of shear walls were predicted to respond approximately the same to harmonic accelerations below 0.15 g.

15. An investigation of the stability of the steady state response of shear walls showed there to be no jump phenomenon associated with the steady state response of nailed walls. This study also showed that unbounded response to resonant frequency accelerations will not occur, and catastrophic failure due to resonance phenomenon is not expected.

16. The theoretical bounds of the resonant frequency ratio, κ^* for timber shear walls, using nails to secure the sheathing were determined to be,

$$\sqrt{\frac{(7-a)-(1-a)3\sqrt{3}}{6\pi}\frac{K_2}{K_0}} \leq \kappa^* \leq 1 \tag{11.1}$$

where, a is the load at zero displacement for the hysteresis, K_2 is the yielded stiffness, and K_0 is the initial stiffness for the wall.

17. There is no significant difference between the performance of waferboard and plywood sheathed shear walls up to loads approximately 50% of the ultimate static load. For higher loads plywood sheathed walls have a lower stiffness than waferboard sheathed walls, causing the plywood sheathed walls to deflect more. Waferboard shear walls will have lower material damage during an earthquake, while plywood shear walls will possible experience lower loads due to their higher ductility. The difference, however, will be small.

11.2 Future Research

The results of this study have shown the need for further research to investigate a number of different topics pertaining to timber shear walls. Many of the problems could be solved, at a significantly reduced expense, by using simplified versions of the two

finite element models presented in this thesis. Some of the topics that research should be directed towards are:

1. A reliability study of timber shear walls should be conducted to help move the present design codes from the deterministic procedures currently used, to procedures based on probability theory and capacity design.

2. The dynamic response of timber shear walls, constructed using different methods of attaching sheathing to the framing should be investigated to ensure that changes are not detrimental. Different fastening techniques, such as adhesives, could increase or decrease the ductility, strength, and stiffness of shear walls. The failure mode could also be changed from the ductile failure of the nails to a brittle failure of the framing or sheathing. Experimental and analytical information about the strength, ductility, and stiffness of shear walls, using the different fasteners, are required to assign values to the pertinent factors used in design equations. Nails from different manufacturers, as well as screws, staples, and adhesives should be included in the study in order to verify that each of the connectors are effective.

3. The response of shear walls to a wide range of earthquake excitations should be investigated, either experimentally or analytically. The analytical investigation would be less expensive, and therefore easier to include a larger number of earthquake records in an investigation. It has been shown in this study that peak acceleration alone is not a good indicator of the damage potential of earthquakes. Rather, the duration and frequency content of the earthquake must also be considered.

4. The results of this and future studies should be extended to include other types of dynamic loading, such as hurricane and other wind loadings, and blast loading.

These are some of the answers that are required before significant improvements to the design and utilization of timber shear walls can be made. All of these topics could utilize simplified versions of the finite element models proposed in this thesis to reduce the time and expense of the investigations. The results of this thesis provide a solid base of experimental results and analysis, representative of the type of loading experienced during earthquakes.

Bibliography

[1] APA, 1987. *APA Design/Construction Guide, Residential and Commercial.* American Plywood Association, Tacoma, Washington.

[2] APA, revised 1987. *APA Design/Construction Guide, Diaphragms.* American Plywood Association, Tacoma, Washington.

[3] ASTM, 1986. "ASTM E72-77 Standard Methods of Conducting Strength Tests of Panels for Building Construction". *Annual Book of ASTM Standards*: pp. 690-701.

[4] ASTM, 1986. "ASTM E564-76 Standard Methods of Conducting Strength Tests of Panels for Building Construction". *Annual Book of ASTM Standards*: pp. 1013-1017.

[5] Adams, N.R., 1987. *Research Report 105, Plywood Shear Walls.* American Plywood Association, Tacoma, Washington.

[6] Applied Technology Council, 1980. *Proceedings of a Workshop on Design of Horizontal Wood Diaphragms.* Berkeley, California, pp. 71–142.

[7] Applied Technology Council, 1981. *Guidelines for the Design of Horizontal Wood Diaphragms.* (ATC-7-1), Berkeley, California.

[8] Atherton, G.H., 1982. *Ultimate Strength of Structural Waferboard and Particleboard Diaphragms.* Forest Research Laboratory, Oregon State University, Corvallis, Oregon.

[9] Atherton, G.H., 1983. "Ultimate Strength of Structural Particleboard Diaphragms", *Forest Products Journal,* Vol. 33, No. 5, pp. 22–26.

[10] Batchelar, M.L. and G.J. Gavanagh, 1984. "Nailed Plywood Gusset Joints for Timber Portal Frames," *Proceedings of the Pacific Timber Engineering Conference, Auckland, New Zealand, Vol. II, Timber Design Theory.* Institution of Professional Engineers, Wellington, New Zealand, pp 631–642.

[11] Belytschko, T., 1978. *Advanced Structural Dynamics.* Edited by J. Donéa. Applied Science Publishers, Ltd.

[12] Bendat, J.S. and A.G. Piersol, 1971. *Random Data: Analysis and Measurement Procedures.* John Wiley and Sons, Inc., New York, N.Y., pp. 286–331.

[13] Boughton, G.N. and G.F. Reardon, 1984. "Simulated Cyclone Wind Tests on a Timber Frame House," *Proceedings of the Pacific Timber Engineering Conference, Auckland, New Zealand, Vol. II, Timber Design Theory.* Institution of Professional Engineers, Wellington, New Zealand, pp. 527–534.

[14] Boughton, G.N., 1988. "Full Scale Structural Testing of Houses Under Cyclonic Wind Loads," *Proceedings, 1988 International Conference on Timber Engineering,* Vol. 2, Forest Products Research Society, Madison, Wisconsin, pp. 82–88.

[15] Bramhall, G. and M. Salamon, 1978. *Combined Species-Temperature Correction Tables for Moisture Meters. Information Report VP-X-103.* Forintek Canada Corp., p. 119.

[16] Buchanan, A., 1984. "Wood Properties and Seismic Design of Timber Structures," *Proceedings of the Pacific Timber Engineering Conference, Auckland, New Zealand, Vol. II, Timber Design Theory.* Institution of Professional Engineers, Wellington, New Zealand, pp. 462–469.

[17] COFI, 1978. *Plywood Sheathing.* Council of Forest Industries of British Columbia, Vancouver, British Columbia.

[18] COFI, 1979. *Douglas Fir Plywood Diaphragms.* Council of Forest Industries of British Columbia, Vancouver, British Columbia.

[19] COFI, 1984. *Plywood Handbook.* Council of Forest Industries of British Columbia, Vancouver, British Columbia.

[20] CSA, 1989. *6th Draft of Proposed New Edition of CSA Standard CAN/CSA–086.1–M89, Engineering Design in Wood (Limit States Design).* Canadian Standards Association, Toronto, Ontario.

[21] CWC, 1986. *Canadian Wood Construction, Shearwalls and Diaphragms.* CWC Datafile WC–1. Canadian Wood Council, Ottawa, Canada.

[22] Carney, J.M., 1975. "Bibliography on Wood and Plywood Diaphragms". *ASCE Journal of the Structural Division,* Vol. 101, No. ST11, pp. 2423–2436.

[23] Carroll, M.N., 1970. "Relationship Between Driving Torque and Screwholding Strength in Particleboard and Plywood," *Forest Products Journal,* Vol. 20, No. 3, pp. 24–29.

[24] Carroll, M.N., 1972. "Measuring Screw Withdrawal with a Torque Wrench," *Forest Products Journal,* Vol. 22, No. 8, pp. 42–46.

[25] Caughey, T.K., 1960. "Sinusoidal Excitation of a System with Bi-linear Hysteresis." *Transactions of the ASME, Journal of Applied Mechanics*, Vol. 27, Series E, Number 4, pp. 640–643.

[26] Cheung, C.K., R.Y. Itani, 1984. "Damping Characteristics of Sheathed Wood Diaphragms," *Proceedings, Pacific Timber Engineering Conference, Auckland, New Zealand, Vol. II, Timber Design Theory,* Institution of Professional Engineers, Wellington, New Zealand, pp. 470–477.

[27] Chou, C. and A. Polensek, 1987. "Damping and Stiffness of Nailed Joints: Response to Drying," *Wood and Fiber Science,* Vol. 19, No. 1, pp. 48–58.

[28] Clough, R.W. and J. Penzien, 1975. *Dynamics of Structures.* McGraw-Hill Book Company, New York, N.Y., pp. 118-128.

[29] Council of American Building Officials, 1985. *National Evaluation Report No. NER-315.* Whittier, California.

[30] Cunningham, Dr. T.P., 1989. *Personal Correspondence.*

[31] Dean, J.A., 1987. *Personal Communication.*

[32] Dean, J.A., W.G. Stewart and A.J. Carr, 1986. "The Seismic Behaviour of Plywood Sheathed Shearwalls," *Bulletin of The New Zealand National Society for Earthquake Engineering,* Vol. 19, No. 1, pp. 48–63.

[33] Dean, J.A., B.L. Deam, and A.H. Buchanan, 1989. "Earthquake Resistance of Timber Structures," *The New Zealand Journal of Timber Construction.* Vol. 14, No. 2, pp. 12–16.

[34] De Klerk, D., 1985. *The Effect of Stud Spacing on the Racking Strength of Timber Frame Walls.* CSIR Special Report Hout 405. National Timber Research Institute, Council for Scientific and Industrial Research, Pretoria, South Africa.

[35] Desai, C.S. and J.F. ABEL, 1972. *Introduction to the Finite Element Method. A Numerical Method for Engineering Analysis.* Van Nostrand Reinhold Company, New York.

[36] Dowrick, D.J., 1986. "Hysteresis Loops for Timber Structures," *Bulletin of The New Zealand National Society for Earthquake Engineering,* Vol. 19, No. 2, pp. 143–152.

[37] Eckelman, C.A., 1975. "Screwholding Performance in Hardwoods and Particleboard," *Forest Products Journal,* Vol. 25, No. 6, pp. 30–35.

[38] Falk, R.H. and R.Y. Itani, 1986. "Dynamic Characteristics of Full Scale Wood Diaphragms". ASCE 3rd Specialty Conference on Dynamics of Structures, Los Angeles, California.

[39] Falk, R.H., 1986. *Experimental and Theoretical Study of the Behavior of Wood Diaphragms.* Thesis submitted in partial fulfillment of Ph.D. degree, Washington State University, Pullman, Washington.

[40] Falk, R.H. and R.Y. Itani, 1987. "Dynamic Characteristics of Wood and Gypsum Diaphragms," *ASCE Journal of Structural Engineering,* Vol. 113, No. 6, pp. 1357–1370.

[41] Falk, R.H. and R.Y. Itani, 1989. "Finite Element Modeling of Wood Diaphragms," *ASCE Journal of Structural Engineering,* Vol. 115, No. 3, pp. 543–559.

[42] Falk, R.H. and R.C. Moody, 1989. "Wood Diaphragms: Performance Requirements and Analytical Modeling." *Structural Design, Analysis, and Testing, Proceedings of the Sessions Related to Design, Analysis, and Testing, Structures Congress '89,* ASCE, New York, N.Y., pp. 101–111.

[43] Filiatrault, A. and S. Cherry, 1989. *Seismic Design of Friction Damped Braced Steel Plane Frames by Energy Methods.* Earthquake Engineering Laboratory Report, Department of Civil Engineering, University of British Columbia, Vancouver, B.C., Canada, Report No. EELR–88–01.

[44] Foschi, R.O., 1969. *Stress Distribution in Plywood Stress-Skin Panels with Longitudinal Stiffeners.* Publication No. 1261, Department of Fisheries and Forestry, Canadian Forest Service, Ottawa, Canada.

[45] Foschi, R.O., 1974. "Load–Slip Characteristics of Nails." *Wood Science,* Vol. 7, No. 1, pp. 69–76.

[46] Foschi, R.O., 1977. "Analysis of Wood Diaphragms and Trusses." *Canadian Journal of Civil Engineering,* Vol. 4, No. 3, pp. 345–362.

[47] Foschi, R.O., 1982. *Load/Slip Results for Nailed Connections using Waferboard Panels. Supplementary Report A.* Report to the Canadian Waferboard Association by Forintek Canada Corp., Vancouver, British Columbia.

[48] Foschi, R.O., 1982. *Performance Evaluation of Shear Walls and Diaphragms with Waferboard Sheathing.* Report to the Canadian Waferboard Association by Forintek Canada Corp., Vancouver, British Columbia.

[49] Foschi, R.O., 1982. *Performance Evaluation of Shear Walls with CDX Plywood Sheathing. Supplementary Report B.* Report to the Canadian Waferboard Association by Forintek Canada Corp., Vancouver, British Columbia.

[50] Futhkowski, R.M. and A.L. Castillo, 1988. "Single- and Double-Sheathed Wood Shear Wall Study," *ASCE Journal of Structural Engineering,* Vol. 114, No. 6, pp. 1268–1284.

[51] Gray, R.G. and E.G. Zacher, 1988. "Dynamic Testing of Wood Shear Panels," *Architecture,* March, pp. 121–124.

[52] Griffiths, D.R., 1984. "Determining the Racking Resistance of Timber Framed Walls," *Proceedings of the Pacific Timber Engineering Conference, Auckland, New Zealand, Vol. I, Timber Construction.* Institution of Professional Engineers, Wellington, New Zealand, pp. 504–512.

[53] Gupta, A.K. and G.P. Kuo, 1985. "Behavior of Wood–Framed Shear Walls," *ASCE Journal of the Structural Division,* Vol. 111, No. 8, pp. 1722–1733.

[54] Gupta, A.K. and G.P. Kuo, 1987. "Modeling of a Wood–Framed House," *ASCE Journal of Structural Engineering,* Vol. 113, No. 2, pp. 260–278.

[55] Gupta, A.K. and G.P. Kuo, 1987. "Wood–Framed Shear Walls with Uplifting," *ASCE Journal of Structural Engineering,* Vol. 113, No. 2, pp. 241–259.

[56] HUD, 1979. *Minimum Property Standards for One and Two Family Dwellings.* United States Department of Housing and Urban Development, Washington, D.C.

[57] Henrici, D., 1986. "Design of Sheathed Wooden Shear–Walls," *Drevársky Výskum,* Zväzok III, pp. 57–69.

[58] Hilton, K.C., A. Polensek and G.H. Atherton, 1976. "Effect of Nail Spacing on Rigidity of a Plywood–Wood Joint," *Wood Science,* Vol. 8, No. 4, pp. 234–236.

[59] Hoyle, R.J., Jr., 1972. *Wood Technology in the Design of Structures.* Mountain Press Publishing Company, Missoula, Montana, pp. 263–282.

[60] Hoyle, R.J., Jr. and J.A. Hsu, 1978. "Shear Strength and Shear Modulus of an Elastomeric Adhesive Subject to Repeated Stress," *Wood Science,* Vol. 11, No. 2, pp. 65–68.

[61] Hoyle, R.J., Jr., 1988. "Design of Wood Shear Joints Fastened with Nails and Structural Elastomeric Adhesives," *Proceedings of the 1988 International Conference on Timber Engineering.* Vol. 1, Forest Products Research Society, Madison, Wisconsin, pp. 38–45.

[62] Hsu, J.K. and R.J. Hoyle, Jr., 1978. "Factors Affecting Measurement of Shear Modulusfor an Elastomeric Construction Adhesive," *Wood Science,* Vol. 10, No. 3, pp. 105–110.

[63] ICBO, 1976. *Uniform Building Code.* International Conference of Building Officials, Whittier, California.

[64] Itani, R.Y. and C.K. Cheung, 1984. "Nonlinear Analysis of Sheathed Wood Diaphragms." *ASCE Journal of the Structural Division,* Vol. 110, No. 2, pp. 2137–2147.

[65] Jenkins, J.L., A. Polensek and K.M. Bastendorff, 1979. "Stiffness of Nailed Wall Joints Under Short and Long Term Lateral Loads," *Wood Science,* Vol. 11, No. 3, pp. 145–154.

[66] Källsner, B., 1984. *Panels as Wind-Bracing Elements in Timber-Framed Walls.* Wood Technology Report Nr. 56, Swedish Institute for Wood Technology Research, Stockholm, Sweden.

[67] Kamiya, F., 1986. "Configuration of Wood Sheathed Walls and Its Racking Resistance," *Bulletin of the Forestry and Forest Products Research Institute,* Japan, No. 340, pp. 169–186.

[68] Kamiya, F., 1988. "Buckeling of Sheathed Walls: Nonlinear Analysis", *ASCE Journal of Structural Engineering,* Vol. 114, No. 3, pp. 625–641.

[69] Kanasewich, E.R., 1975. *Time Sequence Analysis in Geophysics.* The University of Alberta Press, Edmonton, Alberta, pp. 175–190.

[70] Keenan, F.J., 1986. *Limit States Design for Wood Structures.* Morrison Hershfield Limited, Toronto, Canada, pp. 405–411.

[71] Kivell, B.T., P.J.Moss and A.J. Carr, 1981. "Hysteretic Modelling of Moment-Resisting Nailed Timber Joints," *Bulletin of The New Zealand National Society for Earthquake Engineering,* Vol. 14, No. 4, pp. 233–243.

[72] Lhuede, E.P., 1988. "Nail Loads for Plywood/Solid Wood Connections," *Proceedings of the 1988 International Conference on Timber Engineering.* Vol. 1 Forest Products Research Society, Madison, Wisconsin. pp. 3–10

[73] Loferski, J.R. and A. Polensek, 1982. "Predicting Inelastic Stiffness Moduli of Sheathing to Stud Nail Joints," *Wood Science,* Vol. 15, No. 1, pp. 39–43.

[74] Malhotra, S.K. and B. Thomas, 1982. "Behavior of Nailed Timber Joints with Interface Characteristics," *Wood Science,* Vol. 5, No. 2, pp. 161–171.

[75] McCutcheon, W.J., 1985. "Racking Deformations in Wood Shear Walls." *ASCE Journal of Structural Engineering,* Vol. 111, No. 2, pp. 257–269.

[76] McCutcheon, W.J., 1986. "Stiffness of Framing Members with Partial Composits Action," *ASCE Journal of Structural Engineering,* Vol. 112, No. 7, pp. 1623–1637.

[77] McDowall, C.G., 1984. "Qualitative Assessment of Whole House Structural Response to Lateral Wind Loads," *Proceedings of the Pacific Timber Engineering Conference, Auckland, New Zealand, Vol. I, Timber Construction.* Institution of Professional Engineers, Wellington, New Zealand, pp. 519–526.

[78] Medearis, K., 1969. "Structural Dynamics of Plywood Shear Walls". *Wood Science,* Vol. 3, No. 2, pp. 106–110.

[79] Mikkola, M.J., M. Tuomala, and H. Sinisalo, 1981. "Comparison of Numerical Integration Methods in the Analysis of Impulsively Loaded Elasto-Plastic and Viscoplastic Structures". Computers and Structures, Vol. 14, No. 5-6, pp. 469-478.

[80] Moody, R.C. and R.J. Schmidt, 1988. "Lateral Loading of Wood Frame Houses: Analysis and Performance." *Proceedings, 1988 International Timber Engineering Conference.* Vol. 2, Forest Products Research Society, Madison, Wisconsin, pp. 62–72.

[81] NFPA, 1986. *National Design Specification for Wood Construction.* National Forest Products Association, Washington, D.C.

[82] NPA, 1983. Correspondence Between the National Particleboard Association and Council of American Building Officials.

[83] NRCC, 1985. *National Building Code of Canada.* Associate Committee on the National Building Code, National Research Council of Canada, Ottawa, Ontario.

[84] NRCC, 1985. *Supplement to the National Building Code of Canada.* Associate Committee on the National Building Code, National Research Council of Canada, Ottawa, Ontario.

[85] NRCC, 1989. *Proposed 1990 National Building Code of Canada, May 1989.* Associate Committee on the National Building Code, National Research Council of Canada, Ottawa, Ontario.

[86] Naik, T.R., S.K. Kaliszky, and L.A. Soltis, 1984. "Mechanical Nonlinear Shear Wall Model." *ASCE Journal of Engineering Mechanics,* Vol. 110, No. 12.

[87] Naik, T.R., S. Kaliszky, and L.A. Soltis, 1984. "Lateral–Torsional Response of Low–Rise Timber Buildings," *Proceedings, 8th World Confence on Earthquake Engineering,* Vol. IV, Response of Structures, San Francisco, Calif., pp. 663–670.

[88] Newmark, N.M., 1962. "A Method of Computation for Structural Dynamics". *ASCE Transactions,* Vol. 127, Part I, pp. 1406–1435.

[89] Ohashi, Y. and I. Sakamoto, 1988. "Effect of Horizontal Diaphragm on Behavior of Wooden Dwellings Subjected to Lateral Load Experimental Study on a Real Size Frame Model," *Proceedings, 1988 International Conference on Timber Engineering,* Vol. 2, Forest Products Research Society, Madison, Wisconsin, pp. 112–117.

[90] Patton–Mallory, M., R.W. Wolfe, L.A. Soltis and R.M. Gutkowski, 1985. "Light–Frame Shear Wall Length and Opening Effects," *ASCE Journal of Structural Engineering,* Vol. 111, No. 10, pp. 2227–2239.

[91] Patton–Mallory, M. and W.J. McCutcheon, 1987. "Predicting Racking Performance of Walls Sheathed on Both Sides." *Forest Products Journal,* Vol. 37, No. 9, pp. 27–32.

[92] Patton-Mallory, M., R.M. Gutkowski, and L.A. Soltis, 1984. *Racking Performance of Light-Frame Walls Sheathed on Two Sides,* Forest Products Laboratory, Madison, Wisconsin.

[93] Perkins, R.H., 1971. "Nail Withdrawal Resistance in Plantation Red Pine Grown in Indiana," *Forest Products Journal,* Vol. 21, No. 6, pp. 29–32.

[94] Peterson, J., 1983. "Bibliogrphy on Lumber and Wood Panel Diaphragms." *ASCE Journal of Structural Engineering,* Vol. 109, No. 2, pp. 2838–2852.

[95] Polensek, A., 1976. "A Finite Element Analysis of Wood-Stud Walls," *ASCE Journal of Structural Engineering,* Vol. 102, No. ST7, pp. 1317–1335.

[96] Polensek, A., 1978. "Properties of Components and Joints for Rational Design Procedure of Wood-Stud Walls," *Wood Science,* Vol. 10, No. 4, pp. 167–175.

[97] Polensek, A. and B.D. Schimel, 1986. "Rotational Restraint of Wood-Stud Wall Supports." *ASCE Journal of Structural Engineering.* Vol. 112, No. 6, pp. 1247–1262.

[98] Polensek, A. and K.M. Bastendorff, 1987. "Damping in Nailed Joints of Light-Frame Wood Buildings," *Wood and Fiber Science,* Vol. 19, No. 2, pp. 110–125.

[99] Sadakata, K., 1988. "Study on Evaluation of Aseismatic Performance of Neoconventional Wooden Frame Structures Assembled by using Highly Ductile Connection Fittings," *Proceedings, 1988 International Conference on Timber Engineering,* Vol. 2, Forest Products Research Society, Madison, Wisconsin. pp. 73–81.

[100] Sakamoto, I., Y. Ohashi and M. Shibata, 1984. "Theoretical Analysis of Seismic Response of Wooden Dwellings in Japan," *Proceedings, Pacific Timber Engineering Conference, Auckland, New Zealand, Vol. II, Timber Design Theory,* Institution of Professional Engineers, Wellington, New Zealand, pp. 454–461.

[101] Salinas, J.J.and D.I. Massé, 1988. " Reliability of Nailed Connections," *Proceedings of the 1988 International Conference on Timber Engineering.* Vol. 1, Forest Products Research Society, Madison, Wisconsin, pp. 11–19.

[102] Schmidt, R.J. and R.C. Moody, 1989. "Modeling Laterally Loaded Light–Frame Buildings," *ASCE Journal of Structural Engineering,* Vol. 115, No. 1, pp. 201–217.

[103] Seismology Committee, SEAOC, 1988. *Recommended Lateral Force Requirements and Tentative Commentary.* Structural Engineers Association of California, San Francisco, California.

[104] Senft, J.F. and S.K. Suddarth, 1971. "Withdrawal Resistance of Plain and Galvanized–Steel Nails During Changing Moisture Content Conditions," *Forest Products Journal,* Vol. 21, No. 4, pp. 19–24.

[105] Smith, I., L.R.J. Whale, and B.O. Hilson, 1988. "An Integrated Approach to Modeling Load–Slip Behavior of Timber Joints with Dowel Type Fasteners," *Proceedings, 1988 International Conference on Timber Engineering,* Vol. 2, Forest Products Research Society, Madison, Wisconsin. pp. 285–293.

[106] Soltis, L.A., 1984. "Low–Rise Timber Buildings Subjected to Seismic, Wind, and Snow Loads," *ASCE Journal of Structural Engineering,* Vol. 110, No. 4, pp. 744–753.

[107] Soltis, L.A., 1984. "Seismic Performance of Low-Rise Light-Framed Wood Buildings," *The Shock and Vibration Digest,* Vol. 16, No. 11, pp. 27-32.

[108] Soltis, L.A. and P.V.A. Mtenga, 1985. "Strength of Nailed Wood Joints Subjected to Dynamic Load," *Forest Products Journal,* Vol. 35, No. 11/12, pp. 14-18.

[109] Soltis, L.A., S. Karnasudirdja, and J.K. Little, 1987. "Angle to Grain Strength of Dowel-Type Fasteners," *Wood and Fiber Science,,* Vol. 19, No. 1, pp. 68-80.

[110] Somayaji, S., 1985. "Discussion: Low-Rise Timber Buildings Subjected to Seismic, Wind, and Snow Loads, by L.A. Soltis," *ASCE Journal of Structural Engineering,* Vol. 111, No. 5, pp. 1164-1166.

[111] Steida, Dr. C.K., 1989. *Personal Correspondence.*

[112] Stewart, A.H., J.R. Goodman, A. Kliewer, E.M. Salsbury, 1988. "Full-Scale Tests of Manufactured Houses Under Simulated Wind Loads," *Proceedings, 1988 International Conference on Timber Engineering,* Vol. 2, Forest Products Research Society, Madison, Wisconsin, pp. 97-111.

[113] Stewart, A.H., A.Kliewer, J.R. Goodman, and E.M. Salsbury, 1989. "Lateral Force Distribution in Manufactured Housing From Full Scale Testing," *Structural Design, Analysis and Testing, Proceedings, Structures Congress '89,* ASCE, New York, N.Y., pp. 112-123.

[114] Stewart, W., J.A. Dean and A.J. Carr, 1984. "The Seismic Performance of Plywood Sheathed Shearwalls," *Proceedings, Pacific Timber Engineering Conference, Auckland, New Zealand, Vol. I, Timber Construction,* Institution of Professional Engineers, Wellington, New Zealand, pp. 486-495.

[115] Stewart, W.G., 1987. *The Seismic Design of Plywood Sheathed Shearwalls.* Thesis submitted in partial fulfillment of Ph.D. degree, University of Canterbury, New Zealand.

[116] Stewart, W.G., J.A. Dean, and A.J. Carr, 1988. "The Earthquake Behavior of Plywood Sheathed Shearwalls," *Proceedings of the 1988 International Conference on Timber Engineering,* Vol. 2. Forest Products Research Society, Madison, Wisconsin, pp. 248–261.

[117] Sturn, G.E. (ATC-7-1), 1980. *Proceedings of a Workshop on Design of Horizontal Wood Diaphragms.* Berkeley, California.

[118] Sugiyama, H., N. Andoh, T. Uchisako, S. Hirano, N. Nakamura, 1988. "Full–Scale Test on a Japanese Type of Two–Story Wooden Frame House Subjected to Lateral Load," *Proceedings, 1988 International Conference on Timber Engineering,* Vol. 2, Forest Products Research Society, Madison, Wisconsin,pp. 55–61.

[119] TECO, 1980. *Summary of Racking Tests Conducted on Waferboard Sheathing.* Report to the Canadian Waferboard Association. TECO, Eugene, Oregon.

[120] TECO, 1981. *Racking Load Test Report on 3 Application Procedures of 7/16" Waferweld.* Report to the Canadian Waferboard Association. TECO, Eugene, Oregon.

[121] Thomson, W.T., 1981. *Theory of Vibrations with Applications.* Prentice-Hall, Inc., Englewood Cliffs, New Jersey, pp. 367–399.

[122] Thurston, S.T. and P.F. Flack, 1980. *Cyclic Load Performance of Timber Sheathed Bracking Walls.* Central Laboratories Report No. 5–80/10. Ministry of Works and Development, Gracefield, Lower Hutt, New Zealand.

[123] Thurston, S.T. and D.L. Hutchison, 1984. "Cyclic Load Testing of Timber-Sheathed Wall Panels," *Proceedings, Pacific Timber Engineering Conference, Auckland, New Zealand, Vol. I, Timber Construction,* Institution of Professional Engineers, Wellington, New Zealand, pp. 496–503.

[124] Tissell, J.R. and J.R. Elliott, 1986. *Research Report 138, Plywood Diaphragms.* American Plywood Association, Tacoma, Washington.

[125] Tissell, J.R., 1989. "Panel-Sheathed Shear Walls – Past and Future." *Structural Design, Analysis and Testing, Proceedings of the Sessions Related to Design, Analysis, and Testing , Structures Congress '89,* ASCE, New York, N.Y., pp. 124–133.

[126] Toumi, R.L. and W.J. McCutcheon, 1977. "Predicting Racking Strength of Light-Frame Walls". Preprint for ASCE Meeting, San Francisco, Calif., October 18, 1977.

[127] Toumi, R.L. and W.J. McCutcheon, 1978. "Racking Strength of Light–Frame Nailed Walls." *ASCE Journal of Structural Division,* Vol. 104, No. ST7, pp. 1131–1140.

[128] Toumi, R.L., 1978. "Racking Strength of Wood-Frame Walls". *U.S. National Bureau of Standards Publication 523* , pp. VI-25 – VI-34.

[129] Turnbull, J.E. and L.P. Lefkovitch, 1986. "Nail Loads for Truss Connections using Steel vs. Five–Ply and Four–Ply Fir and Spruce Plywood Gussets." *Canadian Agricultural Engineering,* Vol. 28, No. 2, pp. 167–173.

[130] Uang, C. and V.V. Bertero, 1988. *Use of Energy as a Design Criterion in Earthquake–Resistant Design.* Report No. UCEERC–88/18 Earthquake Engineering Research Center, University of California, Berkeley, California.

[131] Van Wyk, W.J., 1986. "The Strength Stiffness and Durability of Glued Nail–Glued and Screw Glued Timber Joints," *South African Forestry Journal,* No. 138, pp. 41–44.

[132] Walford, G.B., 1976. "Derivation of Allowable Loads on Nailed Joints in Diaphragms," *Forest Products Laboratory Report No. FP/TE 68,* May, New Zealand, 18 pp.

[133] Westman, E.F. and J.C. McAdoo, 1969. "Nail Withdrawal Resistance of Douglas–Fir and Western Hemlock," *Forest Products Journal,* Vol. 19, No. 5, p. 38.

[134] Wilkinson, T.L. and T.R. Laatsch, 1970. "Lateral and Withdrawal Resistance of Tapping Screws in Three Densities of Wood," *Forest Products Journal,* Vol. 20, No. 7, pp. 34–41.

[135] Zienkiewicz, O.C., 1977. *The Finite Element Method, Third Edition.* McGraw-Hill Book Company (UK) Limited, London.